

MODELLING FOR THE PREDICTION OF THERMAL  
DAMAGE IN GRINDING

*MICHAEL NIEL MORGAN*

A thesis submitted in partial fulfilment of the requirements of Liverpool John  
Moore's University for the degree of Doctor of Philosophy.

SEPTEMBER 1995

## ABSTRACT

This thesis describes an investigation concerned with the development of a quantitative method to calculate grinding temperatures and predict the onset of workpiece thermal damage. For conventional plunge grinding operations the grinding zone temperature is calculated using heat transfer theory for stationary and moving heat source models that describe the physical interaction of the grinding wheel and the workpiece.

Previous developments in thermal modelling for the grinding process were studied. The need for further work was identified.

An experimental study of the thermal properties of grinding wheel bulk materials is described. It was established from the study that the value of the bulk thermal property  $(\kappa\rho c)^{1/2}$  measured from experiment is similar for alumina and CBN. The improved thermal performance of CBN compared to alumina is consequently not explained through the properties of the bulk wheel compound.

A theoretical analysis is presented to predict the proportion of energy entering the workpiece and the proportion entering the grinding wheel. A transient solution is proposed for the partition ratio,  $R$ . The transient solution was developed by matching the temperature at the surface of a conical grain subject to heat from a stationary source, with the temperature at the surface of a workpiece due to a moving circular heat source. The analysis is extended to include energy transfers to the grinding chips and fluid. Lower bound and upper bound solutions for the critical specific energy are established for the two cases. A theoretical boundary solution for the case where energy transfer to the fluid is excluded, is proposed.

A parametric investigation identified the critical model parameters to be the assumed value of grain thermal properties, grain contact radius and grinding contact length. For a given combination of workpiece material, workspeed and infeed the critical parameter influencing the predicted critical specific energy was found to be the damage temperature assumed for the workpiece.

Results are presented for an experimental study undertaken on a centreless grinding machine. Theoretical values of partition ratio predicted from the theoretical boundary solution are found to correlate extremely well with values of partition ratio evaluated from experimental measurements.

## **ACKNOWLEDGEMENTS**

The author would like to thank Professor W. Brian Rowe for his guidance, supervision and expert advice throughout this work. Acknowledgements are also due to Dr. Alan Boyle for his support and to Professor Ben Mills for permitting this work to be carried out in the School of Engineering and Technology Management.

Further thanks go to Dr. David Allanson, J. Andrew Pettit, Sean Black and other colleagues in the Advanced Manufacturing Technology Research Laboratory for their practical help and often inspirational discussions.

Gratitude is also due to Paul Wright and Peter Moran for their assistance with the experimental studies.

I express my thanks to the Liverpool John Moores University who provided the initial finance and the laboratory resources to support the research work.

Finally, I wish to thank my mother Brigitta, brothers Terence and Francis, sister Monica and in particular my wife Wendy, for continued support, encouragement and tolerance during the course of this undertaking.

## Nomenclature : Upper case symbols

	<b>units</b>
$A_a$ wear flat area ( $A_a = bl_g A$ )	$m^2$
$A_r$ real area of contact	$m^2$
$A$ fraction of wear flat area, given by $A_r/A_a$	
$A_c$ cross sectional area	$m^2$
$A_o$ constant used to determine $A_{eff}$	$m^2$
$A_{eff}$ effective wheel dullness	$m^2$
$B'$ material constant (Malkin)	
$C$ cutting edges per unit area of grinding wheel surface / dimensionless constant (see context)	
$D$ constant of proportionality	
$E_s$ Young's modulus: grinding wheel	
$E_s$ Young's modulus: workpiece material	
$F_{HC}$ horizontal cutting force	N
$F_n$ normal grinding force	N
$F'_n$ specific normal grinding force	N/m
$F_t$ tangential grinding force	N
$H$ dimensionless heat transfer coefficient	
$I(x)$ integral	
$J$ defined by $(e_{cc} - e_{ct})/e_c$	
$K_s$ defined by $(1 - \nu_s^2)/(\pi \cdot E_s)$	
$K_w$ defined by $(1 - \nu_w^2)/(\pi \cdot E_w)$	
$K_0$ modified bessel function of second kind of order zero	
$L$ dimensionless source width	
$Nu$ Nusselt number	
$O, P$ dimensionless position variables	
$P$ grinding power	W
$Pr$ Prandtl number	
$Q$ unit strength of instantaneously generated heat source	J
$Q_w$ volumetric removal rate	$m^3/s$
$R_1$ defined as $(x^2 + y^2 + z^2)$	$m^2$
$R$ partition ratio	
$R_{eff}$ theoretical effective partition ratio at low temperatures	
$R^*_{eff}$ theoretical effective partition ratio at the damage threshold	
$R_{exp}$ measured partition ratio	
$R_{lb}$ theoretical lower bound partition ratio	
$R_{th}$ theoretical boundary solution with fluid boiling	
$R_{sp}$ shear plane partition ratio	
$Re$ Reynolds number	
$R_r$ roughness ratio	
$V$ volume	$m^3$
$X, Y, Z$ cartesian coordinates	m
$X', Z'$ dimensionless coordinate parameters	

Z	material removal rate	$\text{m}^3/\text{s}$
Z'	specific material removal rate	$\text{m}^2/\text{s}$

## Nomenclature : Lower case symbols

		units
a	true depth of cut	m
b	width dimension	m
b'	width of grinding chip perpendicular to cutting direction	m
c	specific heat capacity	J/kgK
d <sub>e</sub>	equivalent wheel diameter	m
d <sub>w</sub>	grinding wheel diameter	m
e <sub>c</sub>	specific grinding energy	J/m <sup>3</sup>
h	convective heat transfer coefficient	J/m <sup>2</sup> sK
h <sub>m</sub>	maximum depth of cut	m
h'	critical depth of cut	m
l	width dimension	m
lg	logarithm to base 10	
l <sub>f</sub>	contact length due to deformation	m
l <sub>g</sub>	geometric grinding contact length	m
l <sub>e</sub>	real grinding contact length	m
m	constant used to determine A <sub>eff</sub>	
p	average contact stress	N/m <sup>2</sup>
p <sub>o</sub>	constant contact stress	N/m <sup>2</sup>
q	rate of heat per unit area(heat flux)	W/m <sup>2</sup>
r	contact radius	m
r <sub>o</sub>	contact radius on plane z = 0	m
t,t'	time	s
t <sub>1,max</sub>	maximum undeformed chip thickness	m
u	integration variable	
v	heat source velocity	m/s
v <sub>f</sub>	infeed velocity	m/s
v <sub>w</sub>	workpiece velocity	m/s
x,y,z	cartesian coordinates	m
x',y',z'	cartesian coordinates	m

## Nomenclature : Greek symbols

		<b>units</b>
$\alpha$	thermal diffusivity, defined as $\kappa/(\rho c)$	$m^2/s$
$\chi$	defined by $r^2/(4\alpha t)$	
$\delta$	equivalent dressing infeed angle	
$\phi$	shear angle	degree
$\gamma$	length dimension	m
$\gamma'$	distance from beginning of undeformed chip	m
$\varphi$	dimensionless model parameter	
$\kappa$	thermal conductivity	W/mK
$\mu$	friction coefficient(see context)	
$\mu$	dynamic viscosity(see context)	Ns/m <sup>2</sup>
$\theta$	temperature, defined in context	K
$\theta_{av}$	average surface temperature	K
$\Delta\theta_c$	chip melting temperature	K
$\theta_{fm}$	fluid boiling temperature	K
$\theta_m$	maximum meanline surface temperature	K
$\bar{\theta}_m$	maximum dimensionless surface temperature	
$\theta^*_m$	critical maximum meanline surface temperature	K
$\rho$	density	kg/m <sup>3</sup>
$\tau$	dimensionless time	
$\tau'$	shear stress	Pa
$\psi$	defined by $2L^{1/2}$	
$\nu$	kinematic viscosity(see context)	$m^2/s$
$\nu$	Poisson's ratio(see context)	
$\xi$	integration variable	
$\zeta$	shape factor	

## Suffices

a	wheel porosity	lb	lower bound
b	wheel bond	pl	ploughing
c	specific	th	theoretical bound
cc	specific (to chip)	s	grinding wheel bulk
cf	specific (to fluid)	sl	sliding
ch	chip formation	sp	shear plane
cut	cutting	tot	total
eff	effective	w	workpiece
g	grain		

# CONTENTS

	Page
Abstract	i
Acknowledgements	ii
Nomenclature	iii
<b>Chapter 1</b> Introduction to the grinding process	<b>1</b>
1.1 Thermally induced damage in grinding	1
1.2 Aims and objectives of the investigation	3
1.2.1 Objectives	3
1.3 The scope of the investigation	4
<b>Chapter 2</b> Basic concepts of heat source models	<b>5</b>
2.1 The fundamental law of heat conduction	5
2.2 One-dimensional instantaneous point source solution	7
2.3 Three-dimensional heat conduction	9
2.4 Three-dimensional heat conduction solution	10
2.5 Instantaneous line and plane source solutions	11
2.6 Continuous point, line and plane source solutions	12
2.7 Moving sources of heat	14
2.8 The moving point source temperature solution	14
2.9 The moving line source temperature solution	15
2.10 The moving band source temperature solution	16
2.11 Numerical results for the moving band heat source temperature solution	17
2.12 Discussion of the numerical results for the moving band heat source	19
2.13 The effect of heat source distribution on maximum temperature	23
2.14 Basic concepts of energy partitioning between two conducting bodies	24
2.15 Conclusions	30
<b>Chapter 3</b> Thermal models of the grinding process	<b>31</b>
3.1 The Outwater and Shaw shear plane model	31
3.2 The Takazawa model	33
3.3 Extension of the Takazawa model	36
3.4 The Malkin model	37
3.4.1 Sliding energy in grinding	38

3.4.2	Ploughing and chip formation energies	39
3.4.3	Energy partitioning at the grit-workpiece interface: (Malkin)	41
3.4.4	The shear plane energy model of Malkin coupled with a temperature solution	43
3.4.5	Malkin's strategy for in-process control of thermal damage	45
3.5	The Des Ruisseaux and Zerkle model	47
3.5.1	Shear plane temperature	48
3.5.2	Contact zone temperature	49
3.5.3	Temperature at plane A	50
3.6	Extension of the Des Ruisseaux and Zerkle model to include the effect of cooling	51
3.7	The Rowe and Pettit model	52
3.7.1	The lower bound solution	54
3.7.2	Convection by the grinding chips	56
3.7.3	Convection by the grinding fluid	57
3.7.4	The upper bound solution	58
3.8	Shaw's simplified model	60
3.8.1	Extension of Shaw's simplified model to include the effect of a grinding fluid	64
3.9	The Lavine model	65
3.9.1	Heat transfer to an abrasive grain	66
3.9.2	Heat transfer to workpiece: background temperature rise	68
3.9.3	Workpiece temperature rise beneath an individual grain	69
3.9.4	Heat transfer to the grinding fluid	70
3.9.5	Coupling the temperature and energy equations	71
3.9.6	The partition solution of Lavine	75
3.9.7	Including the effect of heat generation at the shear planes in the coupled heat transfer model of Lavine	77
3.10	Discussion	77
3.11	Conclusions	80
<b>Chapter 4</b>	<b>An investigation of thermal properties of grinding wheels</b>	<b>82</b>
4.1	Theoretical determination of the bulk thermal property $(\kappa\rho c)^{1/2}$ using the equations proposed by Takazawa	82
4.1.1	Selection of the grinding wheel thermal properties for the Takazawa analysis	84
4.1.2	Results	86
4.1.3	Conclusions	86
4.2	Density measurements	87
4.2.1	Apparatus and procedure	87

4.2.2	Results	87
4.3	Thermal conductivity measurements	88
4.3.1	Apparatus and procedure	89
4.3.2	Results	90
4.3.3	Discussion	91
4.4	Specific heat capacity measurements	91
4.4.1	Apparatus and procedure	91
4.4.2	Results	93
4.4.3	Discussion	93
4.5	An experimental method to directly measure the bulk thermal property of a composite solid	94
4.5.1	Theory	94
4.5.2	Apparatus and procedure	95
4.5.3	Results	98
4.6	Conclusions	99
<b>Chapter 5</b>	<b>Energy partitioning to the grinding fluid and chips</b>	<b>100</b>
5.1	The dry grinding partition solution	100
5.2	The single stage workpiece-wheel-fluid partition model	101
5.3	The two stage workpiece-wheel-fluid partition model	103
5.4	The single stage workpiece-wheel-fluid- chips partition model	104
5.5	The two stage workpiece-wheel-fluid- chips partition model	105
5.6	Evaluation	106
5.7	Discussion	108
5.8	Conclusions	108
<b>Chapter 6</b>	<b>Theory: Model development</b>	<b>109</b>
6.1	Grinding temperatures	109
6.2	The grain - workpiece contact	110
6.3	A model for heat transfer into a cylindrical grain	112
6.4	A model for heat transfer into a conical grain	113
6.5	Heat transfer into the workpiece under a grain	115
6.6	Partition ratio: Lower bound	116
6.7	The workpiece background temperature in the grinding contact zone	122
6.8	Grinding contact length	122
6.9	A solution for the lower bound critical specific energy	124
6.10	A solution for the upper bound critical specific energy	125
6.10.1	Conduction to the grinding chips	125
6.10.2	Convection by the grinding fluid	125

6.10.3 A “Fluid wheel” model	126
6.11 Partition ratio: Upper bound	127
6.12 Parameter relationships in grinding	128
6.13 Summary	129
<b>Chapter 7 Theoretical study</b>	<b>132</b>
7.1 Parametric investigation of the conical grain model	132
7.2 Theoretical limit charts	137
7.3 Theoretical values of partition ratio predicted from the conical grain model and other models.	138
<b>Chapter 8 Experimental study</b>	<b>144</b>
8.1 Aim of the experimental study	144
8.2 Machining arrangement for the experimental study	144
8.2.1 Selection of initial values of grinding parameters	145
8.3 Wheel dressing arrangement	145
8.3.1 Selection of values of wheel dressing parameters	146
8.3.2 Dressing tool infeed and traverse speed measurement	146
8.4 The grinding cycle	146
8.5 Experimental equipment	147
8.6 Inspection of the workpiece surface for thermal damage	148
8.7 Measurement of workpiece size	148
8.8 Grinding power measurement	149
8.9 Experimental procedure	149
8.10 Method used to process the experiment data	150
<b>Chapter 9 Experimental results</b>	<b>153</b>
9.1 Thermal damage boundary values: Preliminary study	153
9.2 Grinding power	154
9.3 Thermal damage boundary values	155
9.4 Specific energy and theoretical boundary solutions	157
9.5 Theoretical and experimental values of partition ratio	162
9.6 Evaluation of the Lavine model	168
9.7 Evaluation of the Rowe and Pettit model	168
9.7.1 Determination of the effective bulk thermal property	168
9.7.2 Results for the Rowe and Pettit model	170
9.8 Concluding discussion	173

<b>Chapter 10</b>	<b>Conclusions</b>	<b>174</b>
<b>Chapter 11</b>	<b>Recommendations for further work</b>	<b>176</b>
<b>References</b>		<b>177</b>

## Appendices

- Appendix A1.1 The derivation of the transient one-dimensional heat conduction equation.
- Appendix A1.2 A summary of the expressions for the average and maximum temperature solutions at the surface of a medium subject to a moving band heat source.
- Appendix A1.3 The derivation of the conical grain temperature solution described by Lavine [42,43].
- Appendix A1.4 The derivation of the partition ratio solution proposed by Lavine [42,43].
- Appendix A2.1 Abrasive grain thermal properties.
- Appendix A2.2 Specific heat capacity: Energy balance equation.
- Appendix A2.3 Thermal properties sensor.
- Appendix A3.1 Etch inspection.
- Appendix A3.2 Thermal model: Flowchart and program listing.

## List of plates

- Plate 1      NITAL Etched workpiece (1).
- Plate 2      NITAL Etched workpiece (2).
- Plate 3      The grinding wheel - workpiece arrangement.
- Plate 4      The single point diamond dressing tool.
- Plate 5      The dressing tool linear scale.
- Plate 6      The torsionally rigid coupling.
- Plate 7      Arrangement of the experimental equipment.

## **Chapter 1 INTRODUCTION TO THE GRINDING PROCESS**

Grinding has an important role in manufacturing processes where high accuracy is required. Developments in abrasives and machine technologies have extended the boundaries of grinding capability so that high removal rate grinding competes with other cutting processes. The extended role of grinding creates overlap between the fields of application of cutting and grinding. However, grinding has distinctive features that give the process an advantage for machining difficult-to-machine materials. Many hard materials cannot be machined cost effectively or with sufficient accuracy by any other process [1].

Grinding is used to modify the shape, size and surface texture of hard and soft materials. Material is removed from the workpiece in the form of chips by the action of abrasive particles moving across the surface of a workpiece at high speed. This description of the material removal mechanism implies grinding is similar to other metal cutting processes, such as milling in which cutting edges move relative to the workpiece being machined. However, despite the analogous relative motions of cutter and workpiece, grinding has a number of features that distinguish it from other processes.

The most significant of these is the high relative speed of the tool and the workpiece. Other distinguishing features relate to the grinding wheel and its composition. The abrasive grains are large in number, possess a relatively uncontrolled geometry, are distributed randomly across the surface of the wheel and are very hard. Self-sharpening occurs from the exposure of new cutting edges as a consequence of abrasive grain fracture or complete grain removal during grinding.

A consequence of grinding is that the surface properties including the hardness and the stress state of the material are modified [2]. The change of state of the material occurs mainly as a result of the temperatures generated within the grinding contact zone.

### **1.1 THERMALLY INDUCED DAMAGE IN GRINDING.**

Almost all of the power consumed in grinding is converted to heat in the region where the wheel contacts the workpiece [3]. Heat is generated within the grinding contact zone as a result of the interaction of abrasive grains with the workpiece surface. The

concentration of heat within the grinding contact zone results in an appreciable rise in the temperature of the sliding contacts. If the temperature exceeds a critical level the workpiece suffers thermal damage [4]. Avoidance of thermal damage can often be achieved by employing low removal rates, so reducing the total thermal energy generated and the risk of thermal damage. However, this reduces production rates and grinding efficiency.

Grinding fluid is frequently used to lubricate the grinding zone. Lubricating the contact zone reduces frictional forces [5]. As a result, the temperature at the sliding contacts is lower than that experienced in dry grinding. However, even in wet grinding operations the temperature often exceeds the boiling point of the fluid [6].

Each workpiece material has a unique temperature above which a particular type of thermal damage occurs. The critical temperature is dependent on the physical properties of the material and the thermal damage criterion. Thermal damage induced by grinding has been investigated principally for the grinding of plain carbon and alloy steels as these steels exhibit identifiable microstructural modifications related to a specific temperature. However, thermal damage induced by grinding is also a problem with other materials [4].

It has been proposed [7] that thermal damage in grinding can be avoided whilst maintaining or improving production rates and grinding efficiency by selecting process parameters with reference to a thermal model within an adaptive system. It is necessary to test this hypothesis and examine the assumptions involved.

A thermal model consisting of a series of equations is required to describe the heat transfer occurring within the grinding contact zone. The equations are to be used to ensure that the heat entering the workpiece is lower than the level which will cause damage with an adaptive system which alters values of grinding parameters. However, it is inevitable that simplifying assumptions will have to be made concerning tribological aspects of the grinding contact and it is therefore necessary to consider the implications of such assumptions.

The earliest attempts to calculate temperatures of the workpiece surface in grinding began with the pioneering work of Outwater and Shaw [8] in 1952. Since then much progress has been made in understanding tribological aspects of the grinding contact. In 1988, Rowe and Pettit [7] published results for the calculation and

measurement of the proportion of the grinding power absorbed by the grinding wheel. Initial studies showed that this was an important consideration. Immediately prior to the completion of this thesis a publication in Japanese by Takazawa [9] was found which showed a similar line of reasoning had been previously employed.

Increased understanding of the contact geometry has been acquired as a result of research undertaken on the tribology of grinding [10]. The contact geometry is a complex time and process dependent phenomenon. A partition ratio in this context may be defined as the proportion of the grinding energy which enters the workpiece. In 1989, Lavine [11] published a thermal model based on the contact between individual grains of the grinding wheel and the workpiece. There was clearly a lack of confidence in the reliability of thermal models to consistently predict the energy threshold associated with the onset of thermal damage. It was realised that there was a need to make a more detailed investigation of assumptions employed by different workers. The research was therefore concerned with the investigation of assumptions made regarding the energy partitioning occurring within the grinding contact zone.

## **1.2 AIM AND OBJECTIVES OF THE INVESTIGATION.**

The aim of the work presented in this thesis was to develop a quantitative method to calculate grinding temperatures and predict the onset of workpiece thermal damage for conventional plunge grinding operations.

### **1.2.1 OBJECTIVES**

The objectives of the work were:

- [i] To develop a thermal model for the prediction of values of specific grinding energy. The strategy for avoidance of workpiece thermal damage will be to constrain material removal rates to a value below the value associated with a critical specific grinding energy.
- [ii] To analyse the implications of different thermal modelling assumptions for the energy flows in the zone of interaction between the grinding wheel and the workpiece at the threshold of thermal damage.

[iii] To establish the partition ratio at the thermal damage threshold in grinding.

### **1.3 THE SCOPE OF THE INVESTIGATION.**

The investigation was primarily concerned with the application of heat transfer theory to the grinding process.

Chapter two presents a review of the basic concepts of thermal models and the nature of the assumptions employed in developing models of various heat transfer situations. A critical analysis of previous work on the application of thermal modelling to grinding is presented in chapter three.

In chapter four an investigation of the thermal properties of grinding wheels is described. The results obtained from the experimental study were used to compare values of partition ratio calculated from a wheel / workpiece contact model with values of partition ratio calculated from grain / workpiece contact models.

In chapter five assumptions concerning the energy partitioning to the fluid and grinding chips are investigated. A conclusion of this investigation is a proposed method for modelling the heat flux partitioning to the fluid. In Chapter 6 a refined thermal model is developed based on an analysis of the abrasive grain contact. The effects of assumptions used in the new thermal model are quantified in a theoretical study.

In chapter eight an experimental study consisting of two series of grinding trials is described. The first, a preliminary series of grinding trials, was undertaken to establish the approximate region of the burn boundary for a range of infeed and workspeed combinations. A further series of grinding trials was undertaken to provide values of specific grinding energy at the burn boundary. The results were then used to estimate values of partition ratio. Values of partition ratio determined from experiment were then compared with theoretical values of partition ratio.

## Chapter 2 BASIC CONCEPTS OF HEAT SOURCE MODELS.

In grinding, most of the energy is dissipated as heat within the grinding contact zone [3]. A proportion of the heat generated is conducted to the workpiece. This proportion is known as the partition ratio. The purpose of modelling the heat transfers in the grinding wheel-workpiece contact zone is to attempt to determine the proportion of the energy conducted into the workpiece surface and hence allow the determination of the maximum temperatures experienced at the surface.

This chapter reviews the basic theory for the determination of temperature distributions under a sliding heat source as developed by Jaeger [12]. This is followed by an introduction to the energy partitioning method proposed by Blok [13]. The relevant equations are developed in full to illustrate the assumptions involved. The accuracy of the governing equations is demonstrated and the assumptions used to obtain simplified solutions are discussed, in relation to the applicability to grinding.

### 2.1 THE FUNDAMENTAL LAW OF HEAT CONDUCTION.

A consequence of the second law of thermodynamics and of experience is that heat can be exchanged between two systems only if the two systems are at different temperatures, and that the direction of the heat transfer is from the higher to the lower temperature system. The fundamental condition for heat transfer by conduction within a solid body therefore requires that a temperature gradient exists and that the resulting heat flow be in a direction of decreasing temperature. The basic law which quantitatively defines heat conduction is generally attributed to Fourier [14]. With reference to Figure 2.1 the one dimensional form of the Fourier law states that the quantity of heat  $dQ$ , conducted in the solid in time  $dt$ , is a product of the area  $A$  normal to the flow path, the temperature gradient  $\partial\theta/\partial x$  and a property  $\kappa$ , of the conducting material. Expressed analytically

$$\frac{dQ_x}{dt} = -\kappa.A \frac{\partial\theta}{\partial x} \tag{1}$$

The negative sign is affixed arbitrarily in order that  $Q$  be positive. Equation 1 is the defining equation for thermal conductivity,  $\kappa$ . Thermal conductivity has the units of watts per metre per celsius degree. The thermal conductivity of a material is a function of temperature and other thermodynamic variables. For small temperature

differences thermal conductivity may be regarded as a constant. Materials with a high value of thermal conductivity are good conductors of heat and conversely materials with a low value of thermal conductivity are good insulators of heat. The quantity  $\kappa/(\rho.c) = \alpha$  is the thermal diffusivity of the material and has units of square metres per second. The larger the value of  $\alpha$  the faster heat diffuses through the material. A high value of  $\alpha$  can result from either a high value of thermal conductivity  $\kappa$ , or from a low value of the product  $\rho.c$  [15]. The product  $\rho.c$  is defined as the thermal heat capacity of a material.

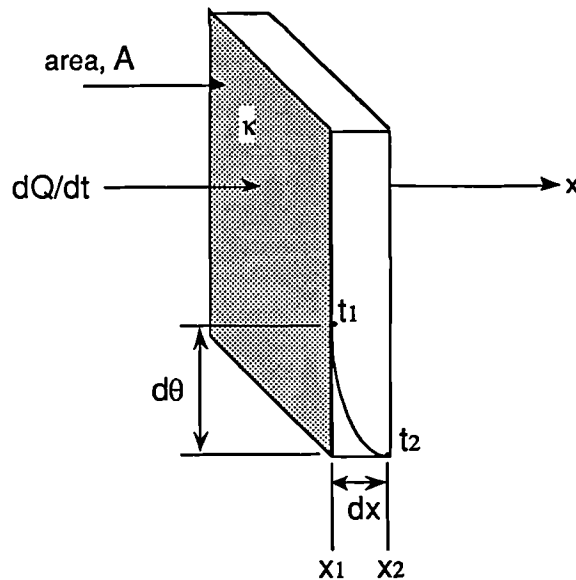


Figure 2.1 Elementary plate for one dimensional heat flow.

In the case of steady conduction where  $\theta$  is a function of  $x$  alone,  $dQ/dt = Q/t = q$ , and equation 1 simplifies to

$$q = - \kappa A \frac{d\theta}{dx} \quad 2$$

The type of process in which the temperature appears as a function of a time coordinate  $t$ , as well as a space coordinate  $x$ , is known as transient conduction. In the transient state of heat conduction the quantity of heat entering and leaving a volume element of the solid is not the same at any given instant. The first law of thermodynamics states that the difference is used to increase the internal energy of the element.

Equation 3 may be derived from equation 1 and is the governing equation that describes transient one-dimensional heat conduction. Equation 3 forms the basis for the solution of many practical problems of heat conduction.

$$\frac{1}{\alpha} \frac{\partial \theta}{\partial t} = \frac{\partial^2 \theta}{\partial x^2} \quad 3$$

Equation 3 is derived from first principles in appendix 1.

## 2.2 ONE -DIMENSIONAL INSTANTANEOUS POINT SOURCE SOLUTION.

The one-dimensional point source solution is of fundamental importance in heat flow, enabling the solution of a large number of important problems to be further derived from first principles. Physically the one-dimensional source solution can be regarded as being the temperature distribution due to an instantaneous source of heat concentrated entirely at the origin in which heat is constrained to flow in one direction.

A solution of the one-dimensional heat equation may be found by application of trial solutions and checking for consistency with equation 3. Equation 4 provides a form of solution which can be shown to be valid. Jaeger [12] presents solutions of a number of forms that are appropriate for different problems.

$$\theta = C.t^{-1/2} .e^{-x^2/(4.\alpha.t)} \quad 4$$

where C is a dimensional constant having units which are the product of time to the power one half and degrees.

The partial derivatives of equation 3 are given in equations 5 and 6.

$$\frac{\partial \theta}{\partial t} = C \left[ -\frac{1}{2t^{3/2}} .e^{-x^2/(4.\alpha.t)} + \frac{x^2}{4.\alpha.t^{5/2}} .e^{-x^2/(4.\alpha.t)} \right] \quad 5$$

$$\frac{\partial^2 \theta}{\partial x^2} = C \left[ -\frac{1}{2.\alpha.t^{3/2}} .e^{-x^2/(4.\alpha.t)} + \frac{x^2}{4.\alpha^2.t^{5/2}} .e^{-x^2/(4.\alpha.t)} \right] \quad 6$$

Substituting from equations 5 and 6 for the partial derivatives in equation 3 demonstrates that equation 4 is a valid solution.

Equation 4 has the properties:

$$\theta \rightarrow 0 \text{ as } t \rightarrow \infty, x \neq 0 \text{ and } \theta \rightarrow \infty \text{ as } t \rightarrow 0, x = 0$$

A graphical solution of equation 4 is shown in Figure 2.2 for different values of  $t$ . In the example shown a value of  $\alpha = 15 \text{ mm}^2/\text{s}$  was used, which is a typical value for steel. Figure 2.2 shows the position - temperature relationship on the surface of a medium at fixed points in time,  $t$ .

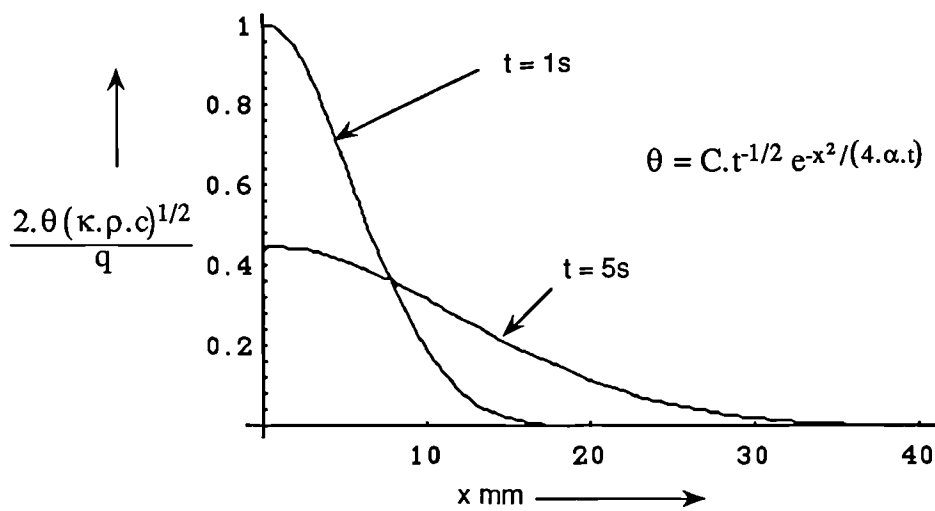


Figure 2.2 Temperature - position solutions on the surface of a medium at fixed points in time,  $t$ .

Since

$$\int_{-\infty}^{\infty} e^{-a^2 \cdot x^2} dx = \frac{\sqrt{\pi}}{a}$$

7

is a standard solution, [12], for the exponential function shown, it may be shown that

$$\int_{-\infty}^{\infty} \theta dx = C.t^{-0.5}.2\sqrt{\pi.\alpha.t} = 2.C\sqrt{\pi.\alpha} \text{ for all } t > 0. \quad 8$$

Applying the result in equation 8 to Fourier's law yields a relationship between the quantity of heat supplied,  $Q_x$ , and the dimensional constant  $C$ , equation 9.

$$Q_x = - \frac{\kappa.A}{\alpha}.2.C\sqrt{\pi.\alpha.} = 2.C\sqrt{\pi.\alpha} \quad 9$$

From the result in equation 9, with  $Q_x/A = q_x$  it can be shown that

$$C = \frac{q_x.\alpha}{2.\kappa\sqrt{\pi.\alpha.}} = \frac{q_x}{2\sqrt{\pi.\kappa.\rho.c}} \quad 10$$

The solution for the one-dimensional differential heat conduction equation is found by substituting for  $C$  in equation 4.

$$\theta = \frac{q_x}{2(\pi.\kappa.\rho.c.t)^{1/2}} e^{-x^2/(4.\alpha.t)} \quad 11$$

### 2.3 THREE-DIMENSIONAL HEAT CONDUCTION.

To determine the governing equation for three-dimensional heat flow the heat conducted in and out of an elemental volume is considered. An elemental volume is illustrated in Figure 2.3.

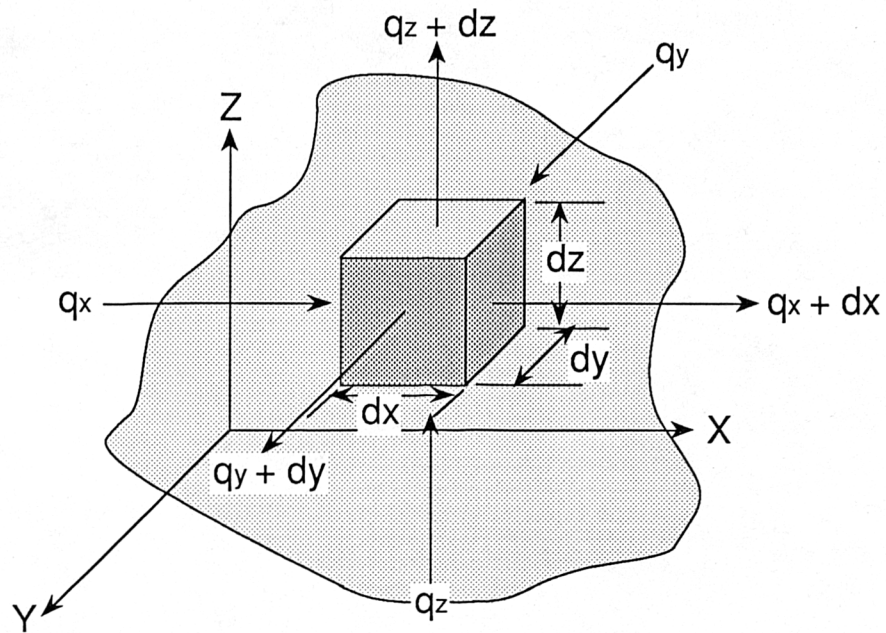


Figure 2.3 Elemental volume for three-dimensional heat conduction analysis.

The fluxes shown in Figure 2.3 are components of the heat flux vector  $q$ , so that

$$q = i q_x + j q_y + k q_z \quad 12$$

The solution for the heat flow within the elemental volume is obtained by applying Fourier's law to each of the coordinate plane surfaces. The governing equation for three-dimensional heat flow is given in a differential form by equation 13 and is termed the differential heat conduction equation.

$$\frac{1}{\alpha} \frac{\partial \theta}{\partial t} = \nabla^2 \theta \quad 13$$

where

$$\nabla^2 = \frac{\partial^2}{\partial x^2} + \frac{\partial^2}{\partial y^2} + \frac{\partial^2}{\partial z^2} \quad 14$$

## 2.4 THREE-DIMENSIONAL HEAT CONDUCTION SOLUTION.

An instantaneous point source is illustrated in Figure 2.4.

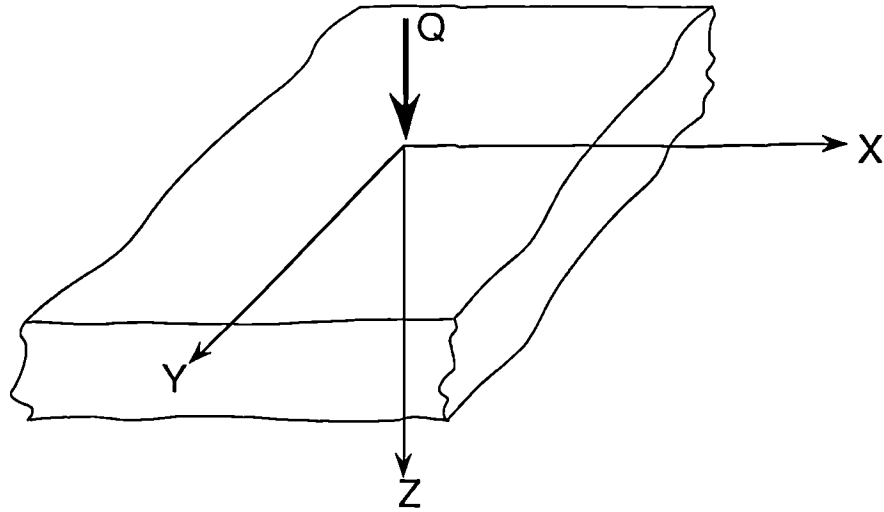


Figure 2.4 An instantaneous point source acting on an infinite solid.

In a similar manner to that given for the solution of the one-dimensional heat equation it can be shown that equation 15 is a solution of equation 13. Equation 15 can be recognised as the product of three one-dimensional source solutions and expresses the temperature distribution due to an instantaneous point source.

$$\theta = \frac{q}{8(\pi \cdot \kappa \cdot \rho \cdot c \cdot t)^{3/2}} \cdot e^{-\{(x-x')^2 + (y-y')^2 + (z-z')^2\}/(4 \cdot \alpha \cdot t)} \quad 15$$

## 2.5 INSTANTANEOUS LINE AND PLANE SOURCE SOLUTIONS.

The integration of the instantaneous point source solution in equation 15 with respect to  $y$  yields equation 16, the solution for an instantaneous line source. The line source solution is equivalent to a uniform distribution of point sources along the  $y$  axis.

$$\theta = \frac{q}{4 \cdot \pi \cdot \kappa \cdot \rho \cdot c \cdot t} \cdot e^{-\{(x-x')^2 + (z-z')^2\}/(4 \cdot \alpha \cdot t)} \quad 16$$

The integration of equation 16 with respect to  $z$ , yields the solution for an instantaneous plane source and is given by equation 17. The plane source solution is equivalent to a distribution of line sources along the line  $x = x'$  and  $y = y'$ .

$$\theta = \frac{q}{2(\pi \cdot \kappa \cdot \rho \cdot c \cdot t)^{1/2}} \cdot e^{-(x-x')^2/(4 \cdot \alpha \cdot t)} \quad 17$$

## 2.6 CONTINUOUS POINT, LINE AND PLANE SOURCE SOLUTIONS.

Solutions for continuous heating may be obtained by integration of the instantaneous source solutions with respect to time. From equation 15, it follows that equation 18 is the temperature solution for the continuous point source.

$$\theta = \frac{q}{2.\pi.\alpha.r} . \text{erfc} \frac{r}{\sqrt{(4.\alpha.t)}} \quad 18$$

where  $r^2 = (x - x')^2 + (y - y')^2 + (z - z')^2$  and  $\text{erfc}\{x\}$  is the complementary error function defined by  $\text{erfc}\{x\} = 1 - \text{erf}\{x\}$ . The error function  $\text{erf}\{x\}$  is defined by

$$\text{erf}(x) = \frac{2}{\pi} \int_0^x e^{-t^2} dt \quad 18a$$

and the complementary error function by

$$\text{erfc}(x) = \frac{2}{\pi} \int_x^{\infty} e^{-t^2} dt \quad 18b$$

From equation 18, the temperature solution for the continuous line source is,

$$\theta = - \frac{q}{4.\pi.\alpha} . \text{Ei} \left( - \frac{r^2}{4.\alpha.t} \right) \quad 19$$

where  $r^2 = (x - x')^2 + (y - y')^2$  and the exponential integral is

$$\text{Ei}(-x) = - \int_x^{\infty} \frac{e^{-u}}{u} du \quad 20$$

$$\text{where } u = \frac{r^2}{4.\kappa(t - t')}$$

From equation 17, the temperature solution for the continuous plane source is,

$$\theta = q \left( \frac{t}{\pi \cdot \alpha} \right)^{1/2} \cdot e^{-\frac{(x-x')^2}{4 \cdot \alpha \cdot t}} - \frac{q |x-x'|}{2 \cdot \kappa} \left( 1 - \operatorname{erf} \frac{|x-x'|}{2\sqrt{\alpha \cdot t}} \right) \quad 21$$

The complementary error function  $\operatorname{erfc}(x) = 1 - \operatorname{erf}(x)$  therefore equation 21 can be rewritten as,

$$\theta = q \left( \frac{t}{\pi \cdot \alpha} \right)^{1/2} \cdot e^{-\frac{(x-x')^2}{4 \cdot \alpha \cdot t}} - \frac{q |x-x'|}{2 \cdot \kappa} \cdot \operatorname{erfc} \frac{|x-x'|}{2\sqrt{\alpha \cdot t}} \quad 22$$

Equation 22 simplifies to equation 23 if the diffusivity is expressed in terms of the conductivity, and the following substitutions are made

$$\xi = \frac{x}{2\sqrt{\alpha \cdot t}}$$

$$t = \frac{l_e}{v_s}$$

$$\theta = \frac{2 \cdot q \cdot l_e^{1/2}}{\pi^{1/2} [\rho \cdot c \cdot \kappa \cdot v_s]^{1/2}} \cdot e^{-\xi^2} - \frac{q |x-x'|}{2 \cdot \kappa} \cdot \operatorname{erfc}(\xi) \quad 23$$

At the surface, the right hand term of equation 23 is zero and the solution for the maximum temperature reduces to equation 24.

$$\theta = \frac{2 \cdot q \cdot l_e^{1/2}}{\pi^{1/2} [\rho \cdot c \cdot \kappa \cdot v_s]^{1/2}} \quad 24$$

The continuous plane source solution given by equation 23 is important for problems in which a stationary source is subject to a constant heat flux for a finite period. It is used in later analyses to determine the temperature of the grinding wheel grain where the grain is subject to a constant heat flux as it passes through the grinding contact zone. For this case, the solid is subject to a constant heat flux for the period  $t = l_e/v_s$ .

## 2.7 MOVING SOURCES OF HEAT.

Jaeger [16] presented temperature solutions for particular models of sliding sources. The model that is used most often for analysing workpiece temperatures is the moving band heat source. The particular problem of a moving band heat source which passes a fixed point with a uniform velocity was solved by integration of the solutions for instantaneous sources with respect to time and the three plane coordinates.

## 2.8 THE MOVING POINT SOURCE TEMPERATURE SOLUTION.

Moving heat source problems can be regarded as problems in which heat is produced at a fixed point past which a body moves. A medium moving past a stationary point source with a uniform velocity parallel to the x - axis is illustrated in Figure 2.5. The heat source emits heat at the rate q at the origin at time t', where t' is greater than t<sub>0</sub>, and continues to emit heat for a period t - t'. The distance travelled by the medium in the period t - t' is x' = v(t - t'). The solution for the moving point source is found by integrating the solution for the instantaneous point source, equation 15, with respect to time and the x - coordinate.

$$\theta = \frac{q}{2 \cdot \kappa \cdot R_1 \cdot \pi^{3/2}} \cdot e^{\frac{v \cdot x}{2 \cdot \alpha}} \int_{\frac{R_1}{2 \sqrt{\alpha (t-t')}}}^{\infty} e^{-\xi^2 - \left( \frac{v^2 \cdot R_1^2}{16 \kappa^2 \xi^2} \right)} d\xi \quad 25$$

Equation 25 is the solution for the moving point source, where  $R_1^2 = (x^2 + y^2 + z^2)$  and  $t - t' = R_1^2 / (4 \cdot \xi^2 \cdot \kappa)$  and  $\xi = R_1 / (2 [\kappa (t - t')]^{1/2})$ .

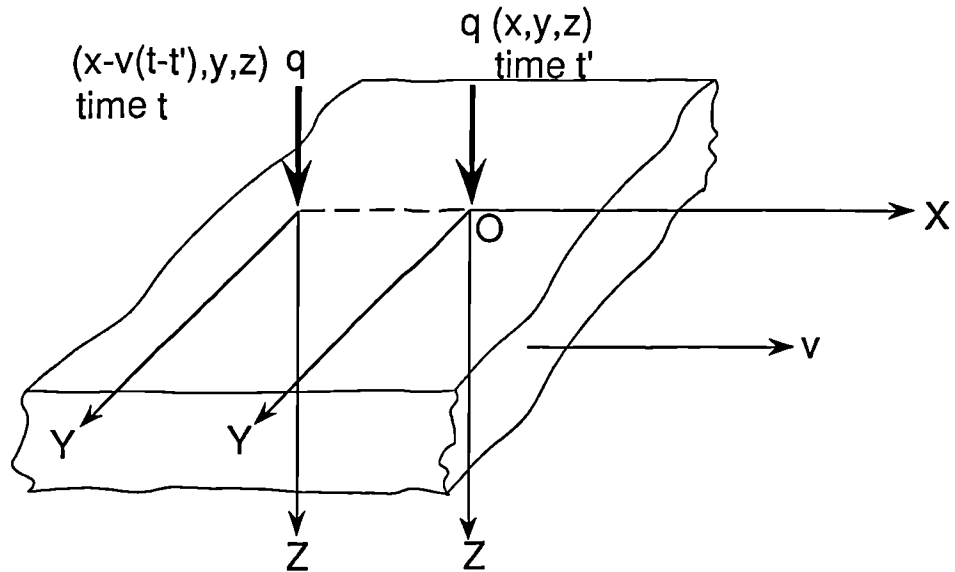


Figure 2.5 An infinite medium moving past a constant point heat source with uniform velocity in fixed space coordinates.

## 2.9 THE MOVING LINE SOURCE TEMPERATURE SOLUTION.

Figure 2.6 shows a line source which emits heat at the rate  $q$ , per unit length along the  $y$ -axis. An infinite medium moves past the line source with a uniform velocity  $v$  parallel to the  $x$ -axis. The steady state temperature solution for the moving line source model is found by integrating equation 25 with respect to  $y$ .

$$\theta = \frac{q}{2\pi\kappa} \cdot e^{-v \cdot x / (2\alpha)} \cdot K_0 \left[ v(x^2 + z^2)^{1/2} / (2\alpha) \right] \quad 26$$

Equation 26 is the solution for the moving line source, where  $K_0(x)$  is the modified Bessel function of the second kind of order zero.

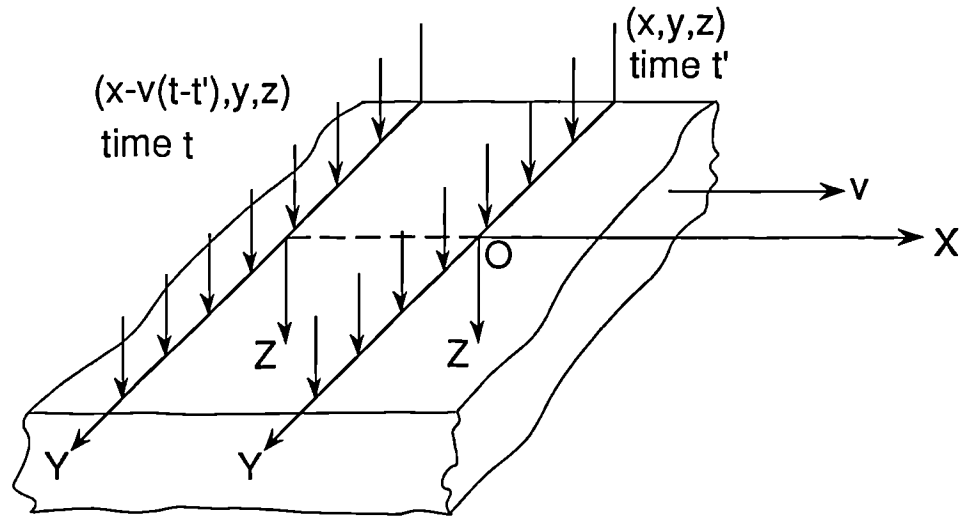


Figure 2.6 An infinite medium moving past a line source with uniform velocity in fixed coordinates.

### 2.10 THE MOVING BAND SOURCE TEMPERATURE SOLUTION.

An infinite medium moving past a plane band source with uniform velocity  $v$  parallel to the  $x$  - axis is shown in Figure 2.7. The band source has dimensions  $-b < x < b$  and  $-\infty < y < \infty$  in the plane  $z = 0$ . Heat is emitted from the band source at a flux  $q$  over the band. The solution for the temperature is found by integration of equation 26 with respect to  $x$  between the limits of  $-b$  and  $b$ .

$$\theta = \frac{q}{2 \cdot \pi \cdot \kappa} \int_{-b}^b e^{v(x-x')/(2\alpha)} \cdot K_0 \left\{ v \left[ \frac{((x-x')^2 + z^2)^{1/2}}{(2\alpha)} \right] \right\} \cdot dx' \quad 27$$

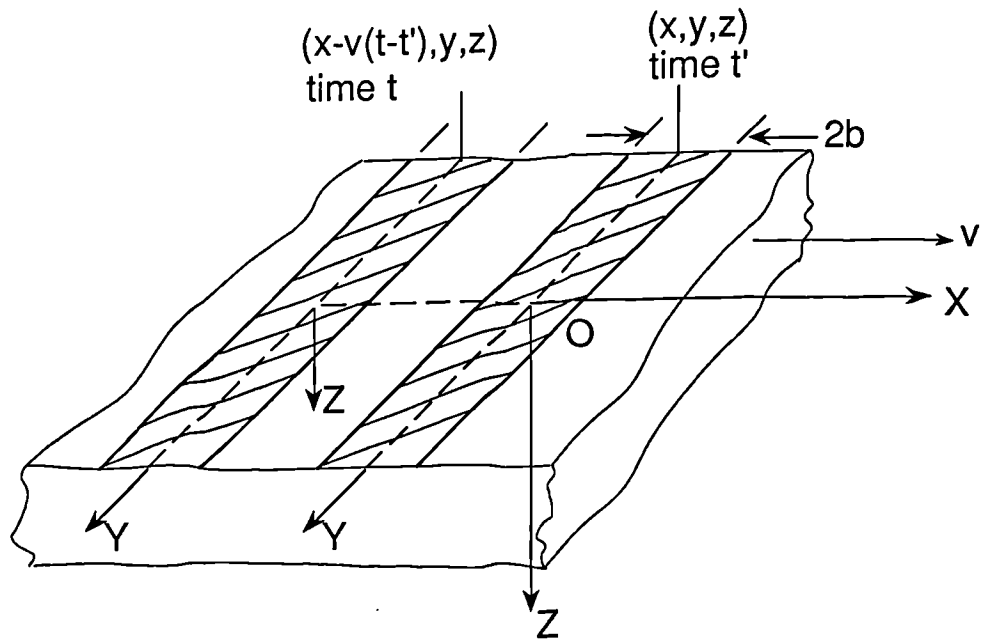


Figure 2.7 An infinite medium moving past a plane band source with uniform velocity in fixed coordinates.

The temperature values given by equation 27 are half the temperature values for the same source moving across a semi-infinite body since heat can flow over the plane  $z$  equals zero and half the heat liberated will go into the plane  $z$  in the negative direction. Equation 27 is an exact equation. The accuracy for a real situation depends only on the inbuilt assumptions. These concern the shape and nature of the heat source. The thermal properties are represented as constants in equation 27. Allowance for varying thermal properties can be incorporated by appropriate describing functions. In a real situation the solid is unlikely to be semi-infinite. All of these issues can be addressed through numerical solutions of equation 15 with appropriate boundary conditions and describing functions for the thermal properties.

## 2.11 NUMERICAL RESULTS FOR THE MOVING BAND HEAT SOURCE TEMPERATURE SOLUTION.

Jaeger performed the integration in equation 27 by a numerical method. The results were presented in a general form using dimensionless parameters. The dimensionless parameters were :

$$X' = \frac{v \cdot X}{2 \cdot \alpha} ; \quad Z' = \frac{v \cdot Z}{2 \cdot \alpha} \quad \text{and} \quad L = \frac{v \cdot b}{2 \cdot \alpha}$$

Equation 27 becomes :

$$\theta = \frac{\alpha \cdot q}{\pi \cdot K \cdot v} \int_{x-L}^{x+L} e^u \cdot K_0(Z^2 + u^2)^{1/2} du \quad 28$$

where  $u = v(x - x')/(2\alpha)$ .

The principal results of Jaegers temperature analysis are illustrated in Figure 2.8. The curves were constructed from tabulated results for the integrals  $I(x)$  and  $I(-x)$  where

$$I(x) = \int_0^x e^{-u} \cdot K_0(|u|) du \quad \text{and} \quad I(-x) = - \int_0^x e^u \cdot K_0(|u|) du \quad 29$$

The results given are for the temperature in a semi-infinite solid caused by a slider of width  $2b$  moving across its surface with a velocity  $v$ .

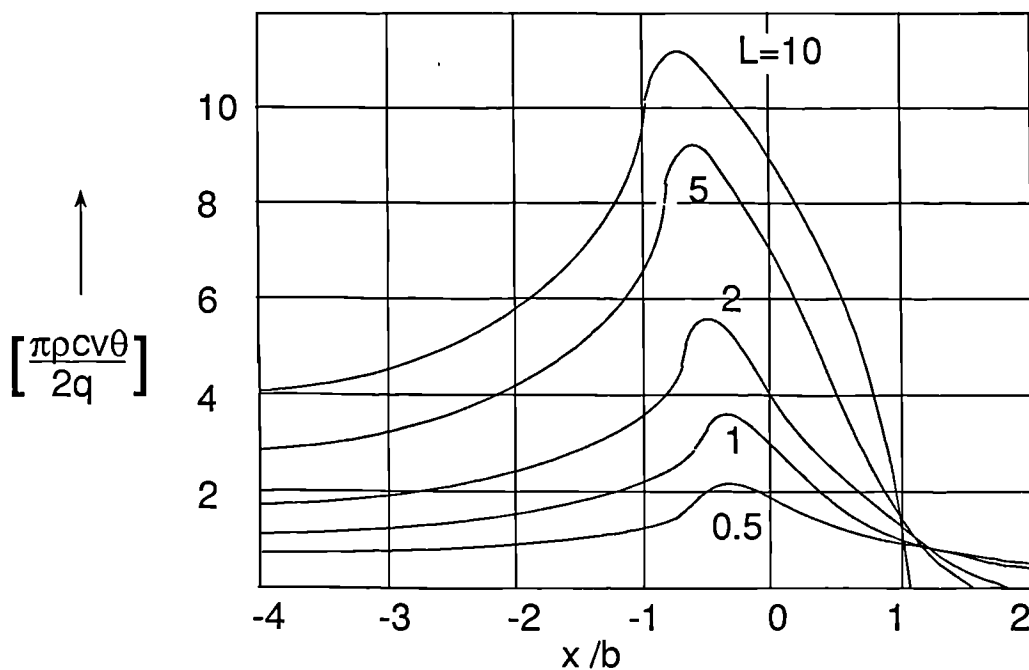


Figure 2.8 Temperature distribution curves for a semi-infinite solid caused by a slider of width  $2b$  moving across a surface with a velocity  $v$  (after Jaeger [16]).

## 2.12 DISCUSSION OF THE NUMERICAL RESULTS FOR THE MOVING BAND HEAT SOURCE.

In Figure 2.8 the values of  $\pi\rho cv\theta/(2q)$  give the temperature variation in the plane of the moving heat source for various values of the Peclet number  $L$ , in terms of the ratio  $X'/L = x/b$ . The value of  $L$  depends on the thermal properties and speeds of the solid and on the contact length.  $L$  is the major non-dimensional parameter governing the heat transfer mechanism in this system. The position of the maximum temperature from Figure 2.8 is seen to approach the trailing edge of the slider as the velocity of the slider increases for large values of  $L$ , and approaches the centre of the slider as the velocity approaches zero.

Jaeger determined relationships between the function  $\pi\rho cv\theta/(2q)$  and the dimensionless parameters  $X'$  and  $L$  by fitting equations to curves similar to those shown in Figure 2.8.

### (i) Solutions for $L < 0.1$

For very small values of  $L$ , that is  $L$  less than 0.1 and for small  $X'$ , the curves are almost symmetrical. The temperature was expressed by equation 30, where  $\lg$  denotes the logarithm to the base 10.

$$\frac{\pi \cdot \kappa \cdot v \cdot \theta}{2 \cdot q \cdot \alpha} = -2.303 (X' + L) \lg|X' + L| + 2.303 (X' - L) \lg|X' - L| + 2.232L \quad 30$$

For values of  $L$  less than 0.1,

$$\lg|X' + L| - \lg|X' - L| \approx 0 \quad 31$$

Applying the relationship in equation 31 allows equation 30 to be simplified. The maximum temperature  $\theta_m$ , and the average temperature  $\theta_{av}$ , for very small  $L$ , are then given by,

$$\theta_m = \frac{4 \cdot q \cdot \alpha}{\pi \cdot \kappa \cdot v} \cdot \{-2.303L \lg L + 1.116L\} \quad 32$$

and

$$\theta_{av} = \frac{4 \cdot q \cdot \alpha}{\pi \cdot \kappa \cdot v} \cdot \{-2.303L \lg(2L) + 1.616L\} \quad 33$$

**(ii) Solutions for L > 5**

For values of L greater than 5, the following approximate solution was given.

$$\frac{\pi \cdot \kappa \cdot v \cdot \theta}{2 \cdot q \cdot \alpha} = (2 \cdot \pi)^{1/2} \{(L - X')^{1/2} - (X' + L)^{1/2}\} \quad 34$$

It may be noted from Figure 2.8 that for values of L greater than 5 the maximum temperature occurs near  $X' = -L$  thus,

$$(L - X')^{1/2} - (X' + L)^{1/2} \approx (2L)^{1/2} \quad 35$$

Simplifying equation 34 using equation 35, substituting the expression for L and rearranging, a solution may be found for the maximum temperature  $\theta_m$ ,

$$\theta_m = 1.60 q \left( \frac{b}{\kappa \cdot \rho \cdot c \cdot v} \right)^{1/2} \quad 36$$

where b is the half width of the heat source.

By appropriate substitutions equation 36 can be expressed in terms of the Peclet number L, and/or the diffusivity  $\alpha$ .

If the numerator and denominator of the right hand term in equation 36 is multiplied by  $\alpha^{1/2}$  an expression is established for the maximum temperature in terms of the diffusivity

$$\theta_m = \frac{1.60 q}{\kappa} \left( \frac{\alpha \cdot b}{v} \right)^{1/2} \quad 36a$$

By replacing the numerical constant in equation 36a with an equivalent term  $\frac{2\sqrt{2}}{\sqrt{\pi}}$ , equation 36a becomes

$$\theta_m = \frac{2 q}{\kappa} \left( \frac{2 \cdot \alpha \cdot b}{\pi \cdot v} \right)^{1/2} \quad 36b$$

If the numerator and denominator of the right hand term in equation 36b is multiplied by  $L^{1/2}$  an expression is established for the maximum temperature in terms of the Peclet number and the diffusivity

$$\theta_m = \frac{2q}{\kappa} \left( \frac{2\alpha \cdot b}{\pi \cdot v} \cdot \frac{v \cdot b}{2\alpha} \cdot \frac{2\alpha}{v \cdot b} \right)^{1/2} = \frac{4q\alpha L^{1/2}}{\kappa \cdot v \cdot \sqrt{\pi}} \quad 36c$$

Equation 36c can be expressed in terms of the Peclet number only, by multiplying the numerator and the denominator of the right hand side by  $L$ , so that

$$\theta_m = \frac{4q\alpha L^{1/2}}{\kappa \cdot v \cdot \sqrt{\pi}} = \frac{4q\alpha L}{\kappa \cdot v \cdot \sqrt{\pi} L^{1/2}} = \frac{4q\alpha \cdot v \cdot b}{\kappa \cdot v \cdot \sqrt{\pi} 2\alpha L^{1/2}}$$

which reduces to

$$\theta_m = \frac{1.13q \cdot b}{\kappa \cdot L^{1/2}} \quad 36d$$

The average temperature,  $\theta_{av}$ , is found from a numerical solution of equation 28, over the area of the source,

$$\theta_{av} = 1.06q \left( \frac{b}{\kappa \rho c v} \right)^{1/2} \quad 37$$

Equation 37 can be manipulated in a similar manner to equation 36 for the average temperature in terms of the Peclet number and/or diffusivity. In the form most commonly encountered

$$\theta_{av} = \frac{0.754q \cdot b}{\kappa \cdot L^{1/2}} \quad 37a$$

The maximum and average temperature solutions described by equations 36 and 37 respectively are important solutions that can be used within thermal analyses concerned with workpiece surface temperatures in grinding.

The expressions for the maximum and average temperature solutions are summarised in appendix A1.2.

**(iii) Solutions for  $0.1 < L < 5$**

For intermediate values of  $L$  the maximum temperatures can be obtained from curves such as those given in Figure 2.8, and the average temperatures evaluated from expressions given in reference 16. Jaeger presented results for intermediate values of  $L$  obtained from the expressions given in reference 12. Jaeger's results are shown in Figure 2.9.

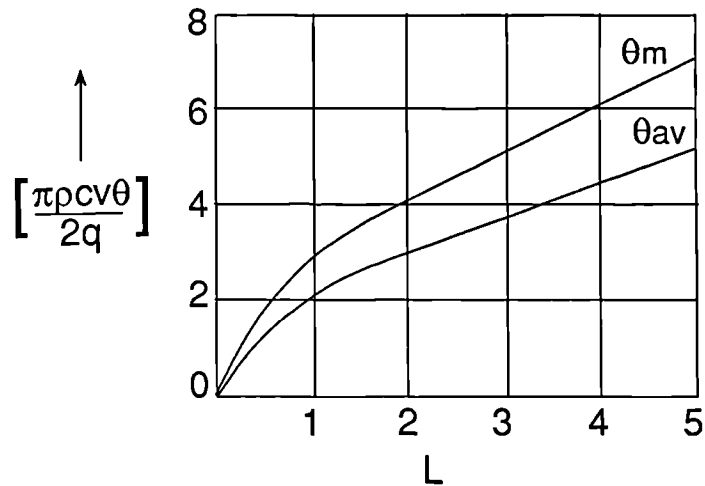


Figure 2.9 Maximum and average temperatures for a moving band source  $0.1 < L < 5$ .

Figure 2.9 shows the relative orders of magnitude of the maximum and average temperatures for cases where the Peclet number is  $0.1 < L < 5$ . In the range  $0.1 < L < 5$  the ratio  $\theta_m/\theta_{av}$  of the maximum temperature to the average temperature varies. When  $L$  is greater than 5, the average temperature is approximately two-thirds of the maximum temperature.

For many grinding situations  $L$  is greater than 5 and equations 36 and 37 may be used for temperature analysis. However, there are other situations in grinding for which it will be shown that  $L$  is much smaller than 5.

A heat source generated at the contacting surface of a perfectly insulated rectangular slider is illustrated in Figure 2.10. The width of the slider is defined by  $-l < x < l$ , and

the length in the y plane is assumed to be much greater than the length in the x plane. It is assumed that no heat transfer occurs in the direction normal to the planes x and z.

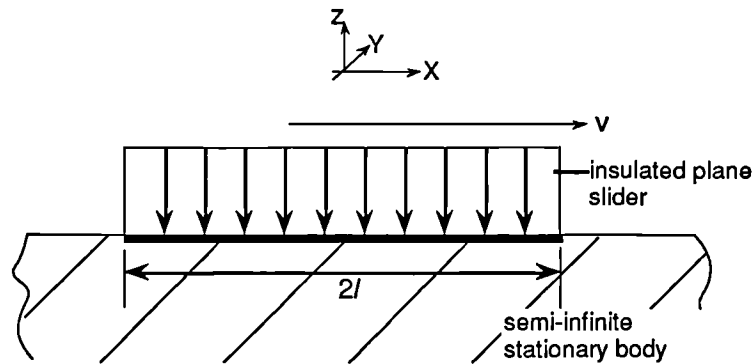


Figure 2.10 A heat source generated by an insulated rectangular slider moving over a semi-infinite stationary body with velocity  $v$ , (after Jaeger [16]).

In the context of thermal damage in the grinding process this physical representation provides a basis for calculation of the temperatures in a workpiece, where a uniform band heat source is moved along its surface. The moving band source is the model quoted in most literature on the subject. However, the model can be questioned because it is difficult to imagine the grinding wheel as an insulated slider. Also, questions arise as to whether a uniform heat source is appropriate. Equation 34 which has been widely used applies to values of  $L$  greater than 5. Inaccuracy will occur when the operating conditions do not satisfy this condition.

### 2.13 THE EFFECT OF THE SHAPE OF THE HEAT SOURCE DISTRIBUTION ON MAXIMUM TEMPERATURE.

The effect of the shape of the heat flux distribution in the contact area has been investigated by Jaeger [16] and by other authors [17, 18]. Results presented for triangular and rectangular heat sources, are illustrated in Figure 2.11 for the case  $L = 1$ .

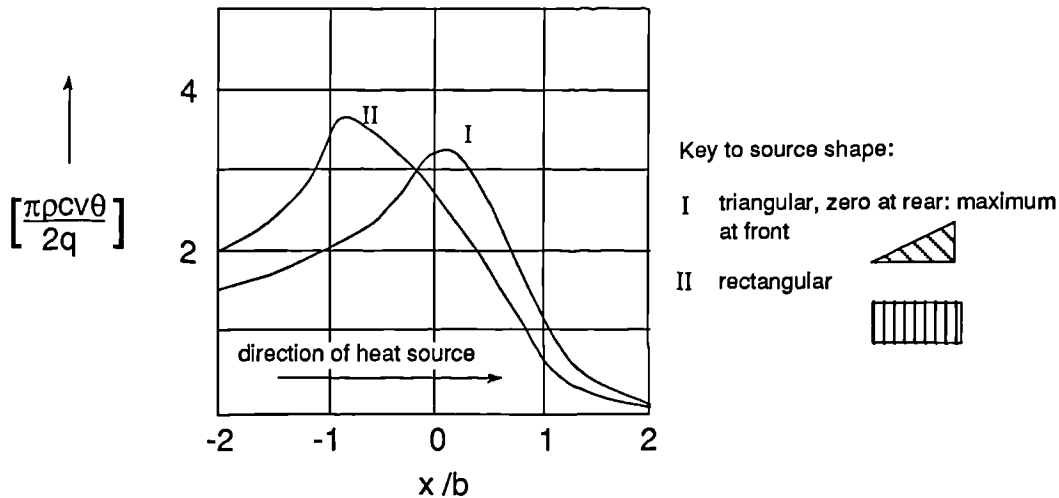


Figure 2.11 The effect of heat flux distribution on maximum temperature (after Jaeger [16])  $L = 1$ .

The values of maximum temperature differ by a maximum of 10%. The shape of the heat source distribution is therefore significant but a second order effect for the determination of the maximum temperature compared with the magnitude of the heat flux.

The curves illustrate the time - temperature relationships for each heat source distribution. The shape of the heat source affects the rates of heating up and cooling down. Snoeys et al [18] refer to the heating and cooling rates of the various distributions. Snoeys et al proposed that since these rates are always extremely high in grinding, quenching of the surface layers will occur in all cases when the maximum temperature exceeds the austenitic transformation temperature. On this basis, the assumption of a rectangular heat source for the evaluation of the maximum temperature in grinding is an approximation which will affect the overall accuracy of the results by up to 10 per cent.

## 2.14 BASIC CONCEPTS OF ENERGY PARTITIONING BETWEEN TWO CONDUCTING BODIES.

In order to determine the effect of a conducting slider it is necessary to examine methods of energy partitioning between two conducting bodies. The earliest analysis found for partitioning between two conducting bodies was presented by Blok [13]. Initially Blok analysed the temperature rise in a stationary body due to a source of

heat evenly distributed over a circular area of contact, as illustrated in Figure 2.12. The dimensions of the heat source were assumed to be small compared to those of the surface of the body to which it was applied. A solution for the temperature rise was obtained using a differential equation proposed by Riemann-Weber. The solution for the temperature rise at time  $t$ , at the centre of a round heat source situated on the plane surface of a larger body, was given as

$$\theta_t = \frac{1}{\sqrt{\pi}} \cdot \frac{q \cdot r}{\kappa} \left\{ \frac{1}{\sqrt{\chi}} (1 - e^{-\chi}) + 2 \int_{-\sqrt{\chi}}^{\infty} e^{-x^2} dx \right\} \quad 38$$

where  $\chi = r^2/(4 \cdot \alpha \cdot t)$ .

Applying equation 7 to equation 38 it may be shown that the maximum temperature rise at time  $t = \infty$  is

$$\theta_m = \frac{r \cdot q}{\kappa} \quad 39$$

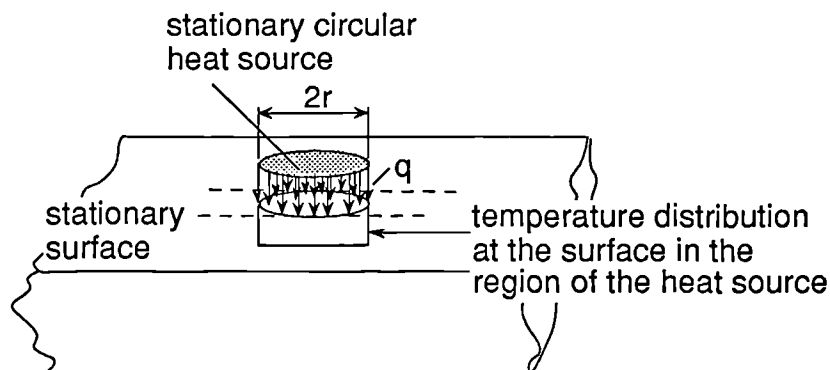


Figure 2.12 Temperature distribution in a plane surface subject to a continuously applied stationary circular heat source, at time  $t = \infty$ .

Blok proceeded to develop a solution for two conducting bodies in contact and proposed a method to partition the heat at the interface between the bodies. The partition ratio was calculated based on the assumption of an even and equal temperature across the length of contact. The heat partitioning principle introduced by Blok is illustrated in Figure 2.13 for a contact between two stationary conductors. The heat source was assumed to be uniformly distributed over a circular area of diameter  $2r$  at the plane of contact.

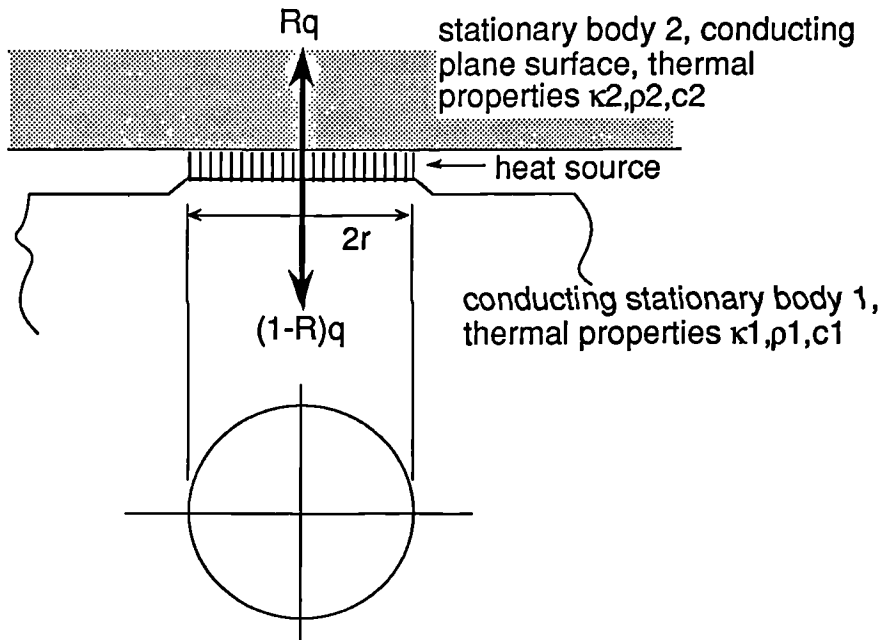


Figure 2.13 The heat source model for two stationary contacting conductors (after Blok [13]).

By applying equation 39 with a modification to the heat flux entering body 1 based on the value of  $(1 - R)$ , the maximum surface temperature of body 1 is,

$$\theta_m = \frac{q \cdot r \cdot (1 - R)}{\kappa_1} \quad 40$$

Similarly, by modifying the heat flux entering body 2 by the fraction  $R$ , the maximum surface temperature of body 2 is,

$$\theta_m = \frac{q \cdot r \cdot R}{\kappa_2} \quad 41$$

Equating the surface temperatures of body 1 and of body 2 yields,

$$R = \frac{\kappa_2}{\kappa_1 + \kappa_2} \quad 42$$

Blok extended the analysis to the determination of temperature distributions due to moving sources of heat applied in the shape of a square, Figure 2.14.

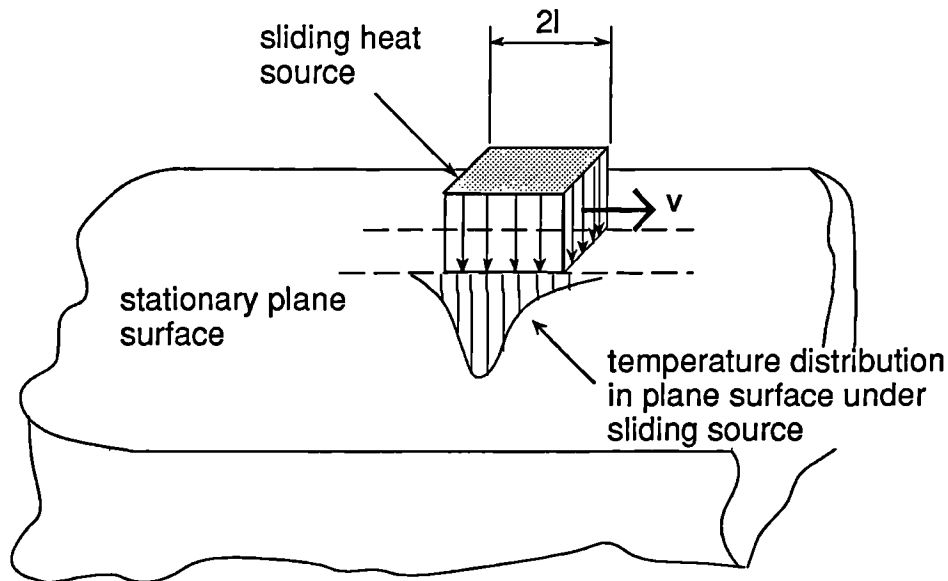


Figure 2.14 Temperature distribution in a stationary plane surface under a square sliding heat source.

The average temperature rise in the infinite surface of Figure 2.14, due to a non-conducting sliding heat source of length  $2l$  moving with a velocity  $v$ , was approximated by curve fitting numerical solutions of the integral of a Riemann-Weber equation deduced for square sources. It was found that for  $L \geq 2$ , the average temperature in the infinite surface was,

$$\theta_{av} = 1.13 q \left( \frac{l}{\kappa \cdot \rho \cdot c \cdot v} \right)^{1/2} \quad 43$$

Equation 43 compares to the band heat source solution of equation 37, and yields a temperature approximately 6 per cent higher.

An approximate solution applicable for lower velocities,  $L \leq 0.1$ , is,

$$\theta_{av} = 1.13 \frac{q \cdot l}{\kappa} \quad 44$$

Thus, at lower velocities  $\theta$  was determined to be independent of the velocity.

Blok proceeded to develop the analysis to include the case where body 2, in Figure 2.13 moved with a high velocity, that is  $L > 10$ , over body 1. The problem solved by

Blok is approximately analogous to that associated with a pin on disc contact, Figure 2.15.

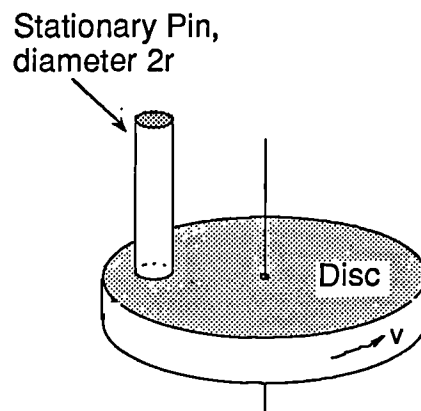


Figure 2.15 Illustration of a pin on disc contact.

There is one important difference however, between the pin on disc contact and the situation modelled by Blok. The round contact of body 1 in Figure 2.13 is a small contact area on a much larger surface so that there is substantial lateral heat transfer in the x-z plane. The lateral heat transfer within a pin would be greatly reduced compared to the lateral heat transfer in a larger body. This distinction will be shown to be important when the time comes to analyse the partitioning of heat at a contact in the grinding zone.

By averaging the temperature field occurring in body 1 and body 2, Blok obtained an approximate solution for the steady state maximum temperature at time,  $t = \infty$ ,

$$\theta_m = 1.6 R \cdot q \left( \frac{l}{\kappa_2 \rho_2 \cdot c_2 \cdot v} \right)^{1/2} \quad 45$$

Equation 45 may be compared with equation 36 for the maximum temperature in an infinite surface due to a moving band source. The magnitudes of  $\theta_m$  for the two cases are virtually identical except for the inclusion of the partition ratio R.

Blok proceeded to derive an expression for the partition ratio. The steady state temperature of a stationary plane surface due to the application of a stationary circular heat source, equation 39, was equated with the temperature in a moving surface under a stationary rectangular heat source, equation 45. The partition ratio given for this case is,

$$R = \frac{\frac{1}{2} \left(1 - \frac{1}{\sqrt{2}}\right) + \frac{\kappa_2}{\kappa_1} \sqrt{\frac{\pi}{2}} \cdot \Psi}{1 + \frac{\kappa_2}{\kappa_1} \sqrt{\frac{\pi}{2}} \cdot \Psi}$$

46

where  $\Psi = 2\sqrt{L}$ .

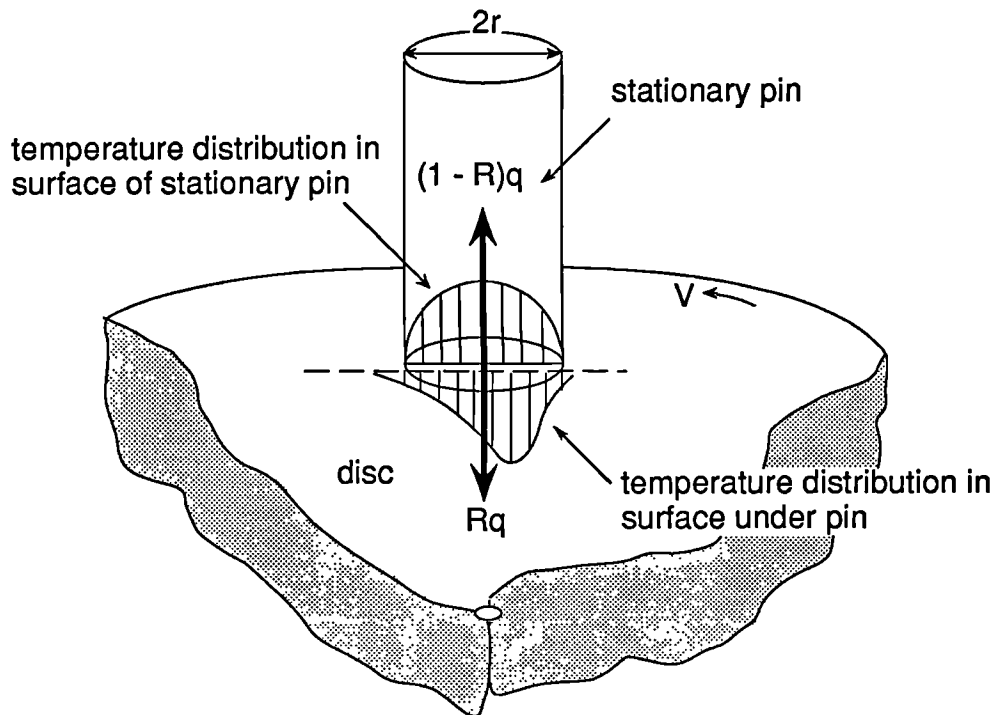


Figure 2.16 Equating the temperature of the two bodies in a pin on disc contact to establish a partition ratio.

An approximate physical representation of the situation modelled by Blok is shown in Figure 2.16. The parabolic temperature distribution at the surface of the stationary pin arises due to lateral heat transfer. This situation can be seen to be rather like the situation seen by a moving wheel grit during a contact with a workpiece. There are however, important differences. The contact time for a grit is relatively short and the extent of lateral heat transfer is unknown. If the pin was perfectly insulated at the boundary represented by the radius  $r$ , the temperature distribution would be expected to be uniform, that is, rectangular.

## 2.15 CONCLUSIONS.

The stationary source model and moving source model solutions presented by Jaeger provide a basis for calculation of the temperatures experienced between a grinding wheel and a workpiece if a partition ratio is used to modify the quantity of heat entering each body.

A method of energy partitioning has been given by Blok. However, a feature of the work proposed by Blok is that an average partition ratio is solved for a small length of contact with a large body at a time  $t = \infty$  for Peclet number  $L > 10$ . This is not generally the situation which applies in grinding.

### Chapter 3 THERMAL MODELS OF THE GRINDING PROCESS.

This chapter presents a review of previous work on thermal modelling in grinding. A distinction is made between the temperature occurring at the surface of a single active grain and the mean-line surface temperature in the grinding wheel-workpiece contact zone.

#### 3.1 THE OUTWATER AND SHAW SHEAR PLANE MODEL.

The application of the band source temperature solution to problems of heat transfer in grinding was first proposed by Outwater and Shaw [8] in 1952. Outwater and Shaw proposed a method to calculate workpiece surface temperature from an analysis of an idealised chip formation process.

In idealised chip production there are three areas where heat is produced through plastic shear or rubbing. As shown in Figure 3.1 heat is generated at the shear plane OA, the chip-grain interface OB and the trailing surface OC. The material is subject to bulk plastic deformation at the shear plane OA.

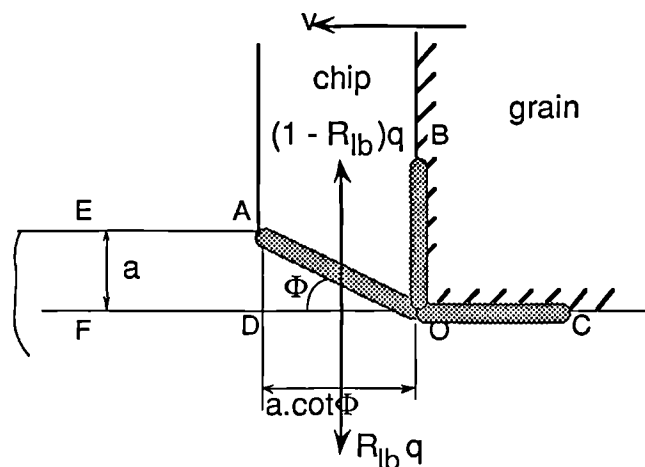


Figure 3.1 Sources of heat generation during grinding.

Outwater and Shaw analysed the energy dissipation within the grinding zone and concluded that the energy dissipated to all other heat sinks was negligible compared to the magnitude of the total grinding energy.

Outwater and Shaw assumed that all the strain due to cutting occurs in a very narrow band extending along shear plane OA, and hence, as in the friction process, all the energy dissipates along the plane, OA. The specific energy  $e_c$ , converted to thermal energy during the shearing process was defined with the assumption of a constant shear stress along the shear plane OA.

Referring to the work of Jaeger [12, 16], Outwater and Shaw argued that at high speeds relatively little heat could escape at the front of the slider (the chip). Thus, the angle of inclination  $\phi$  in Figure 3.1 could be ignored and slider OA could be replaced by slider OD. The temperature at any point in the surface OAE was then approximated to the temperature at the vertical projection of that point on plane surface ODF.

Equation 47 was given as the solution for the average surface temperature along plane ODF.

$$\theta_{av} = \frac{0.752 R_{lb}.q.a .\cot\phi}{2.\kappa.\sqrt{L}} = \frac{0.752 R_{lb}.q (a .\cot\phi)^{1/2}}{(\kappa.\rho.c.v_s)^{1/2}} \quad 47$$

Equation 47 was derived from the band source solution for a sliding contact for values of L greater than 5. A partition ratio  $R_{lb}$  is included in equation 47. The suffix lb is used to identify that the dry partition ratio is a lower bound value, since this value of partition ratio ignores energy convected by the grain and the fluid. Later theories make provision for upper bound solutions which take all effects into account including energy absorbed by the workpiece, the grain, the chips and the fluid.

Equation 47 compares to equation 37 where the slider width  $2b$  is replaced by  $a\cot\phi$ . Thus, the dimensionless source width L was expressed by

$$L = \frac{v_s.a .\cot\phi}{4.\alpha} \quad 48$$

and the heat flux, expressed in terms of the specific energy, by

$$q = \frac{e_c.v_s}{\cot\phi} \quad 49$$

A solution for the partition ratio was derived by equating the interface temperature for the chip and the workpiece using the method described by Blok [13], so that

$$R_{lb} = \frac{0.665 \sqrt{L}}{\sqrt{L} + 0.665 \sqrt{L}} \quad 50$$

where  $R_{lb}$  was said to be the fraction of the total energy entering the workpiece.

The average temperature at the chip surface was given by

$$\theta_{av} = \frac{(1 - R_{lb}) q \cdot \cot\phi}{c \cdot \rho \cdot v} \quad 51$$

Reporting on the results of an analytical and experimental study Outwater and Shaw calculated that approximately 35 - 65 per cent of the total grinding energy transferred to the workpiece, and their solution predicted surface temperatures beneath a grain as high as 1650 degC for a low carbon steel. The large range in the reported values of partition ratio are attributed to the assumed values of mean temperature which were used to obtain a value of thermal conductivity from graphical data. At high temperatures, the thermal conductivity was estimated to be significantly lower than that at lower temperatures. Thus, the higher the assumed mean temperature, the larger was the calculated value of partition ratio. The shear plane angle used in the study, was 19.9 degrees.

In the discussion of results Outwater and Shaw alluded to the time-temperature dependence of workpiece thermal damage. However, no distinction was made between the workpiece temperature that results from the action of a single grain and the average contact zone temperature that results from the interaction of a multitude of grains, which is much lower. The partition ratio solution of Outwater and Shaw was based on the analysis of an idealised chip formation process. Heat conduction to the grinding wheel via the sliding contact along plane OC was ignored, whereas in later analyses heat conduction to the grinding wheel is shown to be significant.

### **3.2 THE TAKAZAWA MODEL.**

Whereas Outwater and Shaw partitioned the grinding energy between the chip and the workpiece, Takazawa in 1964 [9] partitioned the energy between the grinding

wheel and the workpiece. The paper by Takazawa does not appear to have been translated from its original Japanese text into English, however, it is apparent from Takazawa's text that a significant proportion of the grinding energy enters the grinding wheel. Takazawa proposed a method to determine the partition ratio based on the thermal properties of the workpiece and the thermal properties of the grinding wheel. The situation analysed for the determination of the partition ratio at the wheel-workpiece contact level is illustrated in Figure 3.2.

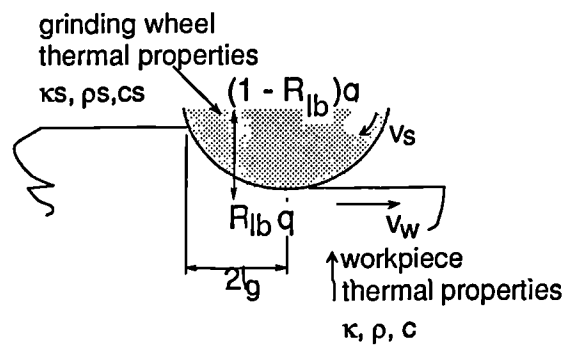


Figure 3.2 Energy partitioning at the wheel-workpiece contact level (after Takazawa [9]).

The thermal properties of the grinding wheel were established from a theoretical analysis based on expressions that included the volume fraction of grain, bond and porosity contained within the wheel. The thermal properties determined by Takazawa were therefore an estimate of the composite properties of the wheel.

Takazawa applied the band source model of Jaeger both to the grinding wheel and to the workpiece contact and equated the temperatures for the wheel and the workpiece to derive expressions for the partition ratio. The partition ratio for  $L > 5$  was

$$R_{lb} = \frac{1}{1 + \sqrt{\frac{\kappa_s \cdot \rho_s \cdot c_s}{\kappa \cdot \rho \cdot c} \cdot \frac{v_s}{v_w}}} \quad 52$$

For values of  $L < 5$  the partition ratio was given as

$$R_{lb} = \frac{1}{1 + 0.6 \sqrt{\frac{\kappa_s \cdot \rho_s \cdot c_s}{\rho \cdot c} \cdot \frac{v_s}{v_w} \cdot \frac{f}{l_g}}} \quad 53$$

where  $f/l_g$  is a coefficient with a magnitude dependent on the value of the infeed rate.

Graphs of partition ratio versus workspeed for an aluminium oxide wheel showed that the partition ratio increased with increasing workspeed. An average partition ratio using equation 52, was estimated to be 0.57. However, in the analytical study presented by Takazawa, a value of  $\kappa_g = 1.55 \text{ W / mK}$  was used. Typical values of  $\kappa_g$  are reported in the range 5 - 45 W / mK, depending on the porosity of the abrasive, and this is discussed in more detail in Chapter 4.

Takazawa's equation for partition ratio, equation 52, appears to have been completely ignored by later workers. It's recent discovery has shown that this was a significant development. Takazawa did not provide experimental values for the thermal properties of the composite wheel and the uncertainty over the calculation of appropriate values may explain why this technique was not taken further or did not become publicised.

In later works, Takazawa [19, 20], also applied the band source model of Jaeger to the workpiece contact to establish the maximum temperature beneath the workpiece surface. The temperature  $\theta_z$  as a function of depth  $z$  beneath the surface was calculated using equation 54. Equation 54 is identical in form to equation 28 except for the inclusion of the partition ratio  $R_{lb}$  determined from equations 52 and 53. Takazawa used the value of  $R_{lb}$  based on bulk wheel properties, from the earlier paper [9].

$$\theta_z = \frac{2.R_{lb}.q.\alpha}{\pi.K.V_w} \int_{x'-L}^{x'+L} e^{-u}.K_0(u^2 + Z^2)^{1/2}.du \quad 54$$

Takazawa integrated equation 54 using a numerical method. Results were presented to illustrate the relationship between temperature and depth below the surface. The theoretical peak temperatures at any depth below the surface were obtained from approximate curve fits of the numerical data.

An approximate curve fit to the results for the maximum temperature for the ranges  $1 < L < 8$  and  $0 < z < 4$  was given by

$$\theta = \frac{2.R_{1b}.q.\alpha}{\pi.K.v} 3.1L^{0.53}.\exp [0.69L^{-0.39}.z]$$

55

It is apparent from equation 55 that the temperature decreases exponentially with increasing distance from the surface.

Takazawa also generated expressions for relationships between the maximum temperature, workpiece speed, wheel depth of cut and grinding wheel speed. The expressions generated by Takazawa enabled him to propose procedures to avoid the occurrence of thermal damage in steels. The critical temperature associated with thermal damage was determined from time-temperature-transformation diagrams. By calculating the heat energy entering the workpiece from the simplified expressions, Takazawa recommended maximum values of the infeed speed, grinding wheel speed and depth of cut to avoid exceeding the critical workpiece temperature in dry grinding operations.

Snoeys, Maris and Peters [18, 21], drew attention to limitations in the range of applicability of the Takazawa approximations. The approximate solutions were matched for values of z between 0 and 4. Snoeys, Maris and Peters identified that the approximations were valid only for gentle grinding conditions because of unacceptable errors if the dimensionless depth z was greater than 4. To cover a broader working range of grinding parameters new equations were established.

### 3.3 EXTENSION OF THE TAKAZAWA MODEL.

The principal equations developed by Snoeys, Maris and Peters are given below

For  $5 < L < 40$  and  $4 < z < 10$ ,

$$\frac{\theta.\pi.K.v}{2.q.\alpha} = 0.66L^{0.93}.\exp [-0.15L^{-0.06}.z] \quad 56$$

For  $5 < L < 40$  and  $10 < z < 20$ ,

$$\frac{\theta.\pi.K.v}{2.q.\alpha} = 0.335L^{1.01}.\exp [-0.08L^{0.044}.z] \quad 57$$

For  $40 < L < 80$  and  $4 < z < 10$ ,

$$\frac{\theta.\pi.k.v}{2.q.\alpha} = 1.64L^{0.67}.\exp[-0.288L^{0.244}.z] \quad 58$$

For  $40 < L < 80$  and  $10 < z < 20$ ,

$$\frac{\theta.\pi.k.v}{2.q.\alpha} = 0.079L^{1.43}.\exp[-0.019L^{0.44}.z] \quad 59$$

Results [18] from the approximate solutions were compared with results from the temperature solutions of Jaeger, and indicated that the simplified band source solutions were accurate within a maximum 5 per cent error. However, it will be noted that solutions were not presented for values of  $L < 5$ .

The partitioning of energy to the workpiece and to the wheel was discussed by Snoeys, Maris and Peters and reference was made to the work of Malkin [4, 22]. However, Snoeys, Maris and Peters excluded the partition ratio in the solutions presented in the paper and failed to indicate whether the partition ratio was included in the equations for which results were compared. Omission of the partition ratio in the workpiece surface temperature solution leads to an artificially high surface temperature.

### 3.4 THE MALKIN MODEL.

Malkin [4, 22] developed a thermal model based on the work of Hahn [23] who described the material removal mechanism in grinding in terms of sliding, ploughing and chip formation. Based on the results of an experimental study Malkin and Cook [24] proposed that each component of abrasive-workpiece interaction could be associated with grinding force components, and hence specific energies. The sum of the specific energies attributed to each component equalled the total specific energy in the grinding process.

$$e_c = e_{sl} + e_{pl} + e_{ch} \quad 60$$

where suffices sl, pl and ch refer to the specific energy components of sliding, ploughing and chip formation respectively.

### 3.4.1 SLIDING ENERGY IN GRINDING.

Evidence of sliding was first identified by Malkin and Cook [24] and occurs because abrasive grains are not perfectly sharp. Sliding forces are said to be generated when abrasive grains move across the workpiece surface without removing or plastically deforming the workpiece material. The wheel dressing process generates flats on the contact surfaces of abrasive grains. As grinding proceeds, the flats become further enlarged through attritious wear and the adhesion of metal particles from the workpiece [3].

The normal grinding force  $F_n$ , was expressed as the sum of a cutting component  $F_{n,c}$  and a sliding component  $F_{n,sl}$ .

The sliding component of the normal force was given by equation 61, in terms of the average contact pressure  $p$  between the wear flats and the workpiece, and the apparent wear flat area  $A_a$ , where  $A_a = b \cdot l_g \cdot A$ , and  $A$  is the proportion of wheel surface area composed of wear flats.

$$F_{n,sl} = p \cdot b \cdot (d_e \cdot a)^{1/2} A \quad 61$$

The sliding component of the tangential force  $F_{t,sl}$ , was obtained by including the friction coefficient  $\mu$ .

$$F_{t,sl} = \mu \cdot p \cdot b \cdot (d_e \cdot a)^{1/2} A \quad 62$$

The average contact pressure,  $p$ , was obtained by differentiating equation 62 with respect to  $A$ , and solving for  $p$ . A curvature difference  $\Delta$ , was defined and a straight line plot of  $p$  versus  $\Delta$  showed that the average contact pressure increased linearly with increasing curvature difference for a particular value of  $A$ . It should be noted that this analysis required the use of measured values of  $A$ .

The value of  $\mu$  was determined from a straight line plot of normal force  $F_n$  versus tangential force  $F_t$ . The value of  $\mu$  was found to be approximately 0.4 for a plain carbon steel.

Malkin reasoned that the sliding energy concept enabled the effect of wheel grade and dressing conditions to be accounted for quantitatively. With harder-grade wheels

and finer dressing, the wear flat area is larger and so the sliding forces are proportionally larger.

### 3.4.2 PLOUGHING AND CHIP FORMATION ENERGIES.

The grinding energy remaining after subtracting the contribution due to sliding was attributed to cutting. Malkin [4] demonstrated that the magnitude of the cutting energy could not be reconciled with the classic chip formation model. The chip formation energy evaluated from earlier metal cutting theory is based on separating the chip formation mechanism into shearing deformation at the shear plane and friction at the rake face. From experimental data Malkin [22] determined that approximately 75 per cent of the total chip formation energy could be attributed to shearing deformation at the shear plane region, the remainder was considered to be expended as friction energy between the grit and the workpiece. None of the chip formation frictional energy was considered to enter the workpiece.

According to Malkin, the shearing energy carried away by the chips is limited to the energy required for melting. The energy required to melt a volume of material can be obtained from enthalpy data. For iron, a change in enthalpy from ambient to melting temperature is 17,685 cal/mol, approximately 10.4 J/mm<sup>3</sup> [3]. Malkin reasoned that since only 75 per cent of the total chip formation energy was attributed to shearing at the shear plane region, the maximum chip formation energy was limited to 13.8 J/mm<sup>3</sup> for steels. Any further increase in cutting energy was considered to be due to an increase in a mechanism other than shearing at the shear plane region. That mechanism was identified as ploughing deformation. The relationship between the ploughing and chip formation energies with material removal is illustrated in Figure 3.3.

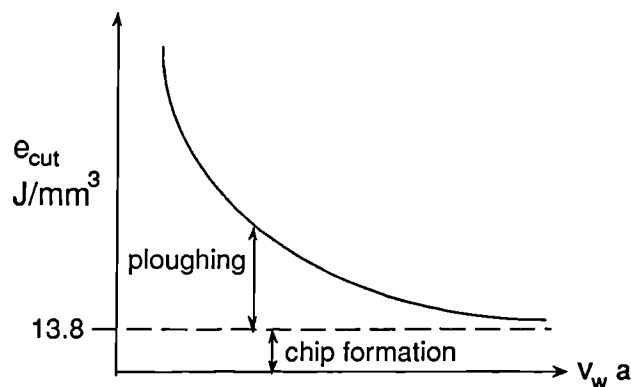


Figure 3.3 Specific cutting energy versus volumetric removal rate. (after Malkin [3])

Ploughing energy is expended by deformation of the workpiece without material removal. A more extensive discussion of ploughing deformation is given in references 24 and 25. The specific cutting energy  $e_{cut}$ , was expressed as the sum of the specific ploughing energy component  $e_{pl}$ , and the specific chip formation energy component  $e_{ch}$ ,

$$e_{cut} = e_{ch} + e_{pl}$$

63

An illustration of the regions of ploughing and chip formation in grinding is given in Figure 3.4.

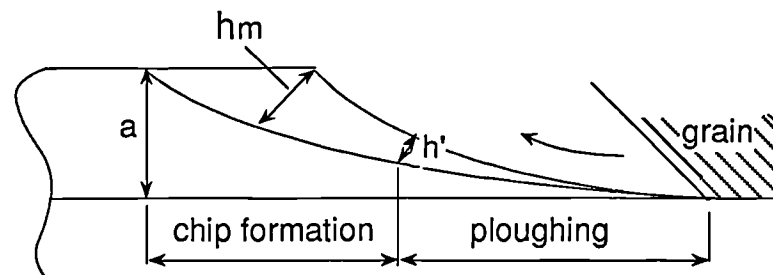


Figure 3.4 Illustration of ploughing and chip formation regions in grinding

Ploughing deformation in upcut grinding occurs as the abrasive grain penetrates the workpiece surface. Ploughing follows the initial elastic contact which is not shown. The depth of cut increases from zero to a maximum of  $h_m$  at the end of the cut. Chip formation occurs when the grain has penetrated to a critical depth of cut  $h'$ . The critical depth of cut depends upon factors such as the grain sharpness, rake angle, grain orientation and the friction coefficient [26].

Malkin proposed that the quantity of energy expended by ploughing was the quantity of cutting energy remaining after the chip formation energy had been subtracted. The portion of the ploughing energy conducted to the workpiece was based on Shaw's analysis of cutting and assumed to be 75 per cent of the total ploughing energy. The reduction was assumed on the basis of the effect of convection losses from the workpiece surface.

In a later analysis by Malkin [27] to determine the threshold value of specific energy for avoidance of thermal damage, convective losses were taken into account

separately so that 100 per cent of the ploughing energy was assumed to conduct to the workpiece.

### 3.4.3 ENERGY PARTITIONING AT THE GRIT-WORKPIECE INTERFACE: (MALKIN).

Malkin used equation 50 proposed by Outwater and Shaw [8] to determine the partition ratio at the shear plane.

Malkin approximated the value of the dimensionless half width  $L$  as half the length of the shear plane. Using a shear angle of  $\phi = 5$  degrees it was calculated from equation 50 that approximately 60 per cent of the shear plane energy expended during chip formation was conducted as heat to the workpiece.

Since only 75 per cent of the chip formation energy is dissipated in the shear plane region, the total fraction of the chip formation energy conducted to the workpiece was then calculated as  $(0.75)(0.60) = 0.45$ . This corresponded to a value of  $6.2 \text{ J/mm}^3$ . However, it was determined from calorimetric methods [4] that approximately 55 per cent of the chip formation energy was conducted to the workpiece. The difference between the theoretically determined and experimentally determined values  $7.6 - 6.2 = 1.4 \text{ J/mm}^3$ , was attributed to convection losses from the workpiece surface.

The fraction  $R_{1b}$  of the total grinding energy  $e_c$  entering the workpiece was therefore given by

$$R_{1b} = \frac{e_{pl} + e_{sl} + 0.55e_{ch}}{e_c} = \frac{e_c - 0.45e_{ch}}{e_c} \quad 64$$

where  $e_{ch}$  = chip formation specific energy =  $13.8 \text{ J/mm}^3$   
 $e_{pl}$  = ploughing specific energy  
 $e_{cut}$  = cutting specific energy  
 $e_{sl}$  = sliding specific energy  
 $e_c$  = total specific energy

$$\text{Thus } R_{1b} = 1 - 6.2/e_c \quad 65$$

Schematically, the energy dissipation proposed by Malkin can be illustrated as shown in Figure 3.5.

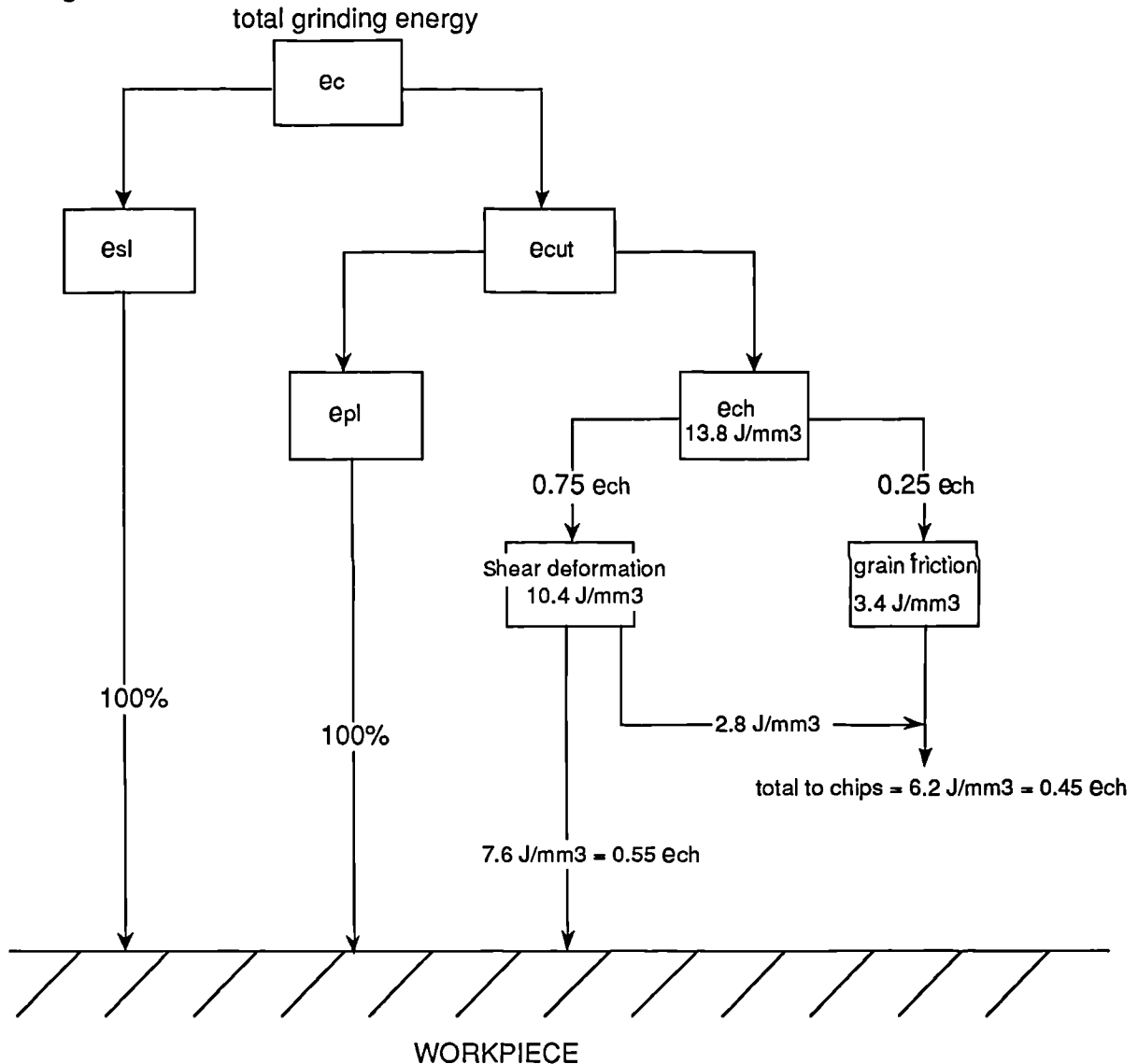


Figure 3.5 Schematic representation of the energy dissipation according to Malkin's shear plane energy model.

The implication of the model proposed by Malkin is that for a given material such as steel, for which the chip formation energy has been determined to be constant at  $13.8 \text{ J/mm}^3$ , the fraction of energy entering the workpiece will increase with an increase in total specific energy. The contribution of chip formation to the total will therefore become less significant and  $R_{IP}$  will approach 1.0. In this case almost all of the energy is transferred to the workpiece through sliding and ploughing mechanisms.

In reference 28, Srivastava, Rogers and Elbestawi employed Malkin's model and reported that values of the fraction of heat entering the workpiece had been measured in the range 60 to 90 per cent and in reference 29 Srivastav, Ulrich and Elbestawi cited typical values in the range 75 to 90 per cent. In reference 4 Malkin reported on the results of an experimental study where the value of  $R_{1b}$  was calculated in the range 0.74 to 0.86.

It is of interest that Malkin referred to the work of Des Ruisseaux and Zerkle [30] and reasoned that the convective cooling coefficient is generally not large enough in shallow cut grinding to significantly affect the peak temperature beneath the source, and therefore the analysis is applicable to both wet and dry grinding operations. The principal benefit of a grinding fluid was described as the lower specific energy resulting from a reduced wear flat area [22].

#### 3.4.4 THE SHEAR PLANE ENERGY MODEL OF MALKIN COUPLED WITH A TEMPERATURE SOLUTION.

By defining the critical temperature related to the onset of workpiece thermal damage, Malkin derived an expression for the maximum allowable grinding power.

For a particular workpiece material and values of grinding parameters the heat flux  $q$  is not generally known. Heat flux  $q$ , was expressed as a function of the specific energy  $e_c$ ,

$$q = \left( \frac{e_c \cdot v_w \cdot a}{l_g} \right) \quad 66$$

Of the total grinding energy only the fraction  $R_{1b}$  is conducted to the workpiece. Combining equations 64 and 66 yields the total specific heat flux entering the workpiece.

$$q = \frac{v_w \cdot a}{l_g} \cdot (e_c - 0.45e_{ch}) \quad 67$$

Substituting for the heat flux in the band heat source solution of Jaeger and rearranging, with  $L = v_w l_g / (4\alpha)$  where  $l_g = (a \cdot d_e)^{1/2}$ , the maximum surface temperature is given by

$$\theta_m = \frac{1.13\alpha^{1/2} \cdot a^{3/4} \cdot v_w(e_c - 0.45e_{ch})}{\kappa \cdot d_e^{1/2}} \quad 68$$

If thermal damage occurs at or above a critical temperature  $\theta_m^*$  the corresponding critical specific energy  $e_c^*$  obtained from equation 68 is given by

$$e_c^* = 0.45e_{ch} + \left( \frac{\kappa \cdot \theta_m^*}{1.13\alpha^{1/2}} \right) \cdot d_e^{1/4} \cdot a^{-3/4} \cdot v_w^{-1/2} \quad 69$$

Equation 69 is in the form  $y = mx + c$ . A plot, Figure 3.6, of  $d_e^{1/4} \cdot a^{-3/4} \cdot v_w^{-1/2}$  versus the total specific energy  $e_c$  gave a slope  $B'$ , proportional to the maximum temperature and an intercept at  $0.45e_{ch}$ , where

$$B' = \frac{\theta_m(\kappa \cdot \rho \cdot c)^{1/2}}{1.13} \quad 70$$

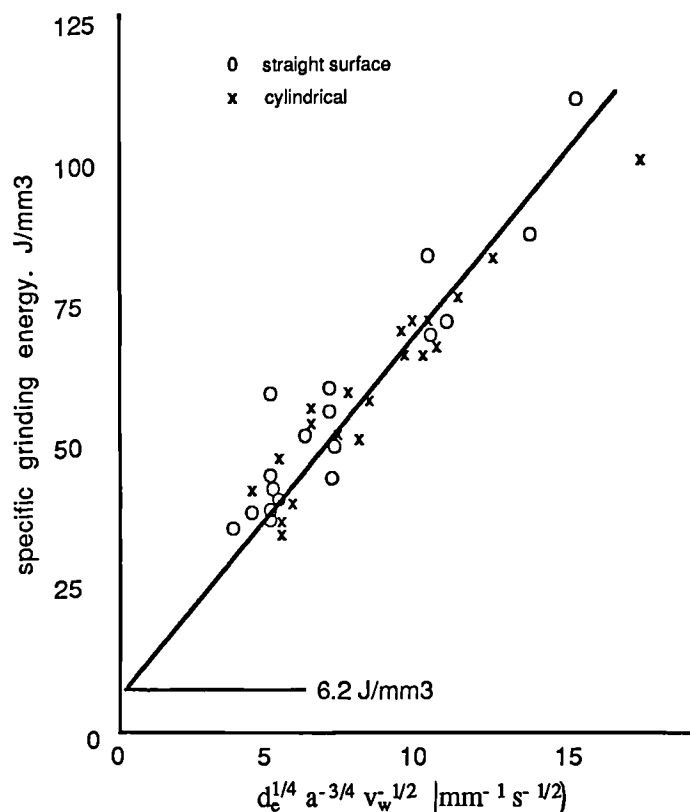


Figure 3.6 Specific energy at workpiece burn threshold for straight surface and cylindrical grinding. (taken from Malkin [22]).

The value of B' determined from experiment was given as a constant, and for most steels was found to be equal to 7.2 J/mm<sup>2</sup>s<sup>1/2</sup> [22].

The allowable power for a maximum temperature  $\theta_m$  was obtained by multiplying the critical specific energy from equation 69 by the volumetric removal rate, Z. The allowable specific power was therefore

$$P' = 0.45 e_{ch}.Z + B'. d_e^{1/4}.a^{-3/4}.v_w^{-1/2}.Z \quad 71$$

The thermal model proposed by Malkin is applicable only to steels and is dependent on experimentally determined values of  $e_{ch}$  and B' which do not apply for all materials. Care must be taken to avoid over-prediction in the assigned values of these parameters as this would lead to over-estimation of allowable power. Malkin's model can be criticised because it ignores conduction into the grains of the wheel and because the partition ratio solution relied on the assumption that all the sliding and ploughing energy was conducted to the workpiece. This assumption can be strongly argued against on the grounds that the grain is effectively a conducting slider that will accept a fraction of the heat generated at the sliding interface. The partition ratio solution proposed by Malkin would require values of sliding energy and ploughing energy to be specified if only a fraction of the sliding energy or ploughing energy was assumed to enter the grain.

It can also be argued that the contact length used should be the true contact length not the geometric contact length as used by Malkin. Any difference in the dimension of the heat source will affect the magnitude of the specific heat flux entering the workpiece. The effects of contact length on predicted maximum temperatures are discussed in a later section.

### **3.4.5 MALKIN'S STRATEGY FOR IN-PROCESS CONTROL OF THERMAL DAMAGE.**

In reference 27 Malkin described an optimisation strategy for cylindrical plunge grinding operations. Material removal rates were constrained by workpiece quality requirements including surface roughness and thermal damage. Two thermal damage constraints were considered: (i) no thermal damage allowed and (ii) thermal damage restricted to a certain depth during the roughing stage. In the latter case it

was proposed that thermal damage was removed during the subsequent finishing stage. The work described below refers only to the no-burn constraint.

A power monitor was installed to measure the wheel spindle power. The measured power during a cycle was then compared with the predicted power from equation 72.

$$P = 0.0138\pi \cdot d_w \cdot v_f + 9.62 \times 10^{-7} v_s + \left[ 8.55 \times 10^{-6} + 2.10 \frac{v_w}{v_s \cdot d_e} \right] \cdot \frac{v_s}{v_w^{1/2}} \cdot (\pi \cdot d_w \cdot v_f \cdot d_e)^{1/2} \cdot A_{\text{eff}} \quad 72$$

Equation 72 is in the form:  $P = P_{\text{ch}} + P_{\text{pl}} + P_{\text{sl}}$  where the total grinding power is the sum of the chip formation, ploughing and sliding components.

The quantity  $A_{\text{eff}}$  was described as the effective wheel dullness. In reference 3 Malkin derived equation 73 which illustrates the relationship between effective wheel dullness and fractional wear flat area  $A$ , the specific normal ploughing force  $F'_{\text{n,pl}}$  and the constant contact stress  $p_0$ .

$$A_{\text{eff}} = \left( \frac{16p_0^2 \cdot v_w}{v_s \cdot d_e \cdot e_{\text{ch}} \cdot F'_{\text{n,pl}} \cdot \kappa} \right)^{1/2} A \quad 73$$

The requirement to determine values of  $A$ ,  $F'_{\text{n,pl}}$  and  $p_0$  prohibited the use of equation 73 in the constraint model. An alternative expression, equation 74, was determined from experimental data and used to relate effective wheel dullness with equivalent dressing infeed angle  $\delta$ , and constants  $A_0$  and  $m$ .

$$A_{\text{eff}} = -0.008A_0 \cdot \log(1.4 \times 10^4 m \cdot \delta) \quad 74$$

The values of  $A_0$  and  $m$  were dependent on the values of the dressing parameters used and were not known *a priori*. The value of  $A_{\text{eff}}$  was therefore obtained at the end of each cycle by matching the measured power with the predicted power from, equation 72, using the least squares criterion.

Values of effective wheel dullness were reported in the range  $0.008 < A_{\text{eff}} < 0.022$ .

In-process control of workpiece thermal damage was achieved by ensuring the measured power did not exceed the critical power level given by equation 71. The critical power corresponded to a critical workpiece temperature considered to be associated with the onset of thermal damage. The critical temperature used by Malkin is discussed in a later section.

### 3.5 THE DES RUISSEAUX AND ZERKLE MODEL.

Des Ruisseaux and Zerkle [31] found that calculated shear plane temperatures did not correspond to temperatures measured experimentally and concluded that the high temperatures in the region of chip formation occurred primarily on the surface of the material which was subsequently removed by grinding. A clear distinction was made between the maximum temperature beneath an individual active grain and the maximum temperature experienced by a workpiece due to a number of cutting points passing across the surface.

Des Ruisseaux and Zerkle idealised the chip shear plane geometry as illustrated in Figure 3.7.

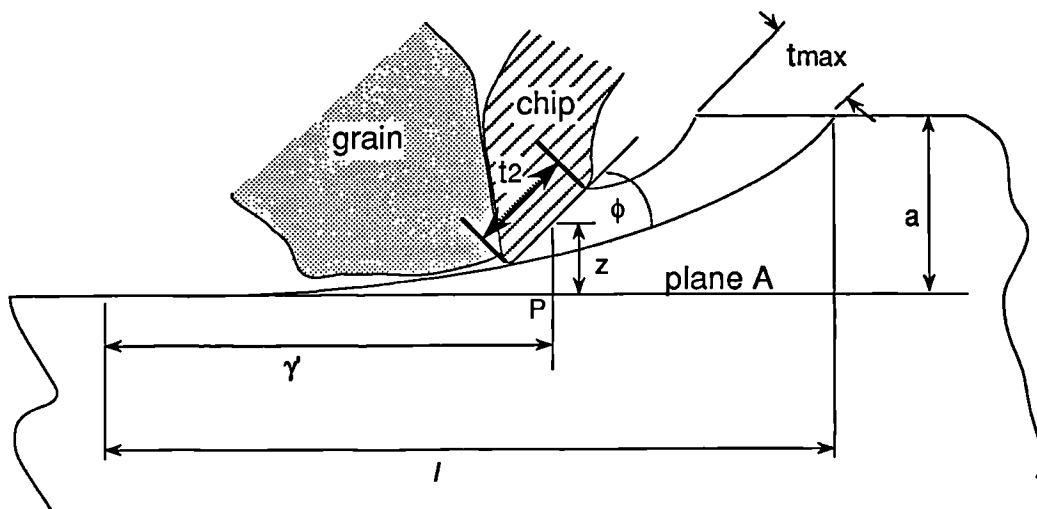


Figure 3.7 Chip shear plane geometry (after Des Ruisseaux and Zerkle [31]).

The maximum temperature at the surface that remained after grinding (Plane A, Figure 3.7), was calculated by superimposing two temperatures: the temperature due to a shear plane heat source, and the temperature due to a band heat source. The temperature at the shear plane was also analysed and this is reviewed first.

### 3.5.1 SHEAR PLANE TEMPERATURE.

The average heat flux which enters the workpiece at the shear plane was expressed in terms of a partition ratio and the shear stress at the shear plane,

$$q_w = R_{sp} \cdot \tau (v_s \pm v_w) \quad 75$$

where the positive sign is for upcut and the negative sign for downcut grinding

$q_w$  = the average shear plane flux into the workpiece

$R_{sp}$  = the fraction of the cutting energy entering the workpiece

Des Ruisseaux and Zerkle referred to the work of Malkin [4, 22] for a value of the partition ratio  $R_{sp}$  at the shear plane, which Malkin reasoned was constant with a value of 0.6.

The shearing stress  $\tau'$ , at the chip shear plane was given by,

$$\tau' = \frac{F_{HC}}{b \cdot l_g \cdot C \cdot (t_{1,max} \cdot b'/2)} \quad 76$$

where  $F_{HC}$  = total horizontal cutting force

$C$  = number of cutting edges per unit area of wheel surface

$t_{1,max}$  = maximum undeformed chip thickness

$b$  = grinding wheel width

$b'$  = width of the grinding chip perpendicular to the cutting direction

$l_g$  = geometric length of the grinding contact zone

The plane heat source dimensionless width was defined by

$$L = \frac{1}{2} \left( \frac{\gamma \cdot t_{1,max}}{l_g \sin \phi} \right) \frac{(v_s \pm v_w)}{2\alpha} \quad 77$$

where  $t_{1,max}$  is the maximum undeformed chip thickness and  $\gamma$  is the distance from the vertical position of the centre of the chip shear plane to the position of entry of the grain into the grinding contact zone, as illustrated in Figure 3.7.

The dimensionless depth variable was defined by

$$z = \left(\frac{\gamma}{l_g}\right)^2 a. \frac{(v_s \pm v_w)}{2\alpha} \quad 78$$

Using typical values of grinding parameters Des Ruisseaux and Zerkle simplified equations 77 and 78, for the dimensionless width and depth variables to

$$L = 3.52 \left(\frac{\gamma}{l_g}\right) \text{ and } z = 30.25 \left(\frac{\gamma}{l_g}\right)^2 \quad 79$$

The temperature at the shear plane was then obtained by substituting the heat flux at the shear plane equation 75, for the total grinding heat flux, and substituting the value  $z = 0$ , for the dimensionless width in equation 55. Equation 55 was proposed by Takazawa as the solution for the maximum temperature below the surface, for the ranges  $1 < L < 8$  and  $0 < z < 4$ . Thus,

$$\theta_m = \frac{3.1 (2q_w \cdot \alpha)}{\pi \cdot \kappa (v_s \pm v_w)} \left(\frac{\gamma}{l_g}\right)^{0.53} \quad 80$$

For the example considered the calculated shear plane temperature approached 2540 degC as the function  $\gamma/l_g$  approached 1.0. Des Ruisseaux and Zerkle proposed that the very high temperature was due to an increase in the heat entering the surface with increasing shear plane area. This temperature is clearly open to doubt since temperatures of this magnitude have never been reported. Malkin [22] reasons that it is impossible for the chip temperature to exceed the melting temperature of the material, since clearly the shear stress for a melted material is much lower than the shear stress employed to calculate the temperature.

### 3.5.2 CONTACT ZONE TEMPERATURE.

The maximum temperature occurring in the grinding contact zone was determined from the moving band heat source solution. The heat source strength for the contact zone was expressed in terms of a different partition ratio and the horizontal component of the grinding force. In this case the partition ratio was defined as the fraction of the total grinding energy entering the workpiece,  $R_{1b}$ .

$$q_w = \frac{R_{lb} \cdot F_H (v_s \pm v_w)}{b \cdot l_g}$$

81

In the results presented by Des Ruisseaux and Zerkle [31] the maximum temperature was calculated for the surface of the contact zone as  $\theta_{max} = 335$  degC. This value was calculated by referring to the work of Malkin [4, 22] for a value of partition ratio which was quoted as  $R_{lb} = 0.8$ .

### 3.5.3 TEMPERATURE AT PLANE A.

The maximum temperature at plane A, the workpiece surface which remains after grinding, due to a shear plane heat source, was determined by substituting equations 77 and 78 into equation 55. The solution obtained was given by

$$\theta_m = \frac{2 \cdot \alpha \cdot q_w}{\pi \cdot \kappa (v_s \pm v_w)} 3.1 \left( \frac{\gamma}{l_g} 3.52 \right)^{0.53} \left\{ \exp \left[ -0.69 \left( \frac{\gamma}{l_g} \right)^2 30.25 \left( \frac{\gamma}{l_g} 3.52 \right)^{-0.37} \right] \right\} \quad 82$$

It is important to note that  $q_w$  is the heat flux strength at the shear plane, defined by equation 75.

For the example given in reference 31 the maximum temperature rise at plane A due to a shear plane heat source was calculated as 535 degC. The maximum temperature rise encountered by the workpiece surface was then obtained from the sum of the maximum contact zone temperature, and the maximum temperature at plane A due to a shear plane heat source. Thus, the maximum temperature rise of the workpiece surface was  $\theta_m = 335$  degC (maximum temperature of the contact zone) + 535 degC (maximum temperature at plane A) = 870 degC. It should be emphasised that equations 80 and 82 are based on an assumption that partition ratio is known. Equations 80 and 82 cannot therefore provide a method to determine the partition ratio.

The work of Des Ruisseaux and Zerkle made clear the distinction between the temperature rise beneath a grit and the average grinding zone temperature and it was suggested that the superposition of the two temperature rises gives the highest temperature that could occur within the interference zone. The grinding zone temperature occurs as a result of a multitude of active grits moving across the workpiece surface. The shear plane temperature occurs beneath a single grit due to

cutting. A partition ratio solution based on idealised chip shear plane geometry was proposed for dry grinding operations. However, the partition ratio solution was in principle the same as that proposed by Outwater and Shaw, and similarly ignored conduction of heat to the grinding wheel.

### 3.6 EXTENSION OF THE DES RUISSEAUX AND ZERKLE MODEL TO INCLUDE THE EFFECT OF COOLING.

In a later work Des Ruisseaux and Zerkle [30] presented results to include the effect of surface cooling on predicted grinding temperatures. The work described how the band source solution of Jaeger could be extended to include the effects of cooling for semi-infinite and cylindrical bodies.

The model analysed by Des Ruisseaux and Zerkle is shown in Figure 3.8. It considers a stationary band source of width  $2l$  acting on the surface of a moving semi-infinite body. Convective cooling was assumed to occur over the entire surface of the body with a constant and uniform heat transfer coefficient  $h$ . The convective coefficient defines the temperature difference between the surface and the fluid required to drive a quantity of energy into the grinding fluid [32]. The two-dimensional steady state temperature distribution due to a rectangular band source reduced to include the effect of cooling was expressed in the following dimensionless form :

$$\frac{\theta \cdot \pi \cdot K \cdot v}{2 \cdot q \cdot \alpha} = \int_{x-L}^{x+L} e^u \cdot K_0(u^2 + Z^2)^{1/2} \cdot du$$

$$- \pi \cdot H \cdot e^{H \cdot Z} \int_0^{\infty} \tau \cdot e^{H^2 \tau^2} \cdot \operatorname{erfc} \left( \frac{Z}{2 \cdot \tau} + H \cdot \tau \right)$$

$$\cdot \left[ \operatorname{erf} \left( \frac{X+L}{2 \cdot \tau} + \tau \right) - \operatorname{erf} \left( \frac{X-L}{2 \cdot \tau} + \tau \right) \right] d\tau$$
83

where  $H = 2\alpha/v$  and  $\tau = v \cdot t / (2\alpha^{1/2})$ .

The first term on the right hand side of equation 83 is seen to be identical to equation 28, the result obtained by Jaeger for the case without cooling. The second term is the temperature decrease due to cooling.

The Des Ruisseaux and Zerkle extension of the band source solution allowed for the effect of cooling to be included in the analysis for rectangular heat sources. Although a closed form solution can be found for the first term in equation 83 no such solution is available for the second term making it necessary to evaluate the equation numerically. Des Ruisseaux and Zerkle calculated temperature distributions for values of  $H = 0.01, 0.1$  and  $1.0$  for a dimensionless half width  $L = 1.0$ . It was reported that for large values of  $H$  and  $L$  convective cooling from the band source region removed a significant portion of the band source energy and so had the effect of reducing the workpiece surface temperature. This important conclusion will be referred to at a later stage.

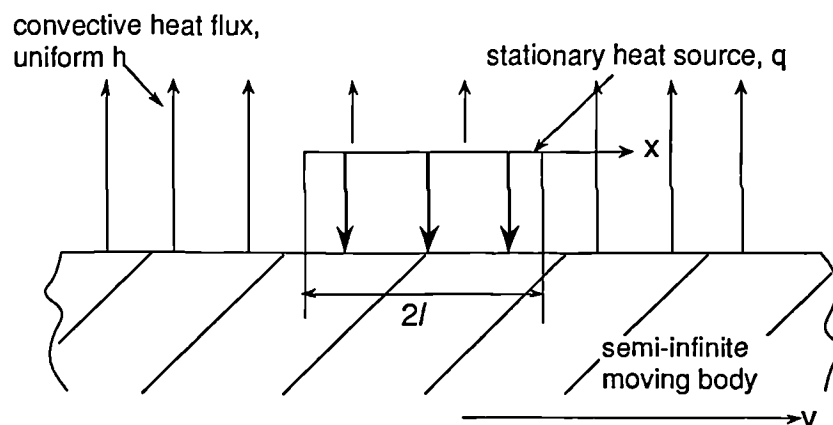


Figure 3.8 Thermal model for a semi-infinite body with cooling (after Des Ruisseaux and Zerkle [30]).

The model also allowed an approximate temperature distribution to be calculated for the area outside the band source region where only convective cooling occurs. This was achieved by increasing the band source strength by an amount equal and opposite to the average convective flux which occurs within the band source region. There is an implicit assumption in this model that convective cooling only takes place outside the band source region.

### 3.7 THE ROWE AND PETTIT MODEL.

Gamble [33] observed that the Jaeger model could equally be applied to either the grinding wheel or the workpiece and that in both cases large temperatures could result. However, the predicted increase in temperature of the grinding wheel,

particularly when using a grinding fluid, may be less apparent than the more substantial rise in temperature of the workpiece. This phenomenon is due mainly to the disparity in speeds between the grinding wheel and the workpiece. A ratio of 100:1 is commonly used for the grinding wheel and workpiece surface speeds [34].

Rowe and Pettit [7] derived a thermal model that employed the bulk thermal properties of the grinding wheel. The bulk thermal properties of the grinding wheel were obtained from experiment [33]. The specific heat capacity of a wheel sample was determined from calorimetric methods. The thermal conductivity of the wheel material was determined using Lee's conductivity apparatus. Experimental methods for the determination of bulk wheel properties are described in the following chapter.

The approaches used by Rowe and Pettit and by Takazawa differ from the case of the conducting slider in that the speed used in the Jaeger model differs for the two bodies in contact. The grinding wheel sees a heat source moving at  $v_s$ , the speed of the grinding wheel. The workpiece sees a heat source moving at  $v_w$ , the speed of the workpiece.

The model of Rowe and Pettit differed from the model of Takazawa in that the analysis was extended to give expressions for the values of critical specific energy at limits associated with either the exclusion or inclusion of heat transfer to the grinding fluid and grinding chips. The limits were termed upper and lower bound solutions.

Further, the specific heat flux defined by Rowe and Pettit differed from the definition of specific heat flux given by other authors in that the real contact length  $l_e$  was used. The effect of modifying the specific heat flux using the real contact length was to reduce the maximum temperature. In fact, if other factors remain unchanged, the maximum workpiece temperature is inversely proportional to  $l_e$  to the power 1/2. Many authors [10, 17, 25, 26, 35 and 36] have investigated grinding contact length and concluded that the real contact length is substantially greater than the geometric contact length. Verkerk [35] investigated the grinding contact length by measuring the heat pulses due to the transition of grains of the wheel past a thermocouple embedded in the workpiece. It was found that the real contact length was substantially greater than the geometrical value. By using a thin thermal junction to form a sensitive thermocouple Gu and Wager [36, 37] established relationships between contact length, cutting depth and workpiece speed. This improved method enabled them to identify three distinct regions of the cutting zone and suggested

contact lengths approximately 30% longer than those measured from previous thermocouple techniques.

Rowe, Qi and Mills [38] analysed the real contact length based on depth of cut and contact deflections. A theoretical model for the real contact length was developed using extant contact mechanics theory and grinding theory. The average real contact length predicted by the model was more accurately representative of measured values than contact length based on other models. The model predicted real contact lengths typically 60% - 150% greater than the geometric contact length, compared with measured contact lengths 50% - 200% greater than the geometric values.

The thermal model of Rowe and Pettit used an equation for the real contact length given by Verkerk [35] as

$$l_e = l_g \left\{ 4.95 \left( \frac{v_s}{v_w} \right)^{-0.216} \cdot \exp \left[ -0.0205 \left( \frac{v_s}{v_w} \right)^{0.33} \right] \log a \right\} \quad 84$$

Rowe and Pettit were the first authors to employ an expression for the real contact length in their equation for the maximum workpiece temperature.

### 3.7.1 THE LOWER BOUND SOLUTION.

The lower bound solution represented a conservative prediction of the critical specific energy and excluded any allowance for heat transfer to the grinding chips and grinding fluid. The lower bound was used to predict the critical specific energy below which thermal damage should not occur.

The total heat flux,  $q$  was defined by,

$$q = \frac{P}{b \cdot l_e} \quad 85$$

In terms of specific energy the total heat flux was given by,

$$q = \frac{e_c \cdot v_w \cdot a}{l_e} \quad 86$$

The heat flux entering the workpiece  $q_w$ , was defined by including a partition ratio in equation 86.

$$q_w = R_{lb} \left( \frac{e_c \cdot v_w \cdot a}{l_e} \right) \quad 87$$

The partition ratio  $R_{lb}$ , was obtained by simultaneous application of the solution for a moving band source to the grinding wheel and the workpiece contact, Figure 3.9.

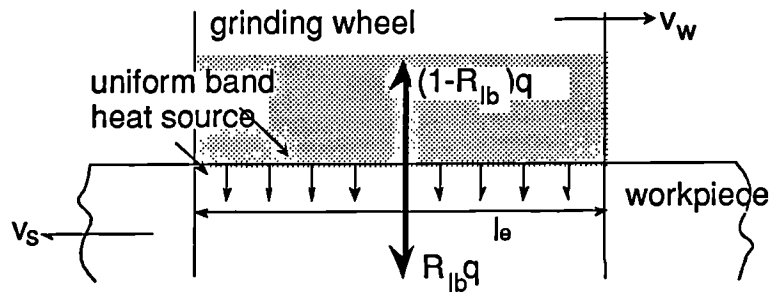


Figure 3.9 The lower bound partition model of Rowe and Pettit [7].

To establish an expression for the temperature at the surface of the workpiece in the model of Figure 3.9 the wheel is considered to be a non-conducting slider moving at a speed  $v_w$  and the workpiece is the fixed surface. Conversely, to establish an expression for the temperature at the surface of the grinding wheel, the workpiece is considered to be a non-conducting slider moving at a speed  $v_s$  and the grinding wheel is the fixed surface. By assuming a common interface temperature the two expressions can be equated. For this case the equation for the partition ratio  $R_{lb}$  is

$$R_{lb} = \frac{1}{1 + \left[ \frac{(\kappa \cdot \rho \cdot c)_s \cdot v_s}{(\kappa \cdot \rho \cdot c)_w \cdot v_w} \right]^{1/2}} \quad 88$$

where suffix s refers to the thermal properties of the grinding wheel. The bulk properties for aluminium oxide wheels were obtained from the experimental work by Gamble [33]. The values were,  $\kappa_s = 0.55 \text{ W / mK}$ ,  $\rho_s = 2287 \text{ kg / m}^3$ ,  $c_s = 0.21 \text{ kJ / kgK}$ .

For a plain carbon steel workpiece material and values of speed ratio between 50 and 100, the partition ratio has values between  $R_{lb} = 0.80$  and  $R_{lb} = 0.73$  respectively. For the case where the thermal properties of the composite wheel are known equation 88 provides a quick and easy method for estimating the partition ratio. However, this model does not explain the physics of the process at the microscopic level of interaction between the grinding wheel and the workpiece, nor can this model be used to explore the sensitivity of thermal partitioning to such factors as grain geometry and wear flats on the grains.

The maximum surface temperature  $\theta_m$ , was obtained by incorporating the partition ratio from equation 88 into the band source solution, equation 36.

$$\theta_m = 3.54L^{1/2} \frac{2\alpha}{\pi.K.v} R_{lb} \left( \frac{e_c.v_w.a}{l_e} \right) \quad 89$$

Rearranging equation 89 in terms of  $\theta_m^*$  the critical maximum temperature above which thermal damage occurs, yields the corresponding value of critical specific energy, which for values of Peclet number  $L > 5$  was

$$e_c^*(\text{lower bound}) = \theta_m^* \left( \frac{l_e}{v_w.\alpha} \right)^{1/2} \frac{0.885K}{R_{lb}.a} \quad 90$$

Equation 90 was defined as a lower bound solution since no account is taken of energy convected by the chips and the fluid. According to this equation, the maximum allowable specific energy depends on the real contact length. It was suggested that previous models had overstated  $\theta_m^*$  to compensate for the lower critical specific energy predicted when the geometric contact length is used.

### 3.7.2 CONVECTION BY THE GRINDING CHIPS.

The maximum specific energy conducted to the grinding chips  $e_{cc}$ , is given by equation 91 in terms of the material removal rate  $Z$ , the density and specific heat capacity of the workpiece material, and the difference between the workpiece melting temperature and ambient temperature.

$$e_{cc} = \rho.c.\Delta\theta_{ch} \quad 91$$

Equation 91 over-estimates the specific energy convected from the grinding zone by the chips in order to produce an upper bound solution. Malkin [4] proposed that the chips cannot absorb more than sufficient energy to melt, and calculated that  $0.45e_{ch}$  is conducted to the workpiece.

### 3.7.3 CONVECTION BY THE GRINDING FLUID.

Most grinding operations take place with fluid applied to the grinding contact zone area. The fluid acts as a lubricant to reduce the amount of frictional heat generated and as a coolant to remove heat energy from the workpiece after it has been heated. Equation 92 expresses the specific energy convected by the fluid in terms of a surface heat transfer coefficient  $h$ , and the difference between fluid boiling and ambient temperatures. Convection is greatly reduced if the boiling point is exceeded [27]. Therefore the maximum specific energy which can enter the grinding fluid is the specific energy required to raise the fluid to boiling temperature

$$e_{cf} = \frac{h \cdot l_e \cdot \Delta\theta_f}{a \cdot v_w} \quad 92$$

Rowe and Pettit presented a solution for the fluid surface heat transfer coefficient employing a cylinder in cross flow model. The justification for this model was based on the assumption of a small area of convection compared to workpiece diameter.

The Reynolds number is typically in the range  $40,000 < Re < 400,000$  for the fluid velocity range  $1 \text{ m/s} < v_{fluid} < 10 \text{ m/s}$ , and a workpiece diameter of 40 mm. The selected relationship for the Nusselt number ( $Nu$ ) and Reynolds number is given by,

$$Nu = D \cdot Re^n \cdot Pr^{1/3} \quad 93$$

where  $D = 0.0266$ ,  $n = 0.805$  and  $Pr = \text{Prandtl number}$ . The Prandtl number, equation 93, has been found to be the parameter which relates the relative thicknesses of the hydrodynamic and thermal boundary layers, and is thus the connecting link between the velocity field and the temperature field [39].

$$Pr = \frac{v}{\alpha} = \frac{\mu/\rho}{\kappa/\rho \cdot c_p} = \frac{\mu \cdot c_p}{\kappa} \quad 94$$

where  $\nu$  is the kinematic viscosity,  $\alpha$  is the thermal diffusivity and  $\mu$  is the dynamic viscosity.

The calculated surface heat transfer coefficient for a water based fluid using equation 93 was within the range  $3,900 < h < 22,750 \text{ W/m}^2\text{K}$ . This range is consistent with the range proposed by Snoeys, Maris and Peters in reference 18.

For a workpiece diameter range of  $0.02 \text{ m} < d_w < 0.1 \text{ m}$  and the fluid velocity range given previously, the Reynolds number is in the range  $20,000 < Re < 90,000$ . Using the relationship for the Nusselt number and Reynolds number given in equation 95 the surface heat transfer coefficient is then calculated to be within the range  $5,500 < h < 15,250 \text{ W/m}^2\text{K}$ .

$$N_u = 0.3 + \frac{0.62 Re^{1/2} \cdot Pr^{1/3}}{\left[1 + \left(\frac{0.4}{Pr}\right)^{2/3}\right]^{3/4}} \left[1 + \left(\frac{Re}{282,000}\right)^{5/8}\right]^{4/5}$$

95

Based on the theoretical analysis of Gamble [33], Rowe and Pettit used a value of  $12,000 \text{ W/m}^2\text{K}$  for the heat transfer coefficient. Equation 95 narrows the range of the heat transfer coefficient and therefore reduces the risk of errors resulting from incorrect selection of the value of the heat transfer coefficient.

Rowe and Pettit argued that heat flow to the fluid was over-estimated because the convection model is based on a complete and full delivery of fluid within the grinding zone.

### 3.7.4 THE UPPER BOUND SOLUTION.

The lower bound solution represents dry grinding conditions and excludes from consideration the heat transferred to the grinding chips and to the coolant. Taking into consideration the maximum heat transferred to the grinding chips and to the grinding fluid gives an upper bound solution representing specific grinding energy levels above which thermal damage should definitely occur.

The maximum workpiece surface temperature including the effects of the grinding chips and the grinding fluid is given in equation 96 and was obtained by substituting for the total heat flux a flux reduced by an amount ( $q_{ch} + q_f$ ).

$$\theta_m = \frac{1.6}{\kappa} \left( \frac{\alpha \cdot l_e}{2 \cdot v_w} \right)^{1/2} \cdot R_{lb} \left[ \frac{e_c \cdot v_w \cdot a}{l_e} - \left( \frac{Z' \cdot \rho \cdot c \cdot \Delta\theta}{l_e} + h \cdot \Delta\theta \right) \right] \quad 96$$

Rearranging equation 96 yields the upper bound solution for the critical specific energy,

$$e_c^* = \left[ 0.89 \theta_m^* \cdot \kappa \left( \frac{v_w}{\alpha \cdot l_e} \right)^{1/2} \cdot \frac{1}{R_{lb}} + \left( \frac{Z' \cdot \rho \cdot c \cdot \Delta\theta}{l_e} + h \cdot \Delta\theta \right) \right] \frac{l_e}{v_w \cdot a} \quad 97$$

Results obtained for the theoretical upper and lower bound solutions were found to enclose the burn boundary results obtained from several publications and also enclosed experimental results obtained in the laboratory. It was concluded that the lower bound solution provided a safe basis for the prevention of workpiece thermal damage. The Rowe and Pettit model presented a simple method for predicting the critical specific energy when grinding with conventional abrasive wheels. Application of the model to grinding with superabrasive materials is discussed in a later section.

The difference between the upper and lower bound solutions for the critical specific energy proposed by Rowe and Pettit, equations 90 and 97, and that proposed by Malkin in equation 69 is readily apparent if the quantity

$$\theta_m^* \left( \frac{l_e}{v_w \cdot \alpha} \right)^{1/2} \cdot \frac{0.89 \kappa}{a}$$

is replaced by an arbitrary function,  $f$ , and the nomenclature standardised. However, it is recognised that each author employs a different length of grinding contact.

Malkin predicts the critical specific energy as

$$e_c^* = 0.45 e_{ch} + f \quad 98$$

whereas Rowe and Pettit predict the lower bound value of critical specific energy as

$$e_c^*(\text{lower bound}) = \frac{f}{R_{lb}} \quad 99$$

and the upper bound value of critical specific energy as

$$e_c^*(\text{upper bound}) = \frac{f}{R_{lb}} + e_{ch} + e_f \quad 100$$

If the upper bound applies the proportion of the total heat entering the workpiece at the threshold of thermal damage is given by

$$R_{eff}^* = R_{lb} \frac{e_c^*(\text{lower bound})}{e_c^*(\text{upper bound})} \quad 101$$

The general solution for the upper bound is

$$R_{eff} = R_{lb} \left( \frac{e_c - e_{cc} - e_{cf}}{e_c} \right) = R_{lb} (1 - J) \quad 101a$$

It is of note that the chip formation energy in equation 98 is assumed to be constant for steels at 13.8 J/mm<sup>3</sup>.

### 3.8 SHAW'S SIMPLIFIED MODEL.

In 1989 Shaw [40] proposed a linearised solution of the band source model to determine the partition ratio in fine grinding operations. Shaw assumed a linear variation in the surface and the sub-surface temperature distributions along the interface of a slider contact. Figure 3.10a illustrates the linear variation in the surface temperature due to a band source of heat for a Peclet number  $L$  greater than 5. In Figure 3.10b the linear variation in the temperature at the trailing edge of the band source beneath the surface is shown by the dotted line. The depth of heat penetration is denoted by  $y'$ . Figure 3.10c is a composite figure that illustrates a linear surface temperature distribution and depth of heat penetration along the slider.

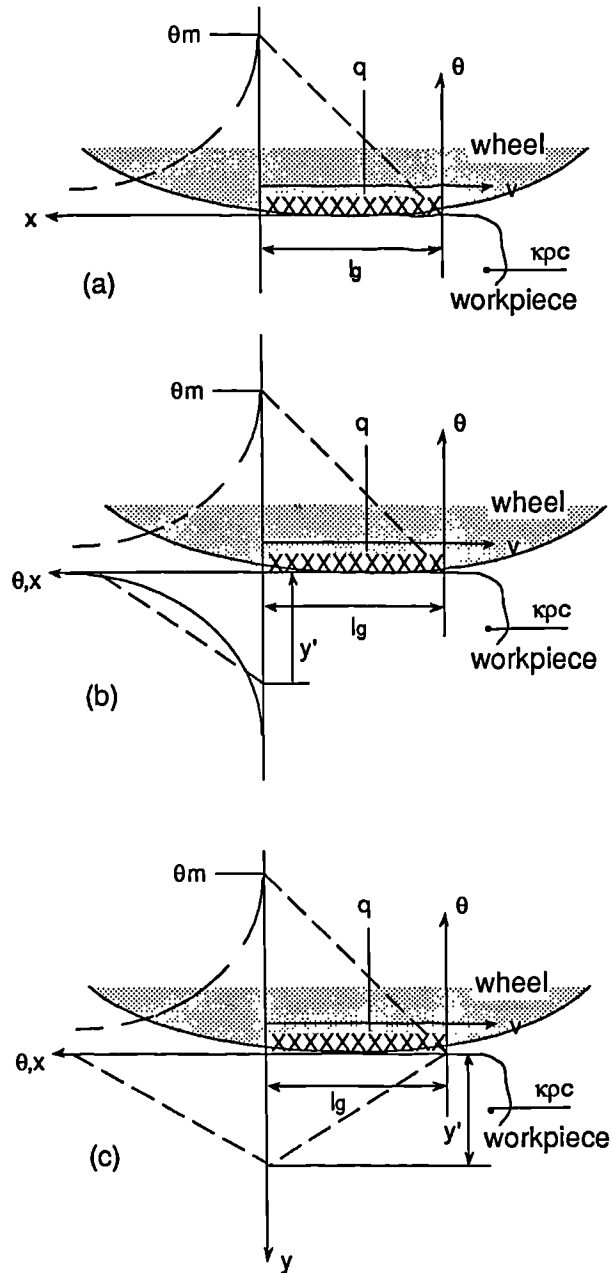


Figure 3.10 The linearised band source model (after Shaw [40]).

Shaw equated the total heat flux conducted to the workpiece to the increase in internal energy of the workpiece using the linearised temperature assumption shown in Figure 3.10c to give,

$$Q = q \cdot l_g \cdot b = \kappa \cdot l_g \cdot b \cdot \frac{\theta_m}{y'} = \rho \cdot c \cdot v \cdot b \cdot \theta_{av} \cdot y'$$

where  $v$  is the velocity, and  $b$  is the width of the heat source. The area of the heat source in Figure 3.10 is given by  $l_g \cdot b$ , thus the Peclet number is  $L = vl_g/\alpha$ .

Since  $\theta_m$  equals  $2\theta_{av}$  for the linearised model it follows that

$$y' = \left[ \frac{2 \cdot l_g \cdot \kappa}{v \cdot \rho \cdot c} \right]^{1/2} \quad 103$$

Substituting for  $y'$  in equation 102 gives

$$\theta_{av} = \frac{0.707q \cdot l_g}{\kappa \cdot L^{1/2}} \quad 104$$

The solution Shaw presented for the average mean-line surface temperature differed from the band source solution by the ratio of the coefficients  $0.752 / 0.707$ , that is approximately 6 per cent.

The partition ratio is defined as the ratio of the energy conducted to the workpiece  $e_{cw}$ , to the total grinding energy  $e_{cw} + e_{cs}$ , so that

$$R = \frac{e_{cw}}{e_{cw} + e_{cs}} \quad 105$$

For dry grinding operations Shaw neglected the energy transferring to the grinding chips so that the total grinding energy was partitioned between the grinding wheel and the workpiece. The specific energy conducted to the workpiece was determined from the linearised model as

$$e_{cw} = \frac{\theta_m \cdot b}{2} \cdot (2 [\kappa \cdot \rho \cdot c]_w \cdot v_w \cdot l_g)^{1/2} \quad 106$$

and the specific energy conducted to the wheel as

$$e_{cs} = \frac{\theta_m \cdot b}{2} \cdot \left( 2 [\kappa \cdot \rho \cdot c]_g \cdot v_s \cdot \frac{A_r \cdot l_g}{A_a} \right)^{1/2} \quad 107$$

The quantity  $(\kappa\rho c)_g$  in equations 106 and 107, expresses the thermal properties of the grains rather than the thermal properties of the grinding wheel as in the Rowe and Pettit analysis.  $A_r$  is the real area of contact and  $A_a$  is the apparent area of contact. The ratio  $A_r/A_a$  was introduced to allow for the fact that the grinding wheel is not a homogeneous solid, and that the thermal product  $(\kappa\rho c)_g$  for the grain is much larger than  $(\kappa\rho c)_s$  for the bulk material of the wheel. Equations 105 - 107 lead to an equation for the partition ratio

$$R_{lb} = \frac{1}{1 + \left( \frac{(\kappa\rho c)_g}{(\kappa\rho c)_w} \cdot \frac{v_s}{v_w} \cdot \frac{A_r}{A_a} \right)^{1/2}} \quad 108$$

For the case when the speed ratio is equal to 100 and the wear flat ratio is equal to 0.01 Shaw gave equation 109 as the approximate solution for the partition ratio

$$R_{lb} = \frac{1}{1 + \left[ \frac{(\kappa\rho c)_g}{(\kappa\rho c)_w} \right]^{1/2}} \quad 109$$

where suffix g refers to the thermal properties of the abrasive grain. For a plain carbon steel workpiece material and grain thermal properties of  $\kappa_g = 20 \text{ W / mK}$ ,  $\rho_g = 3900 \text{ kg / m}^3$ ,  $c_g = 0.75 \text{ kJ / kgK}$ , the partition ratio calculated from equation 109 has a value of  $R_{lb} = 0.65$ .

Shaw [40] assigned a fixed value to the ratio of the real and apparent areas of contact (the wear flat ratio) in recognition of the difficulties of acquiring the actual value. However, the approximation provides a simple solution for the partition ratio as a function of the thermal properties of the grinding wheel and workpiece materials that is independent of the grinding geometry and the value of the grinding parameters.

The partition ratio of Shaw can be compared to the partition ratio proposed by Rowe and Pettit in equation 88. The two definitions of the partition ratio are of the same form and equate with the following relationship

$$(\kappa\rho c)_s = (\kappa\rho c)_g \frac{A_r}{A_a} \quad 110$$

It can be concluded from equations 108 and 109 that Shaw agrees with the method of analysis proposed by Rowe and Pettit although recognising that if grain properties are used a factor is required to change the quantity  $(kpc)_g$  to the same magnitude as  $(kpc)_s$ .

The Shaw model appears to work reasonably well with conventional abrasives, which is a case where the experimentally determined value [33] of  $(kpc)_s$  has been found to differ from the quantity  $(kpc)_g$  by approximately two orders of magnitude. Thus, for a contact area ratio of  $A_r/A_a = 0.01$  the relationship given in equation 100 has a similar order of magnitude. Whether or not it works well with superabrasive materials will depend on the actual value of  $(kpc)_g$  for superabrasive materials. At present there are no reliable data available concerned with the value  $(kpc)_g$  for superabrasive materials. However, the experimental investigation described in chapter 4 aims to address this particular issue and will thus enable the validity of the Shaw model to be tested for this case.

### 3.8.1 EXTENSION OF SHAW'S SIMPLIFIED MODEL TO INCLUDE THE EFFECT OF A GRINDING FLUID.

The analysis by Shaw was developed to include the effect of a grinding fluid [41]. A uniform fluid film over the entire surface of the grinding wheel was assumed. The justification for this assumption was the small value of the ratio  $A_r/A_a$ . The analysis is analogous to the assumption of a fluid grinding wheel.

Heat flow is thus considered to occur between the workpiece and the fluid in the same manner as between the workpiece and the wheel. The energy convected by the fluid using the linearised model was given by equation 111.

$$e_f = \frac{\theta_m b}{2} (2[kpc]_f v_s l_g)^{1/2} \quad 111$$

For wet grinding, energy conducted to the wheel and fluid is summed, therefore

$$e_s = \frac{\theta_m b}{2} \left( 2[kpc]_g v_s \frac{A_r}{A_a} l_g \right)^{1/2} + \frac{\theta_m b}{2} (2[kpc]_f v_s l_g)^{1/2} \quad 112$$

By substituting for equations 106 and 112 into equation 105 a wet grinding partition ratio was derived. A simplified solution is presented in equation 113, based on the following assumptions :

- $v_s/v_w$  is approximately equal to 100
- $A_r/A_a$  is approximately equal to 0.01
- $(k\rho c)_f / (k\rho c)_w$  is approximately equal to one

Suffix f pertains to the fluid and suffix w refers to the workpiece.

With the assumptions above, it was found that

$$R_{\text{eff}} = \frac{1}{2 + \left[ \frac{(\kappa \cdot \rho \cdot c)_g}{(\kappa \cdot \rho \cdot c)_w} \right]^{1/2}} \quad 113$$

For a plain carbon steel workpiece material and grain thermal properties of  $\kappa_g = 20 \text{ W / mK}$ ,  $\rho_g = 3900 \text{ kg / m}^3$ ,  $c_g = 0.75 \text{ kJ / kgK}$ , the wet partition ratio has a value of  $R_{\text{eff}} = 0.40$ .

Shaw refers to the quantity  $(\kappa\rho c)^{1/2}$  as the Geometric Mean Thermal Property (GMTP). In reference [15]  $(\kappa\rho c)^{1/2}$  is referred to as the coefficient of heat penetration, which is a more useful description of the property. A method to directly measure the property  $(\kappa\rho c)^{1/2}$  is described in chapter 4 and results from an experimental investigation are reported. Shaw concludes that the superior thermal performance of a superabrasive is a result of the high GMTP value not only the high value of thermal conductivity, though Shaw in reference 40 confusingly suggests that superabrasives have a low thermal conductivity and low GMTP, whereas in fact superabrasives have a very high thermal conductivity and high GMTP.

Equations 109 and 113 have the great merit of simplicity, but as with the other models described so far, cannot be used to explore the effect of grain geometry.

### 3.9 THE LAVINE MODEL.

A model of heat transfer in grinding was proposed by Lavine [11, 42 and 43] in which heat generation was assumed to occur at the grain - workpiece interface. The model considered the heat removed from the grinding zone by the workpiece, abrasive

grains and the grinding fluid. Heat generation at the shear planes was analysed in a later work, reference 44, and is referred to in a later section.

The analysis of Lavine commenced with the development of separate models for heat transfer to each of the abrasive grain, workpiece and fluid. The models were then coupled to give the workpiece - wheel interface temperature.

### 3.9.1 HEAT TRANSFER TO AN ABRASIVE GRAIN.

The model for heat transfer into an abrasive grain proposed by Lavine is shown in Figure 3.11.

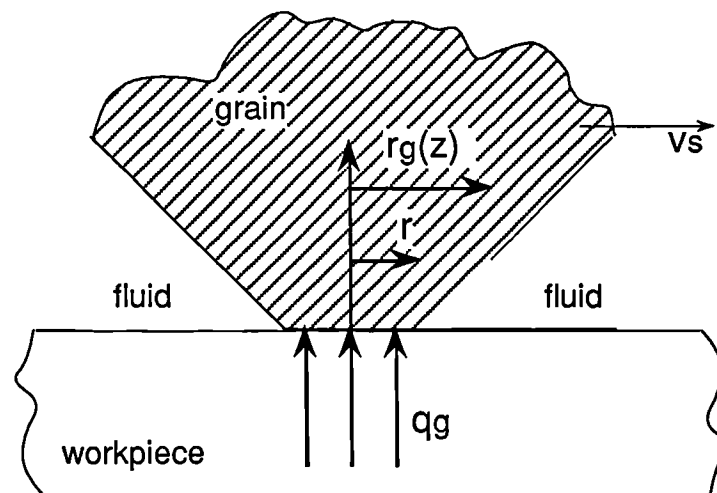


Figure 3.11 Model for heat transfer into an abrasive grain (after Lavine [11, 42]).

The grain was modelled as a frustum of a cone such that the cross-sectional area  $A_c$  was given by,

$$A_c = \pi.r_g^2 = \pi(r_0 + \gamma.z)^2 \quad 114$$

An expression for the grain temperature rise was found from the solution of the governing equation for heat conduction with (i) the assumption  $\gamma = dr_g/dz = 1$  which was made with the justification that on average the grains are as wide as they are high, and (ii) the following boundary conditions,

$$\theta_g(z, t=0) = 0$$

$\theta_g(z \rightarrow \infty, t)$  - finite

$$q_g = -\kappa \frac{\partial \theta_g}{\partial z} \Big|_{z=0}$$

The solution of Lavine is derived in full in appendix A1.3. The derivation details how the application of the Laplace transform rule in equation 115 to the governing differential equation of heat conduction led to a second order homogeneous differential equation with a solution of the form given by equation 116.

$$L[f'(t)] = s\bar{f}(s) - f(0) \tag{115}$$

$$\bar{\theta} = A.e^{\lambda_1 z} + B.e^{-\lambda_2 z} \tag{116}$$

The average grain temperature rise  $\theta_g$ , found by solving equation 116 was

$$\theta_g = \frac{q_g \cdot r_0^2}{\gamma \cdot \kappa_g (r_0 + \gamma \cdot z)} \left\{ \operatorname{erfc} \left( \frac{z}{2\sqrt{\alpha_g \cdot t}} \right) - \exp \left( \frac{\gamma \cdot z}{r_0} + \frac{\gamma^2 \cdot \alpha_g \cdot t}{r_0^2} \right) \right\} \tag{117}$$

Equation 117, valid for values of L greater than 5, may be compared with the temperature solution, equation 22, for a continuous band source. Equation 117 was established by applying the assumption of no temperature gradient in the radial direction. The justification given for this assumption was that the surrounding fluid has a low value of thermal conductivity and insulates the grain, which has a high value of thermal conductivity. The heat transfer analysis was thus reduced to a one-dimensional analysis with a change in cross-section. A further assumption was that the bond material was considered not to be of significance in terms of heat transfer to the grain, although this was considered in a later work, reference 44.

The solution for the maximum surface temperature at the end of the grinding zone,  $\theta_{g,max}$ , reduced to equation 118 following the substitution from equation 119 for  $\zeta$ , which was a factor said to account for the fact that the grain cross-sectional area increases with z.

$$\theta_{g, \max} = \frac{q_g r_0}{\gamma \cdot K_g} [1 - \exp(\zeta^2) \operatorname{erfc}(\zeta)] \quad 118$$

$$\zeta = \left( \frac{\gamma^2 \cdot \pi \cdot \alpha_g \cdot l_g}{A_0^2 \cdot v_s} \right)^{1/2} \quad 119$$

The grain heat flux and surface temperature are related by

$$q_g = h_g \cdot \Delta\theta_g \quad 120$$

where  $h_g$  is given by the solution for the maximum surface temperature rise from equation 118.

For the purpose of matching the solutions for the grain to the solutions for the fluid and the workpiece a local heat transfer coefficient was defined,

$$h_g = \sqrt{\frac{\pi(k \cdot \rho \cdot c)_g v_s}{f(\zeta) 4 \cdot l_g}} \quad 121$$

where the function  $f(\zeta)$ , obtained from equations 118, 119 and 120, was given by

$$f(\zeta) = \frac{2}{\pi^{1/2}} \frac{\zeta}{1 - \exp(\zeta^2) \operatorname{erfc}(\zeta)} \quad 122$$

It is of note that Lavine employs the geometric contact length  $l_g$  and not the real contact length  $l_e$ .

### 3.9.2 HEAT TRANSFER TO THE WORKPIECE: THE BACKGROUND TEMPERATURE RISE.

To calculate the background temperature rise the entire grinding zone was thought of as a uniformly distributed heat source that caused a heat flux  $q_{wb}$  into the workpiece. The workpiece is then a moving semi-infinite medium with a uniform heat flux at its surface, and has a maximum surface temperature given by equation 34 for values of  $L > 5$ . Conduction in the direction of motion was neglected and no dependence on the 'third dimension' was assumed. Given these assumptions the local heat transfer

coefficient  $h_{wb}$ , corresponding to the workpiece background temperature rise  $\Delta\theta_{wb}$ , for values of  $L$  greater than 5, is

$$h_{wb} = \sqrt{\frac{\pi(\kappa.\rho.c)_w v_w}{4.l_g}} \quad 123$$

The heat flux and temperature are related by

$$q_{wb} = h_{wb} \cdot \Delta\theta_{wb} \quad 124$$

where  $\Delta\theta_{wb} = \theta_T - \theta_{amb}$   
 $\theta_{amb}$  = temperature at time,  $t = 0$ .  
 $\theta_T$  = temperature at time,  $t = l_g/v_s$ .

### 3.9.3 WORKPIECE TEMPERATURE RISE BENEATH AN INDIVIDUAL GRAIN.

In reference 42, Lavine presented a solution for the workpiece temperature rise  $\theta_{wg}$ , due to a single grain, in which the grain was taken to be a square heat source and the dependence of the workpiece temperature on the 'third dimension' was included, as was conduction in the direction of motion. The workpiece temperature solution was determined by integrating a point source solution over a square region. An isotherm plot of the workpiece temperature rise underneath the heat source was given to illustrate the position of the maximum temperature, which was identified as occurring near the trailing edge of the heat source. The average workpiece temperature beneath a grain was obtained by integrating the maximum workpiece temperature solution between the limits 0 and  $L_g$ , where  $L_g$  was the equivalent speed parameter for a heat source of grain dimensions. Lavine recognised that the temperature solutions for the grain and the workpiece were incompatible in respect of their geometries since the grain contact is circular and the workpiece contact was modelled as a square and could not therefore be matched locally. Lavine therefore proposed that the average workpiece temperature under a grain should be matched to the maximum grain temperature at the end of its contact with the workpiece. This would be quite reasonable for some values of  $L$  and  $l_g$ . However, in Lavine's paper of 1989, [43], it is clear that the temperatures were not matched in this way and this is discussed further in Section 3.9.5.

In a later publication [44] the analysis was simplified with a uniform band source solution which was reported to yield almost identical results.

The heat flux into the workpiece surface beneath a single grain is given by,

$$q_{wb} = h_{wg} \cdot \Delta\theta_{wg} \quad 125$$

where the temperature rise, measured relative to the background temperature, is  $\Delta\theta_{wg}$  - since the background temperature is the temperature of the workpiece before it encounters the grain.

The heat transfer coefficient from the band source solution was given by,

$$h_{wg} = \frac{3}{2} \sqrt{\frac{\pi(k.\rho.c)_w.v_s}{4.r_o}} \quad 126$$

The factor of 1.5 in front of this heat transfer coefficient is due to the fact that the heat transfer coefficient in equation 126 relates to the average temperature rather than the maximum temperature.

### 3.9.4 HEAT TRANSFER TO THE GRINDING FLUID.

If the fluid is assumed to be at rest with respect to the wheel the fluid heat flux and surface temperature are related by equation 127.

$$q_f = h_f \cdot \Delta\theta_f \quad 127$$

where the heat transfer coefficient at the end of the grinding zone is

$$h_f = \sqrt{\frac{\pi(k.\rho.c)_f.v_s}{4.l_g}} \quad 128$$

and the suffix f refers to the properties of the fluid.

In this model for the heat transfer to the fluid, the fluid is modelled as a solid surface subjected to a moving band source of heat, although no physical justification was presented for this assumption.

### 3.9.5 COUPLING THE TEMPERATURE AND ENERGY EQUATIONS.

In the early paper by Lavine, Malkin and Jen, reference 11, the workpiece, fluid and grain temperatures were equated as illustrated in Figure 3.12.

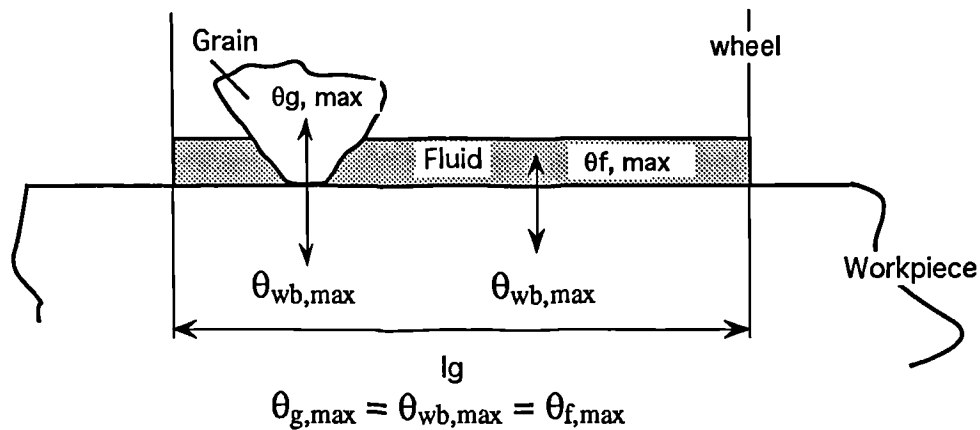
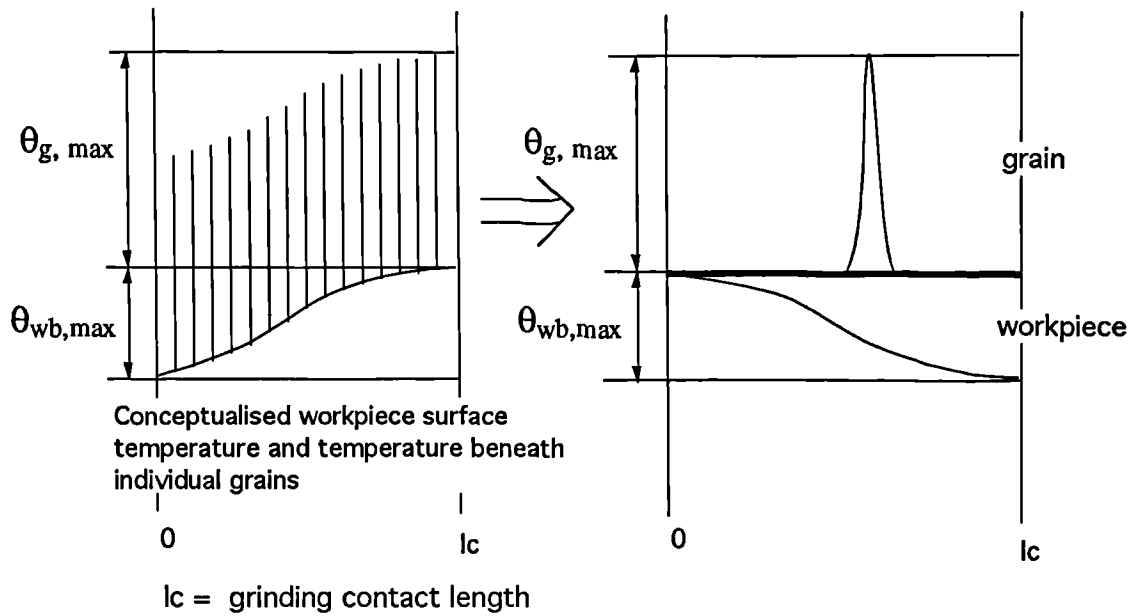


Figure 3.12 Coupling of grain, fluid and workpiece temperatures (Lavine, Malkin and Jen, 1989).

In the model above, it was assumed that the maximum surface temperature was the same for the workpiece, grain and fluid. Each point on the workpiece surface was considered to have a temperature  $\theta_{wb, \max}$ . The fluid temperature rise  $\theta_{f, \max}$  was assumed to be equal to  $\theta_{wb, \max}$ . Lavine noted however, that it was not correct to couple the temperatures in this way and that the assumption would under-predict the conduction into the grain. The error can be simply demonstrated for the case where the fluid convection is negligible. The coupling of the models employed by Lavine for this case is illustrated in Figure 3.13.



$$\theta_{g,\max} = \theta_{wb,\max}$$

Figure 3.13 Matching of the grain and workpiece temperatures (Lavine, Malkin and Jen, 1989).

It is clearly wrong to equate the grain spike temperature with the maximum background temperature and this was intimated in a personal correspondence with Lavine that followed the 1989 publication.

In a later paper, reference 42, Lavine and Jen proposed a different equation of interface temperatures. The total grain temperature rise  $\theta_{g,\max}$ , was considered to be equal to the sum of the workpiece background temperature rise  $\theta_{wb,\max}$  and the workpiece temperature rise due to an individual grain  $\theta_{wg,\max}$ . The method of matching of the grain and the workpiece surface temperatures is shown in Figure 3.14.

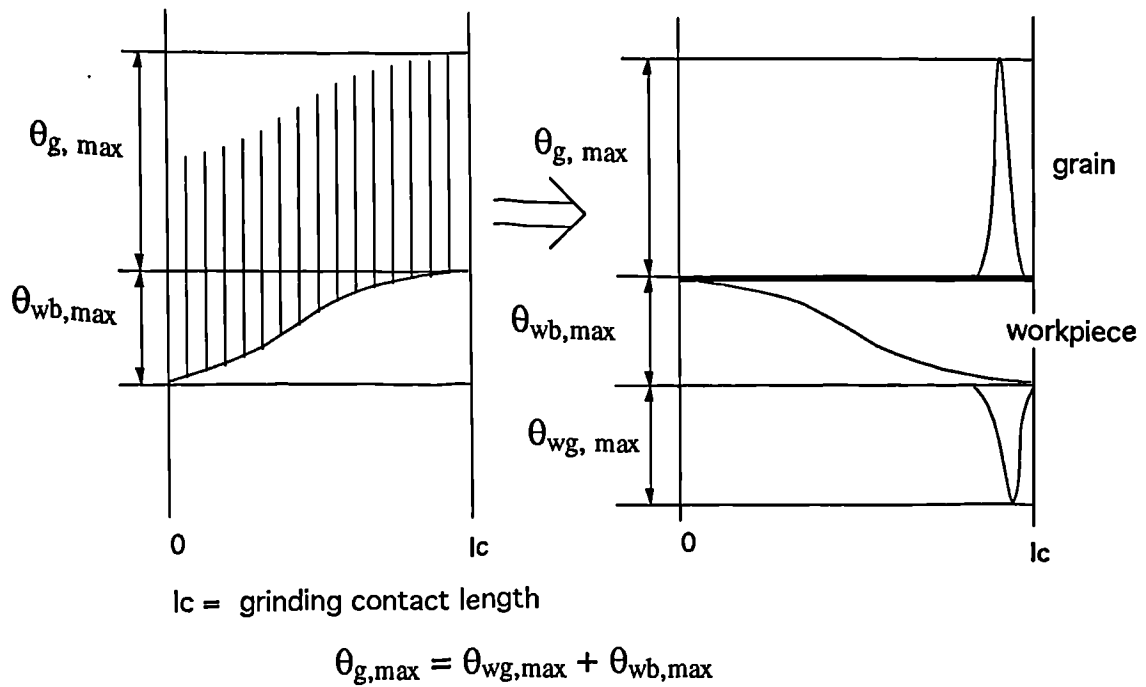


Figure 3.14 Matching of the grain and workpiece temperatures (Lavine and Jen, 1991).

The implication of the coupling illustrated in Figure 3.14 is that the temperature on the surface of the grain is  $\theta_{g,\max}$ , and arises from a proportion of the energy generated at the grain interface, while the temperature on the surface of the workpiece under a grain is  $\theta_{wg,\max} + \theta_{wb,\max}$ , where  $\theta_{wg,\max}$  arises from the remainder of the energy generated at the grain interface and  $\theta_{wb,\max}$  arises from the same energy distributed across the grinding contact length. Equating the temperatures in this way considers the effect of a single quantity of heat, twice, and consequently does not adhere to the principle of energy conservation.

For temperature compatibility and for energy conservation it follows that the two criteria below must be satisfied;

- (i) **Compatibility of temperatures at interface**  
interface temperature on grain = interface temperature on workpiece
- (ii) **Energy conservation at interface**  
total flux at interface - flux into grain - flux into workpiece beneath a grain = 0

A proposed requirement for grain and workpiece temperature compatibility is shown in Figure 3.15. The grain and workpiece temperatures are each treated separately by superposition. For the purpose of clarity the superscript g is used to identify the grain temperatures, and the superscript w is used to identify the workpiece temperatures. Hence  $\theta_{wb}^w$  refers to the workpiece background temperature rise,  $\theta_{wg}^w$  refers to the workpiece surface temperature rise due to a single grain,  $\theta_{wb}^g$  is the workpiece background temperature seen by an individual grain as it enters the grinding contact zone and  $\theta_{wg}^g$  refers to the *additional* grain temperature rise due to its contact with the workpiece. The analysis is consistent with the Lavine analysis with respect to the assumption of a steady state condition.

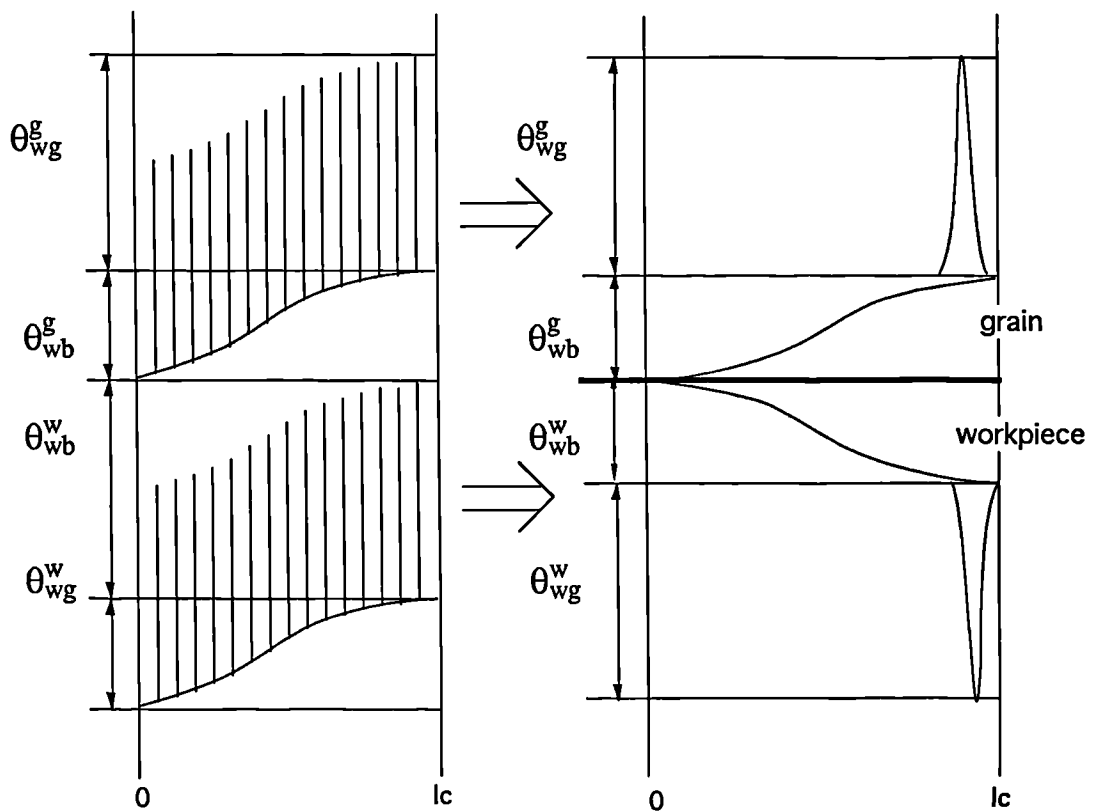


Figure 3.15 Proposed requirement for grain and workpiece temperature compatibility.

It can be recognised from Figure 3.15 that the temperature compatibility criterion is satisfied explicitly in that

$$\theta_{wg}^g + \theta_{wb}^g = \theta_{wg}^w + \theta_{wb}^w$$

and since  $\theta_{wb}^g = \theta_{wb}^w$ ,

$$\theta_{wg}^g = \theta_{wg}^w \quad 130$$

The energy criterion is satisfied by writing

$$q_{grind} = q_g + q_{wg} \quad 131$$

where  $q_{grind}$  is the energy generated at the grain - workpiece interface.

The modified compatibility condition illustrated in Figure 3.15 distinguishes clearly between temperatures at the wheel contact level and temperatures at the grain contact level and avoids the need to include an area ratio, a problem experienced by Lavine's analysis.

It is to be noted that in chapter 6 the corrected temperature compatibility is adopted for the development of a new thermal model.

### 3.9.6 THE PARTITION SOLUTION OF LAVINE.

The solution of interest for the purpose of predicting thermal damage was assumed to be the solution for the workpiece background temperature. The heat flux  $q$  based on the total grinding area was given by equation 132.

$$q = q_{grind} \cdot A \quad 132$$

where  $A$  is the fractional wear flat area and  $q_{grind}$  is the energy generated at the grain - workpiece interface.

Inclusion of the partition ratio  $R_{eff}$  in equation 124 gave the workpiece background temperature,

$$\theta_{wb} = \frac{R_{eff} \cdot q}{h_{wb}} \quad 133$$

By re-arranging the equations given previously the steady state solution for the partition ratio was determined as:

$$\frac{1}{R_{\text{eff}}} = \left[ 1 + \frac{h_f(1-A)}{h_{wb}} \right] \cdot \left[ 1 + \frac{h_g}{h_{wg}} \right] + A \cdot \frac{h_g}{h_{wb}} \quad 134$$

$$= \left[ 1 + \frac{2}{3} \kappa_g f(\zeta) \sqrt{\frac{2 \cdot r_0}{l_g}} \right] + \left\{ \left[ 1 + \frac{2}{3} \kappa_g f(\zeta) \sqrt{\frac{2 \cdot r_0}{l_g}} \right] (1-A) \kappa_f + A \cdot \kappa_g f(\zeta) \right\} \sqrt{\frac{v_s}{v_w}} \quad 135$$

where

$$\kappa_f = \sqrt{\frac{(\kappa \cdot \rho \cdot c)_f}{(\kappa \cdot \rho \cdot c)_w}} \quad \text{and} \quad \kappa_g = \sqrt{\frac{(\kappa \cdot \rho \cdot c)_g}{(\kappa \cdot \rho \cdot c)_w}} \quad 136$$

A proof of the partition solution defined by equation 135 is given in appendix A1.4.

To establish estimates of the value of  $R_{\text{eff}}$ , simplifications of equation 135 were given. A number of assumptions were employed to obtain the simplified expressions. The quantity  $(1 - A)$  was approximated to 1 since the fractional contact area is typically only a few per cent. The dimension of a single grain contact  $2r_0$ , was approximated to 100  $\mu\text{m}$ . For aluminium oxide abrasive grains  $\kappa_g$  was approximated to 0.7, and the function  $f(\zeta)$  was assumed to be equal to 1, which was said to be the approximate value in conventional grinding operations. In wet grinding the simplified solution for  $R_{\text{eff}}$  was given by,

$$\frac{1}{R_{\text{eff}}} \approx 1 + [\kappa_f + A \cdot \kappa_g] \sqrt{\frac{v_s}{v_w}} \quad 137$$

and in dry grinding, where the quantity  $\kappa_f$  for air was approximated to zero, by,

$$\frac{1}{R_{\text{lb}}} \approx 1 + A \cdot \kappa_g \sqrt{\frac{v_s}{v_w}} \quad 138$$

A comparison of the dry grinding partition solution of Lavine given in equation 138 with the partition solution of Rowe and Pettit given in equation 88 illustrates the difference between the two solutions. Lavine's partition solution uses the quantities  $l_g$ ,  $r_0$  and  $A$ , Rowe and Pettit's partition solution uses  $l_e$  and the bulk thermal properties of the grinding wheel. However, it is at this point that one is met with a contradiction of fundamental importance to the solution proposed by Lavine. If, as Lavine suggests, the function  $f(\zeta)$  is approximately equal to one in conventional

grinding operations, then the temperature solution for the conical grain reduces to the temperature solution for the band source applied to a semi-infinite plane surface. As this cannot be true the value of the solution for a 45 deg cone angle is clearly wrong.

### **3.9.7 INCLUDING THE EFFECT OF HEAT GENERATION AT THE SHEAR PLANES IN THE COUPLED HEAT TRANSFER MODEL OF LAVINE.**

Lavine in reference 44 extended the previously described model to include the effect of heat generation at the shear planes. The analysis followed the methodology presented in references 11, 42 and 43 with further consideration given to the heat generated at the shear plane. The effect of the shear plane was small compared to other effects such as  $v_s/v_w$ .

To compare the values of predicted critical specific energy generated from both the Lavine model and the Rowe and Pettit model, Lavine, in a personal correspondence, used the experimental data published in reference 7 by Rowe and Pettit. Similar values of predicted critical specific energy for each model were reported. However, in reference 44 Lavine reported on the results of numerical examples and concluded that the assumption that all the heat is generated at the wear flats led to an over-prediction of the workpiece background temperature rise and would therefore tend to be conservative in predicting the theoretical critical specific energy. For CBN wheels, the assumption of heat generation at the wear flat areas was reported to yield greater errors though Lavine's numerical results showed these errors to be second order.

### **3.10 DISCUSSION.**

Of the total grinding energy consumed in grinding only a fraction  $R$ , is transferred to the workpiece. Thus, a knowledge of the value of  $R$  is required to calculate the workpiece surface temperature. Each author has proposed a solution for  $R$  developed from an analysis of the heat transfer occurring at either the grain - workpiece contact level or at the wheel - workpiece contact level. In Table 3.1 the partition ratios, evaluated from the partition solution of each author, are summarised for the particular case described in Table 3.2.

Table 3.1 Summary of dry partition ratio solutions and typical values for aluminium oxide wheels and steel workpieces.

Author	Partition ratio	Typical values
Outwater / Shaw	$R_{lb} = \frac{0.665\sqrt{L}}{\sqrt{L} + 0.665\sqrt{L}}$	0.49 - 0.62
Takazawa (Model III)	$R_{lb} = \frac{1}{1 + \sqrt{\frac{(\kappa\rho c)_s v_s}{(\kappa\rho c)_w v_w}}}$	0.39
Malkin	$R_{lb} = \frac{e_c - 0.45e_{ch}}{e_c}$	0.87
Rowe / Pettit	$R_{lb} = \frac{1}{1 + \sqrt{\frac{(\kappa\rho c)_s v_s}{(\kappa\rho c)_w v_w}}}$	0.56
Shaw	$R_{lb} = \frac{1}{1 + \sqrt{\frac{(\kappa\rho c)_g v_s A_r}{(\kappa\rho c)_w v_w A_a}}}$	0.64
Lavine (simplified solution)	$R_{lb} = \frac{1}{1 + \frac{A_r}{A_a} \left[ \sqrt{\frac{(\kappa\rho c)_g v_s}{(\kappa\rho c)_w v_w}} \right]}$	(i) 0.93* (ii) 0.86**

The values in Table 3.1 are based on the following conditions, some of which are obtained from Table 3.2.

$$L = 2.8 - 8.7$$

$$v_s/v_w = 100$$

$$A_r/A_a = 0.01$$

$$e_c L/B = 40 \text{ J/mm}^3;$$

grain : bond : porosity ratio = 2 : 1 : 1.

\*(i) was calculated from equation 135 with the following simplifying assumptions:

$$\frac{2}{3} \kappa_g f(\zeta) \sqrt{\frac{2r_0}{l_g}} = 0; \text{ A is neglected relative to 1.}$$

\*\* (ii) was calculated from equation 135 with the following values:

$$2r_o = 100 \times 10^{-6} \text{ m}$$

$$f(\zeta) = 1.5$$

$$l_g = 5 \times 10^{-3} \text{ m}$$

Table 3.2 Material properties used to obtain the values in Table 3.1

	$\kappa$ , W/mK	$\rho$ , kg/m <sup>3</sup>	$c$ , J/kgK
alumina, grain	20	3900	750
alumina, wheel	0.55	2300	900
workpiece, MS	50	7600	480
bond	2.84	2635	1151
air	0.0243	1.3	1026

It is evident from Table 3.1 that substantial variation occurs in the predicted values of partition ratio proposed by each of the referenced authors. In fact, for the case considered, the simplified partition solution of Lavine predicts that nearly all the heat energy enters the workpiece in dry grinding operations. This compares to a value of approximately 50 per cent or lower, predicted by the solutions of Outwater and Shaw and Takazawa.

The models of Malkin and Outwater and Shaw each ignore thermal conduction into the grinding wheel. Malkin proposed a model based on energy considerations and argued that the effect of grinding fluid was accommodated within the model. The reasoning central to Malkin's argument was that the use of grinding fluid reduces the specific grinding energy and hence reduces the partition ratio obtained from the proposed partition solution. The thermal model proposed by Malkin requires that the value of specific chip formation energy is a constant at 13.8 J/mm<sup>3</sup>. The thermal model proposed by Malkin is not amenable to theoretical analysis and requires values of specific energy determined from experiment to yield results for use in a comparative study.

The partition solution of Rowe and Pettit [7] was similar to that proposed by Takazawa [9] in that the bulk properties of the wheel were used. However, Rowe and Pettit determined the wheel bulk properties experimentally and used the real length of contact in the thermal model. The model of Rowe and Pettit also allowed for the cooling effects of a grinding fluid to be included. The partition solutions of Rowe and Pettit and Takazawa are of a simple form, although reliant on appropriate

values of bulk wheel thermal properties. However, reliable data for values of bulk wheel thermal properties are not presently available.

The partition solution of Shaw [40] employed the thermal properties of the grain and a factor based on the wear flat area to reduce the heat energy accepted by the wheel. If the thermal properties of both the grain and the workpiece are known, a value of partition ratio can be determined by adopting simplifying assumptions. The model of Shaw was developed from a consideration of the tribological contact at the grain contact level and at the wheel contact level, however, no heat transfer model was proposed for conduction into the grain.

Lavine [11, 42 and 43] developed a partition solution in a manner much different to that of Shaw [40] yet proposed a partition solution similar in form. The solution proposed by Lavine required the grain thermal properties to be known and included a factor based on the wear flat area. However, the wear flat area ratio appeared in the denominator on the outside of the square root bracket in the Lavine partition solution, and inside the square root bracket in the Shaw partition solution. The effect of having the wear flat area ratio outside, as opposed to inside, the square root bracket, is to increase the value of  $R_{1b}$  for any given value of wear flat area ratio. This would be consistent with the values of  $R_{1b}$  reported by Lavine, which were in the range of 0.63 - 0.92, which compare to the values reported by Shaw, of  $R_{1b}$  in the range 0.51 - 0.70.

The analysis presented by Lavine for conduction into the grain at the value of  $f(\zeta) = 1$  is equivalent to the continuous band source solution. The model can only be reconciled with accurate solutions when a value of cone angle much less than the proposed 45 degrees is used. It is also of note that the work of Lavine was entirely theoretical and results were presented only for the experimental data of other authors.

### **3.11 Conclusions.**

From the previous review of thermal models it can be concluded that each of the proposed partition solutions has merit. However, it is apparent from the difference in the approaches used to establish the partition solution that there is no consensus on the most appropriate modelling technique. There is, therefore, a need to develop a thermal model that makes clear the distinction between the contact speeds, contact lengths and the contact temperatures experienced by the workpiece at each of the

two levels of contact. In this way it will be possible to establish a model that relies more on the accuracy of the physical modelling than on experimentally determined values of parameters that are obtained under particular grinding conditions which may not be repeatable under other grinding conditions.

## Chapter 4 AN INVESTIGATION OF THERMAL PROPERTIES OF GRINDING WHEELS.

This chapter describes an investigation of the thermal properties of aluminium oxide and cubic boron nitride (CBN) grinding wheel materials. A knowledge of the wheel bulk thermal property  $(\kappa\rho c)^{1/2}$  is required for the solution of the partition ratio proposed by Rowe and Pettit. The bulk property  $(\kappa\rho c)^{1/2}$  has previously been referred to by Shaw [40] as the geometric mean thermal property, by Blok [13] as the thermal contact coefficient and is referred to by Grigull and Sandner [15] as the coefficient of heat penetration. Previous work provided theoretical values [9], and experimental values [33], of the wheel bulk thermal properties of one grade of aluminium oxide grinding wheel. However, there are at present no data available for CBN. Further, no data are available to describe the variation in thermal properties as a function of wheel porosity.

The chapter is in three parts. In the first part the bulk property  $(\kappa\rho c)^{1/2}$  is evaluated for aluminium oxide and CBN wheel materials from the theoretical models proposed by Takazawa [9]. The second part describes an experimental investigation in which the density, specific heat capacity and thermal conductivity are each determined independently for three grades of aluminium oxide wheel material and for three grades of CBN wheel material. In the third part a method is developed to directly measure  $(\kappa\rho c)^{1/2}$ . The chapter concludes with a comparison of the results obtained from the three analyses.

### 4.1 THEORETICAL DETERMINATION OF THE BULK THERMAL PROPERTY $(\kappa\rho c)^{1/2}$ USING THE EQUATIONS PROPOSED BY TAKAZAWA.

The density and the specific heat capacity of a composite material can be expressed in terms of the volume percentage of the component parts, such that the density can be determined from

$$\rho_s = \rho_g \cdot V_g + \rho_b \cdot V_b + \rho_a \cdot V_a \quad 139$$

and the specific heat capacity from

$$c_s = \frac{c_g \cdot \rho_g \cdot V_g + c_b \cdot \rho_b \cdot V_b + c_a \cdot \rho_a \cdot V_a}{\rho_s} \quad 140$$

where V is the volume percentage, and suffices g, b and a refer to the grain, bond and porosity respectively.

Takazawa proposed three methods for the determination of the thermal conductivity of the composite wheel material. The basis for the analyses is illustrated in Figure 4.1.

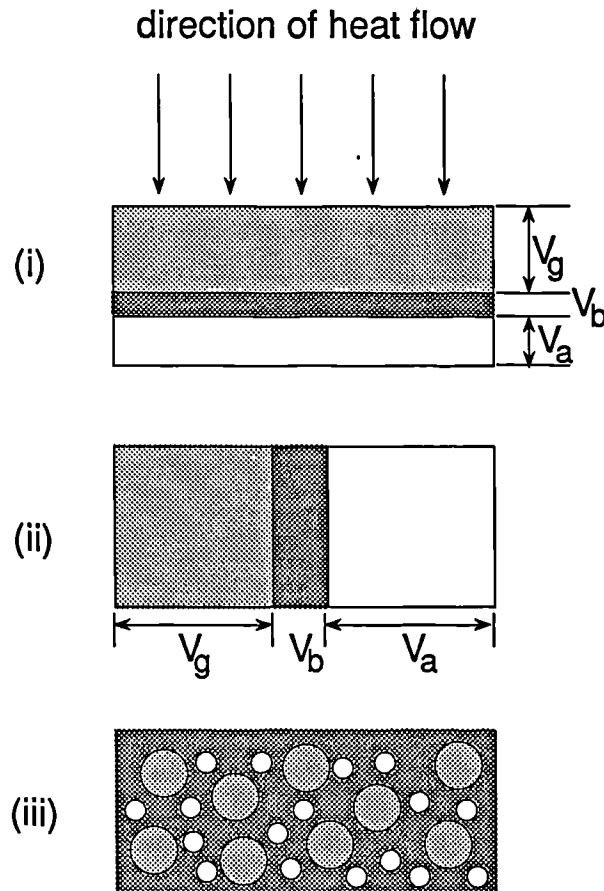


Figure 4.1 Three heat transfer models proposed by Takazawa to determine the bulk wheel thermal conductivity.

The thermal conductivity of the wheel for each model was given by equations 141, 142 and 143.

$$(i) \kappa_s = \frac{1}{\frac{V_g}{\kappa_g} + \frac{V_b}{\kappa_b} + \frac{V_a}{\kappa_a}} \quad 141$$

$$(ii) \kappa_s = V_g \kappa_g + V_b \kappa_b + V_a \kappa_a$$

142

If an analogy to electrical systems is made, then model (i) can be recognised as a series connected resistance, and model (ii) as a parallel connected resistance.

$$(iii) \kappa_s = \kappa_b \cdot \frac{1 - 2 \left[ V_a \cdot \frac{\kappa_b - \kappa_a}{2\kappa_b + \kappa_a} + V_g \cdot \frac{\kappa_b - \kappa_g}{2\kappa_b + \kappa_g} \right]}{1 + \left[ V_a \cdot \frac{\kappa_b - \kappa_a}{2\kappa_b + \kappa_a} + V_g \cdot \frac{\kappa_b - \kappa_g}{2\kappa_b + \kappa_g} \right]}$$

143

#### 4.1.1 SELECTION OF THE GRINDING WHEEL THERMAL PROPERTIES FOR THE TAKAZAWA ANALYSIS.

Takazawa [9] proposed equations 141 - 143 for the theoretical determination of bulk properties of the grinding wheel. The solutions required a knowledge of the volume percentage and thermal properties of the grain, bond and air. There is much conflicting published data relating to the grain thermal properties and Table 4.1 below, summarizes these findings.

Table 4.1 Published values of abrasive grain properties.

Author	Takaza- wa [9]	Ramach - andran [45]	Inasaki [1]	Shaw [40, 41]	Toensh- off [46]	Rowe [7]	Lavine [42 - 44]	Phanind - ranath [47]	Manufa- cturer [48]
<b>Al<sub>2</sub>O<sub>3</sub></b>									
$\kappa_g$ W/mK	1.55	6.3	15	16.7	27	35	46	3.1	19.5
$\rho_g$ kg/m <sup>3</sup>	3900	3800	-	3800	-	3910	3970	3986	3980
$c_g$ J/kgK	754	711	-	753	-	765	765	1233	1100
	G.E [49]	Lavine [42 - 44] *G.E	Gardinie -r [50] *G.E	Rowe [7] *G.E	Kumar [51] *G.E	Hiroshi [52] *G.E	Shaw [40, 41] *G.E	Bailey [53] *G.E	Verniek- es [54] *G.E
<b>CBN</b>									
$\kappa_g$ W/mK	87-							200 -	200 -
	1300	1300	1300	1300	1300	1300	87	700	700
$\rho_g$ kg/m <sup>3</sup>	3450	3450	3450	3450	3450	3450	3450	3450	3450
$c_g$ J/kgK	506	506	506	506	506	506	506	506	506

\*G.E indicates the original source of the published data.

It is evident from Table 4.1 that the most controversial data relates to the value of the grain thermal conductivity. This is possibly due to variations in the purity of the materials which is not indicated in the referenced publications. The range of conductivity values presented may also be due in some part to the variation of conductivity with temperature. From the data published by the manufacturer [48] the thermal conductivity of aluminium oxide varies from 19.5 W/mK at room temperature, to 5.31 W/mK at a temperature of 900 degC. The temperatures for the values of grain conductivity given in Table 4.1, are not indicated in the referenced publications. However, throughout the analyses presented in this thesis the assumption of constant conductivity has been used. This assumption will be investigated later in the thesis and further information is given in appendix A2.1 on the variation of abrasive grain thermal conductivity with temperature.

The published values of conductivity of CBN abrasive properties each find their source in the manufacturers handbook of properties, reference 49. It is of note that the value of 1300 W/mK was stated to be a theoretically determined value, whilst the value of 87 W/mK is a value obtained by extrapolation of data from porous compacts. The value of 200 W/mK, quoted by Bailey [53] and Vernekes [54], is a value measured on a dense polycrystalline compact.

The values of conductivity used to evaluate the bulk wheel properties from the Takazawa models are given below in Table 4.2.

Table 4.2 Values of grain thermal properties used in the Takazawa models.

Grain values	$\kappa_g$ W/mK	$\rho_g$ kg/m <sup>3</sup>	$c_g$ J/kgK
Al <sub>2</sub> O <sub>3</sub>	20.94	3890	819
CBN <sub>(1)</sub>	200	3450	506
CBN <sub>(2)</sub>	1300	3450	506

Where  $\kappa_g$ ,  $\rho_g$  and  $c_g$  are the mean values calculated from Table 4.1, CBN<sub>1</sub> is the lower published value and CBN<sub>2</sub> is the higher published value.

The properties of air and bond [55] are given in Table 4.3

Table 4.3 Properties of grinding wheel bond and air used in the Takazawa models.

	$\kappa$ W/mK	$\rho$ kg/m <sup>3</sup>	$c$ J/kgK
air	0.0243	1.3	1026
bond*	2.84	2635	1151

\*A vitreous silica bond possessing properties equal to those of a corosilicate glass [55] was assumed.

#### 4.1.2 RESULTS.

Table 4.4 Values of thermal conductivity  $\kappa_s$ , for the bulk grinding wheel samples using the Takazawa models.

Wheel sample	$\rho_s$ kg/m <sup>3</sup>	$c_s$ J/kgK	$\kappa_s$ I W/mK	$\kappa_s$ II W/mK	$\kappa_s$ III W/mK
Al <sub>2</sub> O <sub>3</sub> (10% bond)	2209	859	0.061	10.76	6.33
Al <sub>2</sub> O <sub>3</sub> (15% bond)	2341	875	0.069	10.90	5.93
Al <sub>2</sub> O <sub>3</sub> (25% bond)	2604	903	0.096	11.19	5.20
CBN <sub>1</sub> (10% bond)	1989	591	0.061	100.29	9.26
CBN <sub>1</sub> (15% bond)	2121	626	0.069	100.43	8.65
CBN <sub>1</sub> (25% bond)	2384	684	0.096	100.72	7.55
CBN <sub>2</sub> (10% bond)	1989	591	0.061	650.29	9.74
CBN <sub>2</sub> (15% bond)	2121	626	0.069	650.43	9.08
CBN <sub>2</sub> (25% bond)	2384	684	0.096	650.72	7.92

#### 4.1.3 DISCUSSION.

The value of conductivity  $\kappa_s$ , for the bulk grinding wheel evaluated from the Takazawa model (i), equation 141, is relatively insensitive to the conductivity of the grain or the bond material. The equation is most sensitive to the value of the conductivity of air  $\kappa_a$ , and as a consequence the results for this model are considered unreliable.

The value of conductivity evaluated from the Takazawa model (ii), equation 142, is relatively insensitive to the conductivity of the air. This would suggest that the conductivity of the composite would remain constant regardless of the porosity. This is clearly untrue.

The values of thermal conductivity obtained from the Takazawa model (iii), equation 143, are of a similar order of magnitude to the magnitude of the grain and bond values. The results suggest that the thermal conductivity increases with increasing porosity. This tendency occurs because equation 143 does not take into account the lower values of density and specific heat associated with more porous compacts. However, in practice one would expect the thermal conductivity to exhibit the opposite tendency.

## **4.2 DENSITY MEASUREMENTS.**

The density of a substance is defined by the equation  $\rho = m/V$ . For simple geometric shapes the density of a sample can be determined from a knowledge of the mass  $m$  and volume  $V$ .

### **4.2.1 APPARATUS AND PROCEDURE.**

The apparatus included a digital electronic balance, Mettler PM400, with a resolution of 0.001 gramme, a Mitutoyo digital micrometer with a resolution of 10 $\mu$ m and a Mitutoyo Vernier caliper gauge of resolution 0.1 mm. Samples of aluminium, copper and mild steel were tested to determine the accuracy of the measurement method. Samples of wheel material were then tested and the mean value of six diameter measurements and the mean value of eight width measurements were used to establish the volume of the sample. A typical sample had a diameter of 41.20 mm and thickness of 12.50 mm.

### **4.2.2 RESULTS.**

Table 4.5 gives the mean value of density measured for the grinding wheel samples and samples of a known density.

Table 4.5 Density measurement results.

Density, kg/m <sup>3</sup>				
Sample	Measured	Documented		
aluminium	2664	2707		
copper	8920	8954		
mild steel	7610	7650		
Manufacturers data				
Wheel sample	Theoretical value	Experimental value	Measured	Error %, against Manufacturers experimental data
Al <sub>2</sub> O <sub>3</sub> (10% bond)	2600	2520	2550	1.2
Al <sub>2</sub> O <sub>3</sub> (15% bond)	2360	2280	2300	0.9
Al <sub>2</sub> O <sub>3</sub> (25% bond)	2240	2150	2150	0.0
CBN (10% bond)	2350	2290	2280	0.4
CBN (15% bond)	2110	2090	2090	0.0
CBN (25% bond)	1990	1970	1960	0.5

The values quoted for aluminium and copper were for materials of a 100% purity. It is unlikely that the materials tested were of 100% purity and this would account, in some part, for the difference between the measured values and the values quoted from reference [45].

The measured values of density for vitrified alumina and CBN wheel samples agreed with the experimental and the theoretical values provided by the manufacturer, within approximately 1 per cent. The manufacturers theoretical values were determined from a method of mixtures analysis, the experimental values from a method similar to that described above. It was found that for samples of a simple geometry such as those tested, accurate size measurements are adequate to calculate this parameter.

### 4.3 THERMAL CONDUCTIVITY MEASUREMENTS.

The thermal conductivity of a sample of material with known dimensions can be determined from an experimental arrangement that measures the heat flow through a sample of the material [12]. Heat can be provided by an electrical method. The equilibrium temperature gradient across a sample may be used to calculate its

thermal conductivity. This involved solving the one dimensional Fourier equation, equation 1, where the only unknown is the thermal conductivity. For the experimental arrangement shown in Figure 4.2, if  $e$  joules of energy are emitted from each exposed unit area of surface per second per degC above ambient temperature, then the thermal conductivity of the sample can be calculated using equations 144 and 145,

$$e = \frac{\text{voltage} \times \text{current}}{\left[ a_A \theta_A + \frac{a_s \theta_A + \theta_B}{2} + a_B \theta_B + a_C \theta_C \right]} \quad 144$$

$$\kappa = \frac{e.d}{2\pi r^2 (\theta_B - \theta_A)} \left[ \frac{a_s \theta_A + \theta_B}{2} + 2a_A \theta_A \right] \quad 145$$

where  $a_A, a_B, a_C, a_S$  are the exposed surface areas of A, B, C and S respectively.  $\theta_A, \theta_B, \theta_C$  are the temperatures of discs A, B, C at the steady state above ambient temperature. The radius of the sample is  $r$  and the thickness of the sample is  $d$ .

#### 4.3.1 APPARATUS AND PROCEDURE.

Lee's conductivity apparatus is an arrangement of copper discs, Figure 4.2, which make an electrical circuit through which an electrical current is passed to generate heat to the apparatus. Thermometers are placed in each of two discs adjacent to a central third copper disc and on each of the two copper discs adjacent to the sample material. A fourth thermometer is placed close to the apparatus and used to measure ambient temperature. A d.c. power unit was used in this experimental study. In Figure 4.2 the discs are identified, reading from left to right, as C, B, S and A.

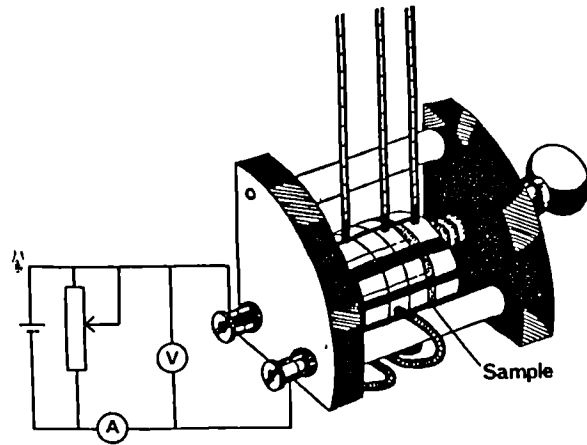


Figure 4.2 Lee's conductivity apparatus used to determine the thermal conductivity of a material.

#### 4.3.2 RESULTS.

The mean values of thermal conductivity measured from experiment for the grinding wheel samples and the calibration sample are given in Table 4.6. The mean value was obtained from the readings of three separate tests.

Table 4.6 Thermal conductivity measurement results.

Sample	Thermal conductivity, W/mK	
	Measured	Documented
Perspex	0.207	0.208
Copper	2.75	386
Aluminium	2.37	204
<b>Wheel sample</b>	<b>Measured</b>	<b>Documented</b>
Al <sub>2</sub> O <sub>3</sub> (10% bond)	0.948	n/a
Al <sub>2</sub> O <sub>3</sub> (15% bond)	0.970	n/a
Al <sub>2</sub> O <sub>3</sub> (25% bond)	0.960	n/a
CBN (10% bond)	1.003	n/a
CBN (15% bond)	0.956	n/a
CBN (25% bond)	1.021	n/a

### **4.3.3 DISCUSSION.**

It was evident from the thermal conductivity values obtained for the calibration samples that the apparatus was inadequate for use with materials possessing a high value of thermal conductivity. From examination of equation 145 it can be seen that the temperature difference between discs B and A at the steady state has a strong influence on the value calculated. For materials possessing a high thermal conductivity the temperature difference is very small and must be measured to a better accuracy than that which was achievable with the test apparatus. This was particularly the case with the copper sample which had the same thermal conductivity as the test apparatus. However, the calibration result for perspex suggests that the apparatus measures to a high accuracy with materials possessing a low thermal conductivity. The measured value of thermal conductivity of the alumina sample was of the same order of magnitude as the published values for the grain material, Table 4.1, and the bond material, Table 4.3. The measured value of thermal conductivity of the CBN sample was approximately one order of magnitude lower than the lowest value published for the grain material, Table 4.1. However, this is not surprising considering the lower thermal conductivity of the bond material.

The thermal conductivity of the vitrified alumina and CBN bulk wheel samples were similar at approximately 1 W/mK. There was no identifiable difference in the value of thermal conductivity with porosity. The results of this test suggest that the bulk wheel thermal property is strongly dependent on the bond material and may not account for the improved thermal performance of CBN compared to alumina.

## **4.4 SPECIFIC HEAT CAPACITY MEASUREMENTS.**

The specific heat capacity  $c$ , of a material is the quantity of heat required to produce unit rise of temperature in unit mass and is defined by the equation  $c = \delta Q / (m \Delta \theta)$ . An equation for the specific heat capacity of a sample was established from an energy balance of the system. The analysis is detailed in appendix A2.2.

### **4.4.1 APPARATUS AND PROCEDURE.**

The apparatus included a Universal Sartorius digital electronic balance with a resolution of 0.01 gramme; a digital thermometer; a commercial standard copper -

copper/nickel thermocouple; samples of a known specific heat capacity and a calorimeter. The calorimeter consisted of a thermos flask with a sealing lid.

The experimental procedure involved immersing a heated sample in the calorimeter which was partially filled with a known quantity of water at a known temperature. The temperature of the sample was measured prior to immersion. The temperature of the water surrounding the sample was measured over a period of time, and the temperature at the steady state recorded. The thermocouple was introduced into the calorimeter via an access port in the lid. The experimental arrangement is illustrated in Figure 4.3. The specific heat capacity of a sample was determined by equating the energy lost from the water to the energy gained by the sample less a correction for energy lost to the water carried across with the sample. To improve correlation and to include the effect of losses an empirically derived correction factor of 1.236 was applied to the grinding wheel sample results. A correction factor for each test value was first defined as the product required to raise the experimental value to the quoted value. An empirical factor was then obtained from a linear curve fit to the individual correction factors. For the purpose of this experiment the specific heat capacity was assumed to be constant over the temperature range: 100 degC - ambient.

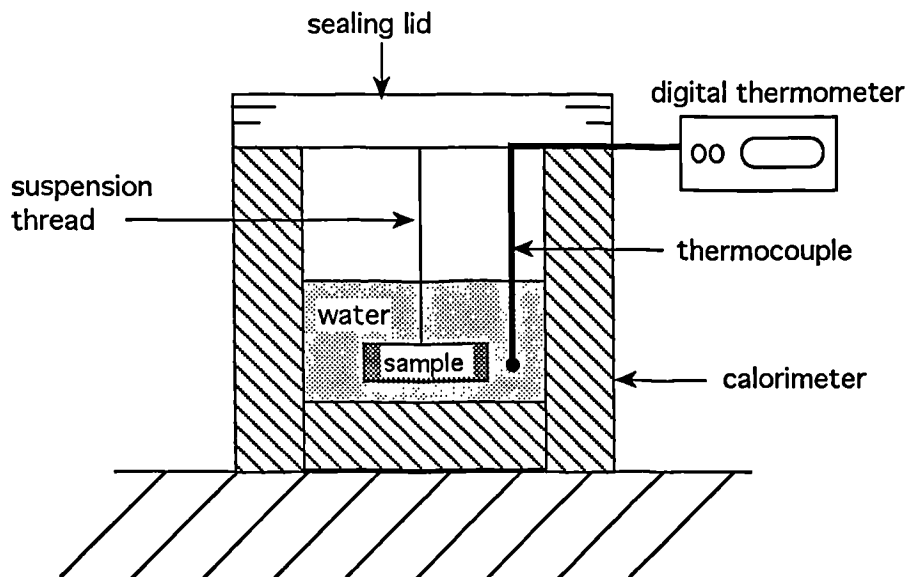


Figure 4.3 Experimental arrangement for the determination of specific heat capacity.

#### 4.4.2 RESULTS.

Table 4.7 gives the mean values of specific heat capacity measured for the grinding wheel samples and the samples of a known specific heat capacity. The mean value was obtained from the readings of three separate tests. A correction factor is included in the results for the grinding wheel samples.

Table 4.7 Specific heat capacity measurement results.

Sample	Specific heat capacity, J/kg K		Standard deviation
	Measured	Documented	
Aluminium	749	896	0.063
Copper	304	383	0.021
Wheel sample	Measured	Documented	Standard deviation
Al <sub>2</sub> O <sub>3</sub> (10% bond)	1,054	n/a	0.100
Al <sub>2</sub> O <sub>3</sub> (15% bond)	964	n/a	0.012
Al <sub>2</sub> O <sub>3</sub> (25% bond)	915	n/a	0.225
CBN (10% bond)	1,027	n/a	0.065
CBN (15% bond)	943	n/a	0.053
CBN (25% bond)	1,068	n/a	0.117

#### 4.4.3 DISCUSSION.

The values determined for the aluminium oxide wheel samples were within the range of values published for the pure abrasive grain, Table 4.1, and tended toward the higher value. This was expected because the specific heat capacity of the bond material and of air is slightly higher than that of the pure abrasive. The results also correlate well with the results obtained from the Takazawa analysis, Table 4.4.

The results for the CBN wheel samples were approximately 1.6 times higher than the values published for the pure abrasive grain, Table 4.1, and again this was expected as the specific heat capacity of the bond material and of air is higher than that of the pure abrasive.

There was no consistent trend relating the porosity of the wheel samples to the specific heat capacity. The aluminium oxide wheel sample results obtained from this

experimental study are very different to those of Gamble [33], who quotes an average value of 210 J/kgK for a similar material.

#### 4.5 AN EXPERIMENTAL METHOD TO DIRECTLY MEASURE THE BULK THERMAL PROPERTY OF A COMPOSITE SOLID.

The physical properties  $\kappa$ ,  $\rho$  and  $c$  are each individually understood, however the physical meaning of the bulk property  $(\kappa\rho c)^{1/2}$  is less apparent. A further understanding of the bulk property can be acquired from consideration of the thermal contact between two semi-infinite bodies of different material sustaining equal and uniform temperature fields

At the contact surface between two bodies the bounding plane can store no heat and a uniform temperature  $\theta_i$  will exist. From equation 24, the solution for the surface temperature of body 1 is given by

$$\theta_i - \theta_1 = \frac{2q_1 t^{1/2}}{\pi^{1/2}(\kappa\rho c)_1^{1/2}} \quad 149$$

where  $q_1$  is the heat flux at the surface. Similarly, the solution for the surface temperature of body 2 is

$$\theta_i - \theta_2 = \frac{2q_2 t^{1/2}}{\pi^{1/2}(\kappa\rho c)_2^{1/2}} \quad 150$$

Therefore,

$$\frac{q_1}{q_2} = \frac{(\kappa\rho c)_1^{1/2}(\theta_i - \theta_2)}{(\kappa\rho c)_2^{1/2}(\theta_i - \theta_1)} \quad 151$$

A solution for the mean contact temperature  $\theta_i$  between two dissimilar bodies each sustaining different uniform temperatures was presented by Grigull and Sandner [15] as

$$\frac{\theta_i - \theta_1}{\theta_2 - \theta_1} = \frac{(\kappa\rho c)_2^{1/2}}{(\kappa\rho c)_1^{1/2} + (\kappa\rho c)_2^{1/2}} \quad 152$$

where it is assumed that the temperature is independent of time.

Equation 152 allows the property  $(\kappa\rho c)^{1/2}$  of a material to be determined when it contacts with a second material of a known  $(\kappa\rho c)^{1/2}$ .

The above fact was used as the basis for the development of a sensor with the objective of measuring  $\theta_i$  between a material of known thermal properties and a sample of grinding wheel material for which the property  $(\kappa\rho c)^{1/2}$  was to be determined.

#### 4.5.2 APPARATUS AND PROCEDURE.

A special sensor was designed in order to measure the interface temperature between two contacting bodies. A simplified illustration of the experimental arrangement is shown in Figure 4.4. A full description of the sensor and the method of assembling the thermocouple is given in appendix A.2.3.

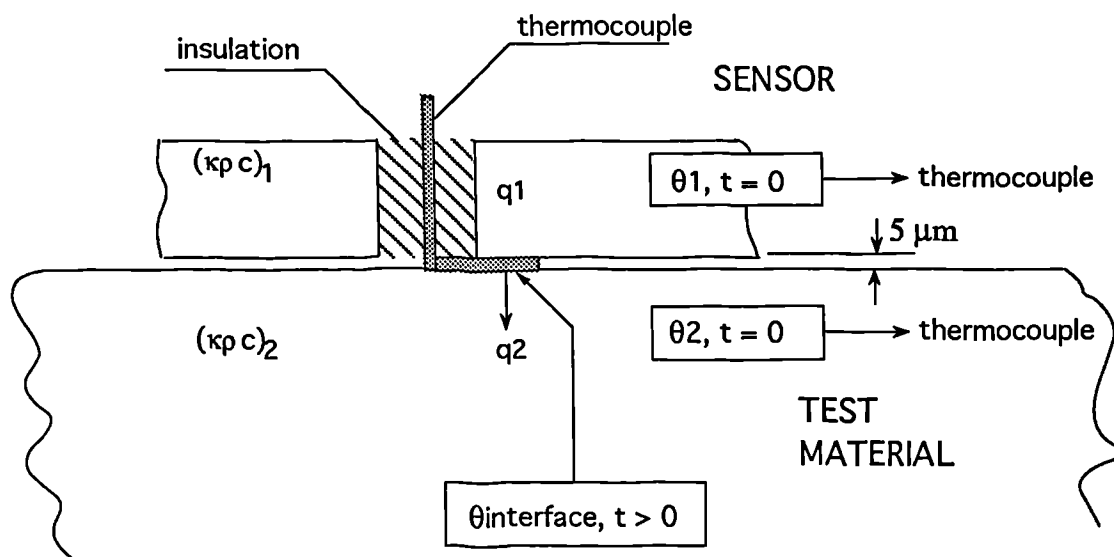


Figure 4.4 Simplified illustration showing the experimental arrangement used to measure the bulk property  $(\kappa\rho c)^{1/2}$  of a material.

The sensor consisted of a commercial standard chromel - alumel type K thermocouple installed between two sections of a mild steel housing. The temperature measuring poles of the thermocouple were positioned proud of the face

of the mild steel housing and adjacent to a polished ground surface. A second thermocouple was placed on the material to be tested and a third on the external body of the sensor.

The sample material was heated on a hot plate to a temperature of approximately 100 deg C. The sensor, held at room temperature, was then placed on the surface of the sample material and the maximum steady state interface temperature was recorded. Approximately ten readings were taken during a single trial to determine the mean value of the steady state temperature. The results were normalised with a calibration factor that was established prior to the trials. The temperature measurements from the thermocouple at the interface were passed via a digital thermometer to an oscilloscope and then to a pc. A trial was repeated three times for each sample and a mean for the three trials was calculated.

A typical time - temperature recording from an individual trial is shown in Figure 4.5. The transient and steady state regions are clearly identifiable. A brief and irregular signal following the initial transient can also be seen and this was a typical feature of many of the recordings. The irregular signal was a consequence of slight movements of the sensor whilst attempting to establish a firm contact.

The initial transient for all the materials tested was very short and the interface temperature reached a maximum very soon after contact. The interface temperature,  $\theta_i$  was determined by extrapolating the maximum steady state value back to the temperature axis.

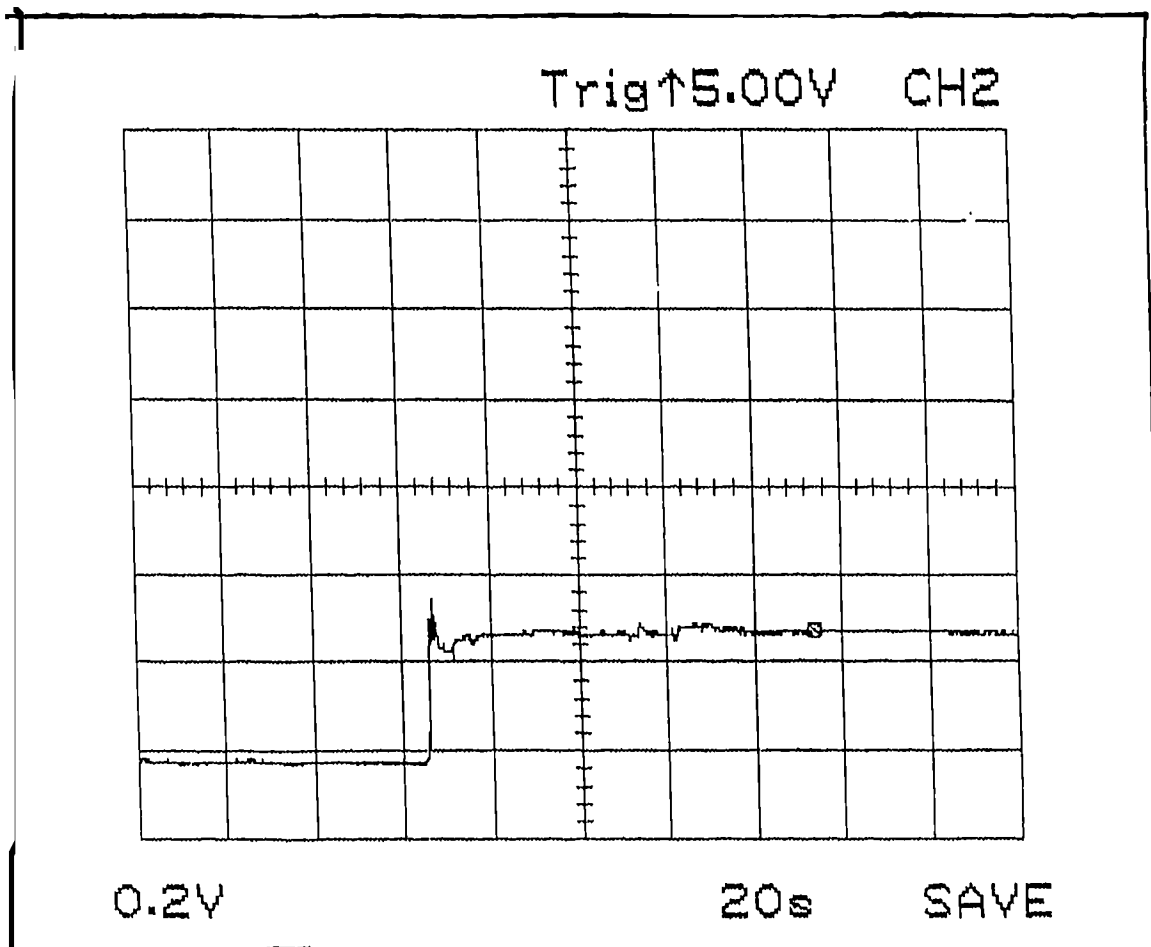


Figure 4.5 A typical time -temperature recording of the interface temperature,  $\theta_i$ .

### 4.5.3 RESULTS.

Table 4.8 gives the mean values of the bulk thermal property  $(\kappa\rho c)^{1/2}$  measured for the grinding wheel samples and the calibration samples.

Table 4.8 Experimental values of bulk thermal property  $(\kappa\rho c)^{1/2}$ .

	$(\kappa\rho c)^{1/2}$ J/s <sup>1/2</sup> m <sup>2</sup> K	$(\kappa\rho c)^{1/2}$ J/s <sup>1/2</sup> m <sup>2</sup> K
sample	Measured	Documented
aluminium	12549	13495
copper	31224	36383
mild steel	18839	22244
<b>Wheel sample</b>	<b>Measured</b>	<b>Documented</b>
Al <sub>2</sub> O <sub>3</sub> (10% bond)	2239	n/a
Al <sub>2</sub> O <sub>3</sub> (15% bond)	1985	n/a
Al <sub>2</sub> O <sub>3</sub> (25% bond)	1911	n/a
CBN(10% bond)	1984	n/a
CBN(15% bond)	2035	n/a
CBN(25% bond)	2039	n/a

Table 4.9 A comparison of the values of the bulk thermal property  $(\kappa\rho c)^{1/2}$  extracted from the three methods.

Wheel sample	Volume percent of bond	Takazawa (Model III) $(\kappa\rho c)^{1/2}$ J/s <sup>1/2</sup> m <sup>2</sup> K	Measured $\kappa$ , $\rho$ and $c$ $(\kappa\rho c)^{1/2}$ J/s <sup>1/2</sup> m <sup>2</sup> K	Sensor measurement $(\kappa\rho c)^{1/2}$ J/s <sup>1/2</sup> m <sup>2</sup> K
Al <sub>2</sub> O <sub>3</sub> (10% bond)	10	3466	1596	2239
Al <sub>2</sub> O <sub>3</sub> (15% bond)	15	3485	1466	1985
Al <sub>2</sub> O <sub>3</sub> (25% bond)	25	3497	1374	1911
CBN <sub>1</sub> (10% bond)	10	3299	1532	1984
CBN <sub>1</sub> (15% bond)	15	3389	1373	2035
CBN <sub>1</sub> (25% bond)	25	3509	1462	2039

The sensor measurement results correspond most closely to the results obtained from the independent  $\kappa$ ,  $\rho$  and  $c$  measurements and similarly exhibit no relationship with porosity. It is of note that all three methods predict that CBN and alumina have similar values of  $(\kappa\rho c)^{1/2}$  despite the order of difference in the magnitude of the CBN grain thermal conductivity and the alumina grain thermal conductivity. The result may partly be explained as a consequence of the dominant effects of the bond and porosity which have similar thermal properties in each case.

The values of  $(\kappa\rho c)^{1/2}$  obtained from the independent  $\kappa$ ,  $\rho$  and  $c$  measurements are approximately 70 per cent of the values obtained from the direct bulk property measurements. As an example, for the case of an alumina wheel with 10 per cent bond,  $(\kappa\rho c)^{1/2} = 1596 \text{ J/s}^{1/2}\text{m}^2\text{K}$ , and from direct bulk property measurements  $(\kappa\rho c)^{1/2} = 2239 \text{ J/s}^{1/2}\text{m}^2\text{K}$ .

Values of  $(\kappa\rho c)_{\text{alumina}}^{1/2}$  obtained from this experimental study will, in a later section, be compared to values of  $(\kappa\rho c)_{\text{alumina}}^{1/2}$  obtained from an inverse method using experimental grinding trial data.

#### **4.6 CONCLUSIONS.**

Three methods to determine the bulk property  $(\kappa\rho c)^{1/2}$  for CBN and alumina wheel materials have been investigated. A new sensor was developed to measure the bulk property  $(\kappa\rho c)^{1/2}$  directly. It is concluded that the bulk property  $(\kappa\rho c)^{1/2}$  has similar values for both CBN and alumina wheel materials. No relationship between the porosity of a wheel material and the bulk property  $(\kappa\rho c)^{1/2}$  was established. The results of this study indicate that the bulk wheel thermal property alone, does not account for the improved thermal performance of CBN compared to alumina.

## Chapter 5 ENERGY PARTITIONING TO THE GRINDING FLUID AND CHIPS.

In this chapter expressions for the heat flux entering the workpiece are given for a series of assumptions relating to the effect of the grinding fluid and the chips. The model of Rowe and Pettit [7] is developed in stages to illustrate how different modelling assumptions affect the theoretical value of heat flux entering the workpiece. In particular it is necessary to decide whether heat in the grinding zone absorbed by the fluid should be treated as entering the coolant directly or only after entering the workpiece or in fact whether the differences in treatment are of significance.

### 5.1 THE DRY GRINDING PARTITION SOLUTION.

Rowe and Pettit [7] proposed that conduction into the grinding wheel could be determined by considering the grinding wheel to be a homogeneous moving surface subject to a heat flux distributed evenly over the grinding contact zone. The assumption required a knowledge of the thermal properties of the grinding wheel, and these were measured from samples of actual grinding wheels. It was established from these measurements that the thermal conductivity of the grinding wheel was much lower than the conductivity of the grain material.

The dry grinding energy partition model of Rowe and Pettit is illustrated in Figure 5.1(a). The model illustrated excludes energy transfer to other heat sinks which were later included to modify the energy applied at the wheel - workpiece interface. The partitioning can be represented graphically as in Figure 5.1(b).

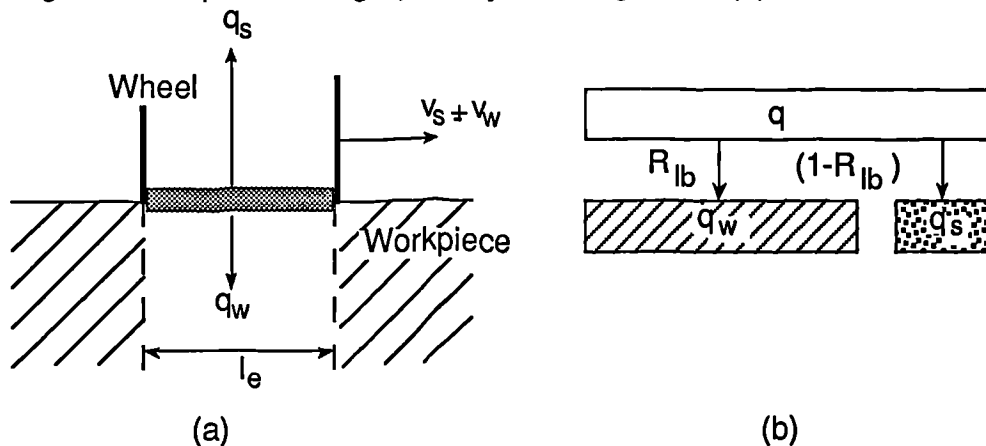


Figure 5.1 (a) The dry grinding energy partition model of Rowe and Pettit, and (b) a graphical representation of heat flux partitioning.

The specific heat flux entering the workpiece is

$$q_w = R \cdot q$$

This method of partitioning provided Rowe and Pettit with a solution termed the 'lower bound solution'. The lower bound solution led to the lowest possible estimate of power level corresponding to a particular maximum workpiece temperature.

## 5.2 THE SINGLE STAGE WORKPIECE - WHEEL - FLUID PARTITION MODEL.

Most grinding operations are performed with the aid of a grinding fluid. The grinding fluid has two main roles: cooling and lubrication which is often more important [57]. Lubrication reduces the friction between the wheel grits and the workpiece, thus improving the efficiency of the process by reducing total grinding forces, power and heat generated in the grinding zone. Reduced grinding forces also result in reduced levels of abrasive wear. The potential benefits of lubrication are illustrated in Figure 5.2.

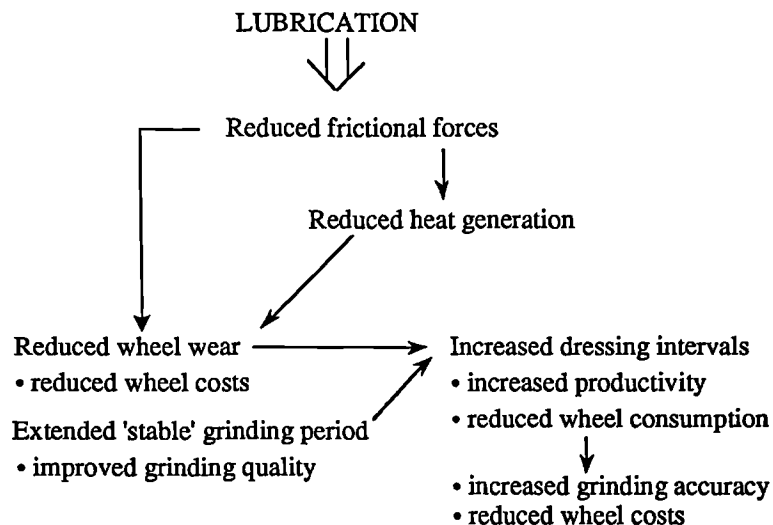


Figure 5.2 Potential benefits of lubrication in grinding operations.

Application of the fluid in grinding involves problems not encountered in other machining processes such as milling or turning. The wheel, rotating at relatively high speeds carries on its surface a layer of air which may divert the stream of fluid from the grinding zone. As a result the fluid reduces the workpiece bulk temperature without having any significant effect upon the grinding process. At a critical fluid velocity the fluid will penetrate the air layer and be convected into the grinding zone by hydrodynamic effects. To secure the optimum lubricating effect of the fluid in the

grinding zone it is therefore important that an effective delivery system is employed that ensures that the critical fluid velocity is exceeded.

Furston [32] used finite element methods to examine workpiece temperatures and the effect of coolant during its passage through the grinding zone in creep feed grinding. Graphical relationships between workspeed and convection coefficient were presented for assumed partition ratios for the fluid-workpiece combination. However, the analysis was applicable only to creep-feed grinding operations. In creep-feed grinding the role of the grinding fluid in provision of cooling in the grinding zone is much greater due to the increased contact length. It was concluded that in some operations the fluid can absorb up to 98 per cent of the heat generated. Okuyama, Nakamura and Kawamura [5] proposed a finite element method for determination of the heat transfer coefficient in shallow-cut grinding operations. Large differences in the value of the heat transfer coefficient were reported due to the effects of fluid nozzle velocity and flow rates, workpiece surface roughness and wheel speed, despite only a limited range of experimental grinding conditions used to test the theoretical model. This serves to highlight the problems in attempting to determine the specific energy convected to the grinding fluid when expressed as a function of the convective coefficient, and this is further discussed in chapter 6.

The workpiece - wheel - fluid model of Rowe and Pettit extends the previous model to include heat flux partitioning to the fluid. Because the temperature of interest is the average of a number of passing grains it is assumed that the cooling effect of the fluid takes place simultaneously with the partition between the wheel and the workpiece, Figure 5.3(a).

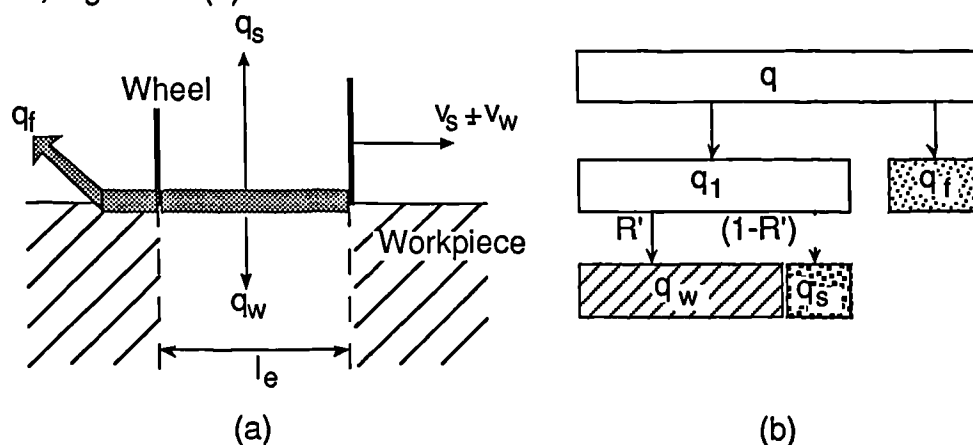


Figure 5.4 (a) The single stage workpiece - wheel - fluid partition model, and (b) a graphical representation of heat flux partitioning.

The specific heat flux entering the workpiece in this case is

$$q_w = R' [q - q_f]$$

$R'$  may be determined by application of appropriate modelling assumptions for the heat flows to the workpiece the grinding wheel and the fluid.

### 5.3 THE TWO STAGE WORKPIECE - WHEEL - FLUID PARTITION MODEL.

In the two-stage model it is proposed that the heat first enters the workpiece and the wheel and later some heat escapes to the fluid, Figure 5.4(a). The heat flux is the result of the averaging effect of a number of grains as in the previous example.

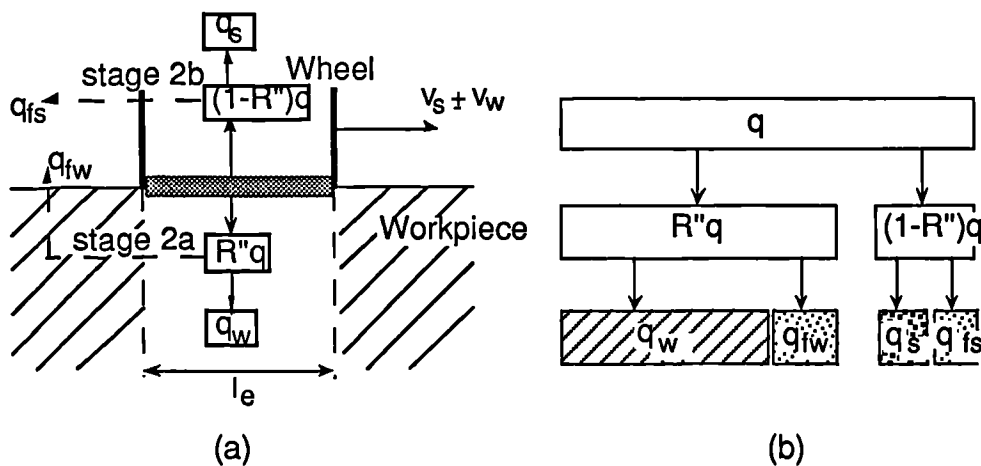


Figure 5.4 (a) The two stage workpiece - wheel - fluid partition model, and (b) a graphical representation of heat flux partitioning.

The stages of the partitioning are as follows:

- [1] The heat is divided initially between the workpiece and the wheel.
- [2a] The heat in the workpiece is further divided between the workpiece and the fluid.
- [2b] The heat in the wheel is divided between the wheel and the fluid.

The specific heat flux entering the workpiece for the two -stage process is

$$q_w = R'' \cdot q - q_{fw}$$

The heat flux entering the fluid via the wheel can be shown to be relatively small and probably has little influence on the workpiece background temperature [58].

A comparison of equation 154 with equation 155 shows that the effect of the fluid on the flux entering the workpiece is less in the single-stage model than in the two stage model. The single-stage model could therefore under-estimate the cooling effect of the fluid on the workpiece and as a consequence the predicted threshold temperature for thermal damage will be slightly higher than actual. However, it is debatable which method most closely agrees with reality purely from physical considerations. It was therefore decided to compare the results given by each method and determine the significance of the difference in treatment.

#### 5.4 THE SINGLE STAGE WORKPIECE - WHEEL - FLUID - CHIPS PARTITION MODEL.

This model develops the analysis to include heat flux partitioning to the grinding chips. In the single stage model the partitioning to the chips is assumed to take place simultaneously with the partitioning to the other heat sinks as shown in Figure 5.5(a).

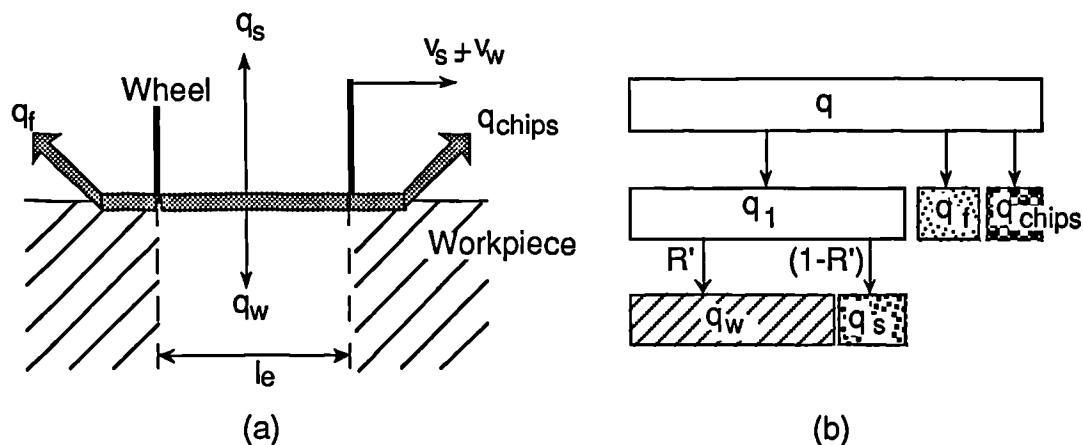


Figure 5.5 (a) The single stage workpiece - wheel - fluid - chips partition model, and (b) a graphical representation of heat flux partitioning.

After solving for  $R'$  the specific heat flux entering the workpiece can be found from,

$$q_w = R' \cdot [q - q_{chips} - q_f] \quad 156$$

For the purpose of determining the possible significance of the chips as a heat sink, it is assumed that the maximum heat which can be convected by the chips is the heat required to reach melting temperature. It has been argued that the actual proportion is less since the chips do not absorb sufficient energy to reach the melting temperature throughout the chip volume during the removal process [3].

The assumption that the chips reach melting temperature is likely to lead to an over-estimate of the heat convected away by the chips and as a consequence will over-estimate the specific energy required to achieve a particular value of maximum workpiece surface temperature. This partitioning model is consistent with the method proposed by Rowe and Pettit for the determination of their upper bound solution.

### 5.5 THE TWO STAGE WORKPIECE - WHEEL - FLUID - CHIPS PARTITION MODEL.

The two stage workpiece - wheel - fluid - chips model extends the two stage workpiece - wheel - fluid model to include energy partitioning to the grinding chips, Figure 5.6.

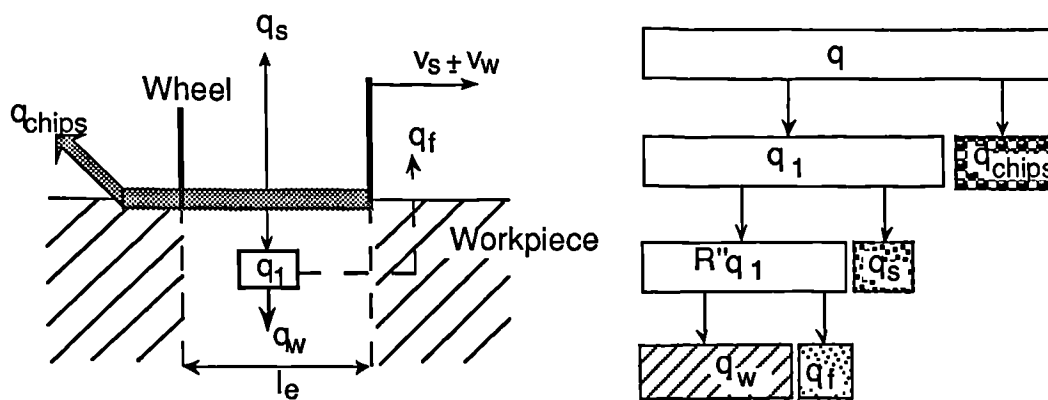


Figure 5.6 (a) The two stage workpiece - wheel - fluid - chips partition model, and (b) a graphical representation of heat flux partitioning.

The two stages of model development are as follows

- [1] The heat generated is divided in the zone of generation between the workpiece, wheel and the chips.
- [2] The heat flux entering the workpiece is further divided between the workpiece and the fluid.

The specific heat flux entering the workpiece for this model is

$$q_w = R'' [q - q_{chips}] - q_f \quad 157$$

## 5.6 EVALUATION.

It is not possible to undertake a direct investigation to test these models. Such an investigation would require temperature distributions to be measured with a better accuracy than is practicably attainable [58]. However, it is possible to calculate the critical value of specific energy predicted from each of the models, by assuming a particular critical temperature. It is also possible to measure the specific energy at the threshold of damage and use this to compare the mean workpiece background temperature predicted by each of the partitioning models. Equations 86, 87, 90, 91, 92 and 97 were used to evaluate the approaches previously outlined. The value of the lower bound partition ratio  $R$ , was calculated from equation 88. The values of the partition ratios  $R'$  and  $R''$  were calculated from equation 101A which was appropriately modified to correspond to the modelling assumptions for the energy flows to the grinding wheel, grinding fluid and grinding chips. The grinding power data was taken from a previously recorded experimental study of the AMTREL. The machining data for the experimental study is given in Table 5.1. The values of the model parameters used for the evaluation are given in Table 5.2. The real contact length was calculated from a relationship given by Verkerk [35], equation 84.

Table 5.1 Machining data.

Grinding machine	: Wickman Scrivener 2K
Process	: Centreless grinding
Grinding wheel	: 19AV60NVS
Workpiece material	: EN9 steel
Wheel speed	: 45 m/s
Workpiece speed	: 0.35 m/s
Infeed rate	: .25 mm/s
Coolant	: Trim VE20, dilution 50:1

Table 5.2 Model parameters.

Convection coefficient, $h$	: 17000 J/m <sup>2</sup> sC
Workpiece critical temperature, $\theta_m^*$	: 430°C
Fluid boiling temperature, $\theta_{fb}$	: 120°C
Grinding wheel thermal diffusivity, $\alpha_s$	: 1.145 x 10 <sup>-6</sup> m <sup>2</sup> /s
Grinding wheel thermal conductivity, $\kappa_s$	: 0.55 W/mK
Workpiece thermal diffusivity, $\alpha_w$	: 1.47 x 10 <sup>-5</sup> m <sup>2</sup> /s
Workpiece thermal conductivity, $\kappa_w$	: 53.7 W/mK

In Figure 5.7 the predicted values of critical specific energy are shown for each of the models outlined. A critical workpiece temperature of 430degC was assumed. At the time this evaluation was being undertaken, preliminary experimental work in the AMTREL suggested that the value of the assumed temperature was reasonable. Figure 5.8 shows the mean workpiece background temperature predicted from each of the models.

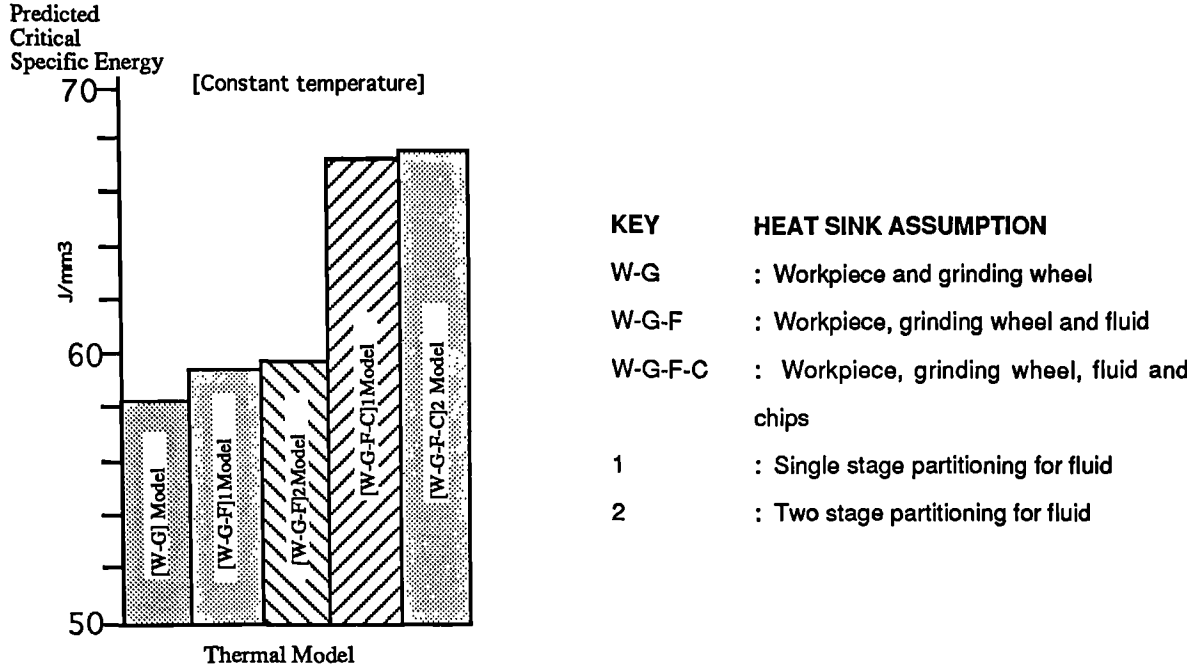


Figure 5.7 Values of critical specific energy predicted from each partitioning model.

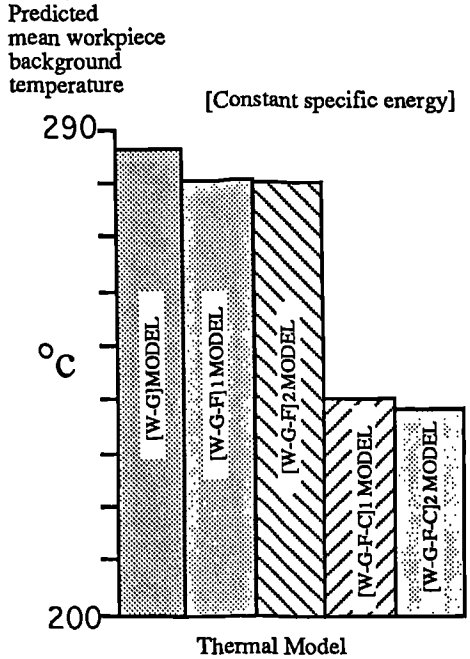


Figure 5.8 A comparison of the values of mean workpiece background temperature predicted from each of the partitioning models.

## **5.7 DISCUSSION.**

The modelling assumptions previously described each yield different equations for the heat flux applied to the workpiece. The single-stage partitioning models are consistent with the models developed by Rowe and Pettit for their upper and lower bound solutions. In contrast, Lavine considered the energy partitioning to the grinding fluid as a two stage process. The heat flux to the fluid enters via the workpiece.

Modelling the partition of heat flux to the fluid as either a single stage or a two stage process has only a marginal effect on the values of critical specific energy predicted by each of the models. This was due to the relatively low cooling effect of the fluid and is consistent with shallow cut grinding where the fluid acts essentially as a lubricant. It can be reasoned that for heavy duty grinding where the cooling effect of the fluid is greater, the difference between the results would be more marked.

The temperatures predicted from each of the models are above the fluid film boiling conditions which suggest it would be appropriate to revert to the dry grinding models.

## **5.8 CONCLUSIONS.**

The two-stage models may possibly describe the physical situation more accurately than the single stage models. However, it is difficult to resolve this question. Furthermore, fluid film boiling conditions reduce the significance of the fluid as a heat sink and the two methods of partitioning, single-stage or two-stage, yield similar results. It was therefore decided to apply the single-stage fluid modelling assumption to the analysis of heat flux partitioning to the fluid.

## Chapter 6 THEORY: MODEL DEVELOPMENT

The contact between the grinding wheel and the workpiece can be analysed at two levels, the grain - workpiece contact level and the grinding wheel - workpiece contact level. At the wheel - workpiece contact level the workpiece surface sees a relative speed of  $v_w$  whilst at the grain - workpiece contact level the workpiece surface sees a relative speed of contact of  $v_s$ . A result of the difference in the length and period of contact is that the workpiece experiences a different temperature phenomenon at each level of contact.

This chapter begins with a description of the tribological contact and grinding temperatures that occur at each level of contact. A new model is then presented that addresses partitioning at the grain level of contact and which overcomes conceptual difficulties inherent in previous approaches. The thermal analysis proceeds in four stages. In the first stage the heat transfer into a single grain is analysed using a conical grain model subject to a stationary heat source for a finite time. The heat transfer into the workpiece surface beneath a single grain is then analysed using a moving circular heat source model. An expression for the partition ratio is then derived using the assumption of an equal average surface temperature for both models. In the final stage a solution for the workpiece background temperature is derived from the solution for a moving band heat source proposed by Jaeger and the partition ratio developed previously. The chapter concludes with a summary of the equations used to describe the proposed thermal model.

### 6.1 GRINDING TEMPERATURES.

During grinding, a temperature spike of very short duration occurs beneath each active grain and a distributed set of much lower temperatures occurs within the grinding zone. In Figure 6.1 the workpiece background temperature and the temperatures beneath single grains are conceptualised.

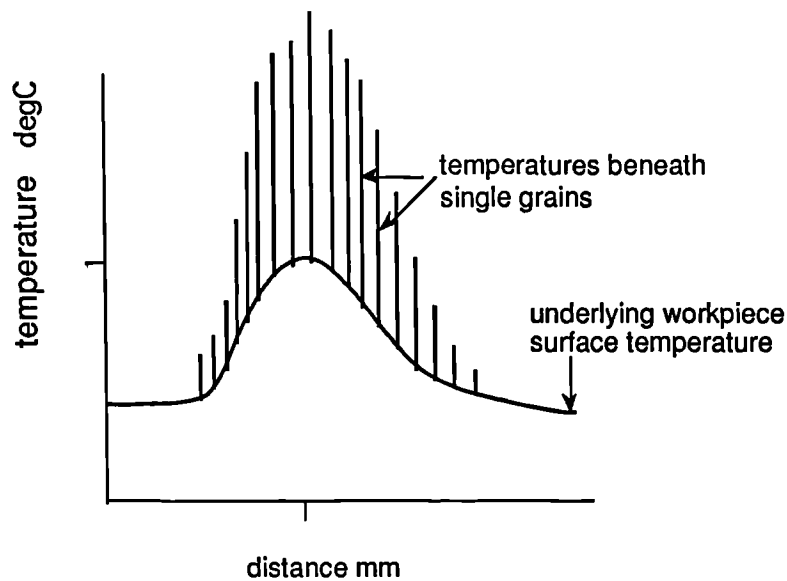


Figure 6.1 Conceptualised workpiece surface temperature and temperatures beneath individual grains.

The occurrence of thermal damage is both temperature and time dependent. Because the spike temperature is of extremely short duration compared with that for the distributed set of temperatures, the temperature of most importance is the mean workpiece background temperature,  $\theta_{wb}$  [7]. The average temperature distribution at the surface and below the surface may lead to damage which penetrates significantly below the surface [17].

## 6.2 THE GRAIN - WORKPIECE CONTACT.

A model representative of the tribological contact at the grain contact level is illustrated in Figure 6.2. A grinding wheel grain is considered to move across the surface of the workpiece at a speed  $v_s \pm v_w$ . The model depicts the wear flats of more than one cutting edge on the grain in contact with the workpiece surface. Each wear flat has a unique and changing length denoted by  $2r_{ox}$  where  $x$  varies up to the number of wear flats per grain.

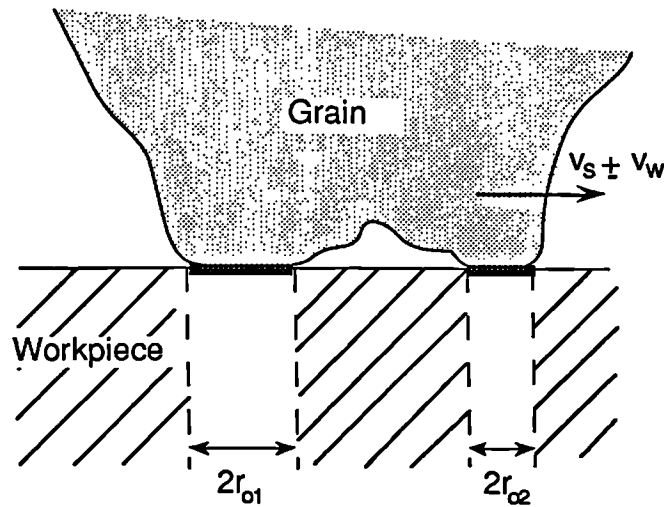


Figure 6.2 The grain level contact in grinding.

Verkerk [35] in a work that aimed to characterize the grinding wheel topography concluded that it was sufficient to consider the cutting edges that belong to the same grain as a single cutting edge. Verkerk reasoned that when there is more than one edge to a grain there is insufficient clearance between the edges to accommodate a chip. The trailing edges cannot therefore be active and the grain acts as a single cutting edge.

On this basis, a simplified model of the grain - workpiece contact can be used to analyse the heat transfer. In the simplified model illustrated in Figure 6.3, a grain with a contact dimension of  $2r_o$  is considered to move across the surface of the workpiece at a speed  $v_s \pm v_w$ .

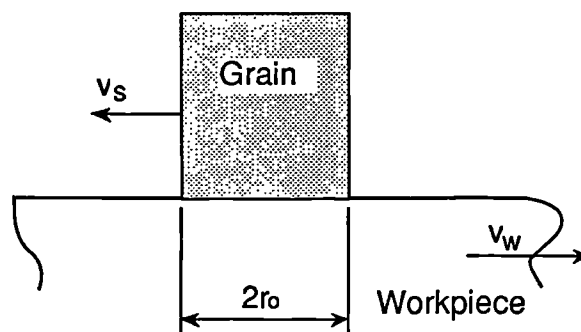


Figure 6.3 A simplified model of the grain level contact in grinding.

This approach is adopted because the contact dimension of the grain with the workpiece is relatively small compared with the arc length of contact of the grain as it passes through the grinding zone.

### 6.3 A MODEL FOR HEAT TRANSFER INTO A CYLINDRICAL GRAIN.

The workpiece experiences different temperature phenomena at the two levels of contact. At the grain level a point on the workpiece is in contact with a grain for a period  $2r_o/(v_s \pm v_w)$ . At the wheel - workpiece level the workpiece experiences a continuous heating over the length of contact  $l_e$  for a period  $l_e/v_w$ .

As an individual grain passes over the surface of the workpiece heat is generated at three locations: the grain - workpiece interface, the grain - chip interface and the shear plane between the workpiece and the chip. Representing each grain and workpiece interaction by the model of a conducting slider on a moving surface, as in Figure 6.3, can be justified on the grounds that the heat generated at the grain - chip interface and the heat generated at the shear plane is largely accounted for by energy to the chips and is therefore taken into account. Thus, only the heat generated at the grain - workpiece interface, which is often much larger, is considered in the partitioning model. By modelling each grain and workpiece interaction in this way the problem is simplified and reduces to a one-dimensional transient heat transfer problem.

According to Jaeger [16] a slider can either be represented as a protuberance on a larger body as shown in Figure 6.4(a), which is typical of many tribological contacts or as a long narrow slider, as shown in Figure 6.4(b), which might be more appropriate for a spikey grain.

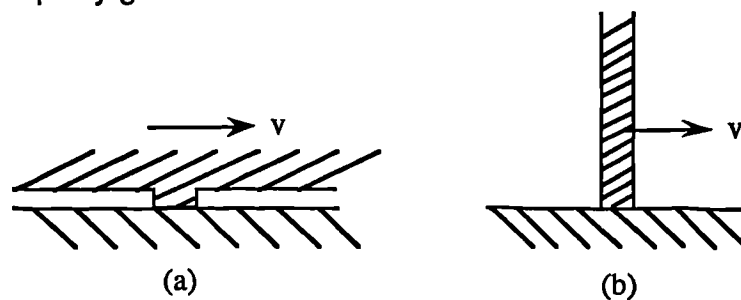


Figure 6.4 Conducting slider on a moving surface (after Jaeger [16]).

If the grain is assumed to be a cylinder of radius  $r$  as in Figure 6.5 then the problem is analogous to that of a continuous plane source, for which there is an exact solution, equation 24. Adopting the subscripts appropriate to Figure 6.5 the maximum surface temperature  $\theta_g$ , equation 158, is found from

$$\theta_g = \frac{2 q_g t^{1/2}}{(\pi \cdot \kappa \cdot \rho \cdot c)_g^{1/2}} \quad 158$$

where  $\kappa, \rho$ , and  $c$  are the conductivity, the density, and the specific heat capacity of the grain,  $q_g$  is the uniform heat flux applied to the grain contact face, and  $v_s$  is the grinding wheel speed.

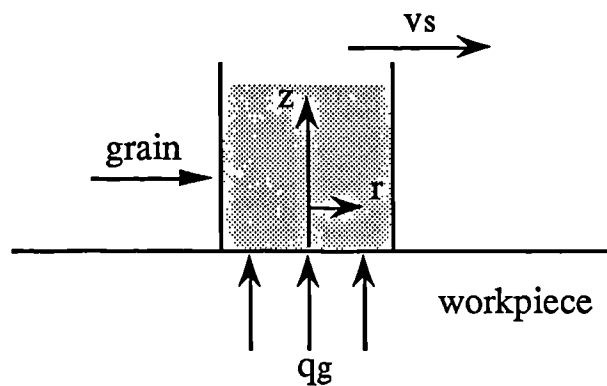


Figure 6.5 Model for heat transfer into a cylindrical grain.

At time  $t = l_e/v_s$ , the time the grain is in contact with the workpiece, equation 158a applies.

$$\theta_g = \frac{2}{\pi^{1/2}} \cdot \frac{q_g l_e^{1/2}}{[(\kappa \rho c)_g v_s]^{1/2}} \quad 158a$$

Equation 158 provides an expression for the transient temperature rise as the grain progresses through the contact zone from time  $t = 0$  to  $t = l_e/v_s$ .

#### 6.4 A MODEL FOR HEAT TRANSFER INTO A CONICAL GRAIN.

By describing the grain as a cylinder in section 6.3 the heat transfer model was simplified and it can be argued that a conical or spherical grain contact model would be more representative of the physical grain geometry.

Lavine [42, 43] appears to propose a solution for heat transfer into a conical grain. However, on close inspection it is found that the model is a one-dimensional analysis with the assumption of a uniform heat flux across a varying grain diameter. Thus temperature gradients are zero within a single plane. The simplification was defended on the basis that the external thermal resistance of the workpiece and the grinding fluid are very high compared with the internal resistance of the grain. However, the simplification is clearly invalid for large values of cone angle.

The analytical solution given by Lavine for the temperature  $\theta_g$  at the contacting surface of the grain was,

$$\theta_g = \frac{2}{\pi^{1/2}} \cdot \frac{q_g l_g^{1/2}}{[(k\rho c)_g v_s]^{1/2} f(\zeta)} \quad 159$$

where

$$f(\zeta) = \frac{2}{\pi^{1/2}} \cdot \frac{\zeta}{1 - \exp(\zeta^2) \cdot \text{erfc}(\zeta)} \quad 160$$

$$\zeta = [(\gamma^2 \alpha_g l_g) / (r_0^2 v_s)]^{1/2} \quad 161$$

and  $\gamma = dr_g/dz$ .  $A_0$  was the contact length of the grain (wear flat length),  $\alpha_g = \kappa/(\rho c)$  for the grain and  $l_g$  was the distance the grain was in contact with the workpiece.

A comparison of equation 159 with equation 158a shows that the two solutions differ by the factor  $f(\zeta)$ . The factor  $f(\zeta)$  was used to account for the increasing cross sectional area of the grain with increasing distance into the grain.

Lavine noted that on average the grains are as wide as they are high and for a conical grain with a cone angle of  $45^\circ$ ,  $\gamma$  is equal to 1. For a cylindrical grain  $\gamma = 0$ ,  $\zeta = 0$ ,  $f(\zeta) = 1$  and equation 159 reduces to equation 158a.

It is considered that the conical grain model describes the physical geometry of the grain more accurately than the cylindrical grain model. It can be argued that a spherical or other grain model shape would be even more appropriate than the

conical grain model. However, the temperature solution for a sphere is non-linear with respect to  $z$ , and so adds further complexity. The conical grain model therefore provides a useful basis from which to develop the thermal analysis.

## 6.5 HEAT TRANSFER INTO THE WORKPIECE UNDER A GRAIN.

The expression for temperature at the surface of the grain needs to be solved simultaneously with the expression for the temperature at the contacting surface on the workpiece. An appropriate solution for the temperature on a surface due to a circular sliding heat source was given by Archard [60], Figure 6.6.

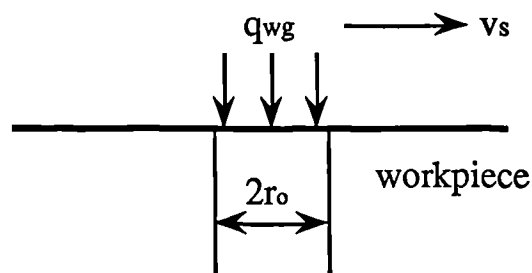


Figure 6.6 A circular heat source moving on the surface of the workpiece.

To derive the surface temperature solution, equation 162, for this case, Archard used the same arguments as Jaeger used for the band source solution.

$$\theta_{wg} = \frac{0.974q_{wg}r_o^{1/2}}{[(k\rho c)_w v_s]^{1/2}} \quad 162$$

where  $\theta_{wg}$  is the average temperature of the workpiece at the grain contact and  $q_{wg}$  is the corresponding heat flux. Equation 162 was said to be valid for values of Peclet number greater than 5, where  $L = (\dot{v}_s r_o)/(2\alpha_w)$ .

The circular heat source model was selected because it is consistent with the circular contact assumed for determination of heat flow into the grain. It is interesting to note that apart from a small change in the constant of proportionality, equation 162 is identical with the equation for a band source given by Jaeger, equation, 37.

## 6.6 PARTITION RATIO: LOWER BOUND.

Ignoring heat convected by the chips and fluid, the fraction of the heat flux entering the workpiece at any instant is  $R_{lb}q$  and the fraction entering the grain is  $(1-R_{lb})q$ . Equating the solution for the maximum temperature at the surface of the conical grain, equation 159, to the solution for the average temperature at the surface of the workpiece under a grain, equation 162, leads to an expression for the value of the partition ratio  $R_{lb}$ ,

$$\frac{2}{\pi^{1/2}} \cdot \frac{(1 - R_{lb})q_g l_e^{1/2}}{[(k\rho c)_g v_s]^{1/2} f(\zeta)} = \frac{0.974 R_{lb} q_w r_0^{1/2}}{[(k\rho c)_w v_s]^{1/2}} \quad 163$$

thus,

$$\frac{1}{R_{lb}} = 0.86 \left[ \frac{(k\rho c)_g}{(k\rho c)_w} \right]^{1/2} \left( \frac{r_0}{l_e} \right)^{1/2} f(\zeta) + 1 \quad 164$$

and

$$R_{lb} = \frac{F}{1 + F} \quad \text{where } F = \frac{1.16}{f(\zeta)} \left[ \frac{(k\rho c)_w}{(k\rho c)_g} \right]^{1/2} \left( \frac{l_e}{r_0} \right)^{1/2} \quad 165$$

Equation 165 represents the maximum value of the partition ratio which occurs at the end of the grinding contact zone.

An expression for the value of the partition ratio at any point  $x$  in the grinding contact zone can be found by replacing the contact length dimension,  $l_e$ , from equation 165, with  $x$  so that

$$R_{lbx} = \frac{F}{1 + F} \quad \text{where } F = \left( \frac{x}{r_0} \right)^{1/2} \left[ \frac{(k\rho c)_w}{(k\rho c)_g} \right]^{1/2} \frac{1.16}{f(\zeta_x)} \quad 166$$

where

$$\zeta_x = [(\gamma^2 \alpha_{g \cdot x}) / (r_0^2 v_s)]^{1/2} \quad 167$$

and

$$f(\zeta_x) = \frac{2}{\pi^{1/2}} \cdot \frac{\zeta_x}{1 - \exp(\zeta_x^2) \cdot \text{erfc}(\zeta_x)}$$

168

The relationship between  $f(\zeta_x)$  and the distance of contact  $x$  was established from a plot of  $\log f(\zeta_x)$  versus  $\log x$ . A typical plot is illustrated in Figure 6.7 for an aluminium oxide abrasive, with values of  $r_o = 25$  microns and  $v_s = 30$  m/s.

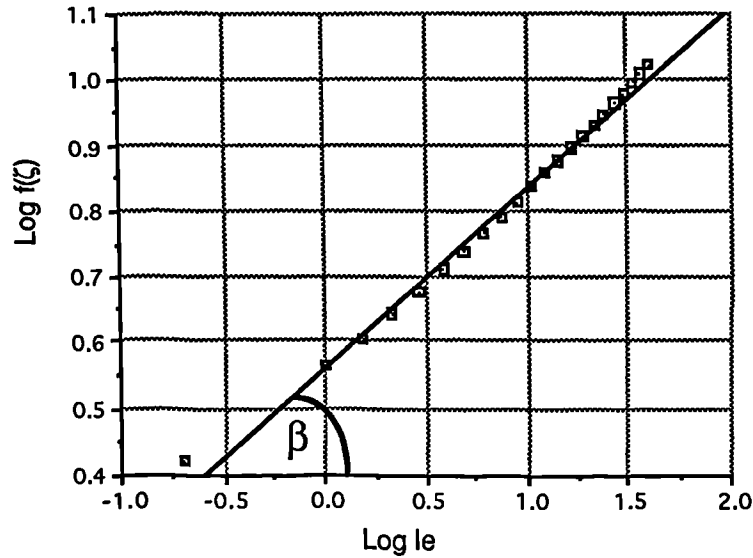


Figure 6.7 A plot of  $\log f(\zeta_x)$  versus  $\log l_e$  for  $r_o = 25$  microns and  $v_s = 30$  m/s.

The quantity  $f(\zeta_x)$  can thus be expressed as a function of  $x$  to the power  $\tan\beta$  where  $\tan\beta$  is the gradient of the curve  $\log f(\zeta_x)$  versus  $\log x$ . The approximate value of  $\beta$  from Figure 6.7 is  $15^\circ$ . A typical range of values of  $\beta$  is  $12^\circ$  to  $19^\circ$ .

It is therefore possible to write:  $f(\zeta_x) = x^{\tan\beta}$  168

and for the case  $x = l_e$ :  $f(\zeta_x) = l_e^{\tan\beta}$  169

A solution for the average partition ratio was found by substituting  $x$  to the power  $\tan\beta$  for  $f(\zeta_x)$  in equation 166 and integrating between the limits of 0 and  $l_e$ .

The relationship between  $F$  and  $x$  from equation 166 and equation 168 is,

$$F \propto \frac{x^{0.5}}{f(\zeta_x)} \equiv \frac{x^{0.5}}{x^{\tan\beta}} \equiv x^{0.5 - \tan\beta} \quad 170$$

Thus, for the average partition ratio,  $F_{av}$ ,

$$F_{av} \propto \frac{1}{l_e} \int_0^{l_e} F dx \quad 171$$

and

$$F_{av} \propto \frac{1}{l_e} \int_0^{l_e} x^{0.5 - \tan \beta} dx \quad 172$$

Integrating equation 172 gives,

$$F_{av} \propto \frac{1}{l_e} \left[ \frac{x^{1.5 - \tan \beta}}{1.5 - \tan \beta} \right]_0^{l_e} \quad 173$$

which evaluates to

$$F_{av} \propto \frac{l_e^{0.5 - \tan \beta}}{1.5 - \tan \beta} \quad 174$$

and can be rewritten as

$$F_{av} \propto \frac{l_e^{0.5}}{l_e^{\tan \beta} [1.5 - \tan \beta]} \quad 175$$

From equation 170 and equation 175

$$F_{av} \propto \frac{F}{1.5 - \tan \beta} \quad 176$$

so that the average partition solution is

$$F_{av} = \left[ \frac{(k\rho c)_w}{(k\rho c)_g} \right]^{1/2} \frac{1.16 F}{(1.5 - \tan \beta) (r_o)^{1/2}} \quad 177$$

With the function  $F$  expressed in terms of  $l_e$  and  $f(\zeta)$  the average partition solution is

$$F_{av} = \left(\frac{l_e}{r_o}\right)^{1/2} \left[\frac{(k\rho c)_w}{(k\rho c)_g}\right]^{1/2} \cdot \frac{1}{f(\zeta)} \cdot \frac{1.16}{1.5 - \tan\beta} \quad 178$$

Using the substitution,

$$\varphi = \frac{1.16}{1.5 - \tan\beta} \quad 179$$

the solution for the average partition ratio can be expressed as

$$R_{lb} = \frac{F_{av}}{1+F_{av}} \text{ where } F_{av} = \left(\frac{l_e}{r_o}\right)^{1/2} \left[\frac{(k\rho c)_w}{(k\rho c)_g}\right]^{1/2} \cdot \frac{\varphi}{f(\zeta)} \quad 180$$

Equation 180 is valid for all values of  $\zeta$ , however, at values of  $\zeta$  greater than 3, the quantity  $[1 - \exp(-\zeta^2) \cdot \text{erfc}(\zeta)]$  in equation 160 approaches 0.85, Figure 6.8, and  $f(\zeta)$  is approximately equal to  $1.13\zeta$ . The error at  $\zeta$  equals 3 is approximately 15 per cent.

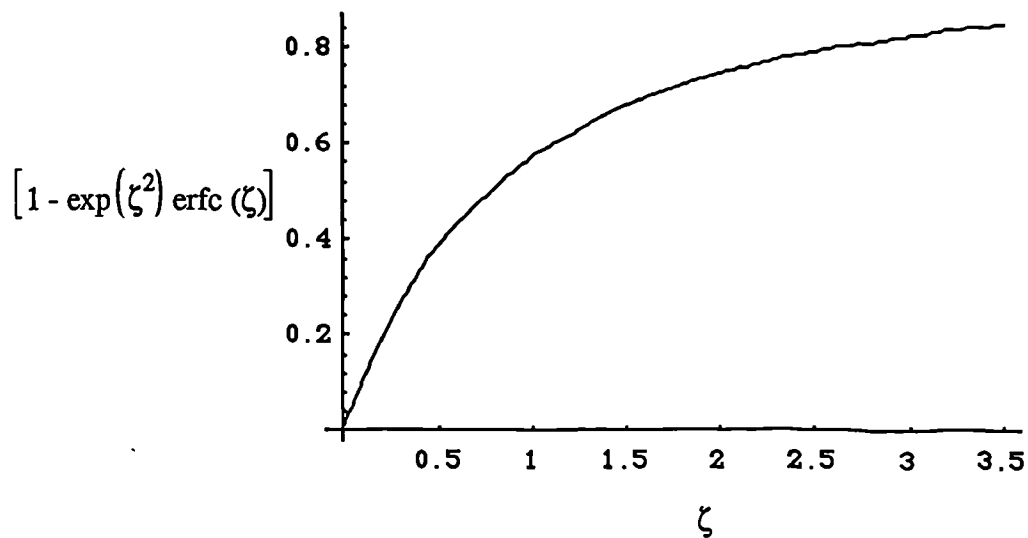


Figure 6.8 The relationship between the quantity  $[1 - \exp(-\zeta^2) \cdot \text{erfc}(\zeta)]$  and zeta.

An approximate solution for the average value of the partition ratio  $R_{lb}$ , at values of  $\zeta$  greater than 3 is

$$R_{1b} = \frac{F_{av}}{1+F_{av}} \text{ where } F_{av} = \left( \frac{l_e}{r_0} \right)^{1/2} \left[ \frac{(kpc)_w}{(kpc)_g} \right]^{1/2} \frac{1}{2\zeta}$$

181

The basis of the analysis for the approximate solution of equation 181 is a transient model, however, the solution is independent of time and reference to a contact length model is not required.

Malkin [3] published an illustration of grain wear flats that appeared on a conventional grinding wheel. The wear flats were observed through an optical microscope and found to be approximately 20 - 50 microns in length. Optical microscopy examinations undertaken in this investigation provided further evidence of wear flats on a conventional grinding wheel that are of similar and smaller dimensions.

The relationship between  $\zeta$  and  $r_0$  is illustrated in Figure 6.9 for an aluminium oxide abrasive and different values of real contact length.

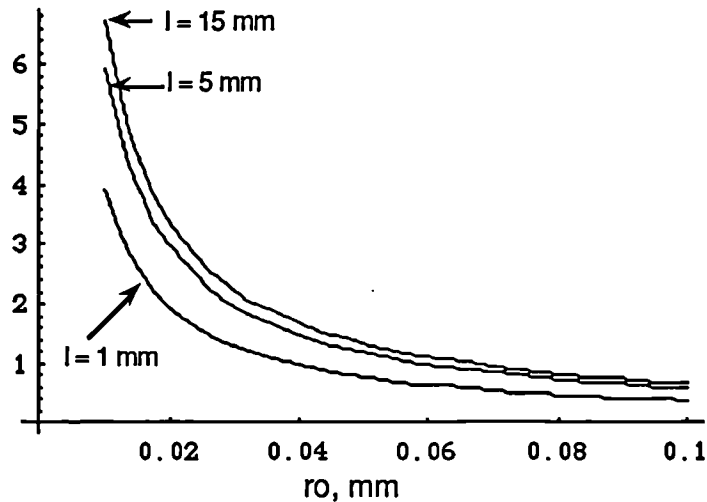


Figure 6.9 The relationship between  $\zeta$  and  $r_0$  for different lengths of contact.

For conventional wheels  $\phi$  is found to vary between 0.85 and 1.0 depending upon the grinding wheel condition and the values of grinding parameters. For the value  $\beta = 15^\circ$  from Figure 6.7,  $\phi = 0.95$ . In Figure 6.10  $\log f(\zeta_x)$  is plotted against  $\log l_x$  for different values of  $r_0$ . At the higher values of  $r_0$  there is little variation in the value of  $\log f(\zeta_x)$  for increasing values of  $\log l_x$ .

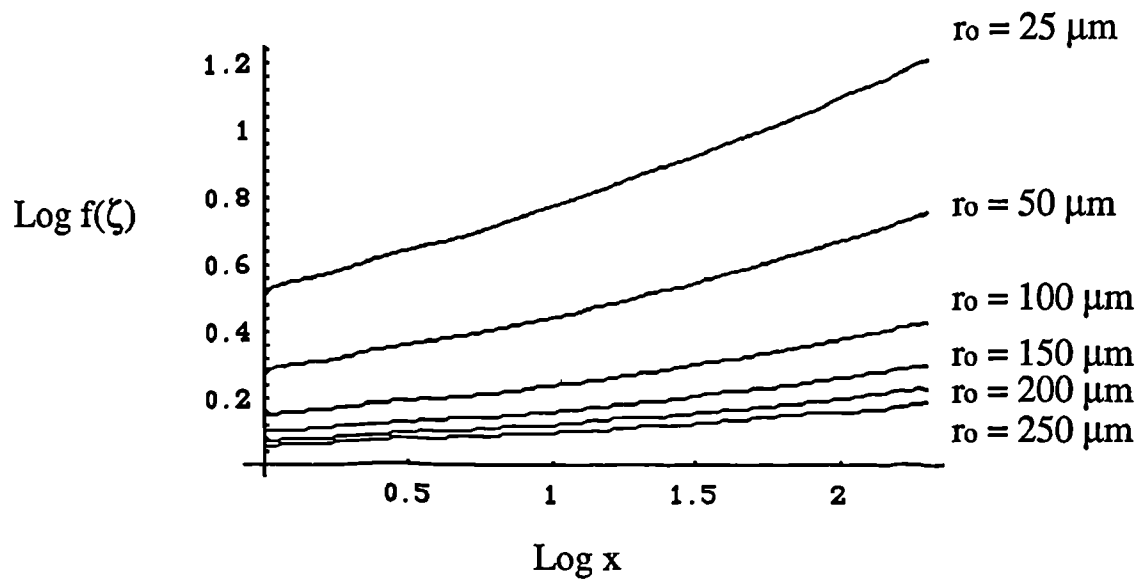


Figure 6.10 A plot of  $\log f(\zeta_x)$  versus  $\log x$  for a range of values of  $r_0$ .

Equations 180 and 181 may be compared to that for the partition ratio in the Rowe and Pettit model which by rearranging is given by,

$$R_{lb} = \frac{F_{av}}{1+F_{av}} \text{ where } F_{av} = \left( \frac{v_w}{v_s} \right)^{1/2} \left[ \frac{(k\rho c)_w}{(k\rho c)_s} \right]^{1/2} \quad 182$$

In the Rowe and Pettit model the suffix s refers to the the properties of the composite wheel rather than the grain properties which are denoted by the suffix g. It will be observed that the speed ratio seen in the Rowe and Pettit model does not feature in the new model. This is a significant difference between the two models which is more pronounced with materials such as CBN which exhibit a very high thermal conductivity.

If the cylindrical grain model is assumed, equating the temperature solution from equation 158 to the temperature solution from equation 162 yields the expression for the partition ratio,

$$R_{lb} = \frac{F_{av}}{1+F_{av}} \text{ where } F_{av} = 1.16 \left( \frac{l_e}{r_0} \right)^{1/2} \left[ \frac{(k\rho c)_w}{(k\rho c)_g} \right]^{1/2} \quad 183$$

which differs from the approximate conical grain partition solution for conventional abrasives by the reciprocal of the shape factor  $\zeta$ .

## 6.7 THE WORKPIECE BACKGROUND TEMPERATURE IN THE GRINDING CONTACT ZONE.

It was previously established in Section 6.1 that the most important measure of temperature for thermal damage is the maximum workpiece background temperature  $\theta_{wb}$  rather than the grain contact temperature  $\theta_g$ . This is because  $\theta_{wb}$  is sustained for a longer period and can lead to effects such as tempering and grain modification of the workpiece surface. The maximum workpiece background temperature at the workpiece surface can be determined for the wheel - workpiece contact in the usual way using the band heat source model and the previously determined value of partition ratio. The thermal flux into the workpiece which has now been determined can be considered as a band source which moves across the stationary workpiece surface at a speed  $v_w$  as illustrated in Figure 6.11, for the real length of contact,  $l_e$ .

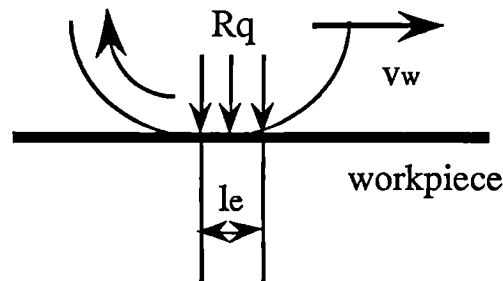


Figure 6.11 A band source moving across a stationary workpiece surface at speed  $v_w$ .

By reference to equation 36 the solution for the maximum workpiece background temperature,  $\theta_m$ , is given by,

$$\theta_m = 1.13 \frac{Rq}{(k\rho c)_w^{1/2} \left[ \frac{l_e}{v_w} \right]^{1/2}} \quad 184$$

where  $R$  is the partition ratio,  $l_e = 2l$ ,  $L = vl/(2\alpha)$  and  $\alpha = \kappa/(\rho c)$ .

## 6.8 GRINDING CONTACT LENGTH.

The grinding contact length is used in the thermal model to define the dimension of the heat source. A difference in the dimension of the heat source will affect the

magnitude of the heat flux entering the workpiece. In Figure 6.12 the geometric contact length and the real contact length calculated from an equation proposed by Rowe and Qi [38] are shown against the depth of cut.

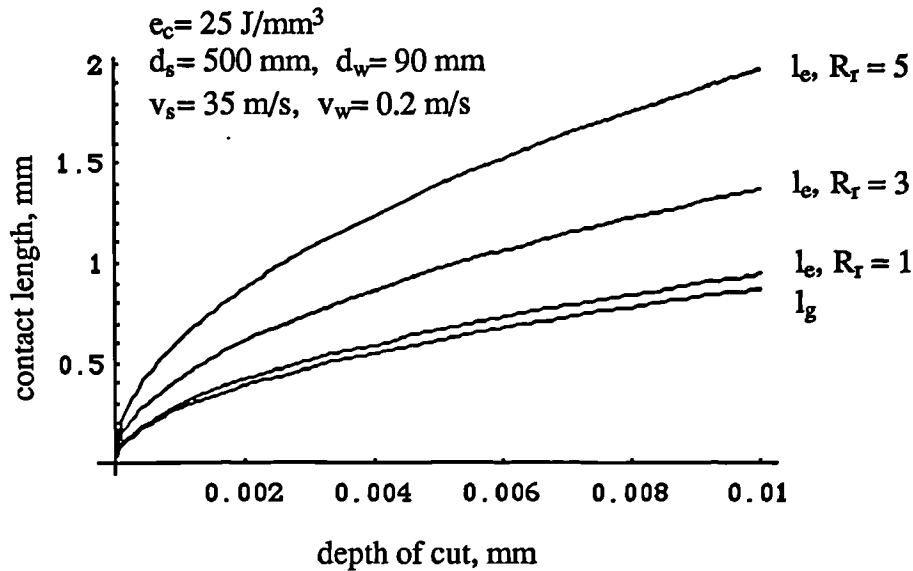


Figure 6.12 Comparison of geometric contact length and real contact length according to Rowe / Qi, for different values of roughness ratio  $R_r$ .

The real contact length  $l_e$ , was represented as the combination of the deformation contact length and the geometric contact length according to the orthogonal relationship given in equation 185.

$$l_e = \sqrt{l_g^2 + l_f^2} \quad 185$$

where  $l_f$ , the contact length due to deformation as a result of applied force, was defined by equation 186.

$$l_f = \left[ 8 R_r^2 F_n' (K_s + K_w) d_s \right]^{1/2} \quad 186$$

The parameters in equation 186 were determined from

$$K_s = (1 - \nu_s^2) / \pi E_s \quad , \quad K_w = (1 - \nu_w^2) / \pi E_w$$

where

$\nu$  = Poisson's ratio

$E$  = Young's Modulus

$F_n'$  = specific normal force,  $\mu = F_t / F_n$

$R_r$  = roughness ratio

Typical values for the parameters were given in reference 38 as

$\nu_s = 0.29$ ,  $\nu_w = 0.22$ ,  $E_s = 213 \text{ KN/mm}^2$ ,  $E_w = 449.6 \text{ KN/mm}^2$ ,  $\mu = 0.4$ ,  $R_r = 5$ .

It is seen from Figure 6.12 that with  $R_r$  equal to 5, the contact length increases to a maximum of approximately three times the geometric contact length for the range of depth of cut considered. It was concluded in reference 38 that further work was required to establish accurate values of  $R_r$ , however, a value of  $R_r$  equal to 5 was proposed as reasonable. The real contact length predicted by the relationship in equation 185 was more accurately representative of measured values than contact length predicted from previous models. Based on this argument, the results of Rowe and Qi were used to determine the contact length required for the thermal analysis.

## 6.9 A SOLUTION FOR THE LOWER BOUND CRITICAL SPECIFIC ENERGY.

By setting the maximum workpiece background temperature equal to the critical workpiece temperature, and substituting for  $q = (e_c v_w a) / l_e$ , the critical specific energy,  $e_c^*$ , in terms of the thermal conductivity  $\kappa$ , has been shown from equation 90 to be equal to

$$e_c^* = 0.89\theta_m^* \left[ \frac{l_e}{v_w} \right]^{1/2} [\kappa \rho c]^{1/2} \frac{1}{R_{Ib} a} \quad 187$$

$\theta_m^*$  is the critical workpiece temperature that should not be exceeded for a particular workpiece material. It is important to realise that the critical temperature selected should be based on the nature of the damage it is intended to avoid. The critical temperature for some materials will be the tempering threshold. For other materials it will be the transformation temperature for the production of austenite. The important requirement is to select the critical temperature according to the change which must be avoided.

Equation 187 does not include terms for the specific energy convected by the chips or the coolant. Thus equation 187 represents a lower bound solution.

## 6.10 A SOLUTION FOR THE UPPER BOUND CRITICAL SPECIFIC ENERGY.

An upper bound solution, equation 188, is obtained when convective terms for the chips,  $e_{cc}$ , and the coolant,  $e_{cf}$ , are included in equation 187.

$$e_c^*(\text{upper bound}) = e_c^*(\text{lower bound}) + e_{cc} + e_{cf} \quad 188$$

When the energy levels exceed the upper bound damage will definitely occur.

### 6.10.1 CONDUCTION TO THE GRINDING CHIPS.

In the previous review of the Rowe and Pettit model [7] it was proposed that the energy conducted to the chips can be expressed in terms of the density, the specific heat capacity and the difference between the ambient temperature and the chip melting temperature.

$$e_{cc} = \frac{P}{Z} = \frac{a.v_w.b.\rho.c.\Delta\theta_c}{a.v_w.b} = \rho.c.\Delta\theta_c \quad 189$$

Equation 189 was considered to over-estimate the specific energy conducted to the chips as it was reasoned that the chips cannot absorb more than sufficient energy to melt. Malkin [22] previously argued that the chips do not usually absorb sufficient energy to reach their melting temperature during the removal process.

### 6.10.2 CONVECTION BY THE GRINDING FLUID.

Expressed in terms of the specific material removal rate and the heat flux, the specific energy entering the fluid is given by,

$$e_{cf} = \frac{P_f}{Z} = \frac{b.h.l_e\theta_f}{a.v_w.b} = \frac{h.l_e\theta_f}{a.v_w} \quad 190$$

The magnitude of the specific energy  $e_{cf}$ , convected by the fluid in the grinding contact zone is strongly dependent on the value of the convection coefficient,  $h$ , and the temperature rise  $\theta_f$ . The units of  $h$  are in watts per square metre per Celsius degree when the heat flux  $q$ , is in watts/square metres.

Equation 191, derived from Newton's law of cooling, is the defining equation for the convection coefficient  $h$ .

$$q = h \cdot \theta_f$$

191

The value of  $h$  may be calculated for some systems. However, in grinding where the true volume of fluid in the grinding zone is not known and where the fluid flow is complex the value of the convection coefficient needs to be estimated experimentally. In all the analytical models referred to in previous chapters a constant convection coefficient was assumed throughout the contact zone. The effect of this assumption would be to over-estimate or under-estimate the cooling effect of the fluid dependent on the error in the value of  $h$  used.

An important tribological principle is the recognition of the difference between the real area of contact ( $A_r$ ) and the apparent area of contact ( $A_a$ ). For grinding, the ratio  $A_r/A_a$  is the ratio of the total wear flat area divided by the total apparent area of the grinding zone. The ratio  $A_r/A_a$  in fine grinding operations is typically of the order of 0.01 [38], thus over most of the grinding zone the fluid is assumed to come into contact with the workpiece surface. This assumption yields the maximum cooling effect possible.

### 6.10.3 A "FLUID WHEEL" MODEL.

If it is assumed that the fluid is at rest with respect to the grinding wheel and is pumped through the grinding zone by the hydrodynamic action of the wheel an estimate of the energy to the fluid can be obtained by considering the fluid as a moving semi-infinite solid with a uniform heat flux applied at its surface. Figure 6.13 illustrates the band heat source model applied to the fluid.

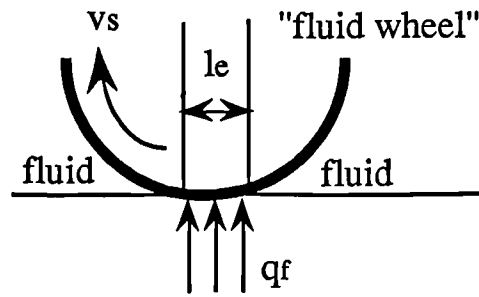


Figure 6.13 A fluid wheel model and a heat source moving at  $v_s$ .

For water based grinding fluids film boiling occurs at a temperature of approximately  $120^\circ\text{C}$  [5]. Above this temperature the cooling effect of the fluid is greatly reduced and the conditions are essentially those of dry grinding. Where the critical temperature for grinding damage exceeds the boiling point of the fluid  $\theta_{fb}$ , the maximum heat convected by the fluid is that quantity of heat required to boil the fluid. By setting the maximum temperature in equation 36 to the boiling point of the fluid less the ambient temperature ( $\theta_{fm} = \theta_{fb} - \theta_{famb}$ ) the maximum specific energy convected by the fluid can be estimated for values of  $L > 5$  from,

$$\theta_{fm} = 1.13 \frac{q_f}{(k\rho c)_f^{1/2} l_e v_s} \left[ \frac{l_e}{v_s} \right]^{1/2} \quad 192$$

By substituting the heat flux with terms for specific material removal rate and specific energy, equation 192 can be rearranged to give an expression for the maximum specific energy convected by the fluid,

$$e_{cf} = \frac{0.89}{a \cdot v_w} \theta_{fm} (k\rho c)_f^{1/2} (l_e v_s)^{1/2} \quad 193$$

### 6.11 PARTITION RATIO: UPPER BOUND.

From equations 187, 189 and 193 the upper bound partition ratio implied by the upper bound solution for the total energy entering the workpiece is given by

$$R_{eff} = R_{lb} \left( \frac{e_c - e_{cc} - e_{cf}}{e_c} \right) = R_{lb} (1 - J) \quad 194$$

## 6.12 PARAMETER RELATIONSHIPS IN GRINDING.

The fundamental grinding parameters are described by their relationship to the kinematics of the process. In centreless grinding, the depth of cut  $a$ , is given by

$$a = \frac{\pi}{2} d_w \frac{v_f}{v_w} \quad 195$$

The equivalent wheel diameter  $d_e$ , which is equivalent to the diameter of a wheel that would be used for surface grinding, is given by

$$d_e = \frac{d_w d_s}{d_w + d_s} \quad 196$$

The material removal rate is,

$$Z = \frac{\pi}{2} d_w v_f b \quad 197$$

A simplified equation for the geometric contact length is,

$$l_g = \sqrt{a d_e} \quad 198$$

Equation 198 is derived from the assumption of a large grinding wheel diameter compared to the depth of cut.

The specific energy is,

$$e_c = \frac{P}{Z} = \frac{P}{a \cdot b \cdot v_w} \quad 199$$

Equations 195 to 199 were used to analyse the results presented in the sections that follow.

## 6.13 SUMMARY

Energy partitioning has been analysed for the average grain contact zone and hence for the whole grinding wheel-workpiece zone. The essential features of the analysis may be summarised as follows:

[i] The model of a stationary conical grain subject to a heat flux applied for a finite time may be used to express the heat conduction into a grain at the grain contact level.

[ii] The model of a moving circular heat source may be used to determine the energy entering the workpiece beneath a single grain.

[iii] The average surface temperature for the conical grain model can be equated to the average surface temperature for the moving circular heat source model to determine an expression for the partition ratio at any point in the contact zone.

[iv] An average lower bound partition ratio may be derived for the real length of contact. The value of the partition ratio is determined from the grain contact level analysis.

[v] At the macro contact level a solution for the maximum background surface temperature is derived by modelling the workpiece subject to a moving band source of strength  $Rq$  and of length  $l_e$ . A solution for the critical specific energy is found by rearranging the terms in the band source temperature solution.

The average partition ratio solution is analytically more accurate than the steady state partition ratio solution proposed by Lavine, which equates the maximum grain temperature at the end of the grinding zone to the average increase in workpiece temperature under a grain plus the average workpiece background temperature in one paper [42] and to the maximum workpiece background temperature in another [11].

The value of the partition ratio is dependent on the ratio of the grain and workpiece thermal properties, the ratio of the real contact length to the grain contact length, and the value of the factor  $\zeta$  which is used to account for the increasing cross sectional area of the grain with increasing distance into the grain. Two partition solutions have

been derived. The first solution, equation 180, is for all values of  $\zeta$ . A second, approximate solution, equation 181, is simpler in form than the first, and can be applied at values of  $\zeta$  greater than 3. The approximate solution is a steady state solution and does not require a contact length model.

At the grain level the workpiece sees a relative speed of  $v_s \pm v_w$  whereas at the grinding zone level the workpiece sees a relative speed of  $v_w$ . The thermal model proposed makes clear the distinction between the relative speed seen by the workpiece at each of the two contact levels.

The equations proposed for the thermal model are summarised in Table 6.1.

Table 6.1 Summary of equations for the proposed thermal model .

[i] Heat transfer into a grain:	$\theta_g = \frac{2}{\pi^{1/2}} \cdot \frac{q_g l_e^{1/2}}{[(k\rho c)_g v_s]^{1/2} f(\zeta)}$
Conical grain model	
$\theta_g$ = maximum grain temperature	
[ii] Heat transfer into the workpiece under a grain:	$\theta_{wg} = \frac{0.974 q_{wg} r_o^{1/2}}{[(k\rho c)_w v_s]^{1/2}}$
Circular heat source model	
$\theta_{wg}$ = average workpiece temperature under a grain	
[iii] Partition ratio	$R_{1b} = \frac{F_{av}}{1+F_{av}} \text{ where } F_{av} = \left(\frac{l_e}{r_o}\right)^{1/2} \left[\frac{(k\rho c)_w}{(k\rho c)_g}\right]^{1/2} \cdot \frac{\phi}{f(\zeta)}$
Conical grain model	
Approximate lower bound solution $\zeta < 3$	
[iv] Partition ratio: Lower bound solution	$R_{1b} = \frac{F_{av}}{1+F_{av}} \text{ where } F_{av} = \left(\frac{l_e}{r_o}\right)^{1/2} \left[\frac{(k\rho c)_w}{(k\rho c)_g}\right]^{1/2} \cdot \frac{1}{2\zeta}$
$\zeta > 3$ - Conical grain model	
[v] Workpiece temperature solution	$\theta_m = 1.13 \frac{Rq}{(k\rho c)_w^{1/2}} \left[\frac{l_e}{v_w}\right]^{1/2}$
$\theta_m$ = maximum background temperature	
[vi] Critical specific energy	$e_c^*(\text{lower bound}) = 0.89 \theta_m^* \left[\frac{l_e}{v_w}\right]^{1/2} [k\rho c]^{1/2} \frac{1}{R_{1ba}}$
Lower bound solution	
[vii] Critical specific energy	$e_c^*(\text{upper bound}) = e_c^*(\text{lower bound}) + e_{cc} + e_{cf}$
Upper bound solution	
[viii] Maximum specific energy convected by the grinding fluid	$e_{cf} = \frac{0.89 \theta_{fm}}{a \cdot v_w} (k\rho c)_f^{1/2} (l_e v_s)^{1/2}$
[ix] Partition ratio: Upper bound solution	$R_{eff} = R_{1b} \left( \frac{e_c - e_{cc} - e_{cf}}{e_c} \right) = R_{1b} (1 - J)$

## Chapter 7 THEORETICAL STUDY.

This chapter is in two parts. In the first part, theoretical results are presented to illustrate the nature of the thermal model. The effect of changes of parameter values  $r_0$ ,  $\phi$ ,  $\gamma$ ,  $\zeta$  and  $\kappa$  on the predicted value of the lower bound partition ratio, equation 180, is examined. Except where explicitly indicated, the results presented are for alumina and CBN abrasive materials and a mild steel workpiece material.

In the second part, theoretical limit charts are derived for the conical grain model. Lower bound values of partition ratio predicted from the conical grain model are then compared with lower bound values of partition ratio predicted from other theories reviewed in chapter 3. For a particular case, upper bound values of partition ratio are shown with lower bound values of partition ratio to illustrate the effect of including heat partitioning to the chips and fluid. The particular equations used are given in the relevant section.

### 7.1 PARAMETRIC INVESTIGATION OF THE CONICAL GRAIN MODEL.

The value of the parameters used for the theoretical study are given in Table 7.1.

Table 7.1 Values of parameters used for the theoretical study.

Parameter	Al <sub>2</sub> O <sub>3</sub>	CBN
$\kappa_g$	35 W/mK	250 W/mK
$\rho_g$	3900 kg/m <sup>3</sup>	3500 kg/m <sup>3</sup>
$c_g$	765 J/kgK	506 J/kgK
$r_0$	50 $\mu$ m	25 $\mu$ m
	<b>Workpiece material</b>	
$\kappa_w$	57 W/mK	
$\rho_w$	7650 kg/m <sup>3</sup>	
$c_w$	460 J/kgK	

$$\phi = 0.85$$

$$\gamma = 1$$

$$d_w = 40 \text{ mm}$$

$$d_s = 450 \text{ mm}$$

$$R_r = 5$$

$$v_s = 35 \text{ m/s}$$

In Figure 7.1 the lower bound partition ratio is shown against grain contact radius  $r_0$ . The grain contact radius is seen to have a strong effect on the value of partition ratio at the lower values of  $r_0$ . At low values of  $r_0$  the Peclet number, evident in the Archard solution, reduces to a value less than 5. The Archard solution used is not valid at Peclet numbers less than 5 and this explains why the model fails at low  $r_0$  values. For typical values of  $r_0$ ,  $25 < r_0 < 100 \mu\text{m}$ , the effect of grain contact radius on the partition ratio is slight. For the particular case examined, the model predicts that CBN is approximately twice as efficient at removing heat energy from the grinding zone than alumina. The relationship illustrated in Figure 7.1 assumes a constant specific energy at varying values of  $r_0$ . This is clearly an invalid assumption, however for illustrative purposes it does allow the tendency of the relationship of partition ratio with  $r_0$  to be presented.

In Figure 7.2 the effect of parameter  $\phi$  on the lower bound partition ratio is shown. Within the typical range of values of  $\phi$ ,  $0.85 < \phi < 0.95$ , the partition ratio varies between 0.68 and 0.71 for alumina and between 0.63 and 0.66 for CBN. In the case illustrated, the partition ratio is similar in magnitude for the two materials. This is due to the assumption of a fixed value of  $\zeta$ .

The effect of cone angle is illustrated in Figures 7.3 and 7.4. The relationship between  $\zeta$  and cone angle for varying values of  $r_0$  is shown first. A large value of cone angle increases  $\zeta$ . A large value of  $\zeta$  increases the time constant of the transient grain response, which can be deduced from equation 161. For a cone angle of  $45^\circ$  the value of  $r_0$  has an increased effect on  $\zeta$  when  $r_0 < 10 \mu\text{m}$ . The results in Figure 7.3 suggest that for most practical situations where  $r_0$  is in the range  $25 < r_0 < 100 \mu\text{m}$ ,  $\zeta$  is less than 3. The effect of cone angle on the value of  $\zeta$  is more pronounced with CBN. In Figure 7.4 the lower bound partition ratio is shown against cone angle. The model predicts only a slight change in the value of lower bound partition ratio with increasing cone angle for alumina. However, for CBN the effect of cone angle is more significant, varying between  $R_{lb} = 0.72$  at a cone angle of  $15^\circ$  and  $R_{lb} = 0.53$  at a cone angle of  $40^\circ$ . This is due to the high value of  $\alpha_g$  (CBN) which features in the equation for  $\zeta$ . The results for CBN indicate that the relationship between grain contact radius and grain thermal properties is more important for materials of a high thermal conductivity.

The lower bound partition ratio is shown against  $\zeta$  in Figure 7.5, for the general solution and for the approximate solution. For values of  $\zeta > 3$  the partition ratio predicted from the approximate solution will be in error by approximately +10 per cent. The results of Figure 7.5 assume a fixed value of cone angle, thermal diffusivity and time constant, consequently the relationship illustrated may thus be interpreted as the effect of grain contact radius.

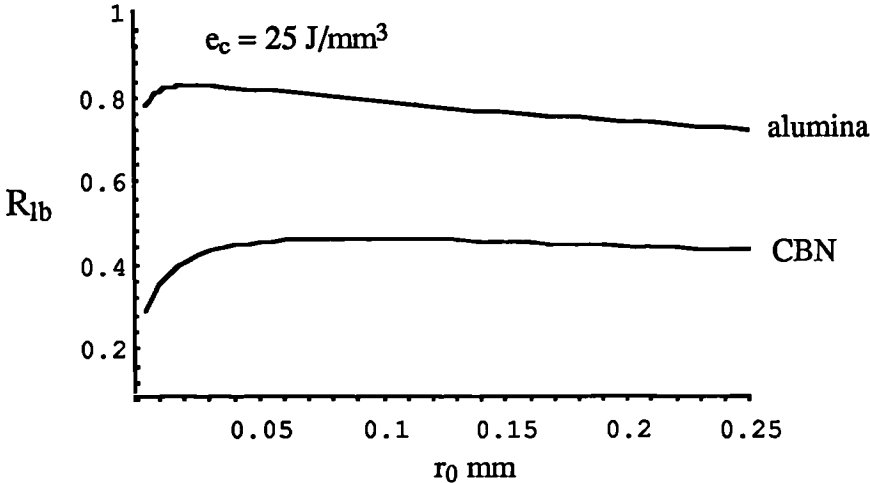


Figure 7.1 The variation of lower bound partition ratio with increasing contact radius,  $r_0$ .

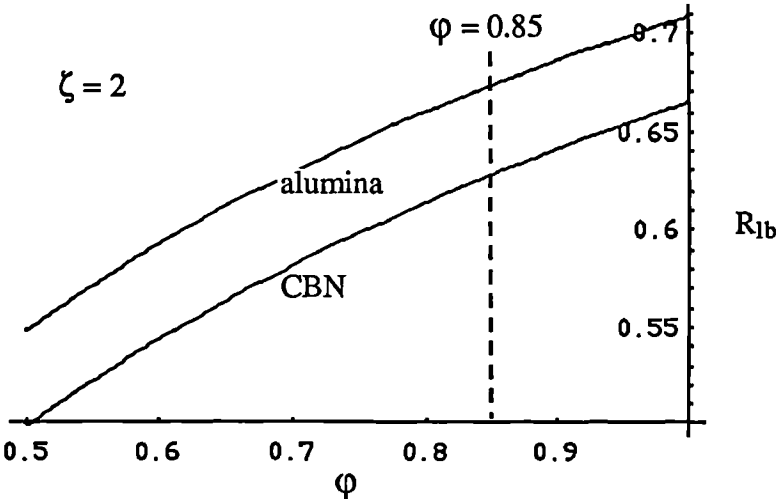


Figure 7.2 The effect of parameter  $\phi$  on the lower bound partition ratio value.

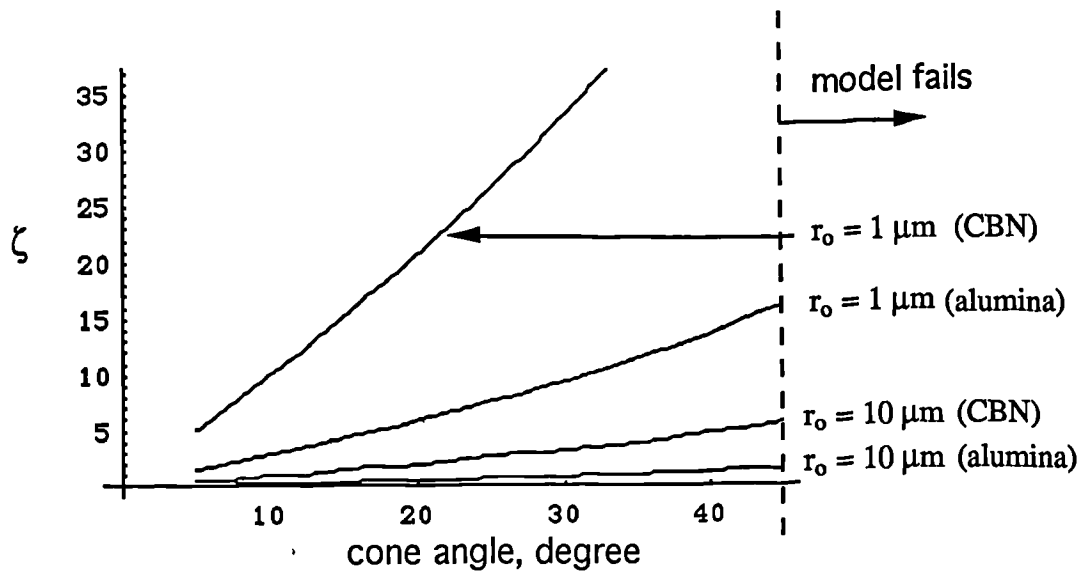


Figure 7.3 The relationship between  $\zeta$  and cone angle at varying values of grain contact radius,  $r_o$ .

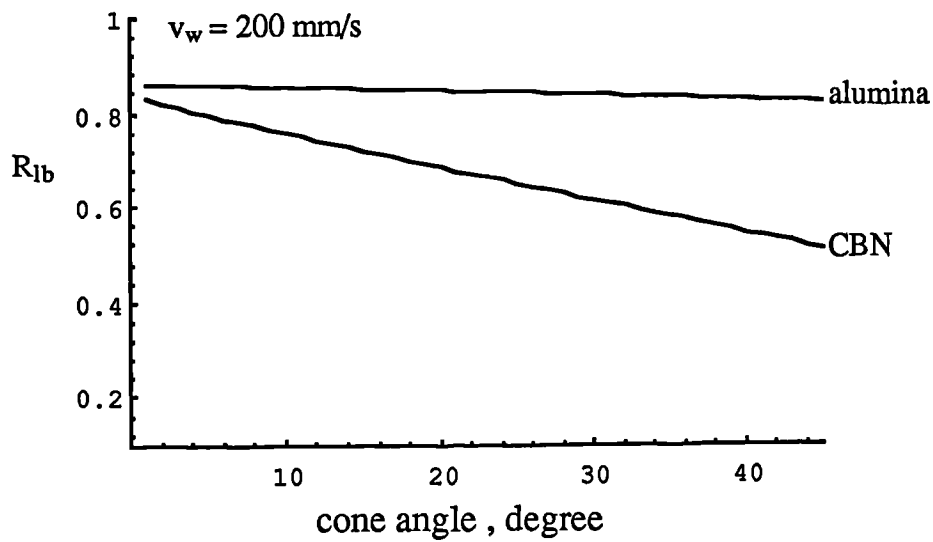


Figure 7.4 The relationship between lower bound partition ratio and cone angle.

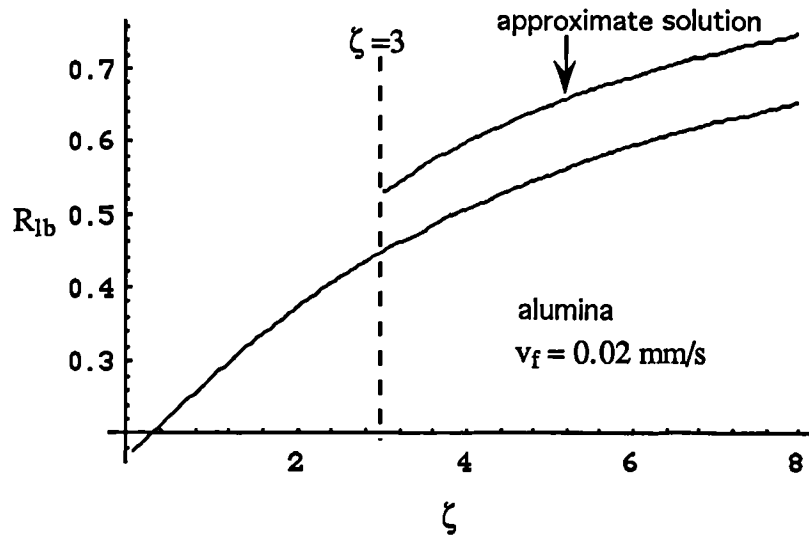


Figure 7.5 The relationship between the lower bound partition solution of the conical grain model and  $\zeta$ . Theoretical results are also shown for the approximate solution, when  $\zeta > 3$ .

In Figure 7.6 values of lower bound partition ratio are plotted against grain thermal conductivity. Values of thermal conductivity quoted in Table 4.1 for CBN and for aluminium grain materials, are indicated on the graph. To generate the results average values of density,  $\rho_g = 3710 \text{ kg/m}^3$ , and specific heat,  $c_g = 635 \text{ J/kgK}$ , were assumed. The average values were calculated from the CBN and aluminium oxide data quoted in Table 4.1.

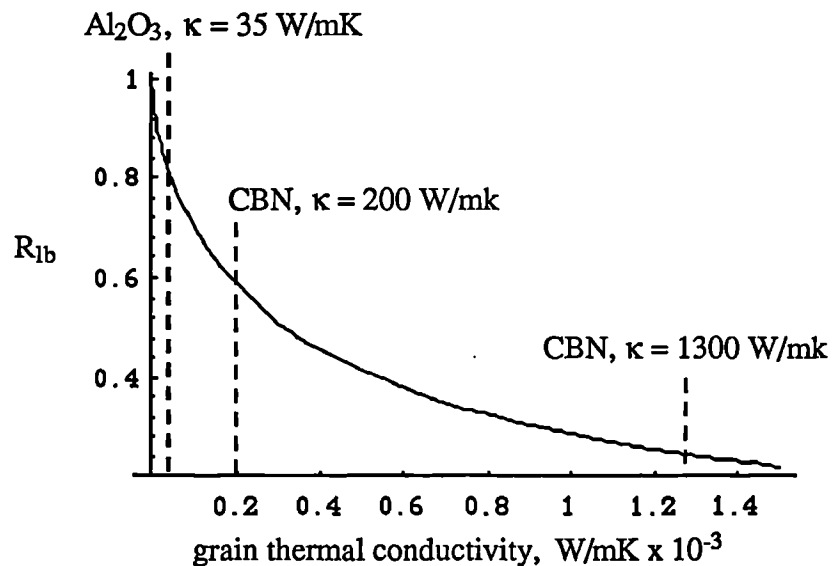


Figure 7.6 The variation of partition ratio with grain thermal conductivity.

It is evident from Figure 7.6 that the predicted partition ratio is lower for CBN than for aluminium. For high values of grain conductivity, the partition ratio is significantly reduced. This in some part accounts for the large variation in predicted values of partition ratio evident in Table 3.1.

## 7.2 THEORETICAL LIMIT CHARTS.

In this section theoretical limit charts are derived from the conical grain model. The limit charts were generated with the aid of a computer program. The computer program calculated an initial value of  $R_{1b}$  from equation 180 for the conical grain model from an input of infeed  $v_{f1}$ , and workspeed  $v_{w1}$ . A value of infeed  $v_{f2}$ , was then calculated from equation 184 for the band source solution using  $R_{1b}$ . The initial infeed  $v_{f1}$  was compared to  $v_{f2}$ . The program then incremented or decremented  $v_{f1}$  depending on the sign of the difference, recalculated  $R_{1b}$  and returned a new value of  $v_{f2}$  from the band source solution, until  $v_{f1}$  was equal to  $v_{f2}$ . The iteration loop was repeated for incremental values of  $v_{w1}$  to the workspeed range illustrated using the previously calculated value of  $R_{1b}$ . The grinding contact length was evaluated from the real contact length model of Rowe and Qi [38], equation 186. A critical workpiece temperature of 350 degC was employed based on the findings of previous research at the AMTREL. The value of 350 degC was reported to be the temperature associated with the onset of temper colours in a cast iron workpiece material.

In Figure 7.7 theoretical limits are shown for different values of specific energy. The results show that lower values of specific energy allow much higher values of infeed to be employed for a particular temperature. The higher values of infeed indicate that much higher removal rates are possible with lower specific energy and high workspeed. At low workspeed, much lower values of infeed are achievable.

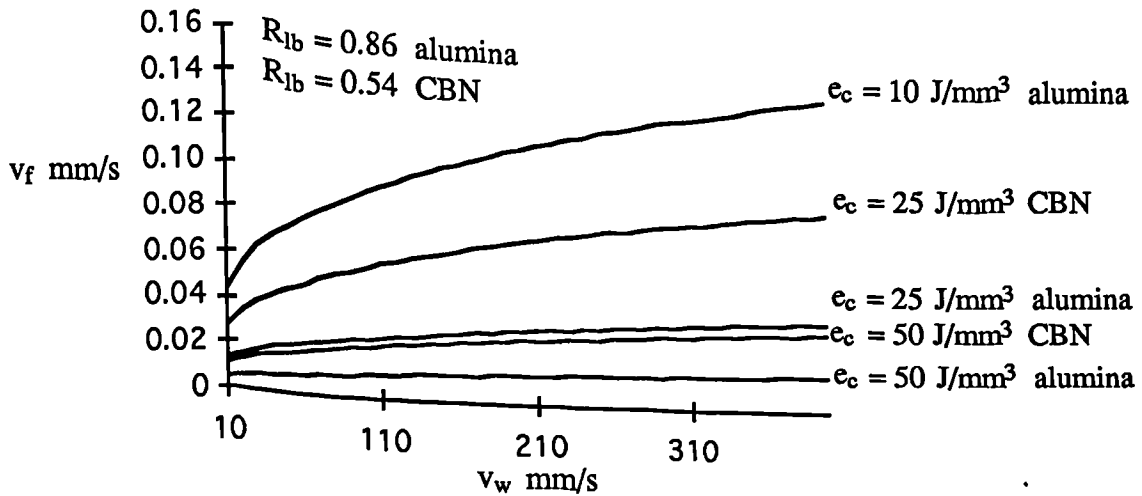


Figure 7.7 Theoretical limit chart for different values of specific energy.

In Figure 7.8 theoretical limit charts are shown for different values of workpiece critical temperature. The results show that at lower workpiece critical temperatures the maximum allowable infeed is considerably lower for a particular specific energy. This has the effect of reducing the removal rates achievable with more temperature sensitive workpiece materials.

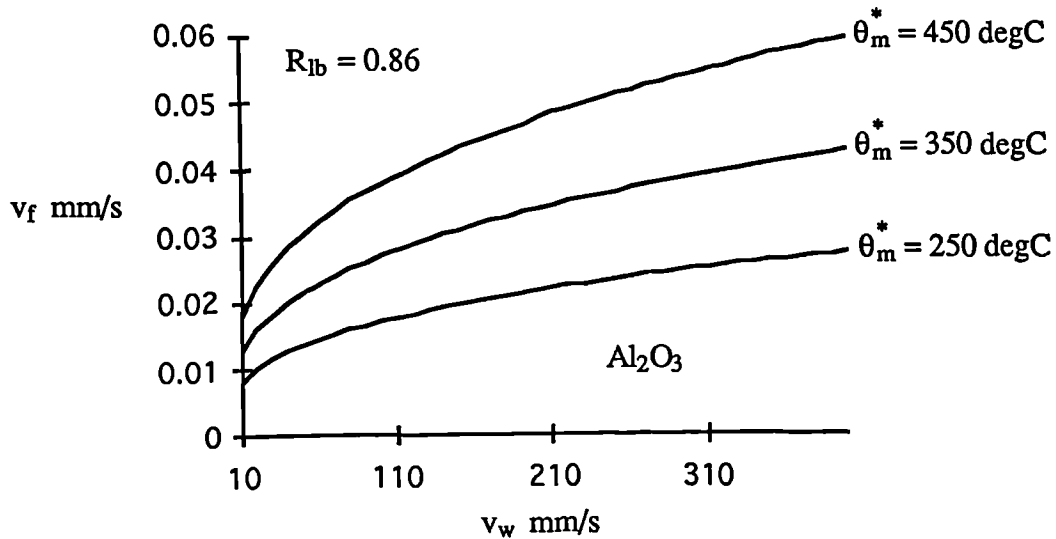


Figure 7.8 Theoretical limits at different values of workpiece critical temperature.

### 7.3 THEORETICAL VALUES OF PARTITION RATIO PREDICTED FROM THE CONICAL GRAIN MODEL AND OTHER MODELS.

In Figures 7.9 - 7.13 results are given for the conical grain model and the models of Shaw [41], Rowe and Pettit [7], Malkin [22] and Lavine [43]. The results were

generated from equation 108 ( $R_{lb}$  Shaw), equation 88 ( $R_{lb}$  Rowe and Pettit), equation 64 ( $R_{lb}$  Malkin), equation 135 ( $R_{lb}$  Lavine) and equation 180 ( $R_{lb}$  Rowe and Morgan). Further to Table 7.1, listed in Table 7.2 are values of parameters used for the graphical results in Figures 7.9 - 7.13.

Table 7.2 Values of parameters used for Figures 7.9 to 7.13.

Parameter	$Al_2O_3$	CBN
$\kappa_s$	0.55 W/mK	1.0 W/mK
$\rho_s$	2350 kg/m <sup>3</sup>	2150 kg/m <sup>3</sup>
$c_s$	210 J/kgK	1012 J/kgK
<b>Grinding fluid</b>		
$\kappa_f$	0.6 W/mK	
$\rho_f$	1000 kg/m <sup>3</sup>	
$c_f$	4200 J/kgK	
$\theta_{fm}$	120 degC	
$\Delta\theta_c$	1500 degC	
$e_c$	25 J/mm <sup>3</sup>	
$A_r/A_a$	0.01	

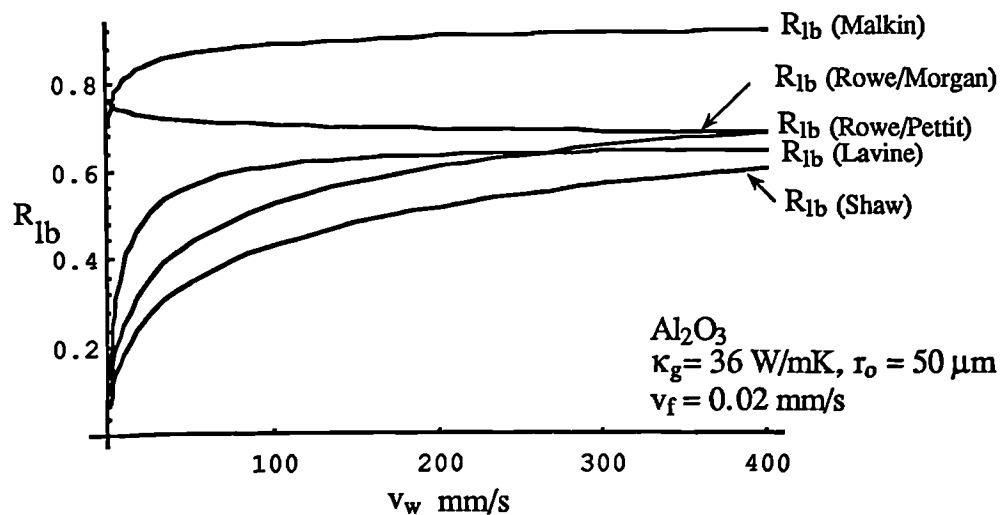


Figure 7.9 Theoretical lower bound values of partition ratio predicted from the conical grain model and other models for the particular case of an alumina abrasive,  $\kappa_g = 36$  W/mK,  $r_o = 50 \mu\text{m}$  and  $v_f = 0.02$  mm/s.

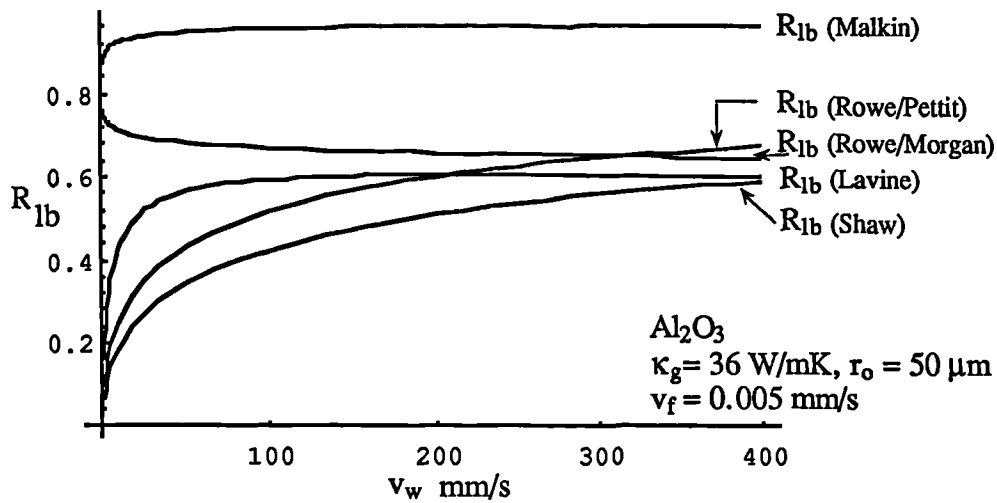


Figure 7.10 Theoretical lower bound values of partition ratio predicted from the conical grain model and other models for the particular case of an alumina abrasive,  $\kappa_g = 36 \text{ W/mK}$ ,  $r_o = 50 \mu\text{m}$  and  $v_f = 0.005 \text{ mm/s}$ .

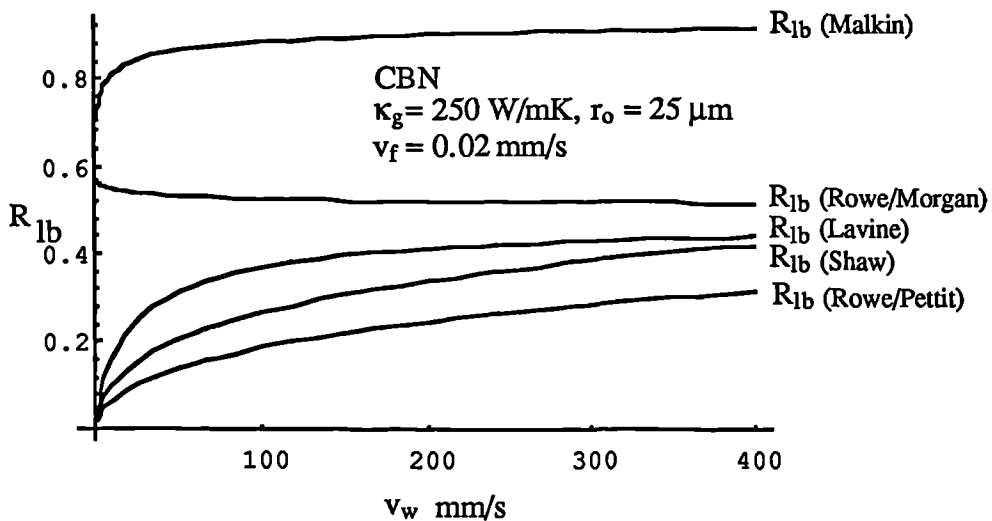


Figure 7.11 Theoretical lower bound values of partition ratio predicted from the conical grain model and other models for the particular case of a CBN abrasive,  $\kappa_g = 250 \text{ W/mK}$ ,  $r_o = 25 \mu\text{m}$  and  $v_f = 0.02 \text{ mm/s}$ .

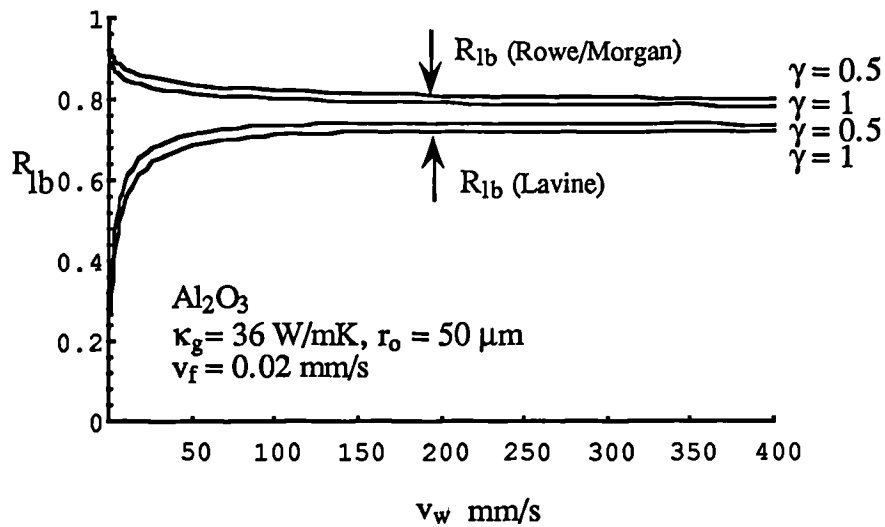


Figure 7.12 Theoretical lower bound values of partition ratio predicted from the conical grain model and the model of Lavine. Partition ratio values are shown for the cases  $\gamma = 0.5$  and  $\gamma = 1$ .

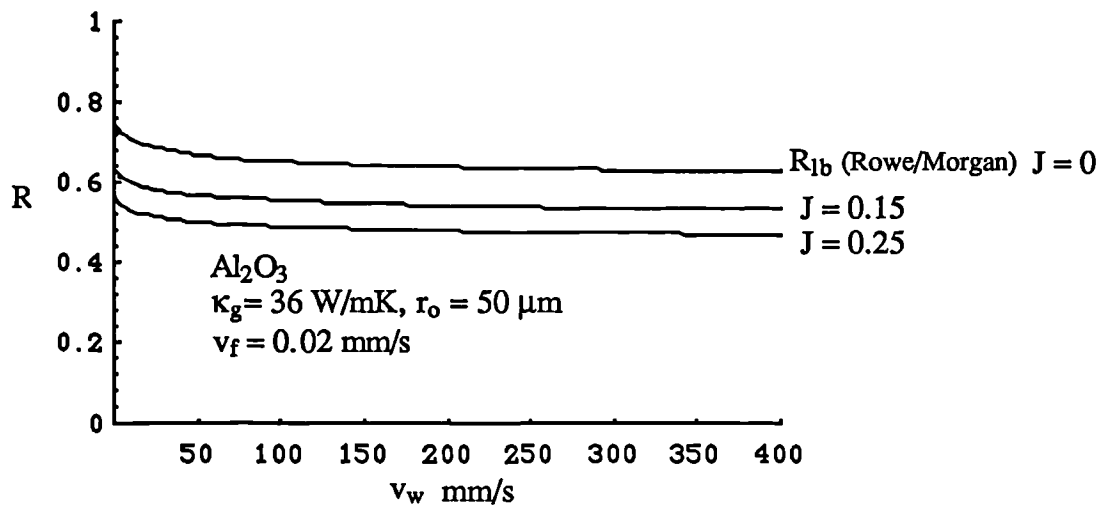


Figure 7.13 Theoretical upper bound and lower bound values of partition ratio predicted from the conical grain model. Upper bound values are shown for the cases  $J = 0.15$  and  $J = 0.25$ .

The value of lower bound partition ratio predicted from each model for a range of work speed is shown in Figures 7.9 -7.11. The Malkin model predicts a partition ratio of approximately 90 per cent and is relatively insensitive to changes in work speed

except at the lower range. It appears from the partition solution proposed by Malkin that very little heat energy will transfer to the chips except at low values of specific energy, when the fraction of the chip formation energy conducted to the chips is more significant.

The Shaw model predicts a maximum partition ratio of approximately 60 per cent for the conditions investigated. The workspeed features in the Shaw model and consequently the results exhibit a sensitivity to this parameter.

The Rowe and Pettit model predicts that, at a maximum, approximately 70 per cent of the heat energy will transfer to the workpiece for the conditions investigated. The Rowe and Pettit model exhibits a similar relationship with workspeed as the Shaw model and correlates well with the Rowe and Morgan model at the higher workspeed range. The value of the bulk wheel thermal properties employed were taken from reference [7]. Increasing the value of the bulk wheel thermal property would have the effect of reducing the partition ratio. The sensitivity of the Rowe and Pettit model to this parameter is evaluated in a later section.

The Rowe and Morgan model and the Lavine model predict similar values of partition ratio at the higher workspeed range, the Rowe and Morgan model predicting the marginally higher values. However, at low workspeeds the Lavine model and all other models become increasingly inaccurate. This is due to the invalidity of the moving band source solution at Peclet numbers less than 5.

Figure 7.10 shows that a slightly lower range of partition ratios are predicted from the Rowe and Morgan model and the Lavine model at  $v_f = 0.02$  compared to  $v_f = 0.005$  mm/s in Figure 7.9. All other models appear insensitive to this parameter.

In Figure 7.11 values of partition ratio are shown for the case of a CBN abrasive. Comparing Figure 7.11 with Figure 7.9 shows the sensitivity of the models to a change in abrasive thermal properties. The Malkin model is insensitive to a change in the abrasive thermal properties while the Shaw model shows a range of partition ratio which is reduced by approximately 20 per cent at the maximum value. The partition ratios predicted from the Rowe and Pettit model appear to change significantly. This is due to the difference in the value of bulk thermal properties used for alumina and CBN. The partition ratios predicted from the models of Rowe and

Morgan and of Lavine are each reduced by approximately 25 per cent. For the Rowe and Morgan model this reduction was predicted previously, Figure 7.6.

In Figure 7.12 lower bound values of partition ratio are shown for the Rowe and Morgan model and the Lavine model for the cases  $\gamma = 0.5$  and  $\gamma = 1$ . The effect of increasing the cone angle from  $\gamma = 0.5$  to  $\gamma = 1$  is to reduce the value of partition ratio predicted from each model by approximately 3 per cent. This effect, for the Rowe and Morgan model, is borne out in Figure 7.4.

In Figure 7.13 theoretical upper bound values of partition ratio are shown with the lower bound values. Heat transfers to the grinding chips and to the grinding fluid are accounted for and varied through inclusion of the parameter  $J = 0.15$  and  $J = 0.25$ . The model predicts that upper bound values of partition ratio are approximately 55 - 60 per cent, and this reduction in the fraction of the total heat energy entering the workpiece would be expected.

It is evident from Figures 7.9 - 7.12 that the Rowe and Morgan model responds to a change in workspeed in a different manner to the other models at the lower workspeed range. It is unreasonable to predict zero values of partition ratio at a zero workspeed, and in this respect the Rowe and Morgan model as a general solution would appear to respond most favourably. The other models fail at low workspeed values because the moving band source solutions employed are not valid at Peclet numbers less than 5. In the case of the Rowe and Morgan model, which features the Peclet number in the analysis of the heat transfer into the workpiece under a grain, the Peclet number criterion is not breached, as it is a function of wheelspeed not workspeed.

## Chapter 8 EXPERIMENTAL STUDY

This chapter describes two series of grinding trials. A preliminary series of trials established the approximate region of the burn boundary for a range of infeed and workspeed combinations and a further series of trials provided values of specific grinding energy at the burn boundary. These results were then used to estimate values of partition ratio.

### 8.1 AIM OF THE EXPERIMENTAL STUDY.

The principal aim of the experimental study was to obtain the grinding power at the threshold of thermal damage for a range of infeed and workspeed combinations. This allowed the specific grinding energy measured from experiment to be compared to the critical specific energy predicted by the thermal model.

### 8.2 MACHINING ARRANGEMENT FOR THE EXPERIMENTAL STUDY.

Experiments were undertaken on a centreless grinding machine. The grinding arrangement is illustrated in Figure 8.1, and shown in Plate 1.

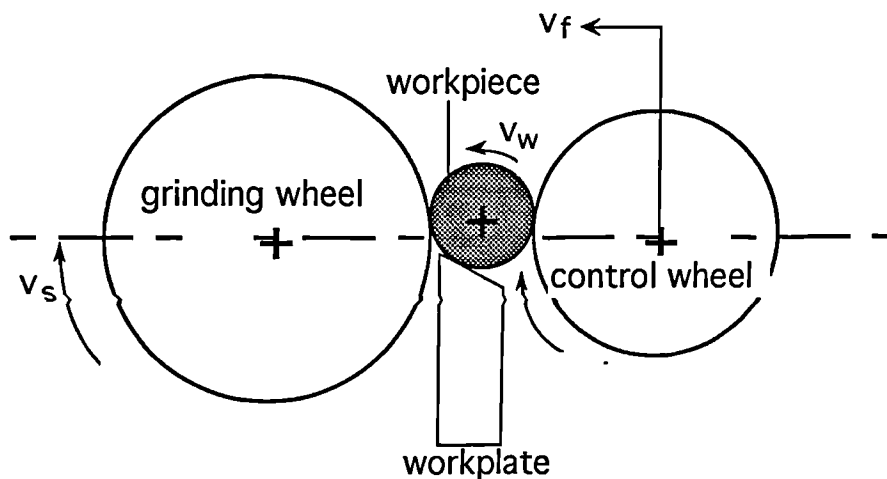


Figure 8.1 The plunge feed centreless grinding arrangement.

The control parameters for centreless grinding are the workpiece speed,  $v_w$ , the grinding wheel speed,  $v_s$ , and the infeed rate,  $v_f$ . The workpiece is supported by a workplate set between the grinding wheel and the control wheel. To remove material the control wheel is advanced towards the grinding wheel. The control wheel infeed

pushes the workpiece up the inclined face of the workplate towards the grinding wheel. The control wheel provides a continuously advancing frictional surface which ensures constant and uniform rotation of the workpiece at the same peripheral speed as that of the control wheel. The directions of rotation of the machining elements are also shown in Figure 8.1.

### 8.2.1 SELECTION OF INITIAL VALUES OF GRINDING PARAMETERS.

Initial values of grinding wheel speed, infeed and workspeed were selected based on results presented by Rowe, Bell and Brough [34] and from information provided in the Machining Data Handbook [61].

### 8.3 WHEEL DRESSING ARRANGEMENT.

Dressing of the grinding wheel generates the required geometric profile on the wheel and conditions the surface grits to provide the desired cutting action. The dressing tool was a single point diamond, Plate 2. The control parameters for the dressing operation are the dressing increment,  $a_d$  and the dressing lead,  $f_d$ . A schematic representation of the dressing arrangement is shown in Figure 8.2.

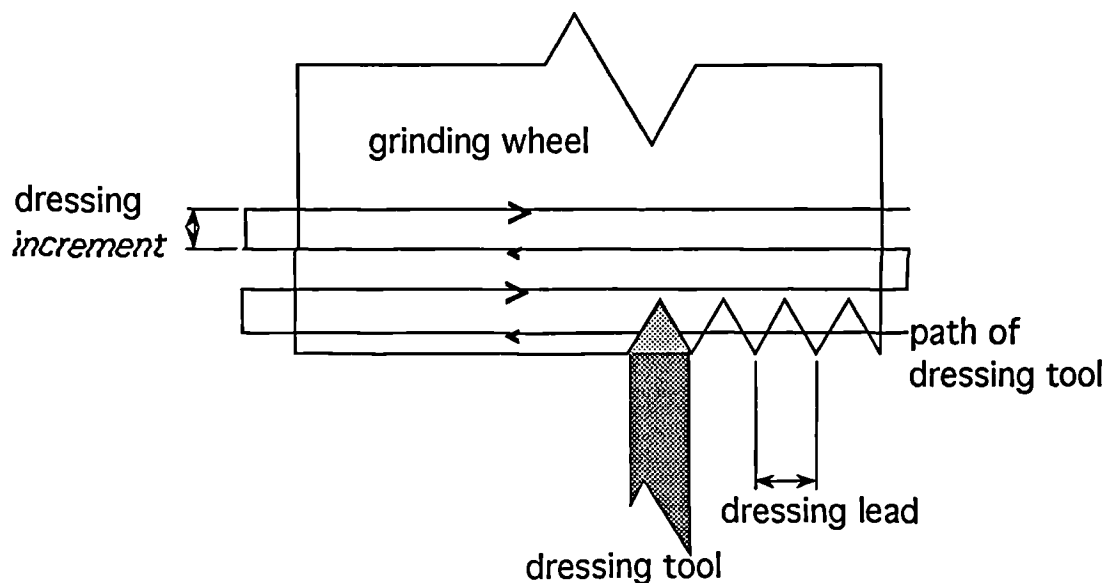


Figure 8.2 Schematic representation of the dressing operation.

### **8.3.1 SELECTION OF VALUES OF WHEEL DRESSING PARAMETERS.**

The values of dressing increment, dressing lead and the number of dressing passes were selected based on experimental results by Chen [62].

The values of dressing parameters were selected for rapid stabilisation of grinding power, workpiece surface roughness and workpiece roundness. From the results achieved by Chen [62] it was established that an optimum wheel condition could be achieved by preparing and dressing the wheel using the following values:

- a dressing lead of 0.1 mm/rev.
- an initial pass with a dressing increment of 100  $\mu\text{m}$ .
- six further passes with a dressing increment of 10  $\mu\text{m}$ .

Chen also established that following a wheel dressing operation the condition of the surface of the grinding wheel is unstable and large changes in grinding power, workpiece surface roughness and workpiece roundness occur before stable grinding conditions are reached. Results from the research project indicated that stable grinding conditions are reached following the removal of approximately 40 - 70  $\text{mm}^3/\text{mm}$  of workpiece material. For this experimental study approximately 50 - 55  $\text{mm}^3/\text{mm}$  of workpiece material was removed to condition the wheel prior to the commencement of a grinding trial.

### **8.3.2 DRESSING TOOL INFEEED AND TRAVERSE SPEED MEASUREMENT.**

The advance of the single point diamond dresser into the grinding wheel was monitored using a linear scale that provided a 0.005 mm resolution. The linear scale was a model MEL 300 55 - 300 manufactured by Goodwin Electronic Measuring Systems, and was linked to a three axis digital readout console, model GEM 33AS20INN50X076, shown in Plate 3. The dressing tool traverse speed was set by timing the dresser unit travel between two fixed points.

## **8.4 THE GRINDING CYCLE.**

In centreless grinding, the approach of the control wheel infeed to the workpiece target size and its subsequent retraction is a controlled sequence of events, termed a grinding cycle. The basic grinding cycle is illustrated in Figure 8.3 and can be modified by altering the infeed rate, altering the dwell period or by a combination of

each. The grinding cycle used throughout the experiments was a plunge feed grinding cycle with no dwell period. Immediate wheel retraction was used to avoid the removal of the surface layer that was subsequently inspected for thermal integrity.

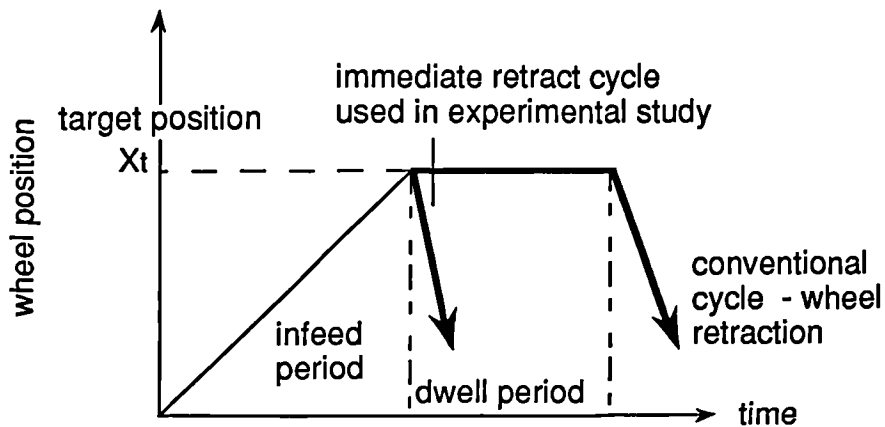


Figure 8.3 A conventional grinding cycle with a dwell period and the grinding cycle without dwell used in the experimental study.

## 8.5 EXPERIMENTAL EQUIPMENT.

**Machine tool:** The machine tool used in the experimental study was a Wickman Scrivener No 2K centreless grinding machine which had been extensively modified by previous researchers. The original machine was manually controlled.

Axis position, grinding wheel speed and workspeed were controlled by an OSAI A-B 8600 CNC. Linear scales provided a machine axis positional feedback resolution of  $2\ \mu\text{m}$ . A high pressure coolant delivery system was installed allowing for the removal of grinding swarf and bulk cooling of the workpiece material during high material removal rate grinding operations.

The machine was fitted with a high speed intelligent AC variable drive system providing 52 kW at continuous operation between base speed of 1500 rpm and maximum speed of 6000 rpm, via a torsionally rigid coupling, shown in Plate 4. The control wheel infeed motor had an encoder fitted giving  $0.1\ \mu\text{m}$  resolution, however, it was reported by the technical staff concerned with the retrofit that backlash led to problems with reliability and the encoder was therefore not used. The machine slides were coated with PTFE and closed-loop lubricated.

An alumina abrasive grinding wheel was used, grade 19AV60NVS. The maximum diameter of the wheel was 506 mm and the maximum width 100 mm. The control wheel was of grade A60 OR, and had a maximum diameter of 260 mm, and width 204 mm. A workplate with a 30° plate angle and tungsten carbide surface was fitted.

The workpiece material selected for the experimental study was grey cast iron BS 1452 grade 17/260, which has a 3.0 - 3.2 per cent carbon content. The physical properties were as follows: thermal conductivity 48.8 W/mK, specific heat capacity 365.0 J/kgK, density 7260.0 kg/m<sup>3</sup>, melting temperature 1325 °C [63]. The maximum dimensions of the workpiece were: 80 mm length and 35 mm diameter.

A chemical emulsion concentrate, TRIM VHP e200, in a dilution of 50:1 with water, was used for the grinding fluid. The specific gravity of the concentrate was 0.95, and the flash point temperature 152 °C.

## **8.6 INSPECTION OF THE WORKPIECE SURFACE FOR THERMAL DAMAGE.**

In the preliminary experimental study workpieces were inspected visually for discoloration. Visual inspection relies on a subjective judgement of thermal damage and as a consequence may not be indicative of grain modification or tempering. In the larger experimental study selected workpieces were inspected for thermal damage using an etch technique. The thermal damage was evident as tempered ferrite / cementite with inclusions of oxides that appeared as a result of material impurities. The arrangement of equipment and procedure for the etch inspection facility is described in appendix A.3.1.

## **8.7 MEASUREMENT OF WORKPIECE SIZE.**

In grinding, size, geometry and surface texture are improved during the dwell period. However, a thermally damaged surface layer is modified during the dwell period. Excluding a dwell period results in workpieces of irregular geometry, inaccurate size, and unpredictable surface texture. However, the purpose of the experimental study was to establish the specific grinding energy at the threshold of thermal damage, which requires a knowledge of the volumetric material removal rate. It was therefore essential to use a grinding cycle without a dwell period. High precision size measurements enable volumetric material removal rates to be determined to a high

accuracy. However, due to the size and geometric inaccuracies resulting from the immediate retract grinding cycle used in this experimental study, size measurements taken from a calibrated hand gauge of 1 micron resolution were considered to be adequate.

## **8.8 GRINDING POWER MEASUREMENT.**

The power consumed by the AC main drive was monitored via a line connection to the drive control unit. The line connection gave an analogue output of 0 - 10 V dc that indicated the percentage of drive usage. The analogue signal was calibrated for a 100 kW motor, thus a + 10.0 V signal indicated maximum utilisation at constant operation. The signal was imported to the line connection via a dc bus in the RAC main spindle controller providing a 12 bit resolution. The signal was calibrated by the manufacturer [64] using a Hall effect transducer. At full scale deflection the signal tolerance was 5 per cent. The losses between the drive and the motor were reported by the manufacturer as up to 5 per cent of total recorded power. Thus, shaft power in kilowatts, was equal to:  $(0.95 \pm 0.025) \times \text{recorded voltage} \times 10,000$ . The analogue signal was amplified using an industry standard precision bi-polar operational amplifier: PCB: OP-07CN. The amplified signal was digitised using an Amplicon analogue to digital converter: PC-30A/D card [65], installed within an Opus 286 pc, model PC V. The experimental arrangement is shown in Plate 5. Interpretation of the power data was subjective. However, the mean power estimated from the displayed power curve was compared to the mean power recorded with a Siemens Functionmeter and the two values were in close agreement. It was concluded that a maximum error of the order of 5 per cent could result from a misreading of the power data.

## **8.9 EXPERIMENTAL PROCEDURE.**

The flowchart shown in Figures 8.6a and 8.6b, summarises the procedure used to identify the region of thermal damage for a range of infeed and workspeed combinations. In the preliminary experimental study the approximate region of the thermal damage boundary was established. In the further series of experimental trials the thermal damage boundary was accurately established. The grinding parameters and machining data are summarised in Table 8.1.

Table 8.1 Grinding parameters and machining data

Grinding machine	: Wickman Scrivener 2K
Process	: Centreless grinding
Grinding wheel	: 19AV60NVS
Workpiece material	: Grey cast iron
Wheel speed	: 38.8 m/s
Workpiece speed	: 0.125 - 0.6 m/s
Infeed rate	: 0.067 - 0.60 mm/s
Coolant	: Trim VE20, dilution 50:1

Test 1: The wheel was dressed and conditioned as described in Section 8.3.1 prior to the commencement of a grinding trial. A single grinding trial consisted of the grinding of one batch of ten workpieces. Initially, a batch of workpieces were ground at a known safe value of workpiece speed at the lowest infeed rate, 0.067 mm/s. A further series of trials were undertaken at the selected infeed rate, with workpiece speed progressively reduced until workpiece temper colours were observed.

Test 2: Test 1 was repeated for an increased value of infeed rate.

Further tests were completed with infeed rate increased incrementally up to the maximum value of 0.60 mm/s.

#### **8.10 METHOD USED TO PROCESS THE EXPERIMENTAL DATA.**

The experimental data was processed using an Opus 286, model PC V and Apple Macintosh pc's. A computer program was written in the FORTRAN language to calculate specific grinding energies, partition ratios and other quantities that were required for analysis and / or comparison. A listing and flowchart of the program is given in appendix A.3.2. For the purpose of presentation, the grinding power data recorded from the trials were transferred to the Macintosh as a text file via the Apple File Exchange utility.

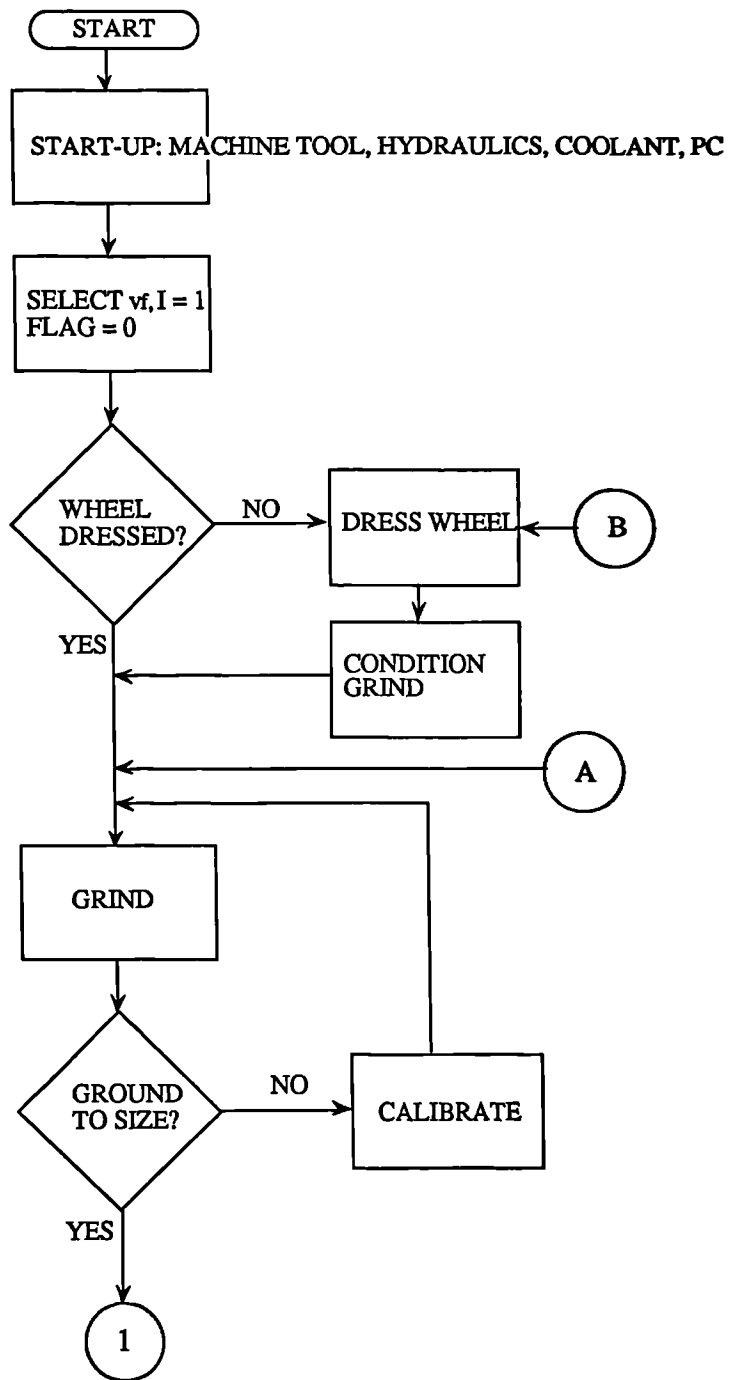


Figure 8.6a A flowchart showing the procedure used in the experimental study.

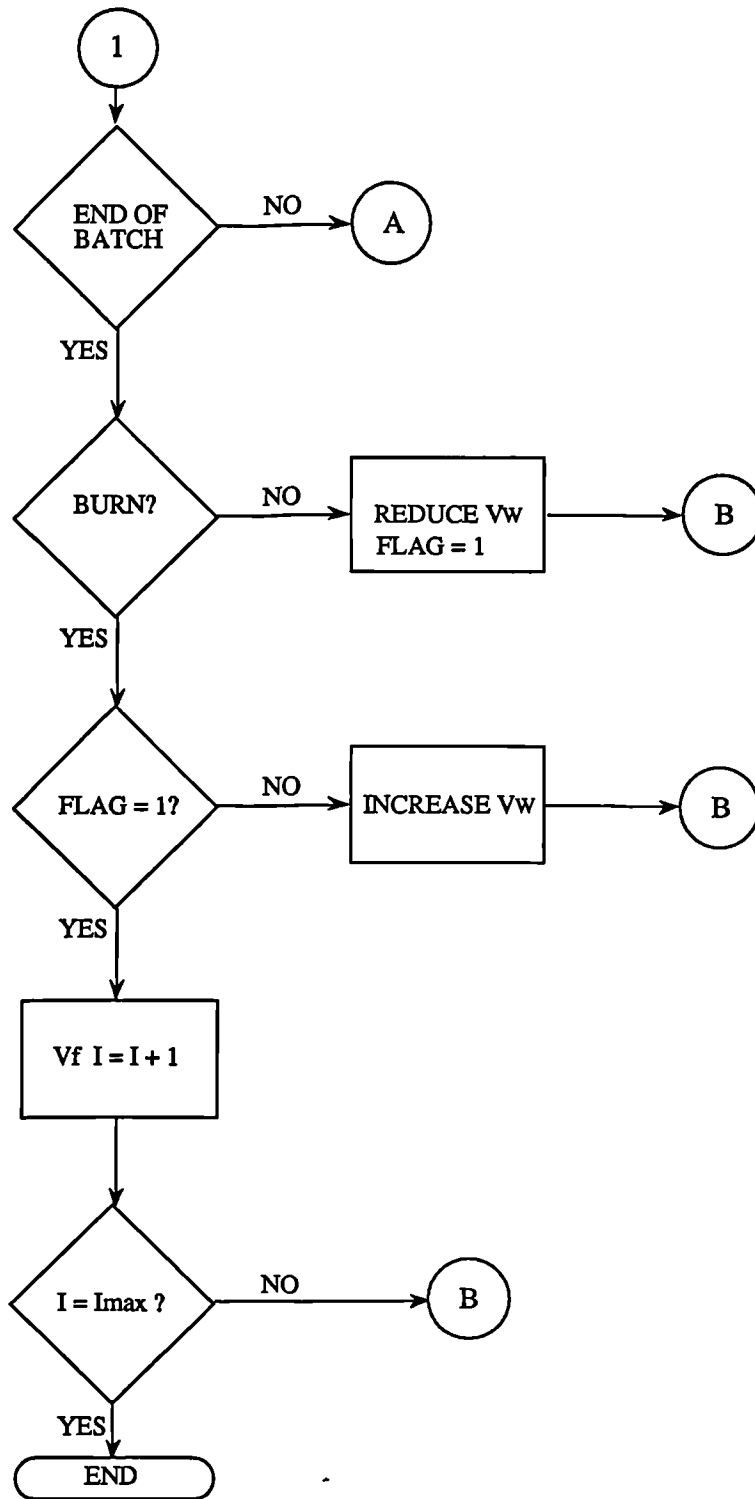


Figure 8.6b A flowchart showing the procedure used in the experimental study.

## Chapter 9 EXPERIMENTAL RESULTS.

The aim of this experimental study was to determine the value of partition ratio predicted by the thermal model and compare this value with the partition ratio,  $R_{exp}$ , obtained from the measured power and material removal rate at the threshold of damage. At the burn threshold the partition ratio has a critical value corresponding to the equality  $\theta_m = \theta_m^*$ . A threshold temperature of  $\theta_m^* = 480$  deg C was assumed for the workpiece material, based on the experimental work of Rowe, Black and Mills [59]. Critical values of partition ratio were determined for combinations of values of infeedrate  $v_f$ , and workspeed  $v_w$ . The burn boundary was approached using incremental changes to the workspeed for a particular value of infeedrate .

The first section of this chapter summarises the results recorded from the preliminary series of trials that were undertaken to establish the approximate region of the burn boundary for the range of infeedrate and workspeed combinations.

### 9.1 THERMAL DAMAGE BOUNDARY VALUES: PRELIMINARY STUDY.

The burn boundary is defined by a combination of values of infeedrate and workspeed. In grinding operations the burn boundary can be avoided by increasing the workspeed, reducing the infeedrate or reducing the specific energy by using a coarser wheel dressing condition or changing to a softer wheel [34].

In Figure 9.1 the region of the burn boundary is shown for the range of values of infeedrate and workspeed used in the preliminary study. Visible thermal damage was evident at the lower range of workspeed for all infeedrate values. At the higher values of infeedrate , damage was evident at all but the highest workspeeds. It was found that an infeedrate of 0.6 mm/s was close to the maximum infeedrate achievable for any value of workspeed without incurring thermal damage, for the particular cast iron workpiece and alumina abrasive.

The results shown in Figure 9.1 provided a basis from which values of infeedrate and workspeed were selected for the further experimental study.

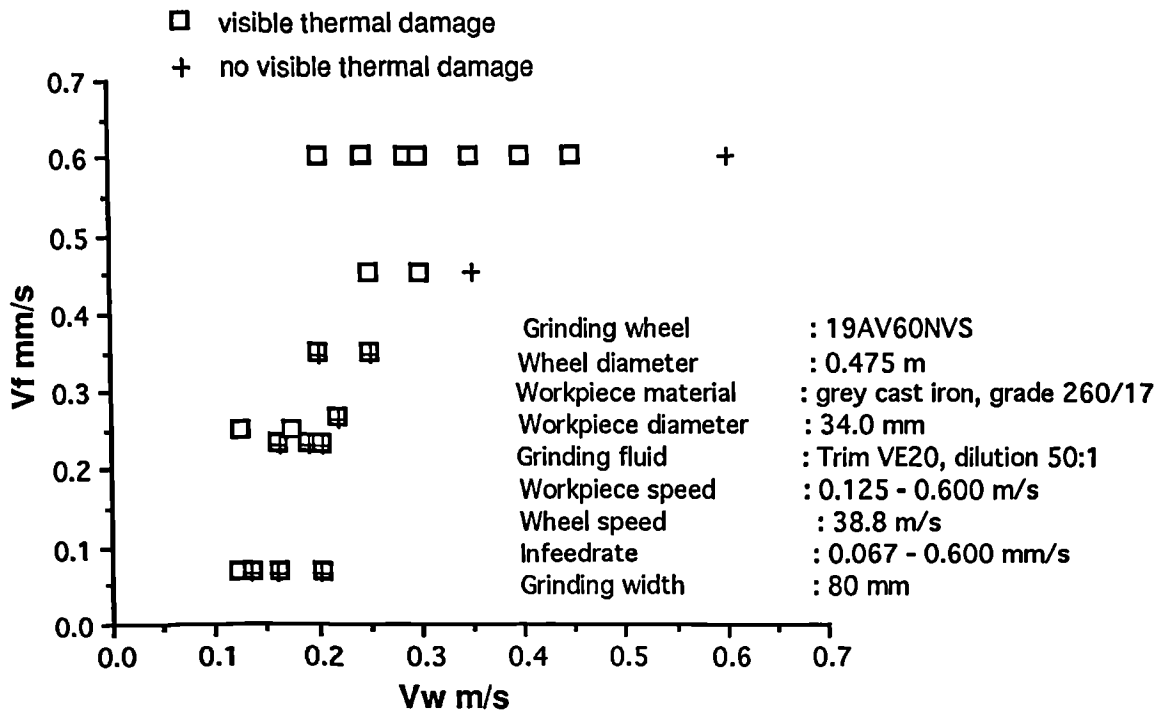


Figure 9.1 Thermal damage results used to define the boundary.

## 9.2 GRINDING POWER.

Grinding power data recorded from the grinding trials are shown in Figures 9.2 and 9.3. In Figure 9.2 the power data from four separate grinding trials are shown together. In the case illustrated, the workspeed was fixed at a value  $v_w = 200$  mm/s and the infeedrate incremented from an initial value of  $v_f = 0.167$  mm/s to the higher value  $v_f = 0.417$  mm/s. Power at the no-load condition was approximately 6 kW. The grinding power can be seen to increase with each incremental value of infeedrate.

At the higher values of infeedrate it was difficult to determine whether or not the grinding power had achieved a maximum value equal to the steady state value, before wheel retraction occurred. In Figure 9.3 power data from a grinding cycle used in the experimental study is shown with power data from a single grinding trial in which the cycle was extended to allow steady state values to be achieved. It can be seen that the maximum power values correspond for the two sets of power data and hence it can be reasoned that the maximum power values recorded were valid. The effect of wheel conditioning, identified as a reduction in power, is apparent from the power data for the extended cycle.

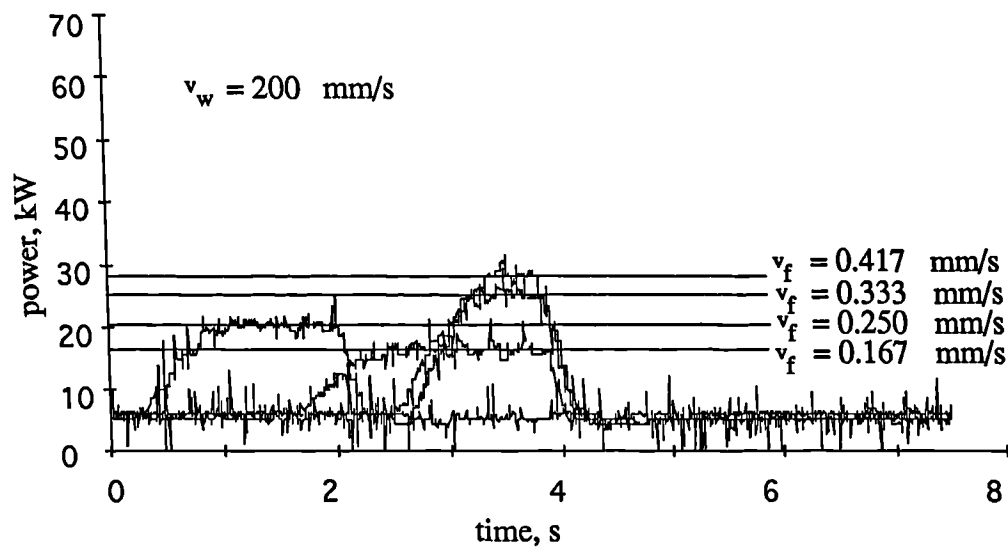


Figure 9.2 Power data from four separate grinding trials, for the case of a fixed workspeed and incremental values of infeedrate.

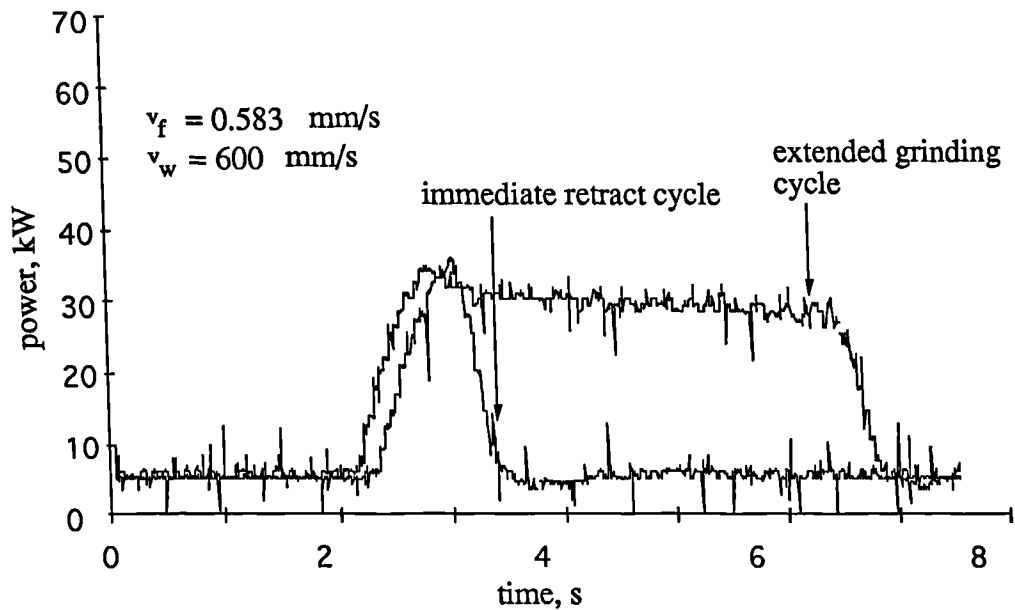


Figure 9.3 Power data from a cycle used in the experimental study and from an extended cycle, where workspeed  $v_w = 600$  mm/s and infeedrate  $v_f = 0.583$  mm/s.

### 9.3 THERMAL DAMAGE BOUNDARY VALUES.

In Figure 9.4 each point corresponds to the average result obtained for a batch of 5 workpieces. The combination of infeedrate and workspeed values that define the

burn boundary correspond with the preliminary trial results shown in Figure 9.1. At the lower range of infeedrate,  $0.083 \text{ mm/s} < v_f < 0.25 \text{ mm/s}$ , increasing workspeed to a value greater than  $v_f = 200 \text{ mm/s}$  has the effect of reducing the risk of thermal damage. Increasing the workspeed reduces the period over which the heat source is applied and increases the periodicity of the heat source. It may be concluded from Figure 9.4 that there is a safe combination of workspeed and infeedrate for a particular grinding set-up. In practice, consideration would have to be given to the operating limits for power and chatter to ensure a safe operating regime and finished workpieces of desired surface quality.

Also evident in Figures 9.1 and 9.4 is a region of indeterminacy at the lower workspeed and infeed range. In this region the thermal damage boundary is vertical, which implies that thermal damage will occur at all values of infeedrate for a particular workspeed. This result is contrary to the theoretical results of Figures 7.7 and 7.8 which predict an increased risk of thermal damage with an increase in infeedrate for any particular workspeed, throughout the workspeed range investigated for constant specific energy. In practice the specific energy increased at low workspeed.

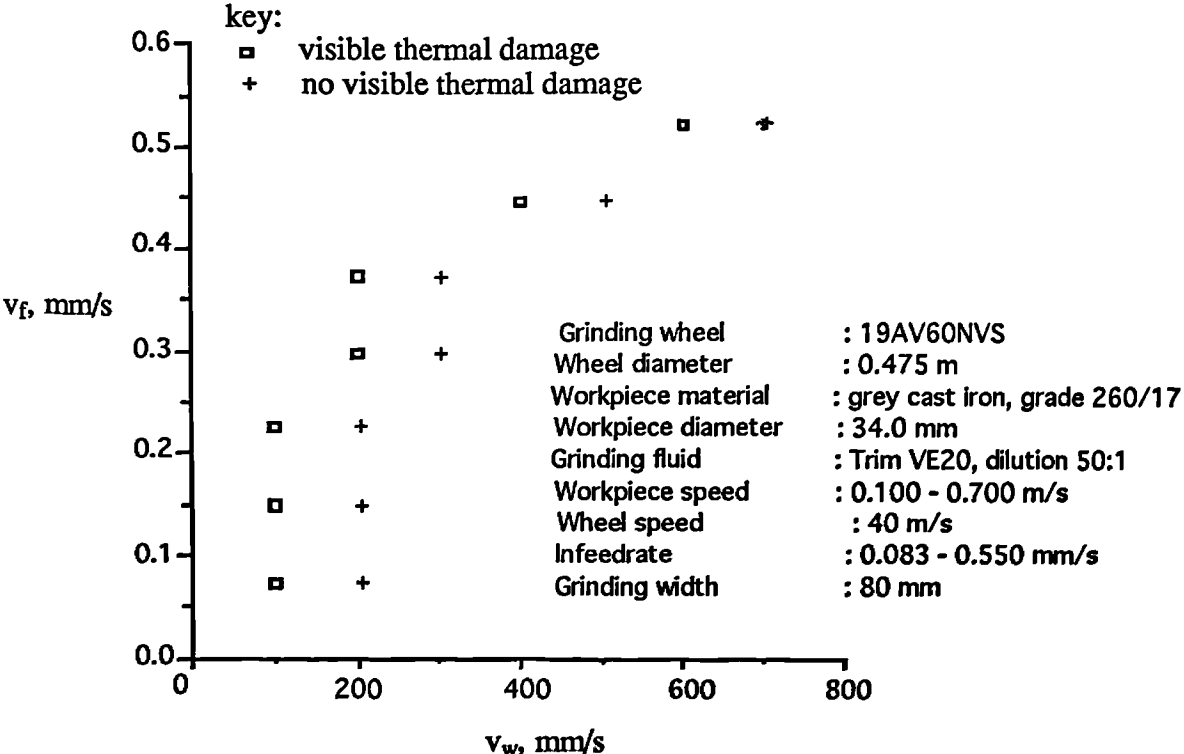


Figure 9.4 An experimental thermal damage boundary.

## 9.4 SPECIFIC GRINDING ENERGY AND THEORETICAL BOUNDARY SOLUTIONS.

In this section, values of specific energy obtained from experimental measurements are compared with theoretical lower bound and upper bound values of specific energy. The experimental data were obtained from grinding batches of workpieces at combinations of infeedrate and workspeed that corresponded to the thermal damage boundary limits established in Figure 9.4. Table 9.1 summarises the values of grinding parameters and machining data. The experimental procedure is fully described in chapter 8.

Table 9.1 Grinding parameters and machining data

Grinding machine	: Wickman Scrivener 2K
Process	: Centreless grinding
Grinding wheel	: 19AV60NVS
Workpiece material	: Grey cast iron
Coolant	: Trim VE20, dilution 50:1
Wheel speed	: 40 m/s
Workpiece speed	: 0.125 - 0.6 m/s
Infeed rate	: 0.083 - 0.583 mm/s
Grinding cycle	: constant infeedrate and retract
Dressing tool	: single point diamond
Dressing parameters	: dressing lead 0.1 mm/rev : initial increment of 100 $\mu\text{m}$ : six further passes, increment of 10 $\mu\text{m}$

Values of specific energy corresponding to the lower bound solution were calculated from equation 187 and exclude energy transfers to the chips and to the fluid. Values of specific energy corresponding to the upper bound solution were calculated from equation 188. Also shown are values of specific energy for a theoretical solution  $e_c(\text{th})$ , which includes energy partitioning to the wheel, workpiece and chips only, and was calculated from equation 200.

$$e_c(\text{th}) = e_c(\text{lower bound}) + e_{cc}$$

200

The experimental specific energy was determined from the measured power and removal rate.

The theoretical lower bound and upper bound values of partition ratio were calculated from equation 180 and equation 194 respectively, where  $e_c$  was the measured value of specific energy. The theoretical boundary values  $R_{th}$ , excluded energy transfers to the fluid and were calculated from equation 201.

$$R_{th} = R_{lb} \left( \frac{e_c - e_{cc}}{e_c} \right) = R_{lb} (1 - J') \quad 201$$

where  $J' = \frac{e_{cc}}{e_c}$

Grinding contact length was calculated from equation 185, which was proposed by Rowe and Qi [38] as the solution for the real contact length. The parameters used in the real contact length model are given in Table 9.2.

Table 9.2 Parameters used in the real contact length model, Rowe and Qi [38].

$v_s = 0.29$	$v_w = 0.22$
$E_s = 213 \text{ KN/mm}^2$	$E_w = 450 \text{ KN/mm}^2$
Friction coefficient, $\mu = 0.4$	
Roughness ratio, $R_r = 5$	

Energy transfers to the grinding chips  $e_{cc}$ , were calculated from equation 189. Energy transfer to the grinding fluid  $e_{cf}$ , was calculated from equation 193 using water properties and a fluid boiling temperature of 120 degC.

The boundary results for no visible thermal damage are shown in Figure 9.5.

### Machining data and model parameters

Grinding wheel	: 19AV60NVS
Wheel diameter	: 0.475 m
Workpiece material	: grey cast iron, grade 260/17
Workpiece diameter	: 32 mm
Grinding fluid	: Trim VE20, dilution 50:1
Wheel speed	: 40 m/s
Grain contact radius, $r_0$	: 50 $\mu\text{m}$
$\gamma$	: 1
$\varphi$	: 0.85
$\theta_m^*$	: 480 deg C
$(\kappa\rho c)_g^{1/2}$	: 10220 J/s <sup>1/2</sup> m <sup>2</sup> K
$(\kappa\rho c)_w^{1/2}$	: 14160 J/s <sup>1/2</sup> m <sup>2</sup> K
$e_{cc}$	: 5.28 J/mm <sup>3</sup>

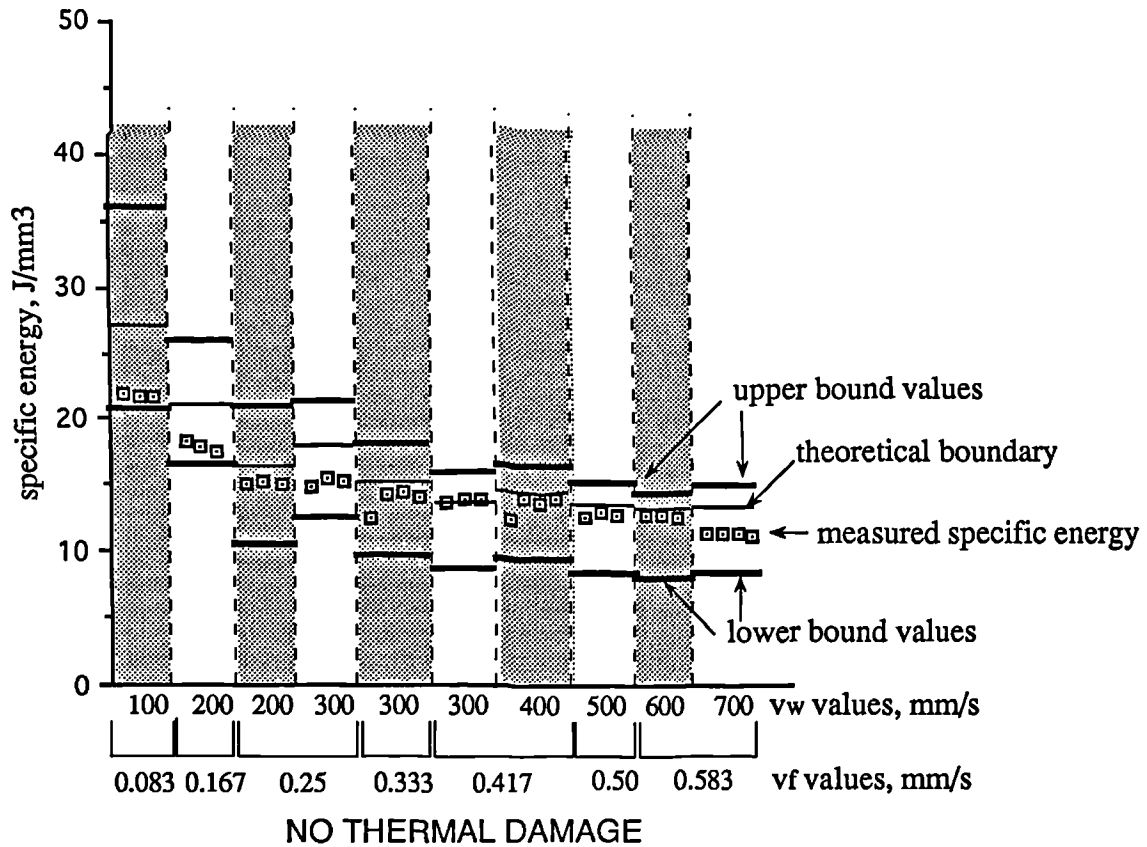


Figure 9.5 Measured and theoretical boundary values of specific energy for infeedrate and workspeed combinations in the range 100 mm/s <  $v_w$  < 700 mm/s and 0.083 mm/s <  $v_f$  < 0.583 mm/s.

The lower bound solution predicts values of specific energy between  $8 \text{ J/mm}^3 < e_c(\text{lower bound}) < 21 \text{ J/mm}^3$  for the infeedrate and workspeed range investigated. The theoretical upper bound values of specific energy predict that further increases in specific energy can take place before thermal damage will definitely occur. The measured values of specific energy all lie between the values predicted from the lower bound solution and the theoretical boundary solution. However, the experimental values correspond to the side of the boundary where damage has not occurred and therefore the actual temperature may have been slightly lower than 480 degC. For a lower temperature the lower bound values should be reduced which should improve the match between experimental values and the theoretical boundary values.

At all but the lower workspeed and infeedrate values the measured specific energy remained relatively constant at an average value of approximately  $14 \text{ J/mm}^3$ . At the lower infeedrate and workspeed values the measured specific energy increased to a maximum of  $23 \text{ J/mm}^3$ . This result can partly be explained by the size effect. A consequence of reducing both infeedrate and workspeed for a given wheel speed is to reduce the size of the chip generated by each grit. Any increase in the specific energy is then primarily due to a proportional increase in the ploughing and sliding energy components associated with chip removal.

The results for workpiece material at the onset of thermal damage are shown in Figure 9.6. The theoretical results and experimental results exhibit similar tendencies to those described for Figure 9.5. The theoretical boundary solution exhibits excellent agreement with the experimental results with the exception of the particular case of a low infeedrate and a low workspeed. The theoretical boundary solution predicts that the workpiece material should exhibit the first indications of thermal damage, and this was evident as a very light straw discoloration.

As an experiment to compare theoretical results it was unfortunate that the specific energies were so low. This had the effect of increasing the sensitivity of the theoretical results to the chip energy and reducing the sensitivity of the results to the abrasive. This can be seen more clearly from Figure 9.6a in which the fractions of energy associated with the workpiece, wheel, chips and fluid are indicated.

### Machining data and model parameters

Grinding wheel	: 19AV60NVS
Wheel diameter	: 0.475 m
Workpiece material	: grey cast iron, grade 260/17
Workpiece diameter	: 32 mm
Grinding fluid	: Trim VE20, dilution 50:1
Wheel speed	: 40 m/s
Grain contact radius, $r_0$	: 50 $\mu\text{m}$
$\gamma$	: 1
$\varphi$	: 0.85
$\theta_m^*$	: 480 deg C
$(\kappa pc)_g^{1/2}$	: 10220 $\text{J/s}^{1/2}\text{m}^2\text{K}$
$(\kappa pc)_w^{1/2}$	: 14160 $\text{J/s}^{1/2}\text{m}^2\text{K}$
$e_{cc}$	: 5.28 $\text{J/mm}^3$

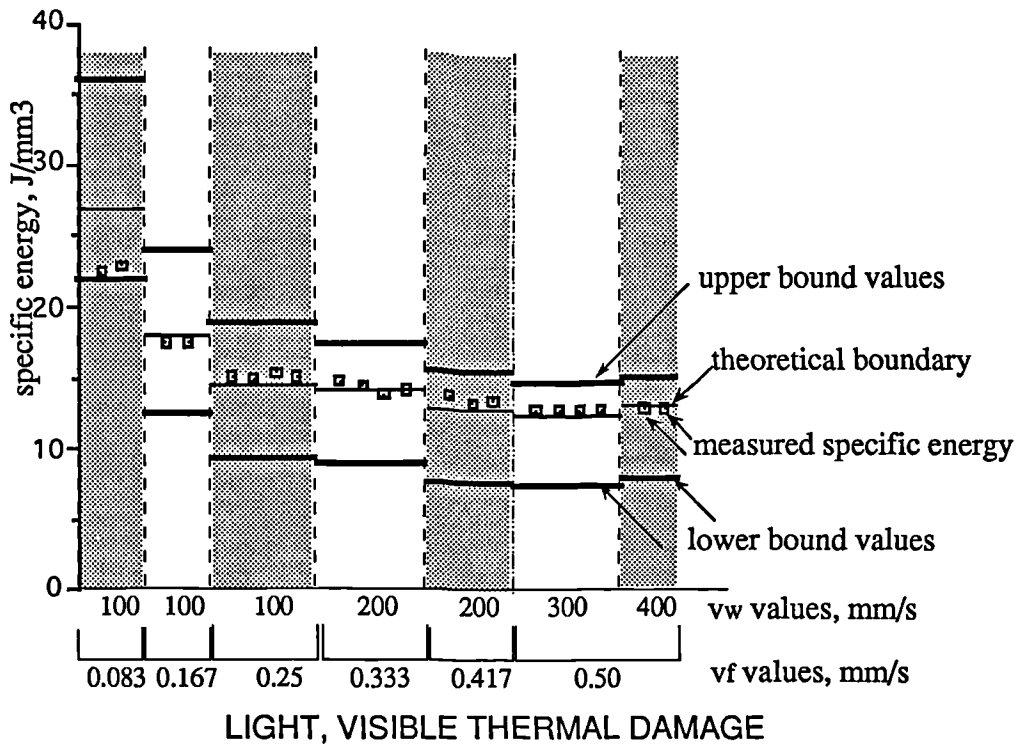


Figure 9.6 Measured specific energy and theoretical boundary values of specific energy at infeedrate and workspeed combinations corresponding to the onset of thermal damage.

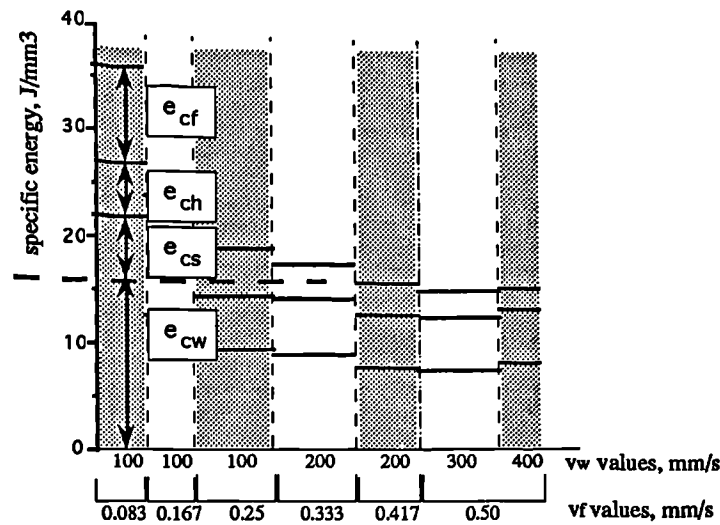


Figure 9.6a Illustration of the energy distributions.

In Figure 9.6a the energy distributed between the wheel and the workpiece is shown by a dashed line. It is evident from Figure 9.6a that the fractions of energy to the chips and to the fluid predicted from the model are significant at low specific energies.

## 9.5 THEORETICAL AND EXPERIMENTAL VALUES OF PARTITION RATIO.

In this section, values of partition ratio calculated from experimental measurements are compared with theoretical values of partition ratio predicted from the thermal model.

The measured values of partition ratio  $R_{exp}$  were calculated from the band source solution for a uniform heat flux re-arranged in terms of  $R$ , equation 202. A threshold temperature of  $\theta_m^* = 480$  degC, Rowe, Black and Mills [59], was assumed for the calculation of  $R_{exp}$ . The specific energy  $e_c$  was determined from the measured power and removal rate.

$$R = \frac{0.89 \theta_m^* (\kappa_{pc})_w^{1/2} l_c^{1/2}}{v_f^{1/2} a e_c} \quad 202$$

Values of  $R_{exp}$  were calculated for the two cases: (i)  $l_c = l_g$  and (ii)  $l_c = l_e$ . The lower bound partition ratio was calculated from equation 180. Upper bound values of

partition ratio were calculated from equation 194. The theoretical boundary  $R_{th}$  values were calculated from equation 201. Grinding contact length was calculated from equation 185. Energy transfer to the grinding chips  $e_{cc}$ , was calculated from equation 189. Energy transfer to the grinding fluid  $e_{cf}$ , was calculated from equation 193 using water properties and a fluid boiling temperature of 120 degC.

Theoretical lower and upper bounds, and theoretical boundary values of partition ratio are shown with measured values of partition ratio in Figure 9.7. The results in Figure 9.7 correspond to the case of no visible thermal damage. In Figure 9.7 the theoretical lower bound has a value approximately equal to 0.83 for the range of infeedrate and workspeed investigated. These results are consistent with the results presented in the theoretical study, Figures 7.19 - 7.12. Theoretical upper bound values of partition ratio vary between 0.32 and 0.38 with the lower values occurring at the lower workspeed and infeedrate range. The theoretical boundary values vary between a maximum of  $R_{th} = 0.63$  at the lower values of workspeed and infeedrate to a minimum of  $R_{th} = 0.45$  at the higher workspeed and infeedrate range. The tendency of the  $R_{th}$  values is explained through the effect of  $e_{cc}$ , which is less pronounced at the lower workspeeds where the total specific energy is greater. The value of  $e_{cc}$  was constant at 5.28 J/mm<sup>3</sup>.

For case (i), where the grinding contact length was based on the geometric contact  $l_g$ , the measured values of partition ratio were not enclosed by the lower bound and theoretical partition values in all instances. For case (i), the theoretical boundary failed to provide an upper bound.

For case (ii), where the grinding contact length was based on the real contact  $l_r$ , all measured values of partition ratio, with one exception, were enclosed by the lower bound and theoretical partition ratio values. The theoretical boundary did provide an upper bound for this case. The results for case (ii) also suggest that the maximum energy transfer to the grinding chips is lower than predicted from equation 189.

### Machining data and model parameters

Grinding wheel	: 19AV60NVS
Wheel diameter	: 0.475 m
Workpiece material	: grey cast iron, grade 260/17
Workpiece diameter	: 32 mm
Grinding fluid	: Trim VE20, dilution 50:1
Wheel speed	: 40 m/s
Grain contact radius, $r_0$	: 50 $\mu\text{m}$
$\gamma$	: 1
$\phi$	: 0.85
$\theta_m^*$	: 480 deg C
$(\kappa\rho c)_g^{1/2}$	: 10220 $\text{J/s}^{1/2}\text{m}^2\text{K}$
$(\kappa\rho c)_w^{1/2}$	: 14160 $\text{J/s}^{1/2}\text{m}^2\text{K}$
$e_{cc}$	: 5.28 $\text{J/mm}^3$

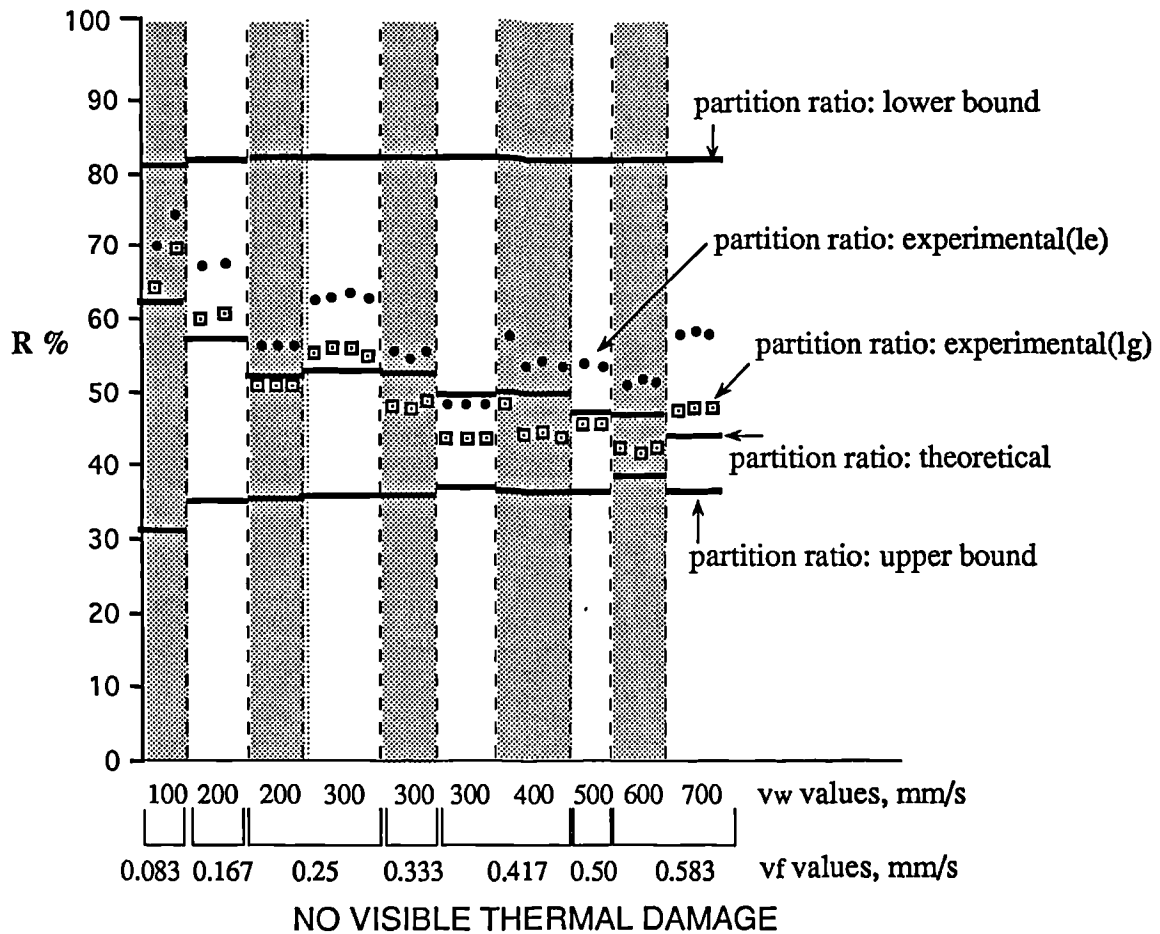


Figure 9.7 Theoretical and measured values of partition ratio.

The theoretical and measured values of partition ratio corresponding to the onset thermal damage are shown in Figure 9.8. The theoretical lower bound has a value approximately equal to 0.83 for the range of infeedrate and workspeed investigated. In all cases the results lay between the lower and upper bounds. However, the shape of a line through the results best agrees with values corresponding to the theoretical boundary solution. Measured values of partition ratio based on the real contact length give improved correlation with the theoretical boundary results compared to the measured values of partition ratio based on the geometric contact length. With the exception of the particular case where workspeed  $v_w = 100$  mm/s and infeedrate  $v_f = 0.083$  mm/s, thermal damage was encountered at values of partition ratio lower than the value predicted from the theoretical boundary solution. The upper bound solution predicts values of partition ratio that are approximately 10 - 50 per cent lower than the theoretical boundary solution. The results suggest that the upper bound solution was a pessimistic boundary for the prediction of definite thermal damage compared to the theoretical boundary.

Better agreement between experimental results and the theoretical boundary at the lower workspeed and infeed combination could be achieved by increasing the energy partitioning to the chips. Alternatively, the result could be interpreted as an indication that the partitioning to the wheel is under-estimated at the lower workpseed range or the critical temperature is lower than 480 degC due to bulk cooling, or a combination of effects. However, to test the validity of each alternative explanation would require an unreasonably large experimental study.

Grinding wheel : 19AV60NVS  
 Wheel diameter : 0.475 m  
 Workpiece material : grey cast iron, grade 260/17  
 Workpiece diameter : 32 mm  
 Grinding fluid : Trim VE20, dilution 50:1  
 Wheel speed : 40 m/s  
 Grain contact radius,  $r_0$  : 50  $\mu\text{m}$   
 $\gamma$  : 1  
 $\varphi$  : 0.85  
 $\theta_m^*$  : 480 deg C  
 $(\kappa\rho c)_g^{1/2}$  : 10220 J/s<sup>1/2</sup>m<sup>2</sup>K  
 $(\kappa\rho c)_w^{1/2}$  : 14160 J/s<sup>1/2</sup>m<sup>2</sup>K  
 $e_{cc}$  : 5.28 J/mm<sup>3</sup>

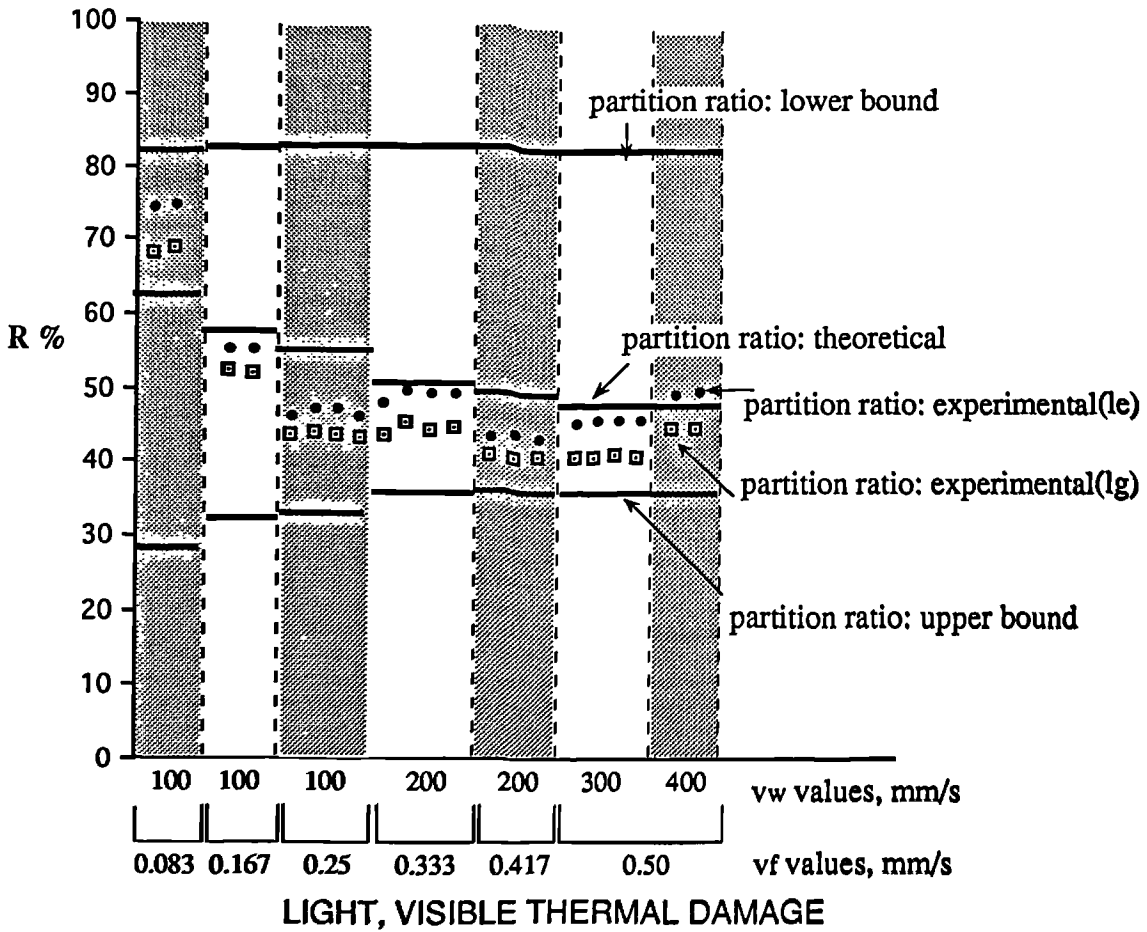


Figure 9.8 Theoretical and measured values of partition ratio.

Grinding wheel	: 19AV60NVS
Wheel diameter	: 0.475 m
Workpiece material	: grey cast iron, grade 260/17
Workpiece diameter	: 32 mm
Grinding fluid	: Trim VE20, dilution 50:1
Wheel speed	: 40 m/s
Grain contact radius, $r_0$	: 50 $\mu\text{m}$
$\gamma$	: 1
Area ratio, $A_r / A_a$	: 0.01
$\theta_m^*$	: 480 deg C
$(\kappa\rho c)_g^{1/2}$	: 10220 J/s <sup>1/2</sup> m <sup>2</sup> K
$(\kappa\rho c)_w^{1/2}$	: 14160 J/s <sup>1/2</sup> m <sup>2</sup> K
$(\kappa\rho c)_f^{1/2} / (\kappa\rho c)_w^{1/2}$	: 0.145
$e_{cc}$	: 5.28 J/mm <sup>3</sup>

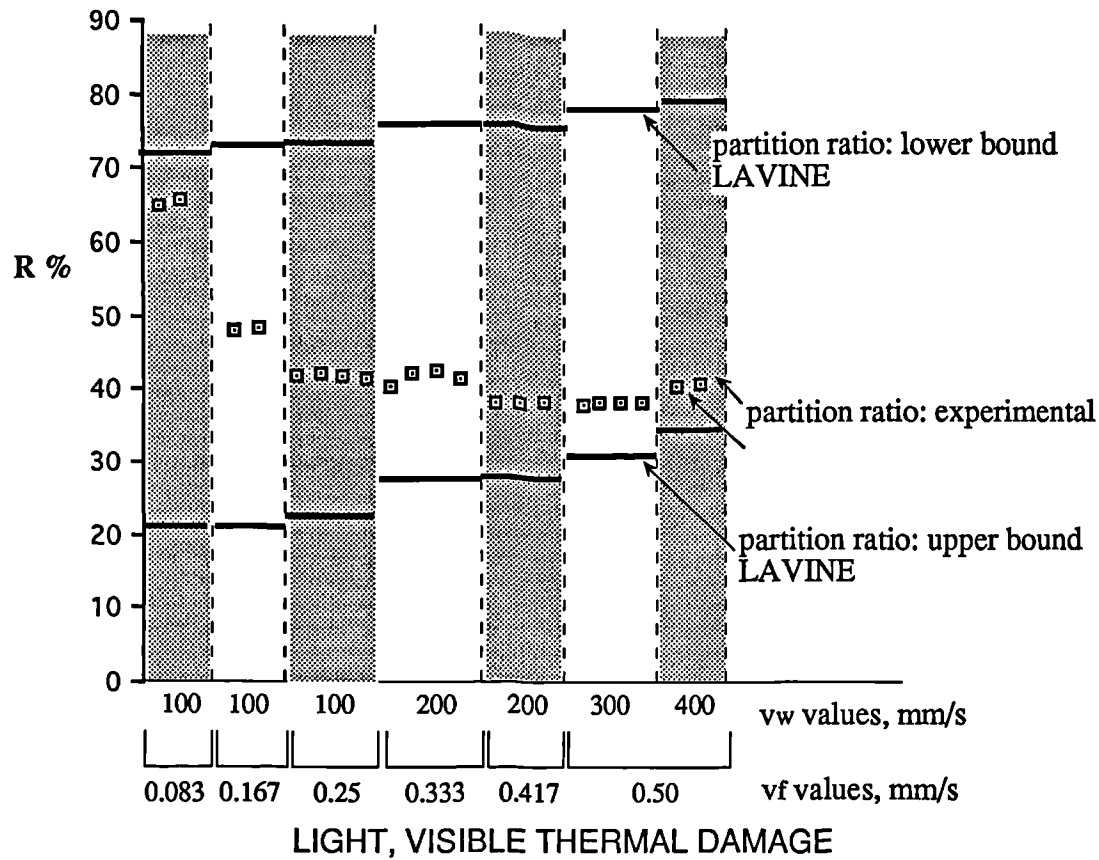


Figure 9.9 Measured values of partition ratio and theoretical lower bound and upper bound values of partition ratio predicted from the model of Lavine [42].

## 9.6 EVALUATION OF THE LAVINE MODEL.

Figure 9.9 shows experimental partition ratios compared with theoretical values from the Lavine model. It is evident from Figure 9.9 that the theoretical upper bound solution proposed by Lavine gave broadly similar results to the new model for the prediction of thermal damage, although the lower bound partition ratios reduce towards the lower workspeed and infeedrate range. The tendency of the the upper bound and lower bound solutions is less consistent with the experimental results as explained in section 9.4.

As suggested previously, it was unfortunate that the specific energies were so low as this had the effect of increasing the sensitivity of the models to the chip energy and reducing the sensitivity to the abrasive. It was not possible therefore, to make a fair comparison between the new model and the Lavine model.

## 9.7 EVALUATION OF THE ROWE AND PETTIT MODEL.

In this section, the effective bulk thermal property  $(\kappa\rho c)_s^{1/2}$  of an alumina wheel is *determined by correlating data from experimental measurements with predictions from the Rowe and Pettit model [7].* The effective bulk thermal property determined from the correlated results was then employed in the partition ratio solutions of Rowe and Pettit. In Figure 9.10 results from the lower bound partition ratio and a theoretical boundary solution are shown with the experimental partition ratio. The theoretical boundary solution excludes the effects of energy transfers to the fluid and was calculated from equation 203.

$$R_{\text{exp}} = \frac{1}{1 + \sqrt{\frac{(\kappa\rho c)_s v_s}{(\kappa\rho c)_w v_w}}} (1 - J') \quad 203$$

### 9.7.1 DETERMINATION OF THE EFFECTIVE BULK THERMAL PROPERTY.

Re-arranged for the bulk thermal property  $(\kappa\rho c)_s^{1/2}$  equation 203 becomes

$$(\kappa\rho c)_s^{1/2} = \left(\frac{v_w}{v_s}\right)^{1/2} (\kappa\rho c)_w^{1/2} \left\{ \left[ \frac{1}{R_{\text{exp}}} (1 - J') \right] - 1 \right\} \quad 204$$

The value of other parameters required for the determination of the bulk thermal property are given in Table 9.3.

Table 9.3 Values of parameters required for the calculation of  $(\kappa\rho c)_s^{1/2}$ .

Grinding wheel speed	: 40 m/s
Workpiece bulk thermal property, $(\kappa\rho c)_w^{1/2}$	: 14160 J/s <sup>1/2</sup> m <sup>2</sup> K
Energy transferred to chips, $e_{cc}$	: 5.28 J/mm <sup>3</sup>

As examples, two extreme cases are considered:

- (i)  $v_w = 100$  mm/s;  $v_f = 0.083$  mm/s.
- (ii)  $v_w = 600$  mm/s;  $v_f = 0.583$  mm/s.

The specific energy  $e_c$ , required for the calculation of  $J'$ , was the value obtained from the measured power and material removal rate at the workspeed and infeedrate combinations corresponding to case (i) and case (ii). Similarly, the values of measured partition ratio  $R_{exp}$ , were the values calculated for the workspeed and infeedrate combinations corresponding to case (i) and case (ii). The values of partition ratio and specific energy for each case were

- (i)  $R_{exp} = 0.72$ ;  $e_c = 22$  J/mm<sup>3</sup>.
- (ii)  $R_{exp} = 0.41$ ;  $e_c = 14$  J/mm<sup>3</sup>.

The effective bulk thermal property calculated from the experimental results is given in Table 9.4 with values of  $(\kappa\rho c)_s^{1/2}$  determined from independent  $\kappa$ ,  $\rho$  and  $c$  measurements and with values of  $(\kappa\rho c)_s^{1/2}$  obtained from sensor measurements. The value of  $e_{cc}$  was 5.28 J/mm<sup>3</sup> and this corresponds to a maximum value. The value of  $(\kappa\rho c)_s^{1/2}$  quoted in columns 1 and 2 of Table 9.4 are averaged values from Table 4.9.

Table 9.4 A comparison of the effective bulk thermal property  $(\kappa\rho c)_s^{1/2}$  with measured values, for an alumina wheel.

	Averaged value from $\kappa$ , $\rho$ and $c$ measurements	Averaged value from sensor measurements	Case (i) : $v_w = 100$ mm/s : $v_f = 0.083$ mm/s	Case (ii) : $v_w = 600$ mm/s : $v_f = 0.583$ mm/s
Wheel material	$(\kappa\rho c)^{1/2}$ J/s <sup>1/2</sup> m <sup>2</sup> K	$(\kappa\rho c)^{1/2}$ J/s <sup>1/2</sup> m <sup>2</sup> K	$(\kappa\rho c)^{1/2}$ J/s <sup>1/2</sup> m <sup>2</sup> K	$(\kappa\rho c)^{1/2}$ J/s <sup>1/2</sup> m <sup>2</sup> K
Al <sub>2</sub> O <sub>3</sub> $e_{cc} = 5.28$ J/mm <sup>3</sup>	1479	2045	40	900

In case (i), the value of effective bulk thermal property does not match well with measured values. The workspeed and infeedrate values used in case (i) correspond to the region of indeterminacy of Figure 9.4 and it can reasonably be argued that the result for this case is not reliable.

In case (ii), the value of effective bulk thermal property is of the same order as the measured values, and it is proposed that the effective value is probably in the range  $900 < (\kappa\rho c)_s^{1/2} < 2045 \text{ J/s}^{1/2}\text{m}^2\text{K}$ , since the value estimated for case(i) represents a situation where the model is beginning to break down for reasons which are not fully explained.

### 9.7.2 RESULTS FOR THE ROWE AND PETTIT MODEL.

In this section, values of partition ratio predicted from the Rowe and Pettit model [7] are compared with the values of partition ratio measured from experiment. The lower bound partition ratio was calculated from equation 88 using the values of parameters given in Table 9.5.

Table 9.5 Values of parameters used to calculate the lower bound partition ratio from the Rowe and Pettit model.

Grinding wheel speed	: 40 m/s
Specific energy to chips, $e_{cc}$	: 5.28 J/mm <sup>3</sup>
Workpiece bulk thermal property, $(\kappa\rho c)_w^{1/2}$	: 14160 J/s <sup>1/2</sup> m <sup>2</sup> K
Effective wheel bulk thermal property, $(\kappa\rho c)_s^{1/2}$	: 900 J/s <sup>1/2</sup> m <sup>2</sup> K

The theoretical boundary partition ratio was calculated from equation 101a, modified to exclude the effect of energy partitioning to the fluid. The measured specific energy and corresponding value of workspeed were taken from the experimental study. The values of  $e_{cc}$  and  $(\kappa\rho c)_s^{1/2}$  used were based on the results of the previous section, 9.6.1.

In Figure 9.10 the experimental values are seen to lie between the boundary solutions except at low workspeeds. Better agreement across the range of results could be achieved using a lower value for the effective thermal properties of the

wheel. However, at the lower workspeeds the Rowe and Pettit model predicts the opposite tendency to the measured results. The result, which is consistent with previous theoretical results illustrated in chapter seven, was attributed to the effect of modelling assumptions concerned with the Peclet number. At low values of workspeed the Peclet number criterion is breached and the model is no longer valid.

Grinding wheel :19AV60NVS  
 Wheel diameter : 0.475 m  
 Workpiece material : grey cast iron, grade 260/17  
 Workpiece diameter : 32 mm  
 Grinding fluid : Trim VE20, dilution 50:1  
 Wheel speed : 40 m/s  
 $e_{cc}$  : 5.28 J/mm<sup>3</sup>  
 $(\kappa pc)_s^{1/2}$  : 900 J/s<sup>1/2</sup>m<sup>2</sup>K  
 $(\kappa pc)_w^{1/2}$  : 14160 J/s<sup>1/2</sup>m<sup>2</sup>K

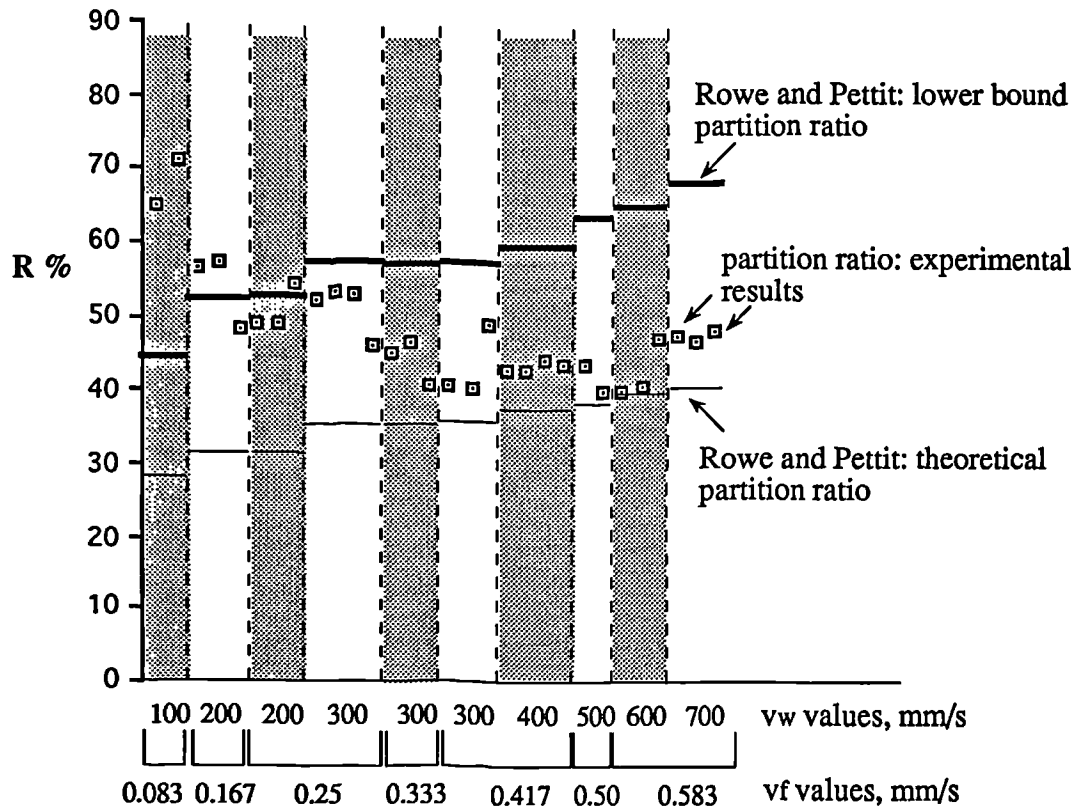


Figure 9.10 Theoretical values of partition ratio predicted from the Rowe and Pettit model with experimentally measured values of partition ratio.

## 9.8 CONCLUDING DISCUSSION.

The new model gives improved agreement with experimental results. It is clearly shown, that the specific energy to the chips is an important element in the actual process. Good agreement is only achieved by including the specific energy to the chips and the energy to the grinding wheel in the partitioning model.

Damage does not always occur at specific energies corresponding to the theoretical boundary. However, agreement is close so that the theoretical boundary is a realistic working model. For monitoring purposes, the lower bound could be considered as a warning limit and the theoretical boundary as an action limit.

The results shown in Figures 9.5 to 9.8 provide strong evidence to suggest that the energy transfers to the fluid are smaller than predicted from equation 193. The assumptions concerning the fluid require further investigation.

Advantages could be gained from ensuring that the wheel surface is free from workpiece material and this would be particularly significant with CBN since the relative difference between the thermal properties of the workpiece and those of the grain material is high. The accuracy of the theoretical results beyond the lower workspeed and infeedrate range suggest that all of the heat energy entering the active grains is dissipated prior to re-engagement with the workpiece. The results provide justification for the assumption of an initial ambient grain temperature.

In this study, effective values of the bulk thermal property  $(\kappa\rho c)_s^{1/2}$  have been presented for an alumina wheel. Prior to this study very few data relating to the bulk property were available, nor were the data available corroborated with experimental evidence. As a consequence, it is the first time an evaluation of the bulk thermal properties model has been undertaken.

## Chapter 10 CONCLUSIONS.

1. The stationary source model and moving source model solutions presented by Jaeger have been shown to provide a useful basis for the calculation of temperatures experienced between a grinding wheel and workpiece if a partition ratio is used to modify the quantity of heat entering each body.
2. A new model has been developed based on the thermal analysis of a stationary conical grain and a moving circular heat source. A transient solution and an approximate steady state solution have been proposed for the partition ratio. The transient solution allows the partition ratio to be estimated at each point through the grinding zone and hence leads to an overall estimate of the proportion of the total heat which enters the workpiece in the grinding zone. In effect, this allows interface temperatures to be equated at each point through the grinding zone. While this solution overcomes some problems inherent in previous approaches, the conical grain model cannot be used for cone angles greater than  $45^\circ$  since in this case the heat transfer into the grain would exceed the value for the plane solution which is a boundary solution.
3. Upper bound and lower bound solutions have been developed. The theoretical lower bound solution over-estimates the heat energy transferring to the workpiece. Allowance for energy transfers to the chips and to the fluid yields an upper bound prediction of the energy transferring to the workpiece. A theoretical boundary solution  $R_{th}$ , for the partition ratio that excludes energy transfer to the fluid, predicts values of partition ratio that correlate well with results from an experimental study.
4. A significant difference in the proposed model and other approaches is the contact length employed. Experimental evidence strongly indicates that real contact lengths are typically 2 - 3 times greater than geometric contact lengths. Theoretical results using the real contact length correlate well with results from an experimental study. Theoretical results that employ the geometric contact length result in lower values of partition ratio.
5. The new approach is different from the approach adopted by Rowe and Pettit, who proposed upper and lower bound solutions, in that the analysis of heat transfers is undertaken at the grain contact level.

6. Energy modelling to the fluid can be undertaken as: (i) a single stage process, where it is proposed that the cooling effect of the fluid takes place simultaneously with the energy partitioning between the wheel and the workpiece, or (ii) a two-stage process, where it is proposed that the heat first enters the workpiece and wheel and later transfers to the fluid. It was concluded that either modelling assumption yields similar values of critical specific energy.

7. The effect of the transient on the value of the partition ratio is not strong for the recommended range of values,  $0.80 < \phi < 0.90$ . The principal parameters affecting the value of partition ratio are the contact length, grain contact length and shape effect,  $f(\zeta)$ . Recommended values of grain contact length are  $50 \mu\text{m} < r_o \text{ (alumina)} < 100 \mu\text{m}$ , and  $25 \mu\text{m} < r_o \text{ (CBN)} < 50 \mu\text{m}$ .

8. The bulk thermal property  $(\kappa\rho c)_s^{1/2}$ , has similar values for both CBN and alumina wheel materials. The results of this study indicate that the bulk wheel property alone, does not account for the improved thermal performance of CBN compared to alumina. The value of  $(\kappa\rho c)_s^{1/2}$  for the alumina wheel used was in the range  $900 < (\kappa\rho c)_s^{1/2} < 2045 \text{ J/s}^{1/2}\text{m}^2\text{K}$ .

9. The work presented in this thesis provides strong evidence to support the hypothesis that a heat transfer analysis of the grinding process based on appropriate heat transfer assumptions, can provide a satisfactory reference for an adaptive system to control or monitor workpiece thermal damage. It has been shown that at high workspeeds either the Rowe and Pettit model or the new model can be employed with appropriate values for thermal properties. However, the Rowe and Pettit model, and all other models fail the test of agreement with experimental results at low workspeeds. The new model is the only model which gives good agreement at low workspeeds.

## **Chapter 11 RECOMMENDATIONS FOR FURTHER WORK.**

There remains some uncertainty concerning the value of particular model parameters. The thermal properties of abrasive grain materials and composite wheel compounds, at ambient and at elevated temperatures, requires further investigation. During grinding, the wear flat length is a dynamic property of the abrasive grain. Further experimental evidence is needed to establish an empirical model for wear flat lengths under particular grinding conditions. It has been shown that the length of contact over which the heat source is applied affects the intensity of the heat source distribution. Further work is needed to establish quantifiable evidence for applying particular values of parameters in the real contact length model.

The workpiece thermal damage criteria and the associated workpiece critical temperature need to be determined for a range of workpiece materials. Determination of the damage criteria is particularly important for materials common to the aerospace and automotive industries, where the thermal integrity of a component is often critical.

Further work is required to investigate the effect of fluid on specific energy values.

The thermal model was validated against the results of centreless grinding experiments. Development of the work for application to internal, face and form grinding operations, where boundary conditions and contact geometry are different to those investigated, is recommended.

Further work is suggested to establish if the proposed thermal model will provide an appropriate basis from which to develop a model for the prediction of residual tensile stress levels.

## REFERENCES

- [1] Inasaki, I., Toenshoff, H.K., Howes, T.D., 1993, 'Abrasive machining in the future', Keynote paper, Annals of the CIRP volume 42/2.
- [2] Torrance, A.A., 1978, 'Metallurgical effects associated with grinding', Proceedings of 19th International Machine Tool Design and Research Conference, Manchester, pp 637 - 644.
- [3] Malkin, S., 1989, 'Grinding technology - theory and applications of machining with abrasives', Publishers - Ellis Horwood Ltd.
- [4] Malkin, S., 1978, 'Burning limit for surface and cylindrical grinding of steels', Annals of the CIRP, volume 27/1, pp 233-235.
- [5] Okuyamar, S., Nakamura, Y., Kawamura, S., 1992, 'Cooling action of grinding fluid in shallow grinding', International Journal of Machine Tools Manufacturing, volume 33, n 1, pp 13 - 23.
- [6] Pearce, T., 1993, 'Simple rules for correct use of coolant in general grinding applications', Proceedings of the Institute of Grinding Technology Seminar, held at the University of Bristol, 16 February.
- [7] Rowe, W.B., Pettit, J.A., Boyle, A., Moruzzi, J.L., 1988, 'Avoidance of thermal damage in grinding and prediction of the damage threshold', Annals of the CIRP, volume 37/1, pp 327-330.
- [8] Outwater, J.O., Shaw, M.C., 1952, 'Surface temperatures in grinding', Transactions of A.S.M.E., 74, pp 73-85.
- [9] Takazawa, K., 1964, 'The flowing rate into the work of the heat generated by grinding', Journal Japan Society, Precision Engineering, volume 30 Part 12, pp 914 -920.
- [10] Rowe, W.B., Qi, H.S., Morgan, M.N., Zheng, H., 1993, 'The effect of deformation on the contact area in grinding', Annals of the CIRP, volume 42/1, pp 409 - 412.
- [11] Lavine, A.S., Malkin, S., Jen, T.C., 1989, 'Thermal aspects of grinding with CBN wheels', Annals of the CIRP, 38/1, pp 557-560.
- [12] Carslaw, H.S., Jaeger, J.C., 1990, 'Conduction of heat in solids', Second Edition, Published by Oxford University Press, New York.
- [13] Blok, H., 1937, 'Theoretical study of temperature rise at surfaces of actual contact under oiliness lubricating conditions', Proceedings of the General Discussion on Lubrication and Lubricants, Institution of Mechanical Engineers, London, volume 2, p 222 - 235.

- [14] Herivel, J., 1975, 'Joseph Fourier - The Man and the Physicist', Published by Clarendon Press Oxford.
- [15] Grigull, U., Sandner, H., 1984, 'Heat Conduction', First Edition, Published by Hemisphere Corporation, International Series in Heat and Mass Transfer.
- [16] Jaeger, J.C., 1942, 'Moving sources of heat and the temperature at sliding contacts, Proceedings of the Royal Society of New South Wales, 76, pp 203-224.
- [17] Vanserven, Ir.E., 1987, 'A subsurface integrity model in grinding', Ph.D. Thesis, Katholieke Universiteit Leuven, Belgium.
- [18] Snoeys, R., Maris, M., Peters, J., 1978, 'Thermally induced damage in grinding', Annals of the CIRP, volume 27/2, pp 571-581.
- [19] Takazawa, K., 1966, 'Effects of grinding variables on surface structure of hardened steel', Bulletin of the Japan Society of Precision Engineering, volume 2, n 1, pp 14-21.
- [20] Takazawa, K., 1972, 'Thermal aspects of the grinding operation', Industrial Diamond Review, April, pp 143-149.
- [21] Maris, M., Snoeys, R., 1973, 'Heat affected zone in grinding operations', Proceedings of the 14th International Machine Tool Design and Research Conference, Manchester, pp 659 -669.
- [22] Malkin, S., 1974, 'Thermal aspects of grinding. Part 1 - Energy partition, Part 2 - Surface temperatures and workpiece burn', Journal of Engineering for Industry, 96, pp 1184-1191.
- [23] Hahn, R.S., 1962, 'On the nature of the grinding process', Proceedings of Third International Machine Tool Design and Research Conference, pp 129 - 154.
- [24] Malkin, S., Cook, N.H., 1971, 'The wear of grinding wheels, Part 2 - Fracture wear', Journal of Engineering for Industry, November, pp 1129-1133.
- [25] Gu, D., 1992, 'The contact zone in surface grinding', Ph.D. Thesis, University of Western Australia, Australia.
- [26] Okuyamar, S., Kawamura, S., 1979, 'On the interference length of surface grinding', Journal Japan Society of Precision Engineering, volume 45, n 4.
- [27] Xiao, G., Malkin, S., Danai, K., 1994, 'Autonomous system for multi-stage cylindrical grinding', Transactions ASME, Journal of Dynamic Systems, Measurement and Controls.
- [28] Srivastava, S., Rogers, D.B., Elbestawi, M.A., 1992, 'Workpiece burn and surface finish during controlled force robotic disk grinding', International Journal of Machine Tools Manufacturing', volume 32, n 6, pp 797-809.

- [29] Srivastava, S., Ulrich, B.J., Elbestawi, M.A., 1990, 'Analysis of rigid-disk wear during robotic grinding', *International Journal of Machine Tools Manufacturing*, volume 30, n 4, pp 521-534.
- [30] Des Ruisseaux, N.R., Zerkle, R.D., 1970, 'Temperature in semi-infinite and cylindrical bodies subjected to moving heat sources and surface cooling', *Journal of Heat Transfer*, 92, pp 456-464.
- [31] Des Ruisseaux, N.R., Zerkle, R.D., 1970, 'Thermal analysis of the grinding process', *Journal of Engineering for Industry*, 92, pp 429-435.
- [32] Fursdon, P.M.T., 1989, 'The continuous dress creep feed form grinding of titanium alloys', PhD thesis, University of Bristol.
- [33] Gamble, K., 1987, 'Thermal aspects of grinding', B.Sc Engineering Thesis, Liverpool John Moores University.
- [34] Rowe, W.B., Bell, W.F., Brough, D., 1987, 'Limit charts for high removal rate centreless grinding', *International Journal of Machine Tools Manufacture*, volume 27, no1, pp 15 - 25.
- [35] Verkerk, J., 1975, 'The real contact length in cylindrical and plunge grinding', *Annals of the CIRP* volume 24 / , pp 259 - 263.
- [36] Gu, D.Y., Wager, J.G., 1988, 'New evidence on the contact zone in grinding contact length, sliding and cutting regions', *Annals of the CIRP*, volume 37/1, pp 335 - 340.
- [37] Gu, D.Y., Wager, J.G., 1990, 'Further evidence on the contact zone in surface grinding', *Annals of the CIRP*, volume 39/1, pp 349 - 352.
- [38] Rowe, W.B., Qi, H.S., Morgan, M.N., Zheng, H.W., 1993, 'The effect of deformation on the contact area in grinding', *Annals of the CIRP*, volume 42/1, pp 409 - 412.
- [39] Holman, J.P., 1986, 'Heat transfer', Sixth edition, Publishers - McGraw-Hill.
- [40] Shaw, M.C., Ramanath, S., 1988, 'Abrasive grain temperature at the beginning of a cut in fine grinding', *Journal of Engineering for Industry*, February, volume 110, pp 15 - 18.
- [41] Shaw, M.C., 1990, 'A simplified approach to workpiece temperatures in fine grinding', *Annals of the CIRP*, volume 39/1, pp 345-347.
- [42] Lavine, A.S., Jen, T.C., 1991, 'Coupled heat transfer to workpiece, wheel, and fluid in grinding, and the occurrence of workpiece burn', *International Journal of Heat and Mass Transfer*, volume 34, no 4/5, pp 983-992.
- [43] Lavine, A.S., 1989, 'Thermal aspects of grinding : Heat transfer to workpiece, wheel and fluid', In *Collected Papers in Heat Transfer ASME HTD* volume 123, pp 267-274.

- [44] Lavine, A.S., 1991, 'Thermal aspects of grinding : The effect of heat generation at the shear planes', *Annals of the CIRP*, 38/1, pp 557-559.
- [45] Ramachandran, K.I., Vijayaraghavan, L., Krishnamurthy, R., Ganesan, N., 'Thermal stresses in grinding wheels'.
- [46] Toenshoff, H.K., Brinksmeier, E., Wobker, H.G., 1989, 'Evaluation of surface layers of machined ceramics', *Annals of the CIRP*, volume 38/2, pp 699 - 708.
- [47] Phanindrananth, V., Babu Ramesh, N., 'A theoretical model for prediction of groove geometry on laser dressed grinding wheel surface'.
- [48] Universal Grinding Wheel Company, 1994, 'Treibacher artificial corundum: General characteristics', Personal correspondence.
- [49] DeVries, R.C., 1972, 'Cubic Boron Nitride: Handbook of properties', General Electric Technical Information Series, General Electric Company Corporate Research and Development, No 72CRD178
- [50] Gardinier, C.F., 1988, 'Physical properties of superabrasives', *American Ceramic Society Bulletin*, volume 67, no 6, pp 1006 - 1009.
- [51] Kumar, K.V., 1990, 'Superabrasive grinding of Titanium alloys', Society of Manufacturing Engineers, 4th International Grinding Conference, Dearborn Michigan, USA, MR90-505, pp 1 - 17.
- [52] Hiroshi, E., Kishi, K., 1975, 'The newly developed CBN cutting tool', *Journal American Ceramic Society*, volume 57.
- [53] Bailey, M.W., 1992, 'Ultra-hard abrasives in engineering production application notes and illustrations'. Personal correspondence.
- [54] Verniekes, N., 1987, 'CBN grinding wheels with ceramic bonding for cost-effective grinding', *Ball and Roller Bearing Engineering*, FAG 30, pp30 - 35.
- [55] Kingery, W.D., 1963, 'Structure and properties of vitrified-bonded abrasives', *Ceramic bulletin* 42/5, pp 297 - 303.
- [56] *Smithells Metals Reference Book*, 1992, Published by Butterworth Heinemann Ltd, 7th Edition.
- [57] Mittal, R.N., Porter, T.M., Rowe, G.W., 1984, 'Lubrication with cutting and grinding emulsions', *Lubrication Engineering*, volume 40, pp 160 -162.
- [58] Rowe, W.B., Morgan, M.N., Pettit, J.A.P., Lavine, A.S., 1990, 'A discussion of thermal models in grinding', Society of Manufacturing Engineers, 4th International Grinding Conference, Dearborn Michigan, USA, MR90-516, pp1-14.
- [59] Rowe, W.B., Black, S.C.E., Mills, B., Qi, H.S., 1994, 'Experimental energy partitioning in grinding', *Proceedings of EuroMetalWorking Conference*, Udine, Italy, pp 1 - 8.

- [60] Archard, J.F., 1958, 'The temperature of rubbing surfaces', *Wear*, volume 2, pp 438 - 455.
- [61] *Machining Data Handbook*, 1980, Published by Machinability Data Center, Metcut Research Associates Inc, Cincinnati, Ohio, Third Edition, volume 2.
- [62] Rowe, W.B., Chen, X., Morgan, M.N., 1993, 'The identification of dressing strategies for optimal grinding wheel performance', *Proceedings of the 30th Int. MATADOR Conference*, pp 195 - 202..
- [63] *Iron and Steel specifications Handbook*, 1986, Published by British Steel Corporation, 6th Edition.
- [64] Rexroth Indramat, AC Main Drive User's Manual IA74788 REV.A 10/91.
- [65] Amplicon Liveline Limited, 1990, PC-30PGL and PC-30PGH User Manual, Companion Manual PC-30 Driver Software.
- [66] Rowe, W.B., Black, S.C.E., Mills, B., Qi, H.S., Morgan, M.N., 'Experimental investigation of heat transfer in grinding', submitted to CIRP 1995.

## APPENDICES

## APPENDIX 1.1

### THE DERIVATION OF THE TRANSIENT ONE-DIMENSIONAL HEAT CONDUCTION EQUATION.

Reference is made to Figure 2.1 for the terms used in this derivation.

The heat entering the elemental volume of width  $dx$  is equated to the heat leaving the elemental volume plus the increase in internal energy. Expressed analytically as

$$E_{\text{enter}} = E_{\text{out}} + E_{\text{internal}} \quad \text{A1.1.1}$$

$$E_{\text{enter}} = q = -kA \frac{\partial \theta}{\partial x} \quad \text{A1.1.2}$$

$$E_{\text{internal}} = \rho c A \frac{\partial \theta}{\partial t} dx \quad \text{A1.1.3}$$

$$E_{\text{out}} = q_{x+dx} = -kA \left. \frac{\partial \theta}{\partial x} \right|_{x+dx} = -A \left[ \kappa \frac{\partial \theta}{\partial x} + \frac{\partial}{\partial x} \left( \frac{\partial \theta}{\partial x} \right) dx \right] \quad \text{A1.1.4}$$

The term on the right hand side of equation A1.1.4 is obtained from Taylor's theorem, and uses the first two terms of the expansion only, such that

$$f(x+h) = f(x) + hf'(x)$$

Substituting for A1.1.2, A1.1.3 and A1.1.4 in A1.1.1

$$-kA \frac{\partial \theta}{\partial x} = \rho c A \frac{\partial \theta}{\partial t} dx - A \left[ \kappa \frac{\partial \theta}{\partial x} + \frac{\partial}{\partial x} \left( \frac{\partial \theta}{\partial x} \right) dx \right] \quad \text{A1.1.5}$$

Simplifying and rearranging A1.1.5 gives

$$\frac{\partial^2 \theta}{\partial x^2} = \frac{1}{\alpha} \frac{\partial \theta}{\partial t} \quad \text{A1.1.6}$$

Where equation A1.1.6 is termed the governing equation for transient one-dimensional heat conduction.

## APPENDIX A1.2

A SUMMARY OF THE EXPRESSIONS FOR THE AVERAGE AND MAXIMUM TEMPERATURE SOLUTIONS AT THE SURFACE OF A MEDIUM SUBJECT TO A MOVING BAND HEAT SOURCE.

The following equations are valid for values of Peclet number greater than 5.

The maximum dimensionless surface temperature,  $\bar{\theta}_m$  is given by

$$\bar{\theta}_m = \left( \frac{\pi \cdot \kappa \cdot v}{2 \cdot \alpha \cdot q} \right) \theta_m = 3.54 L^{1/2} \quad \text{A1.2.1}$$

The maximum surface temperature,  $\theta_m$  is given by

$$\theta_m = \frac{1.60q}{\kappa} \left( \frac{\alpha \cdot l}{v} \right)^{1/2} \quad \text{A1.2.2}$$

$$\theta_m = \frac{2q}{\kappa} \left( \frac{2 \cdot \alpha \cdot l}{\pi \cdot v} \right)^{1/2} \quad \text{A1.2.3}$$

$$\theta_m = \frac{4 \cdot q \cdot \alpha}{\kappa \cdot v \cdot \pi^{1/2}} L^{1/2} \quad \text{A1.2.4}$$

$$\theta_m = \frac{1.13q \cdot l}{\kappa \cdot L^{1/2}} \quad \text{A1.2.5}$$

The average surface temperature,  $\theta_{av}$  is given by

$$\theta_{av} = \frac{0.754q \cdot l}{\kappa \cdot L^{1/2}} \quad \text{A1.2.6}$$

$$\theta_{av} = \frac{1.064q}{\kappa} \left( \frac{\alpha \cdot l}{v} \right)^{1/2} \quad \text{A1.2.7}$$

For values of Peclet number less than 5, the maximum surface temperature expressed in terms of the non-dimensional temperature parameters  $\bar{f}$  and  $f_m$  is

$$\theta_m = \frac{0.636q \cdot \alpha}{\kappa \cdot v} f_m = \frac{f_m}{\bar{f}} \bar{\theta} \quad \text{A1.2.8}$$

### APPENDIX A1.3

#### THE DERIVATION OF THE CONICAL GRAIN TEMPERATURE SOLUTION DESCRIBED BY LAVINE [42, 43].

The governing equation for one-dimensional heat conduction with reference to Figure 3.11 is

$$\frac{\partial \theta_g}{\partial t} = \frac{\alpha_g}{A_c} \frac{\partial}{\partial z} \left( A_c \frac{\partial \theta_g}{\partial z} \right) \quad \text{A1.3.1}$$

where

$$A_c = \pi r^2 \text{ and } r = r_0 + \gamma z$$

$$\text{Let } \hat{\theta} = r \theta_g \text{ then } \theta_g = \frac{1}{r} \hat{\theta}$$

so

$$\frac{\partial \theta_g}{\partial z} = \frac{\partial}{\partial z} \left( \frac{1}{r} \hat{\theta} \right) \quad \text{A1.3.2}$$

The partial derivative of the right hand term is

$$\frac{\partial \theta_g}{\partial z} = \frac{1}{r} \frac{\partial \hat{\theta}}{\partial z} + \frac{\partial}{\partial z} \left( r^{-1} \hat{\theta} \right) \quad \text{A1.3.3}$$

Substituting for 'r' gives

$$\frac{\partial \theta_g}{\partial z} = \frac{1}{r} \frac{\partial \hat{\theta}}{\partial z} + \frac{\partial}{\partial z} (r_0 + \gamma z)^{-1} \hat{\theta} \quad \text{A1.3.4}$$

Completing the differentiation of A1.3.4

$$\frac{\partial \theta_g}{\partial z} = \frac{1}{r} \frac{\partial \hat{\theta}}{\partial z} - (r_0 + \gamma z)^{-2} \gamma \hat{\theta} \quad \text{A1.3.5}$$

Substituting for  $(r_0 + \gamma z)$  in equation A1.3.5

$$\frac{\partial \theta_g}{\partial z} = \frac{1}{r} \frac{\partial \hat{\theta}}{\partial z} - \frac{\gamma \hat{\theta}}{r^2} \quad \text{A1.3.6}$$

From equation A1.3.1 and A1.3.6

$$\frac{\alpha_g}{A_c} \frac{\partial}{\partial z} \left( \frac{A_c \partial \theta_g}{\partial z} \right) = \frac{\partial}{\partial z} \left[ A_c \left( \frac{1}{r} \frac{\partial \hat{\theta}}{\partial z} - \frac{\gamma \hat{\theta}}{r^2} \right) \right] \quad \text{A1.3.7}$$

$$\frac{\partial}{\partial z} \left( \frac{A_c \partial \theta_g}{\partial z} \right) = \frac{\partial}{\partial z} \left[ \pi r^2 \left( \frac{1}{r} \frac{\partial \hat{\theta}}{\partial z} - \frac{\gamma \hat{\theta}}{r^2} \right) \right] \quad \text{A1.3.8}$$

$$\frac{\partial}{\partial z} \left( \frac{A_c \partial \theta_g}{\partial z} \right) = \pi \frac{\partial}{\partial z} \left[ r \frac{\partial \hat{\theta}}{\partial z} - \gamma \hat{\theta} \right] \quad \text{A1.3.9}$$

$$\frac{\partial}{\partial z} \left( \frac{A_c \partial \theta_g}{\partial z} \right) = \pi \left( r \frac{\partial^2 \hat{\theta}}{\partial z^2} + \gamma \frac{\partial \hat{\theta}}{\partial z} - \gamma \frac{\partial \hat{\theta}}{\partial z} \right) \quad \text{A1.3.10}$$

$$\frac{\partial}{\partial z} \left( \frac{A_c \partial \theta_g}{\partial z} \right) = \pi r \frac{\partial^2 \hat{\theta}}{\partial z^2} \quad \text{A1.3.11}$$

Also,

$$\frac{\partial \theta_g}{\partial t} = \frac{1}{r} \frac{\partial \hat{\theta}}{\partial t} \quad \text{A1.3.12}$$

Substitute A1.3.11 and A1.3.12 in A1.3.1,

$$\frac{1}{r} \frac{\partial \hat{\theta}}{\partial t} = \frac{\alpha_g}{A_c} \pi r \frac{\partial^2 \hat{\theta}}{\partial z^2} \quad \text{A1.3.13}$$

or

$$\frac{\partial \hat{\theta}}{\partial t} = \alpha_g \frac{\partial^2 \hat{\theta}}{\partial z^2} \quad \text{A1.3.14}$$

The boundary and initial conditions for  $\hat{\theta}$  are

- 1 At time  $t = 0$ ;  $\theta_g(z, t = 0) = 0$  and  $\hat{\theta}(z, t = 0) = 0$
- 2 At the steady state, i.e.  $z = \infty$ ;  $\theta_g(z = \infty, t)$  - finite, and  $\hat{\theta}(z = \infty, t)$  - finite.
- 3 The heat flux at the surface of the grain =  $\theta_g$  and

$$q_g = -\kappa \left. \frac{\partial \theta_g}{\partial z} \right|_{z=0} \quad \text{A1.3.15}$$

From A1.3.6

$$q_g = -\kappa \left[ \frac{1}{r} \frac{\partial \hat{\theta}}{\partial z} - \frac{\gamma \hat{\theta}}{r^2} \right]_{z=0} \quad \text{A1.3.16}$$

$$\frac{-q_g r_0^2}{\kappa} = r_0 \left. \frac{\partial \hat{\theta}}{\partial z} \right|_{z=0} - \gamma \hat{\theta} \Big|_{z=0} \quad \text{A1.3.17}$$

Taking the laplace transform in time,

$$\hat{\theta}(z, t) \rightarrow L[\hat{\theta}(z, s)] = \bar{\theta}(z, s)$$

and using the rule  $L[f'(f)] = s f'(s) - f(0)$

the differential equation of A1.3.14 becomes

$$s \bar{\theta} - \hat{\theta}(0) = \alpha_g \frac{\partial^2 \bar{\theta}}{\partial z^2} \quad \text{A1.3.18}$$

the initial condition of  $\hat{\theta}(0) = 0$  gives

$$\bar{\theta} = \alpha_g \frac{\partial^2 \bar{\theta}}{\partial z^2} \quad \text{A1.3.19}$$

r

$$\frac{\partial^2 \bar{\theta}}{\partial z^2} - s \bar{\theta} = 0 \quad \text{A1.3.20}$$

This is a second order homogeneous differential equation and can be solved by the trial method. A number of different trial solutions are described in, for example, references [68 and 69], however, the solution used by Lavine [42, 43] is given below.

The general solution to equation A1.3.20 is assumed to be of the form  $y = Ae^{\lambda z}$  then,  $\frac{d^2 y}{dx^2} = A \lambda^2 e^{\lambda z}$  and  $\bar{\theta} = a_1 e^{\lambda z} + a_2 e^{-\lambda z}$ . Where  $\lambda = \sqrt{\frac{s}{\alpha_g}}$ .

The transformed boundary conditions from A1.3.15 are

( $z = \infty, s$ ) - finite, therefore  $a_1 = 0$

and from A1.3.17

$$\frac{q_g r_0^2}{\kappa} \frac{1}{s} = r_0 \frac{\partial \bar{\theta}}{\partial z} \Big|_{z=0} - \gamma \bar{\theta} \Big|_{z=0} \quad \text{A1.3.21}$$

for the condition  $a_1 = 0$

$$\bar{\theta} = a_2 e^{-\lambda x} \quad \text{A1.3.22}$$

$$\text{thus, } \frac{d\bar{\theta}}{dz} = -\lambda a_2 e^{-\lambda x} \quad \text{A1.3.23}$$

and A1.3.20 is expressed as

$$r_0 (-\lambda a_2 e^{-\lambda x})_{z=0} - \gamma a_2 e^{-\lambda x} |_{z=0} = -\frac{q_g r_0^2}{\kappa_g} \frac{1}{s} \quad \text{A1.3.24}$$

$$-r_0 \lambda a_2 - \gamma a_2 = -\frac{q_g r_0^2}{\kappa_g} \frac{1}{s} \quad \text{A1.3.25}$$

$$-a_2 (r_0 \lambda + \gamma) = -\frac{q_g r_0^2}{\kappa_g} \frac{1}{s} \quad \text{A1.3.26}$$

and

$$a_2 = \frac{q_g r_0^2}{\kappa_g} \frac{1}{s(r_0 \lambda + \gamma)} \quad \text{A1.3.27}$$

From A1.3.22 and A1.3.27

$$\bar{\theta} = \frac{q_g r_0^2}{\kappa_g} \frac{e^{-\lambda x}}{s(r_0 + \gamma)} \quad \text{A1.3.28}$$

This is a standard Transform of the form  $\frac{e^{-qx}}{p(q+h)}$ , where the inverse solution for  $\bar{\theta}(p)$  is

$$\frac{1}{h} \operatorname{erfc}\left(\frac{x}{2\sqrt{\alpha t}}\right) - \frac{1}{h} e^{hx + \alpha h^2 t} \operatorname{erfc}\left(\frac{x}{2\sqrt{\alpha t}} + h\sqrt{\alpha t}\right) \quad \text{A1.3.29}$$

Multiplying the numerator and denominator of the right hand term in A1.3.28 by  $1/r_0$  gives

$$\bar{\theta} = \frac{q_g r_0}{\kappa_g} \frac{e^{-\lambda z}}{\left(\lambda + \frac{\gamma}{r_0}\right)}$$

So that,  $p = \frac{q_g r_0}{\kappa_g}$ ,  $h = \frac{\gamma}{r_0}$  and  $x = z$

Substituting in A1.3.29 for  $p$ ,  $h$  and  $x$

$$\begin{aligned} & \frac{1}{h} \operatorname{erfc}\left(\frac{x}{2\sqrt{\alpha t}}\right) - \frac{1}{h} e^{hx + \alpha t h^2} \operatorname{erfc}\left(\frac{x}{2\sqrt{\alpha t}} + h\sqrt{\alpha t}\right) \\ \equiv & \frac{r_0}{\gamma} \operatorname{erfc}\left(\frac{z}{2\sqrt{\alpha t}}\right) - \frac{r_0}{\gamma} e^{\frac{\gamma}{r_0} z + \alpha \left(\frac{\gamma}{r_0}\right)^2 t} \operatorname{erfc}\left(\frac{z}{2\sqrt{\alpha t}} + \sqrt{\left(\frac{\gamma}{r_0}\right)^2 \alpha t}\right) \end{aligned} \quad \text{A1.3.30}$$

$$= \frac{q_g r_0^2}{\gamma \kappa_g} \left[ \operatorname{erfc}\left(\frac{z}{2\sqrt{\alpha t}}\right) - e^{\frac{\gamma}{r_0} z + \alpha \left(\frac{\gamma}{r_0}\right)^2 t} \operatorname{erfc}\left(\frac{z}{2\sqrt{\alpha t}} + \sqrt{\left(\frac{\gamma}{r_0}\right)^2 \alpha t}\right) \right] \quad \text{A1.3.31}$$

Then

$$\theta_g = \frac{1}{r} \hat{\theta} = \frac{q_g r_0^2}{\gamma \kappa_g (r_0 + \gamma z)} \left[ \operatorname{erfc}\left(\frac{z}{2\sqrt{\alpha t}}\right) - e^{\frac{\gamma}{r_0} z + \alpha \left(\frac{\gamma}{r_0}\right)^2 t} \operatorname{erfc}\left(\frac{z}{2\sqrt{\alpha t}} + \sqrt{\left(\frac{\gamma}{r_0}\right)^2 \alpha t}\right) \right] \quad \text{A1.3.32}$$

At the position  $z = 0$  and at time  $t = \frac{l_g}{v_s}$  equation A1.3.32 reduces to

$$\theta_g = \frac{q_g r_0^2}{\gamma \kappa_g r_0} \left[ 1 - e^{\frac{\alpha l_g \gamma^2}{v_s r_0^2}} \operatorname{erfc}\left(\sqrt{\frac{\alpha l_g \gamma^2}{v_s r_0^2}}\right) \right] \quad \text{A1.3.33}$$

If the substitution  $\xi = \left(\frac{\alpha l_g \gamma^2}{v_s r_0^2}\right)^{1/2}$  is made A1.3.33 can be expressed as

$$\theta_g = \frac{q_g r_0}{\gamma \kappa_g} \left\{ 1 - \exp(-\xi^2) \operatorname{erfc}(\xi) \right\} \quad \text{A1.3.34}$$

Where equation A1.3.34 is the solution given by Lavine in references [42, 43].

## APPENDIX 1.4

A DERIVATION OF THE PARTITION RATIO SOLUTION PROPOSED BY LAVINE [42, 43].

Reference is made to Chapter 3, section 3.9 for the terms used below.

The describing equations for the heat transfer solution were given by

$$\theta_f = \theta_{wb} \quad \text{A1.4.1}$$

$$\theta_g = \theta_{wb} + \theta_{wg} \quad \text{A1.4.2}$$

$$q_{wb} = h_{wb}\theta_{wb} \quad \text{A1.4.3}$$

$$q_{wg} = h_{wg}\theta_{wg} \quad \text{A1.4.4}$$

$$q_g = h_g\theta_g \quad \text{A1.4.5}$$

$$q_f = h_f\theta_f \quad \text{A1.4.6}$$

$$q = q_{grind}A = q_{wg}A + q_gA \quad \text{A1.4.7}$$

$$\theta_{wb} = \frac{Rq}{h_{wb}} = \frac{q_{wb}}{h_{wb}} \quad \text{A1.4.8}$$

$$A = \frac{A_g}{A_{tot}} \quad \text{A1.4.9}$$

$$q_{wg}A_g = q_{wb}A_{tot} + q_f(A_{tot} - A_g) \quad \text{A1.4.10}$$

From A1.4.9 and A1.4.10

$$q_{wg}A = q_{wb} + q_f(1 - A) \quad \text{A1.4.11}$$

From A1.4.2, A1.4.3, A1.4.4 and A1.4.5

$$\frac{q_g}{h_g} = \frac{q_{wb}}{h_{wb}} + \frac{q_{wg}}{h_{wg}} \quad \text{A1.4.12}$$

From A1.4.12

$$q_{wg} = q_g \frac{h_{wg}}{h_g} - q_{wb} \frac{h_{wg}}{h_{wb}} \quad \text{A1.4.13}$$

From A1.4.1, A1.4.6 and A1.4.8

$$\frac{Rq}{h_{wb}} = \frac{q_f}{h_f} \quad \text{A1.4.14}$$

From A1.4.11 and A1.4.13

$$Aq_g \frac{h_{wg}}{h_g} - q_{wb} A \frac{h_{wg}}{h_{wb}} = q_{wb} + q_f(1 - A) \quad \text{A1.4.15}$$

From A1.4.8, A1.4.14 and A1.4.15

$$Aq_g \frac{h_{wg}}{h_g} - RqA \frac{h_{wg}}{h_{wb}} = Rq + Rq \frac{h_f}{h_{wb}}(1 - A) \quad \text{A1.4.16}$$

Rearrange for the 'Rq' terms

$$Aq_g \frac{h_{wg}}{h_g} = Rq + Rq \frac{h_f}{h_{wb}}(1 - A) + RqA \frac{h_{wg}}{h_{wb}} \quad \text{A1.4.17}$$

From A1.4.7 and A1.4.17

$$Aq_{grind} \frac{h_{wg}}{h_g} - Aq_{wg} \frac{h_{wg}}{h_g} = Rq + Rq \frac{h_f}{h_{wb}}(1 - A) + RqA \frac{h_{wg}}{h_{wb}} \quad \text{A1.4.18}$$

From A1.4.7 and A1.4.18

$$q \frac{h_{wg}}{h_g} - Aq_{wg} \frac{h_{wg}}{h_g} = Rq + Rq \frac{h_f}{h_{wb}}(1 - A) + RqA \frac{h_{wg}}{h_{wb}} \quad \text{A 1.4.19}$$

From A1.4.11 and A1.4.19

$$q \frac{h_{wg}}{h_g} - [q_{wb} + q_f(1 - A)] \frac{h_{wg}}{h_g} = Rq + Rq \frac{h_f}{h_{wb}}(1 - A) + RqA \frac{h_{wg}}{h_{wb}} \quad \text{A1.4.20}$$

Expand the left hand term

$$q \frac{h_{wg}}{h_g} - q_{wb} \frac{h_{wg}}{h_g} - q_f(1 - A) \frac{h_{wg}}{h_g} = Rq + Rq \frac{h_f}{h_{wb}}(1 - A) + RqA \frac{h_{wg}}{h_{wb}} \quad \text{A1.4.21}$$

From A1.4.8, A1.4.14 and A1.4.21

$$\frac{h_{wg}}{h_g} - Rq \frac{h_{wg}}{h_g} - Rq(1-A) \frac{h_f h_{wg}}{h_{wb} h_g} = Rq + Rq \frac{h_f}{h_{wb}} (1-A) + RqA \frac{h_{wg}}{h_{wb}} \quad A1.4.22$$

Rearrange for terms in 'Rq'

$$q \frac{h_{wg}}{h_g} = Rq + Rq \frac{h_f}{h_{wb}} (1-A) + RqA \frac{h_{wg}}{h_{wb}} + Rq \frac{h_{wg}}{h_g} + Rq(1-A) \frac{h_f h_{wg}}{h_{wb} h_g} \quad A1.4.23$$

Divide throughout by 'Rq' and multiply both sides by the term  $h_g/h_{wg}$

$$\frac{1}{R} = \frac{h_g}{h_{wg}} + A \frac{h_g}{h_{wb}} + (1-A) \frac{h_g h_f}{h_{wg} h_{wb}} + 1 + (1-A) \frac{h_f}{h_{wb}} \quad A1.4.24$$

Expand the terms on the right hand side

$$\frac{1}{R} = \frac{h_g}{h_{wg}} + A \frac{h_g}{h_{wb}} - A \frac{h_g h_f}{h_{wg} h_{wb}} + \frac{h_g h_f}{h_{wg} h_{wb}} + 1 + \frac{h_f}{h_{wb}} - A \frac{h_f}{h_{wb}} \quad A1.4.25$$

Group together the like terms

$$\frac{1}{R} = \left[ 1 + \frac{h_f}{h_{wb}} - A \frac{h_f}{h_{wb}} \right] \left[ 1 + \frac{h_g}{h_{wg}} \right] + A \frac{h_g}{h_{wg}} \quad A1.4.26$$

Where equation A1.4.26 is the solution for the partition ratio, given by Lavine [42, 43].

**APPENDIX A2.1**  
**ABRASIVE GRAIN THERMAL PROPERTIES.**

Recommended thermal conductivity of alumina (sapphire)  $\text{Al}_2\text{O}_3$

(See Fig. 4.A-2)

Recommended values (High-purity synthetic sapphire single crystal)			
$T_1$	$k_1$	$T_2$	$k_2$
K	watt·cm <sup>-1</sup> ·k <sup>-1</sup>	°F	BTU·hr <sup>-1</sup> ·ft <sup>-1</sup> ·°F <sup>-1</sup>
0	0	-459.7	0
1	(0.039)*	-457.9	(2.25)
5	4.1	-450.7	237
10	29	-441.7	1 680
15	87	-432.7	5 030
20	157	-423.7	9 070
25	202	-414.7	11 700
30	207	-405.7	12 000
35	177	-396.7	10 200
40	120	-387.7	6 930
45	77	-378.7	4 450
50	52	-369.7	3 010
60	26.5	-351.7	1 530
70	15.3	-333.7	884
80	9.6	-315.7	555
90	6.4	-297.7	370
100	4.5	-279.7	260
150	(1.5)	-189.7	(86.7)
200	(0.82)	-99.7	(47.4)
250	(0.58)	-9.7	(33.5)
273.2	(0.52)	32.0	(30.0)
300	0.46	80.3	26.6
350	0.38	170.3	22.0
400	0.324	260.3	18.7
450	0.279	350.3	16.1
500	0.242	440.3	14.0
600	0.189	620.3	10.9
700	0.154	800.3	8.90
800	0.130	980.3	7.51
900	0.115	1160	6.64
1000	0.105	1340	6.07

*Remarks.* The recommended values are for high-purity synthetic sapphire single crystal with heat flow at 60 degrees to the hexagonal axis. The recommended values that are supported by experimental thermal conductivity data are thought to be accurate to within 10 to 15% of the true values at temperatures above 60 K. The thermal conductivity near below the corresponding temperature of its maximum is highly sensitive to small physical and chemical variations of the specimens, and the recommended values below 60 K are intended as typical values for indicating the general trend.

\* Values in parentheses are extrapolated or interpolated.

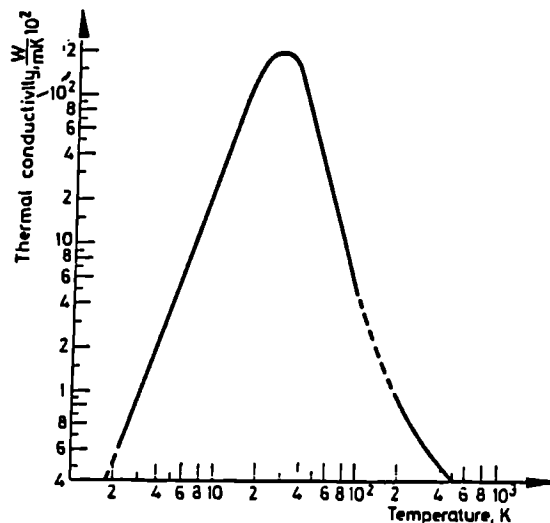
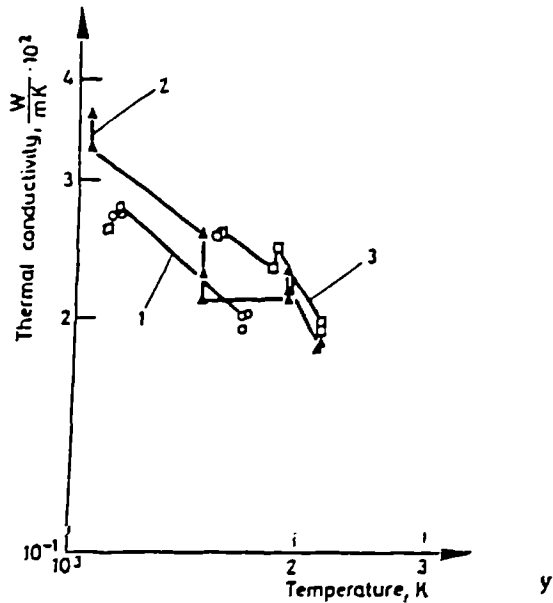


Fig. 4A-2 Recommended thermal conductivity of alumina,  $\text{Al}_2\text{O}_3$

Table 4A-7

Data of thermal conductivity of boron nitride, BN  
 (Temperature, T, K; thermal conductivity, k,  
 Watt cm<sup>-1</sup> K<sup>-1</sup>  
 (See Fig. 4A-5)

T	k	T	k
<i>Curve 1</i>		1933.2	0.233*
1112.1	0.270	2108.7	0.183
1130.4	0.270	2110.9	0.185
1130.4	0.279	2112.1	0.184*
1670.9	0.201	2114.3	0.185
1679.3	0.193		
1696.5	0.202		
<i>Curve 2</i>			
1047.1	0.362	1102.6	0.262
1047.1	0.329	1102.6	0.260
1474.8	0.256	1540.4	0.256
1475.4	0.227	1542.6	0.254
1488.7	0.210	1549.3	0.258
1910.4	0.212	1834.3	0.233
1917.1	0.234	1850.4	0.247
1928.2	0.219	2120.4	0.194
		2125.9	0.194*
		2129.3	0.198
<i>Curve 3</i>			



\* Not shown on plot

Fig. 4A-5 Thermal conductivity of boron nitride, NB

Table 4A-8

Specification, thermal conductivity of boron nitride, BN  
 (For data reported in Fig. 4A-5 and Table 4A-7)

Curve No.	Method used	Temp. range, K	Name and specimen designation	Composition (mass %), specifications and remarks
1	R	1112-1697	1	Specimen 1.9 cm long, 1.9 cm O.D., and 0.635 cm I.D.; surface scratches eliminated by grinding and polishing
2	R	1047-2114	1	Second run of the above specimen
3	R	1103-2129	2	Similar to the above specimen

Data of thermal conductivity of grinding grains (according to Touloukian, Y. S.; Lilay, P. E.; Saxena, S. C.: *Thermal Conductivity of Non-metallic Solids*. IFI Plenum, New York, Washington, 1970).

Detailed data and specification of thermal conductivity are continued in Tables 4A-1-4A-9 and in Figs 4A-1-4A-6.

Table 4A-1

Recommended thermal conductivity of alumina  $Al_2O_3$   
(See Fig. 4A-1)

Recommended values (For 99.5% pure, 98% dense, polycrystalline $Al_2O_3$ )			
$T_1$	$k_1$	$T_2$	$k_2$
K	watt·cm <sup>-1</sup> ·K <sup>-1</sup>	°F	BTU·hr <sup>-1</sup> ·ft <sup>-1</sup> ·°F <sup>-1</sup>
0	0	-459.7	0
100	1.33	-279.7	76.9
150	0.77	-189.7	44.5
200	0.55	-99.7	31.8
250	0.434	-9.7	25.1
273.2	0.397	32.0	22.9
300	0.360	80.3	20.8
350	0.307	170.3	17.7
400	0.264	260.3	15.3
500	0.202	440.3	11.7
600	0.158	620.3	9.13
700	0.126	800.3	7.28
800	0.104	980.3	6.01
900	0.089	1160	5.14
1000	0.0785	1340	4.54
1100	0.0710	1520	4.10
1200	0.0655	1700	3.79
1300	0.0613	1880	3.54
1400	0.0583	2060	3.37
1500	0.0566	2240	3.27
1600	0.0556	2420	3.21
1700	0.0554	2600	3.20
1800	0.0559	2780	3.23
1900	0.0574	2960	3.32
2000	0.0600	3140	3.47
2100	(0.0644)*	3320	(3.72)*

Remarks. The recommended values are for 99.5% pure, 98% dense, polycrystalline  $Al_2O_3$ . The recommended values are thought to be accurate to within 6% of the true values at temperatures from 500 to 1000 K and 6 to 10% at other temperatures.

\* Values in parentheses are extrapolated

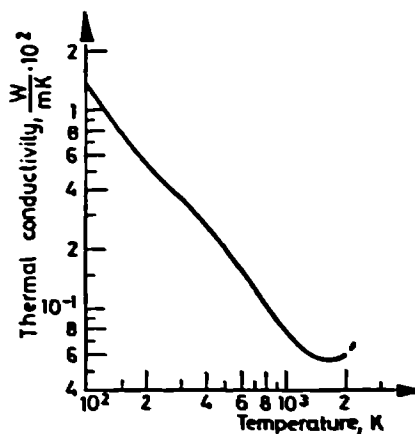


Fig. 4A-1 Recommended thermal conductivity of alumina,  $Al_2O_3$

## APPENDIX A2.2

### SPECIFIC HEAT CAPACITY - ENERGY BALANCE EQUATION.

Theory.

An equation for the specific heat capacity of the sample was established from an energy balance for the system. The equation assumes no losses to the environment.

energy at start = energy at end

energy at start = energy imparted to grinding wheel + energy inherent in water  
+ equivalent of calorimeter + energy in water carried over

energy at start =  $m_s C_{ps} \theta_s + m_w C_{pw} \theta_w + m_{wco} C_{pw} \theta_s$

energy at end =  $m_s C_{ps} \theta_{ss} + m_w C_{pw} \theta_{ss} + m_{wco} C_{pw} \theta_{ss}$

Equating the two equations and rearranging for an expression in terms of the specific heat capacity of the sample gives

$$C_{ps} = m_{wco} C_{pw} (\theta_{ss} - \theta_s) + m_w C_{pw} (\theta_{ss} - \theta_w) / [m_s (\theta_s - \theta_{ss})]$$

where

Mass of sample	$m_s$
Initial calorimeter temperature	$\theta_w$
Temperature of sample before immersion	$\theta_s$
Mass of calorimeter dry (a)	
Mass of calorimeter with water (b)	
Mass of water (b - a)	$m_w$
Mass of calorimeter with water and sample (c)	
Mass of water carried over (c - $m_s$ - $m_w$ - a)	$m_{wco}$
Temperature at steady state	$\theta_{ss}$
Specific heat capacity of water	$C_{pw}$

The following suffices are used:

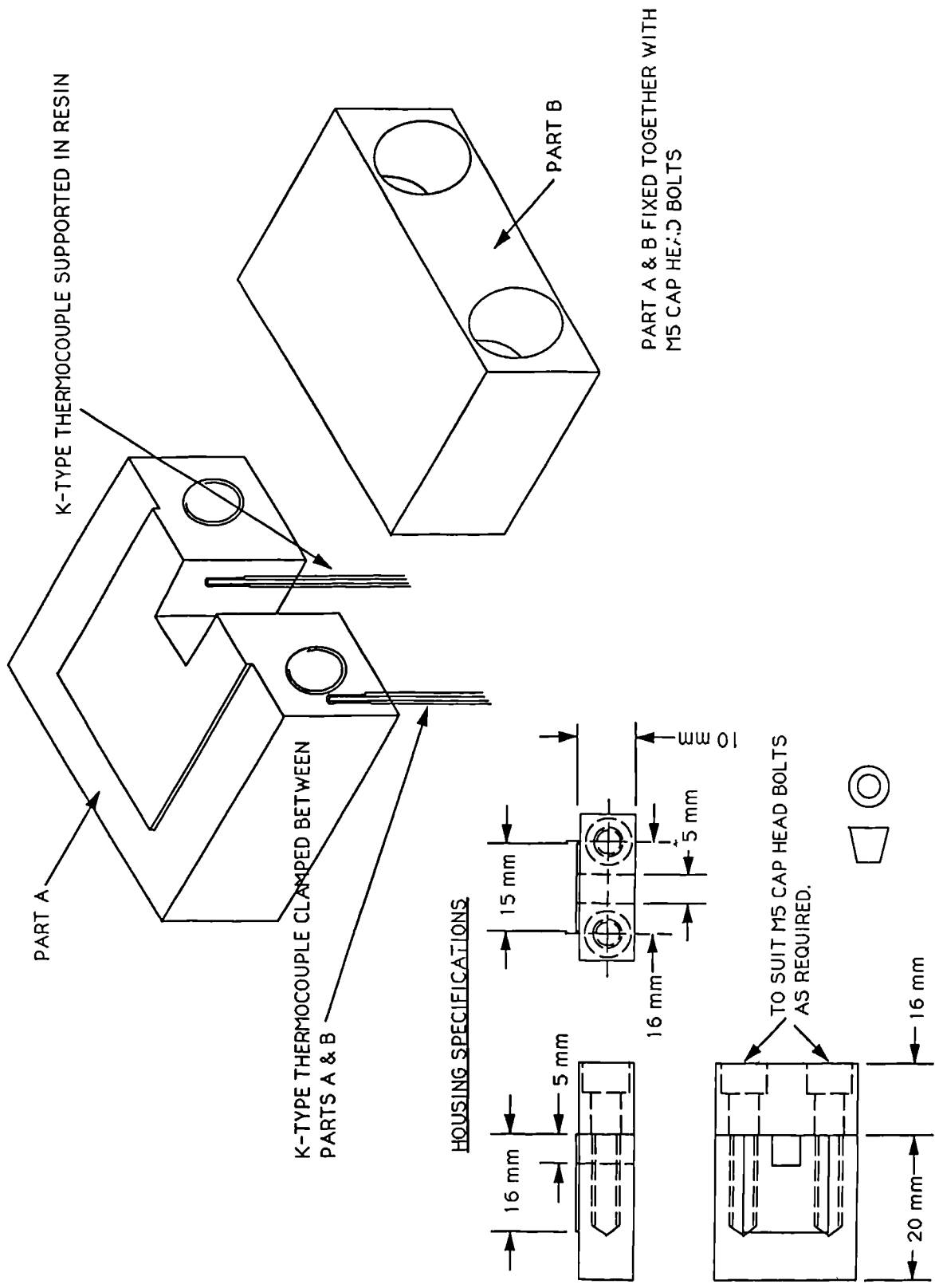
s = sample

ss = steady state

w = water

wco = water carried over

APPENDIX A2.2



## **APPENDIX A3.1**

### **ETCH INSPECTION**

*Extracts from Process Instruction manual:*  
Etch Inspection - (JAR-3N Etchant)

#### **1 Health and Safety Requirements**

The acids used in the process and their solutions can be injurious to health. protective clothing, goggles and gloves should be worn when making-up and operating processing baths. If skin contact occurs, wash off immediately. If eye contact occurs, wash copiously with clean cold water and seek medical advice. Smoking and naked flames are prohibited in processing areas.

#### **2 Approved Materials**

Nitric Acid (sg 1.42)	Good commercial quality
Distilled / De-mineralised water	Good commercial quality
Trichloroethylene	Good commercial quality
Trichloroethane	BS 580 Type 2
De-watering fluid	BS 4487
Light lubricating (OM-13)	DEF STAN 68 - 11 (PX-10)
Anti-smutting agent	JAR-3N

#### **3 Equipment Requirements**

Process tanks:

Tanks are required for each liquid used in the process, i.e. water, nitric acid solution, de-watering fluid and light lubricating oil. Each tank must be large enough to allow for complete submersion of the component(s), impervious to the contained solution and prominently identified.

Acid etchant and de-greasing tanks must have adequate fume extraction facilities.

Other equipment:

Suitable bristle brushes. Suitable jig/baskets/handling equipment for immersing component(s) in etching solutions; wash tanks, de-watering fluid etc. Filtered, dry air supply.

#### **4 Etching Solution Make-up and Control**

Initial make-up of solution shall be by the controlling laboratory and conform to the concentration given below:-

Constituent	Concentration	Operating temperature
Nitric Acid (sg 1.42)	30 ml	ambient
*Anti-smutting agent	45ml	ambient
Distilled / De-mineralised water	0.75 Litre	ambient

\*It is not possible to measure quantities once in solution. Anti-smutting agent strength is not critical but small additions should be made if smutting occurs within the normal etching times and conditions.

Etchant bath shall be changed frequently depending on work load but at a minimum of twice per week. New baths shall be made up by the processors controlling laboratory or quality department approved personnel. The solutions in the tanks shall be maintained at constant level when in use.

#### **5 Etching Procedure**

Note:- Etching must be carried out prior to any shot peening or other surface compressive treatments as these may obscure any imperfections present.

- (a) Ensure that all components are free of oil and other contaminants prior to operation (b).
- (b) Vapour degrease in trichloroethylene vapour or cold de-grease by swabbing or immersion in trichloroethane. (Genklene, Inhibisol, etc).
- (c) Immerse in clean water to cool.
- (d) Immerse in etching solution and agitate.
- (e) Thoroughly rinse in clean water. Light smut may be removed by soft bristle brushing.
- (f) Allow to drain or blow off excess water with filtered air supply. DO NOT attempt to dry completely.
- (g) Immerse in de-watering fluid and allow to drain.
- (h) Inspect in accordance with (6).

## 6 Inspection

Visually inspect component surface under a binocular microscope having a magnification of (x2).

Note: The optimum viewing conditions for etched surfaces is when the lighting is oblique to the angle of view and such that highlights are avoided. An independent, low power light source is essential and ambient background light in the inspection area should be subdued and not exceed 250 lux.

A satisfactory condition of a hardened part is indicated by a uniform grey matt appearance. A case hardened or nitrided surface develops a darker grey colour.

Surface imperfections will be indicated as follows:

- (i) Grinding burns, re-hardened areas, and soft spots - light and /or dark areas contrasting against a matt background.
- (ii) Cracks - dark ragged lines (usually associated with soft spots, burns, or re-hardened areas).
- (iii) General lack of hardness - usually indicated by dark straight lines or lines of dots.
- (iv) Local softening on ground cylindrical components - spirals of dark shade against a lighter matt background.

Components indicating any of the above imperfections shall be rejected.

Plate 1      NITAL Etched workpiece:  
Grey cast iron, grade 260/17, diameter 32 mm

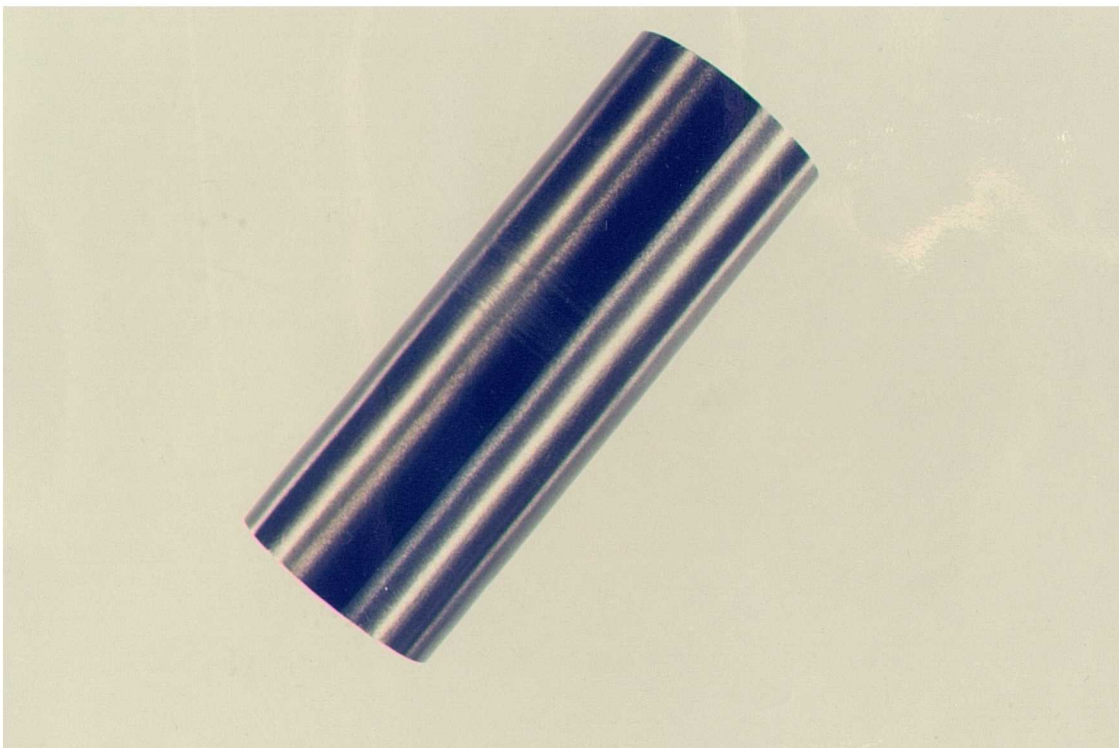
Machine	:Wickman Scrivener 2K
Process	:centreless grinding
Grinding wheel	:19AV60NVS
Wheelspeed	:40 m/s
Grinding fluid	:TRIM VE20, dilution 50:1
Workspeed	:200 mm/s
Infeed	:0.083 mm/s



No visible thermal damage

Plate 2      NITAL Etched workpiece:  
Grey cast iron, grade 260/17, diameter 32 mm

Machine	:Wickman Scrivener 2K
Process	:centreless grinding
Grinding wheel	:19AV60NVS
Wheelspeed	:40 m/s
Grinding fluid	:TRIM VE20, dilution 50:1
Workspeed	:200 mm/s
Infeed	:0.300 mm/s



Light visible thermal damage

## **APPENDIX A3.2**

**THERMAL MODEL: PROGRAM LISTING.**

```

C      THIS PROGRAM CALCULATES THE CRITICAL SPECIFIC GRINDING ENERGY
C      AND PARTITION RATIO'S FOR CENTRE, CENTRELESS AND SURFACE
C      GRINDING OPERATIONS - Version 2
C      (version 1: parameter values = input prompt)
C      (version 2: parameter values = allocated)

      integer csorcl
C      = CENTRE / SURFACE OR CENTRELESS GRINDING?

      real cg,rhog,cpg,diffg,rnort
C      GRAIN PROPERTIES and GRAIN CONTACT LENGTH

      g cw,rhow,cpw
C      WORKPIECE PROPERTIES

      g tburn,tamb,themax,thetamelt
C      WORKPIECE TEMPERATURES 1. (BURN-AMB)=MAX 2.THETAMELT=CHIP MELT TEMP

      g vs,vw,vf
C      GRINDING PARAMETERS

      g cf,rhof,cpf,thetaf,tboil,tambf
C      FLUID PROPERTIES and FLUID TEMPERATURES (BOIL-AMB)=MAX

      g al
C      GEOMETRIC CONTACT LENGTH

      g remc,remc,remcl,eccalc,pwr
C      REMOVAL RATES - CENTRE,SURFACE,CENTRELESS and
C      SPECIFIC GRINDING ENERGY DERIVED FROM MEASURED POWER and
C      RECORDED POWER

C      (1) SURFACE GRINDING
      g ds,wids,as
C      WHEEL DIAMETER, WORKPIECE(orwheel)WIDTH, TRUE DEPTH OF CUT

C      (2) CENTRE GRINDING
      g dwp,dcgs,widc,de
C      WORKPIECE DIAMETER,WHEEL DIAMETER,WORKPIECE WIDTH
C      and EQUIVALENT DIAMETER

C      (3) CENTRELESS GRINDING
      g dwpcl,dclgs,widcl
C      WORKPIECE DIAMETER,WHEEL DIAMETER,WORKPIECE WIDTH

      g ecfluid,ecchips,eccritub,eccritlb
C      QUANTITY OF ENERGY TRANSFERRING TO FLUID,CHIPS and
C      CRITICAL SPECIFIC GRINDING ENERGY UPPER BOUND,LOWER BOUND
      g rub,rlbc,rlbf
C      PARTITION RATIO UPPER BOUND,LOWER BOUND (ZETA>3), (ZETA<

C      VARIABLES USED IN EQUATIONS :

      real ap,aq,ar,at,au,el
C      LABELS FOR VARIABLES USED IN CALCULATION OF ZETA
      g zeta,erfzeta,erfczeta
      g aa,ab,ac,ad,ae,t,aj
C      FIXED REAL VARIABLES USED IN POWER SERIES FOR CALCULATION OF
C      ERFCZETA where ERFCZETA=1-ERFZETA
      g ca,cb,cc,fav,fzeta,pthi
C      LABELS FOR VARIABLES USED IN CALCULATION OF PARTITION
C      RATIO WHEN ZETA IS LESS THAN 3
      g elsqr,elfsqr,alsqr,rr,rrsqr
      g bks,bkw,simas,sigmaw
      g eess,eew

```

```

C LABELS FOR VARIABLES USED IN CALCULATION OF REAL CONTACT LENGTH
g fa,fb,fc,fd,fe,fg
C LABELS FOR VARIABLES USED IN CALCULATION OF PARTITION
C RATIO WHEN ZETA IS GREATER THAN 3

g ga,gb,gc,gd,gf,gg
C LABELS FOR VARIABLES USED IN CALCULATION OF LOWER BOUND
C CRITICAL SPECIFIC ENERGY

g ea,eb,ec
C LABELS FOR VARIABLES USED IN CALCULATION OF ENERGY TO FLUID

g am,df
C LABELS FOR VARIABLES USED IN CALCULATION OF CONTACT LENGTH

C -----
C ***** ALLOCATE VALUES TO PARAMETERS

2 cg=35*1e-3
4 rhog=3910*1e-6
6 cpg=765*1e-3
8 rnort=25*1e-3
10 cw=57*1e-3
12 rhow=7650*1e-6
14 cpw=0.46
16 tburn=471
18 tamb=21
20 thetamelt=1500
22 vs=40000
24 cf=1*1e-3
26 rhof=1000*1e-6
28 cpf=4200*1e-3
30 tboil=120
32 tambf=27
34 sigmas=0.0484
36 sigmaw=0.0841
38 eew=213
40 eess=49.6
42 rr=5
44 pi=3.141592654

C -----
C ***** INPUT PROMPT, vw

160 write (9,165)
165 format('Enter vw in this form xxx.x mm/s')
read(9,170)vw
170 format(f6.1)

C -----
C ***** CALCULATE DEPTH OF CUT CENTRE / SURFACE

write (9,180)
180 format('Enter "1" for centre,"2" for surface,
g "3" for centreless')
read(9,185)csorcl
185 format(' ',i1)

C -----
C ***** CENTRE GRINDING -->

190 if (csorcl.eq.1) then
write (9,195)
195 format('Enter workpiece diameter in this form
g xx.xxx m')
read(9,200)dwp
200 format(f6.3)

```

```

205         write(9,205)
           g   format('Enter Grinding wheel diameter in this
                form xxx.xx mm')
           read(9,210)dcgs
210         format(f6.2)

           write(9,215)
215         g   format('Enter feed rate in this
                form x.xxx mm/s')
           read(9,220)vf
220         format(f5.1)

           write(9,225)
225         g   format('Enter workpiece width in this
                form xx.xx mm')
           read(9,230)widc
230         format(f5.2)

           write(9,235)
235         g   format('Enter recorded power in this
                form xxxxx.x W')
           read(9,240)pwr
240         format(f7.1)

           remc=(pi)*dwp*vf*widc
           eccalc=(pwr/remc)

           de=(dwp*dcgs)/(dwp+dcgs)
           as=((pi*dwp)*vf)/vw
           df=as*de
           al=sqrt(df)

           endif

C -----
C ***** SURFACE -->

250     if (csorcl.eq.2) then

           write(9,255)
255         format('Enter wheel diameter in this form xxx.x mm')
           read(9,260)ds
260         format(f5.1)

           write(9,280)
280         g   format('Enter grinding wheel/ workpiece width in this
                form xx.x mm')
           read(9,285)wids
285         format(f4.1)

           write(9,290)
290         g   format('Enter recorded power in this
                form xxxxx.x W')
           read(9,295)pwr
295         format(f7.1)

296         write(9,297)
297         format('Enter true depth of cut in this form xx.xxx mm')
298         read(9,298)as
           format(f6.3)

           rems=vw*wids*as
           eccalc=(pwr/rems)

           am=as*ds
           al=sqrt(am)
           endif

```

```

C -----
C ***** CENTRELESS -->
300  if (csorcl.eq.3) then
      write(9,305)
305      format('Enter workpiece diameter in this form
g      xx.xxx mm')
      read(9,310) dwpcl
310      format(f6.3)

      write(9,315)
315      format('Enter Grinding wheel diameter in this
g      form xxx.xx mm')
      read(9,320) dclgs
320      format(f6.2)

      write(9,325)
325      format('Enter feed rate in this
g      form x.xxxx mm/s')
      read(9,330) vf
330      format(f6.4)

      write(9,335)
335      format('Enter workpiece width in this
g      form xx.xxx mm')
      read(9,340) widcl
340      format(f6.3)

      write(9,345)
345      format('Enter recorded power in this
g      form xxxxx.x W')
      read(9,350) pwr
350      format(f7.1)

      remcl=(pi/2)*dwpcl*vf*widcl
      eccalc=(pwr/remcl)

      de=(dwpcl*dclgs)/(dwpcl+dclgs)
      as=((pi/2)*dwpcl*vf)/vw
      df=as*de
      al=sqrt(df)

      endif

C -----
C ***** CALCULATE REAL CONTACT LENGTH / ZETA

      alsqr=al**2
      rrsqr=rr**2
      bks=(1-sigmas)/(pi*eess)
      bkw=(1-sigmaw)/(pi*ew)
      elfsqr=4*rrsqr*eccalc*pi*dwpcl*vf*dclgs*(bks+bkw)/vs
      elsqr=elfsqr+alsqr
      el=sqrt(elsqr)

      diffg=cg/(rhog*cpg)
      zeta=sqrt((diffg*el)/((rnort**2)*vs))

C -----
C ***** CALCULATE R LOWER BOUND

      t=1/(1+0.3275911*zeta**2)
      aa=0.254829592
      ab=-0.284496736
      ac=1.421413741

```

```

          ad=-1.453152027
          ae=1.061405429
          aj=exp(-zeta**2)
          erfzeta=1-((aa*t)+(ab*t**2)+(ac*t**3)+(ad*t**4)+
          (ae*t**5))*aj
          erfczeta=1-erfzeta
          ca=exp(zeta**2)
          fzeta=(2*zeta)/(sqrt(pi))*(1-ca*(erfczeta))
          pthi=0.90
          cb=el/rnort
          cc=((cw*rhow)*cpw)/((cg*rhog)*cpg)
          fav=((sqrt(cb)*sqrt(cc))*pthi)/fzeta
          rlbc=fav/(1+fav)

```

```

C -----
C ***** CALCULATE LOWER BOUND SPECIFIC ENERGY

```

```

themax=tburn-tamb
ga=el/vw
gb=(cw*rhow)*cpw
gc=sqrt(ga)*sqrt(gb)
gd=gc*0.89
eccritlb=(gd*themax)/(rlbc*as)

```

```

C -----
C ***** CALCULATE ENERGY TO CHIPS

```

```

ecchips=((rhow*cpw)*thetamelt)

```

```

C -----
C ***** CALCULATE ENERGY TO FLUID

```

```

thetaf=tboil-tambf
ea=(cf*rhof)*cpf
eb=el*vs
ec=sqrt(ea)*sqrt(eb)
ecfluid=((ec*thetaf)*0.89)/(as*vw)

```

```

C -----
C ***** CALCULATE UPPER BOUND SPECIFIC ENERGY

```

```

eccritub=(eccritlb+ecchips+ecfluid)

```

```

C -----
C ***** CALCULATE R UPPER BOUND

```

```

          rub=rlbc*((eccalc-ecchips-ecfluid)/eccalc)

```

```

C -----
C ***** OUTPUT FORMATS

```

```

write (6,600)rlbc
write (6,700)rub
write (6,800)eccritlb
write (6,850)eccalc
write (6,900)eccritub
write (6,910)ecchips
write (6,920)ecfluid
write (6,930)el
write (6,935)al

```

✓

```

write (6,1000) zeta
write (6,1100)
write (6,1110)
write (6,1115)
write (6,1120)
write (6,1130)
write (6,1140) cg, rhog, cpw, rnort, vs
write (6,1150)
write (6,1160)
write (6,1170)
write (6,1180) cw, rhow, cpw, thetamelt, vw
write (6,1185)
write (6,1190)
write (6,1200)
write (6,1210) cf, rhof, cpf, thetaf, themax
write (6,1220)
write (6,1221)
write (6,1222)
write (6,1223) pwr
write (6,1225)
write (6,1226)
if (csorcl.eq.1) then
    write(6,1230)
    write(6,1240)
    write(6,1245)
    write (6,1250) dwp, dcgs, vf, as, widc
endif
if (csorcl.eq.2) then
    write(6,1260)
    write(6,1270)
    write(6,1275)
    write (6,1280) ds, as, wids
endif
if (csorcl.eq.3) then
    write(6,1282)
    write(6,1284)
    write(6,1286)
    write (6,1288) dwpcl, dclgs, vf, as, widcl
endif
write (6,1290)
write (6,1300)

write(6,1310)
write(6,1320) pthi

```

```

600    format(' ', 'R lower bound =', f5.3)

700    format(' ', 'R upper bound =', f5.3)
800    format(' ', 'eccritlb=', f6.2, ' ', 'J/mm3')
850    format(' ', 'eccalc =', f6.2, ' ', 'J/mm3')
900    format(' ', 'eccritub=', f6.2, ' ', 'J/mm3')
910    format(' ', 'ecchips =', f6.2, ' ', 'J/mm3')
920    format(' ', 'ecfluid =', f6.2, ' ', 'J/mm3')
930    format(' ', 'real contact length(le) =', f10.8, ' ', 'mm')
935    format(' ', 'geometric contact length(lg) =', f10.8, ' ', 'mm')
1000   format(' ', 'zeta =', f9.5)
1100   format(' ')
1110   format(' ', 'THE VALUES EMPLOYED WERE AS FOLLOWS :-')
1115   format(' ')

1120   format(' ', 1x, 'cg', 5x, 'rhog', 4x, 'cpw', 4x, 'rnort', 5x,
g      'vs')
1130   format(' ', 'W/mmK', 3x, 'g/mm3', 3x, 'J/gK', 4x, 'mm', 5x, '
g      mm/s')
1140   format(' ', f5.3, 1x, f8.6, 2x, f5.3, 2x, f5.3, 4x, f7.1)
1150   format(' ')

1160   format(' ', 1x, 'cw', 6x, 'rhow', 4x, 'cpw', 4x, 'thetamelt', 2x,

```

```

g 'vw')
1170 format(' ', 'W/mmK', 4x, 'g/mm3', 3x, 'J/gK', 6x, 'C', 4x, '
g mm/s')
1180 format(' ', f5.3, 2x, f8.6, 2x, f5.3, 2x, f6.1, 3x, f6.2)
1185 format(' ')

1190 format(' ', 1x, 'cf', 5x, 'rhof', 4x, 'cpf', 4x, 'thetaf', 3x,
g 'themax')
1200 format(' ', 'W/mmK', 3x, 'g/mm3', 2x, 'J/gK', 4x, 'C', 8x, '
g C')
1210 format(' ', f5.3, 2x, f8.6, 2x, f5.3, 2x, f5.1, 4x, f6.1)
1220 format(' ')

1221 format(' ', 'Power')
1222 format(' ', ' W')
1223 format(' ', f7.1)
1225 format(' ')
1226 format(' ')

1230 format(' ', 'CENTRE GRINDING DATA --->')
1240 format(' ', 3x, 'dw', 8x, 'ds', 7x, 'vf', 13x, '"as"', 8x, 'width')
1245 format(' ', 3x, 'm', 10x, 'm', 7x, 'm/s', 14x, 'm', 12x, 'm')
1250 format(' ', e10.3, 2x, f5.3, 2x, e9.3, 5x, f10.8, 6x, e10.3)

1260 format(' ', 'SURFACE GRINDING DATA --->')
1270 format(' ', 1x, 'ds', 5x, '"as" true', 10x, 'width')
1275 format(' ', 1x, ' m', 8x, 'mm', 12x, 'mm')
1280 format(' ', e7.2, 2x, e10.3, 5x, e10.3)

1282 format(' ', 'CENTRELESS GRINDING DATA --->')
1284 format(' ', 3x, 'dw', 8x, 'ds', 7x, 'vf', 7x, 'width')
1286 format(' ', 3x, 'mm', 8x, 'mm', 7x, 'mm/s', 6x, 'mm')
1288 format(' ', 3x, f4.1, 4x, f5.1, 3x, f6.4, 5x, f5.2)

1290 format(' ')
1300 format('**FLUID PROPERTIES WERE THOSE OF WATER**')

1310 format(' ')
1320 format(' The assumed value of pthi for this run was =', f4.2)

end

```

**Plate 3      The grinding wheel - workpiece arrangement**

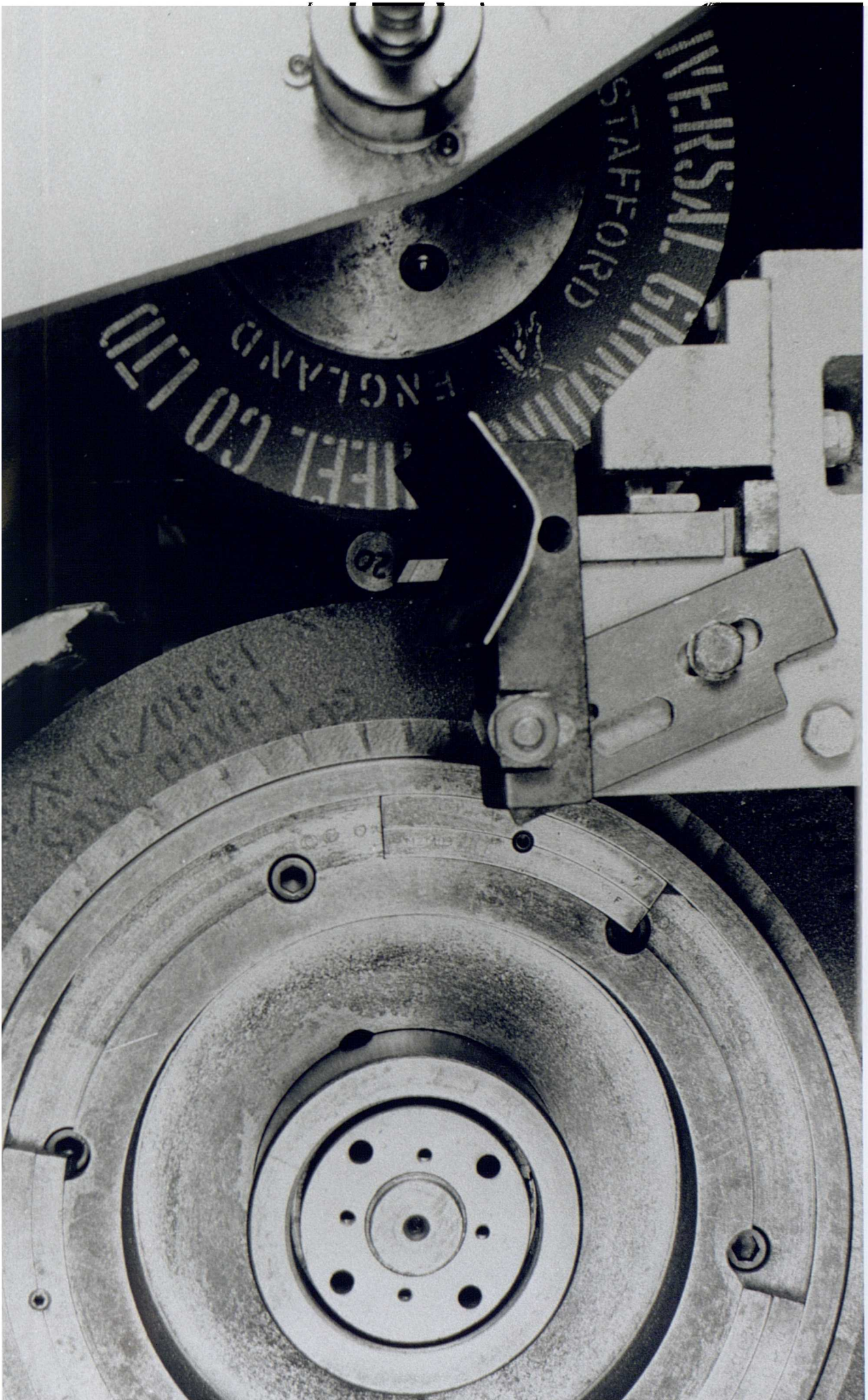


**Plate 4      The single point diamond dressing tool**

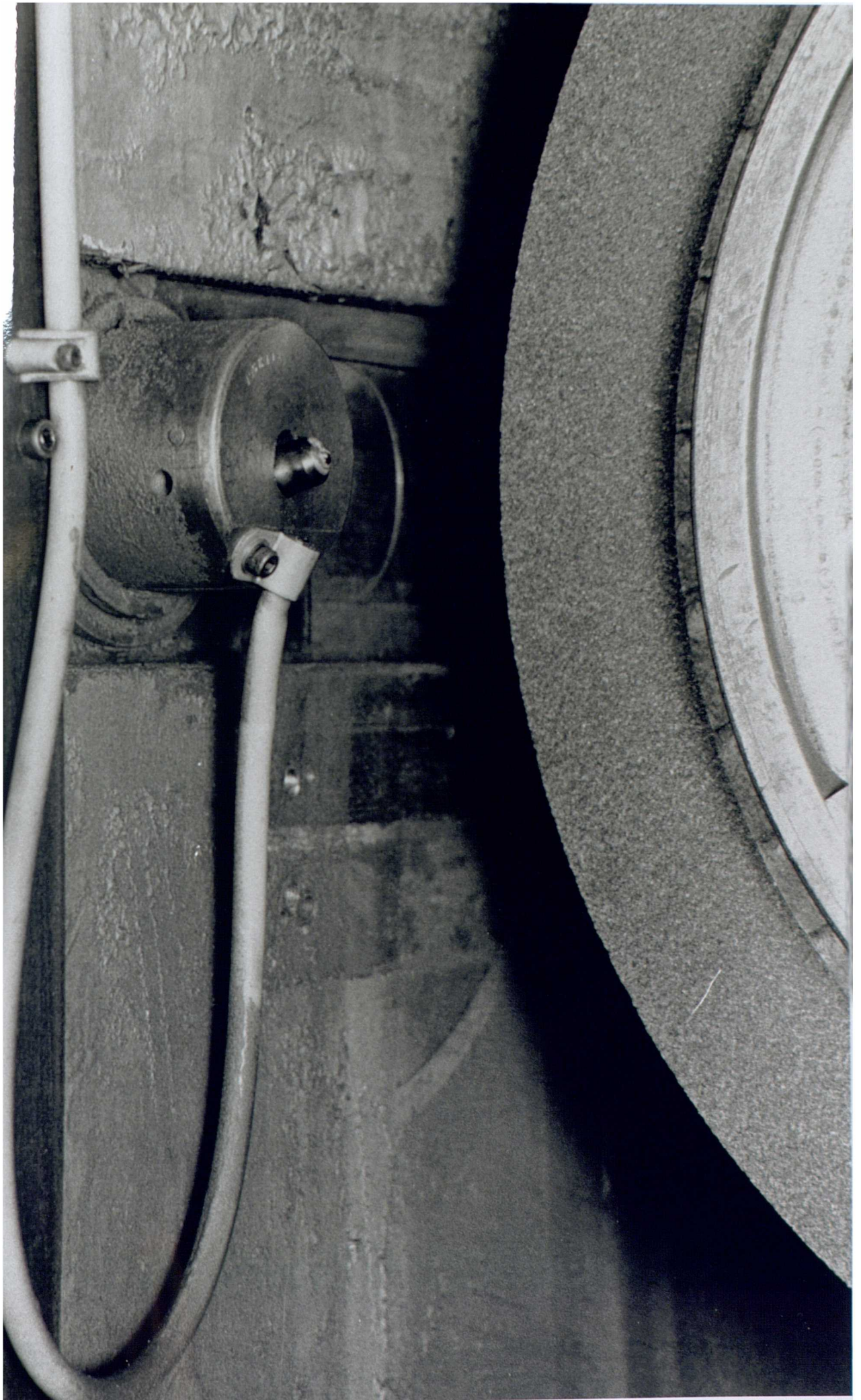


**Plate 5      The dressing tool linear scale**

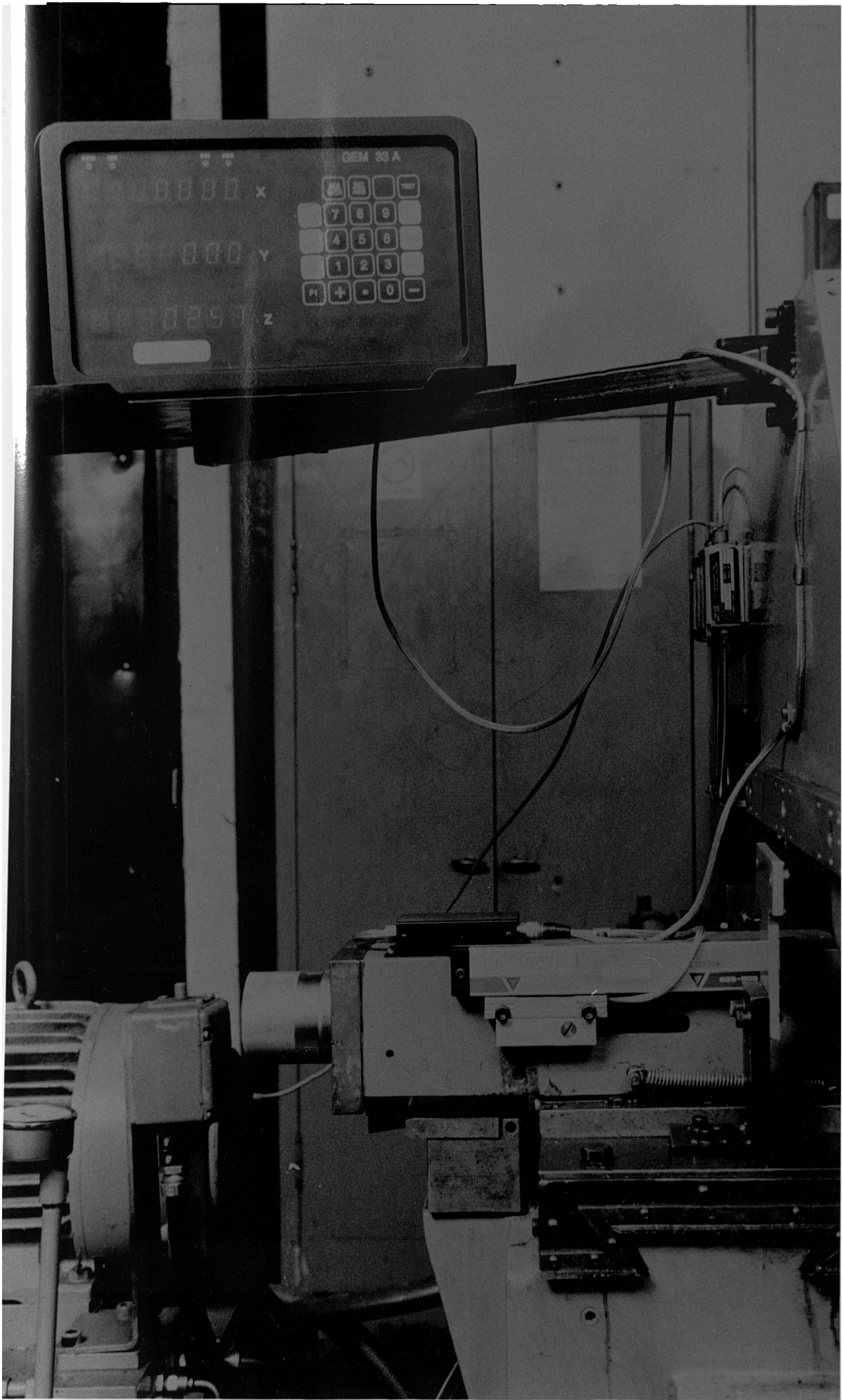


**Plate 6      The torsionally rigid coupling**

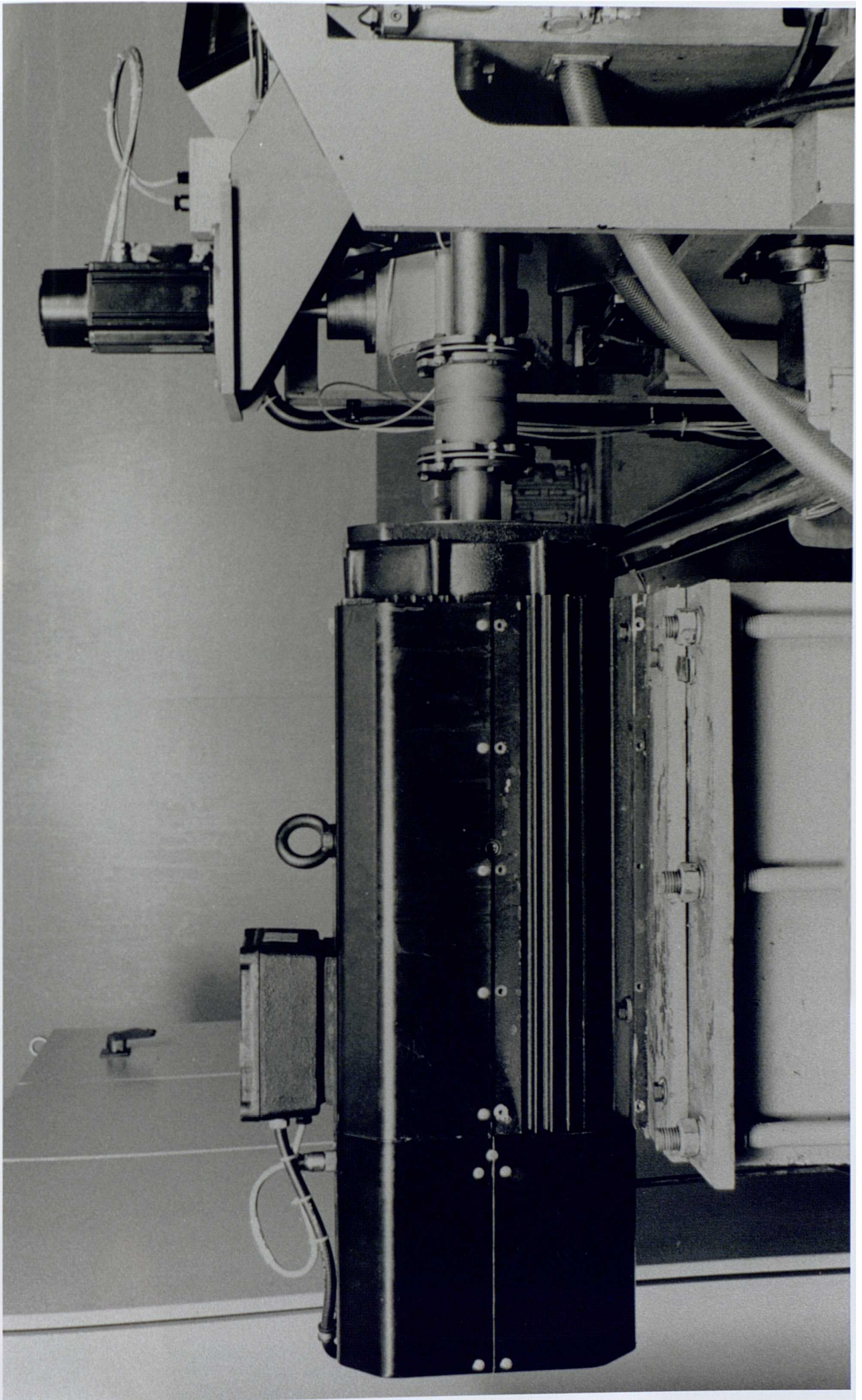


**Plate 7      Arrangement of the experimental equipment**

